DEPARTMENT OF AERONAUTICS AND ASTRONAUTICS

MODELLING OF SATELLITE CONTROL THRUSTER PLUMES

by

Iain D. Boyd

A thesis submitted for the degree of

Doctor of Philosophy

University of Southampton,

Southampton, England.

October 1988

CONTENTS

University of Southampton

ABSTRACT

Faculty of Engineering and Applied Sciences

Department of Aeronautics and Astronautics

Doctor of Philosophy

MODELLING OF SATELLITE CONTROL THRUSTER PLUMES

by Iain D. Boyd

Deleterious effects such as surface heating and turning moments can arise as a consequence of the impingement of thruster plumes with spacecraft surfaces. Such thrusters are normally fired for attitude control. The prediction of such effects must be undertaken at the design stage of the vehicle.

In this study, the modelling of such plumes was undertaken. The following prediction techniques were implemented into computer programmes: (a) the Simons model, (b) the Method of Characteristics (MOC), and (c) the Direct Simulation Monte Carlo method (DSMC). The first two methods are derived from continuum equations whilst the third adopts a discrete particle approach.

Several DSMC schemes exist for treating the collisional behaviour of the gas, and it was unclear which would be best suited for the intended application. A thorough assessment of the implementation and performance of several such schemes was therefore completed.

Having determined the most suitable DSMC scheme, the three modelling techniques were then applied to the isentropic core expansion of a small hydrazine thruster plume. It was found that significant errors occur in the determination of impingement quantities through application of the continuum methods in the flow regime lying between the continuum and free molecular limits.

The DSMC technique was also used to calculate the nozzle lip and backflow expansion regions of the same hydrazine thruster. A significant degree of backflow was found with flow angles of up to 140°. The sensitivity of the calculations to the conditions initially assumed were assessed and found to be important.

ACKNOWLEDGEMENT

The author wishes to express his gratitude to Dr.J.P.W. Stark for his supervision and consultation during the project, together with his most helpful comments in reviewing the manuscript.

In additiona, the author would like to thank Dr.J.C.Lengrand of CNRS, Meudon, France, and Dr.H.Legge, Dr.G.Dettleff and R.D.Boettcher of DFVLR, Gottingen, F.R.G., for their contributions to the work, and for sharing their experimental data. Thanks are also extended to Prof.H.Neunzert and his colleagues at AGTM, University of Kaiserslautern, F.R.G., for their hospitality during my short stay. The encouragement provided by all of the aforementioned is gratefully acknowledged.

The author acknowledges the financial support of an IBM/SERC CASE award. Additional thanks are extended to Dr.T.Heywood for obtaining funds which enabled the author to attend two conferences, and to all at the IBM United Kingdom Scientific Centre, Winchester, for their support.

The contents of this thesis are dedicated to mum, dad, and my wife Kath.

NOMENCLATURE

A	Simons model plume constant
a, b	Modified Simons model constants
$\underline{c}$	molecular velocity vector
c_m	velocity in centre of mass frame
c_r	relative velocity of collision
E_a	activation energy of reaction
E_c	total collision energy
E_{int}	internal energy
E_{tr}	translational energy
f	molecular distribution function
Kn	Knudsen number
k	Boltzmann constant
k_f, k_r	forward and reverse rate coefficients
L	number of time-step subdivisions
Ma	Mach number
m	molecular mass
m_r	reduced mass of collision
N_m	number of simulated molecules
n	number density
P	continuum breakdown parameter
P_{t2}	Pitot pressure
P_{ij}	collision probability of molecules i,j
p	pressure
p_0	thruster chamber pressure
Re	Reynolds number
S	speed ratio
T	temperature
T_0	thruster chamber temperature
T_{ref}	Variable Hard Sphere reference temperature
t	time

U	stream velocity
u, v, w	component velocities
V	volume of computational cell
W	weight or physical scaling factor
α	dissociation degree of ammonia
β	reciprocal of mean thermal speed
Γ	gamma function
γ	ratio of specific heats
δ	boundary layer thickness
ζ	number of internal degrees of freedom
ϕ	fraction of collisions which are inelastic
θ	flow angle
θ_v	characteristic temperature for vibration
λ	mean free path
μ	molecular gas viscosity
ν	collision rate
ρ	density
σ_{ref}	Variable Hard Sphere reference collision cross section
σ_T	total collision cross section
ω	Variable Hard Sphere temperature exponent
Δt_m	decoupling time step
$\Delta\tau$	reduced time step in Modified Nanbu scheme

1. INTRODUCTION

1.1 Background

Spacecraft are usually manoeuvred by the use of jets (or plumes) exhausting from rocket engines. Movement of a spacecraft may be required for orbital transfer or for attitude control. The jets emanating from the spacecraft thrusters expand into the very low ambient pressures experienced in the space environment.

The presence of a low external pressure results in the jet turning through very large angles at the lip of the thruster nozzle so that backflow becomes an important phenomena. A significant amount of impingement between the jet and neighbouring spacecraft surfaces is therefore difficult to avoid. The effects of such impingement should be analysed at the design stage of the spacecraft.

Typical impingement effects include:

(i) unwanted turning moments

(ii) heating of spacecraft surfaces

(iii) charging of spacecraft surfaces

(iv) contamination of spacecraft surfaces

(v) thrust loss.

The possibility of turning moments has consequences on the attitude control system of a spacecraft. Both normal and tangential forces must be accounted for. The need for the correction of unforeseen forces will result in the depletion of valuable onboard

fuel resources. In addition, such forces are responsible for reductions in thruster efficiency resulting in overconsumption of fuel. Thus the operational lifetime of the spacecraft may become impaired.

Failure to take proper account of the heating effects of plume impingement will lead to instability in the thermal balance of the spacecraft. In particular, excessive local heating may cause permanent damage to such sensitive surfaces as solar arrays.

Charging of spacecraft surfaces may lead to defective operation of onboard instrumentation and is particularly harmful to spacecraft carrying scientific payloads.

Also, optical instrumentation and solar cells may lose effectiveness by the deposition of solid and liquid components present in the jet, thus reducing the operational lifetime of the spacecraft.

Finally, the impingement of the thruster exhaust plume will generally result in a loss in the effective thrust provided. This can be as much as 40% [1] depending on the particular spacecraft configuration.

Clearly, the effective determination of such deleterious events is of great importance in the design and the management of a spacecraft.

1.2 Spacecraft Thrusters

The thrusters employed on spacecraft vary greatly in design according to their intended application. The thrust requirements for orbital manoeuvres and for precision pointing of the spacecraft may vary from 500N down to less than 0.5N respectively.

The thruster system may be divided into three regions:

(i) the combustion chamber, in which the fuel(s) are ignited

(ii) the nozzle, through which the products of combustion are expanded

(iii) the plume, which consists of the expansion of the combustion products into the near vacuum of space.

The conditions in the combustion chamber will be effectively determined by the propellant(s) together with the chamber pressure and temperature. Three types of propellant are commonly used: (a) gaseous propellant, e.g. cold gas, (b) liquid propellant, e.g. mono and bi-propellant, and (c) solid propellant.

The combustion products directly affect flow conditions through the nozzle. The nozzle geometry is also of key importance. In particular, the ratio of the exit to throat cross sectional area and the shape of the nozzle wall will determine the properties at the nozzle exit. In the nozzle itself, such phenomena as viscous effects, chemical reactions and two phase flow (unburnt droplets of fuel, solid particles) may occur. Viscous effects result in the formation of a boundary layer along the wall of the nozzle. The nature of the boundary layer from laminar to turbulent may be characterised by Reynolds number.

Finally, we come to the exhaust plume itself. This is initially characterised by the results of the nozzle flow phenomena. In addition, the external pressure will affect the degree of expansion experienced by the jet at the nozzle lip.

In the plume, rarefaction effects are important. In addition, relaxation, condensation and chemical reactions may take place. The expansion of the plume is divided into that of the isentropic core and that of the boundary layer. Clearly, any backflow must be associated with the expansion of the boundary layer. This region of the flowfield is characterised by extreme rarefaction, thermal nonequilibrium, and the species separation effects. It is evident that such phenomena present a severe challenge to both experimental and theoretical investigation.

1.3 Experimental Investigation

Ideally, the prediction of impingement effects would best be investigated by using the actual thrusters in the laboratory. It is clear that even in the largest test facilities, only thrusters of small dimensions can be examined under reasonable vacuum conditions. At the University of Hamburg, Trinks [2 – 4] has tested a range of bipropellant thrusters. The aim of this work is to construct a database of information linking the effects of certain fuels when impinging on certain materials. Such a database should greatly aid the prediction and prevention of some of the effects men-

tioned earlier. At the DFVLR Institute for Experimental Fluid Mechanics, Gottingen, F.R.G., work has concentrated on small hydrazine thrusters [5,6]. Lengrand et al [7 – 9] have used small nozzles and scaling relations to simulate larger rocket engines at the CNRS Aerothermodynamics Laboratory, Meudon, France. Whilst it is certain that similar experimental programmes must exist in the U.S.A., due to the sensitive nature of the subject matter, their results rarely appear in the open literature.

Phenomena which may be investigated in the laboratory include:

(i) heat transfer, using thermocouples,

(ii) Pitot pressure (from which flow angle may also be deduced [10]), using small probes,

(iii) force, using aerodynamic balances,

(iv) velocity, using time of flight measurements,

(v) density, using electron beam fluorescence.

However, the simulation of the low pressure space environment in a laboratory presents major technical difficulties. In many spacecraft configurations the majority of impingement occurs in the outer regions of the exhaust plume. Thus low chamber pressures must be maintained during the firing periods of the thruster under consideration. In addition, Bailey [10] has found that the properties in the backflow region are very sensitive to variations in the laboratory background pressure achieved. In the present day technology, cryogenic devices alone seem to offer the pumping speeds required to maintain a realistic low pressure ambient environment. Such facilities are, of course, extremely expensive.

1.4 Theoretical Investigation

In the absence of experimental facilities recourse must be made to theoretical methods. It is the aim of the present research to make prediction of plume properties

through the use of such techniques. It is then possible to derive in an approximate fashion the impingement effects resulting from a particular plume flowfield.

From a theoretical standpoint, the plume should be subdivided into three distinct flow regimes. These regimes are characterised by the collision rate (or number density) present in the various regions of the expansion for a particular thruster. In regions of the plume where relatively large number densities exist, the collision rate is sufficiently fast such that equilibrium is maintained. This means that the temperatures associated with the various translational and internal modes of the molecules are all equal to the overall temperature. Such flow may be solved using the continuum approach from either the Euler or Navier-Stokes equations depending on viscosity effects and will normally be associated with the nozzle flow of the thruster.

If we travel along a streamline away from the nozzle exit the gas becomes increasingly rarefied until a point is reached at which the collision rate is no longer large enough to maintain thermal equilibrium. The various thermal modes in the gas are observed to separate, and the continuum equations become invalid. The transition regime has been reached. One appropriate mathematical model for this region is the Boltzmann equation. Whilst the Boltzmann equation is of course valid throughout the continuum flow regime, difficulties in its solution means that it should only be applied where alternative equations do not exist. Further procession along the streamline will eventually lead to a point at which no further collisions occur in the gas. This is the free molecular limit. Calculation of flow beyond this point is simplified as flow properties become frozen. The ideas described in this paragraph are displayed in Figure 1.1 which is taken from Ref. 5.

It of vital importance that the three flow regimes just described (continuum-transition-free molecular) be accurately identified. A parameter derived by Bird [11] from numerical investigations is conveniently employed. This continuum breakdown parameter is defined as the ratio of the Lagrangian mean free path to the density scale length and is given by

$$P = \frac{U}{\rho v} \left| \frac{d\rho}{ds} \right| \tag{1.1}$$

where ρ is the density, U is the stream velocity, ν is the local collision rate and s is the distance along a streamline. The parameter was first employed to predict the breakdown of thermal equilibrium in one dimensional flow [11] where the transverse and radial temperatures were seen to depart when the parameter is close to 0.05. The breakdown of rotational equilibrium was also predicted by the same parameter. Subsequently, it has been shown to predict the same phenomena in two dimensions [12] and has been verified experimentally [13].

The same parameter may be used to define the point at which freemolecular flow begins. Usually, the onset of collisionless flow is taken along the locus $P = 2$. Thus, by the use of this single parameter, the three flow regimes are completely characterised.

1.5 Publications

As a direct consequence of the research carried out in this project, the following papers have been accepted for publication:

"Comparison of the Implementation and Performance of the Nanbu and Bird Direct Simulation Monte Carlo Methods", Physics of Fluids.

"On the Use of the Modified Nanbu Direct Simulation Monte Carlo Method", Journal of Computational Physics.

In addition, the following conference papers have been presented:

"Comparison of Monte Carlo Techniques for Nozzle Lip Expansion", Euromech 225, Cranfield, England, July 1987.

"Discrete Particle Simulation of an Expanding Gas", Graphics Techniques for Simulation Conference, London, England, May 1988.

"Modelling of Small Hydrazine Thruster Plumes Using Discrete Particle and

Continuum Methods", AIAA Thermophysics, Plasmadynamics and Lasers Conference, San Antonio, Texas, June 1988.

"Modification of the Simons Model for Calculation of Nonradial Expansion Plumes", 16th International Symposium on Rarefied Gas Dynamics, Pasadena, California, July 1988.

"Statistical Fluctuations in Monte Carlo Calculations", 16th International Symposium on Rarefied Gas Dynamics, Pasadena, California, July 1988.

1.6 Layout

The aim of the project was to undertake the modelling of typical satellite control thruster plumes from which impingement effects could be deduced. For this purpose, the Simons model [14] and the Method of Characteristics [15] have been implemented into computer codes. These techniques are two of the most commonly applied to calculation of rocket plumes and are based on continuum equations. The application of these methods in the transition flow regime of the plume must therefore be viewed with caution. These methods are described, together with their implementation, in Chapter 2. When comparing the Simons model and MOC solutions it was found that large discrepancies existed under certain conditions. The MOC solutions for density along the plume axis were found to agree well with experimental data whilst the Simons model results were in error by as much as a factor of two. By comparison of these two sets of calculations a new model termed the Modified Simons model [16] was developed. This analysis is also contained in Chapter 2.

In order to assess any errors associated with the continuum techniques, a third computer code was developed which adopts a discrete particle approach. The technique implemented is the Direct Simulation Monte Carlo method (DSMC) [17] which readily allows treatment of the thermal nonequilibrium and species separation effects found in rocket plume expansion [18]. In fact, two DSMC computer programmes have been written. The first code has been designed principally for the calculation of expansion plumes, but with small modifications could be applied to a variety of flow problems. A description of the ideas incorporated into the code forms the first part of Chapter 3. A code written for the investigation of chemical reactions using the

DSMC technique is then described. Difficulties encountered in the determination of the amount of internal energy contributing to the breaking of chemical bonds have been overcome with the derivation of a new simulation model [19].

At the development stage of the plume expansion code it was not clear from the literature which of the major DSMC techniques was the most appropriate for application to engineering problems. A series of investigations [20 – 24] was conducted in which several such schemes were assessed in terms of implementation and performance. The results of this study are described in Chapter 4. From this analysis it was then possible to identify the simulation method most suited to the requirements of the intended calculations.

The project has been funded through an SERC/IBM CASE award with contact at the IBM UK Scientific Centre in Winchester, England. Their interest lies in the use of visual techniques to aid interpretation and understanding of a variety of scientific data. Whilst some progress was made for three-dimensional chemical data [25], it was found that such procedures were inapplicable to the flowfields generated for plume expansions. However, the computer graphics facilities at IBM are found to be of great value in the assessment of statistical fluctuations in the DSMC methods [24] and the description of their use is included in Chapter 4.

In Chapter 5, the calculation of the plume flowfield of a small hydrazine thruster is discussed. The physical aspects of such flows are first considered. The validity of employing continuum techniques in the transition flow regime is then assessed by applying the three solution techniques which have been implemented to the isentropic core expansion of the thruster [26]. This was the first time that a detailed DSMC solution has been obtained for the isentropic core of a real thruster. The DSMC technique is also used to obtain solutions in the nozzle lip and backflow expansion regions of the same hydrazine thruster. The sensitivity of the results to the conditions initially assumed in the calculations are assessed. The requirements for the experimental validation of the results obtained is also considered.

The main conclusions drawn from the work performed in the project are described in Chapter 6. Finally, Chapter 7 discusses some possible areas for future study.

2. CONTINUUM SOLUTION TECHNIQUES

2.1 Method of Characteristics

2.1.1 Description

The Method of Characteristics (MOC) is a computational technique for providing an exact solution to the set of nonlinear differential equations describing inviscid flow. It is a method which takes advantage of a unique property of hyperbolic differential equations that enables the solution to be found by a step-by-step procedure [27]. In the following sections the implementation of the method into a numerical algorithm is described. The application of the technique to the solution of plume expansion problems is explained. Finally, details of the computer code are provided together with some example calculations.

The MOC technique considered is that for axisymmetric flow. In the following, the sign convention for the flow angle θ and the Mach angle α are strictly adhered to.

Consider Figure 2.1 in which the flow properties are known at points A and B (the boundary conditions). The line AC is a left running characteristic line whose equation is given by

$$\frac{dr}{dx} = \frac{r_C - r_A}{x_C - x_A} = \tan(\theta_A + \alpha_A) \qquad (2.1)$$

Similarly BC, which is a right running characteristic, is found from

$$\frac{dr}{dx} = \frac{r_C - r_B}{x_C - x_B} = \tan(\theta_B - \alpha_B) \qquad (2.2)$$

Simultaneous solution of Eqns. (2.1) and (2.2) gives the co-ordinates of point C. Details of the procedures for obtaining the relevant flow quantities such as flow and Mach angle, together with flow velocity, at each point, are contained in Reference 28. In addition, special treatment of points near to the centreline, on the centreline, and at the plume boundary are discussed. Quantities such as Mach number, temperature, pressure and density at each point are then determined from the isentropic relationships.

The MOC calculations may also be used to determine the parameter which characterises the flow regime at the current point. The parameter, described in Chapter 1, is given by

$$P = \frac{U}{\rho\nu} \left| \frac{d\rho}{ds} \right|$$

where $\nu \propto \rho T^{0.5-\omega}$ and ω is the viscosity temperature exponent.

The parameter is therefore given by

$$P = \frac{\phi U}{\rho^2 T^{0.5-\omega}} \left| \frac{\rho - \rho'}{\Delta s} \right|$$

where ϕ is a constant, ρ' is the density at a point just upstream of the current point and lying on the same streamline, and Δs is the distance between the two points just described.

The density ρ' is found in the following manner. Consider Figure 2.2 which shows the general point solution described earlier. Once the flow properties at C have been found from those at A and B, the point D is calculated as the intersection between a streamline passing through C, and the line AB. The flow properties at D are then found by interpolation between those at A and B. Thus both ρ' and Δs are determined, from which the parameter P is calculated.

Having described the procedures necessary for the calculation of the flowfield, the application of the Method of Characteristics to the modelling of a plume expansion is now considered.

2.1.2 Calculation of a Plume Expansion

The application of the Method of Characteristics to the expansion of jet plumes has been described in detail by Vick et al [28]. The procedures adopted rely solely on the nozzle exit conditions together with the ambient pressure ratio outside the nozzle. The explanation of the treatment of the work of Vick is best understood with reference to Figure 2.3 which shows the configuration of the MOC solution. The numbered points are of the following types:

(1) nozzle lip, where a two-dimensional Prandtl-Meyer fan is calculated

(2),(3),(4),(5) data on the line defining the boundary inside which the flow is unaffected by the prevailing external conditions, and is referred to as the leading characteristic.

(6) last point on the leading characteristic and the first point on the plume centreline

(7)-(13) general points

(14) jet boundary points

(15) same family points (internal shock)

(16) points adjacent to the centreline

(17) centreline points

Before the main algorithm is entered, the Prandtl-Meyer fan and the leading characteristic must be determined from the existing conditions. The method then proceeds as follows:

1. The general points are calculated thus:
Point (7) is determined from the 1st expansion ray and point (2)

Point (8) is determined from the 2nd expansion ray and point (7)
Point (11) is determined from the 5th expansion ray and point (10)

Special treatment is then required to calculate the jet boundary point.

2. The following is repeated by moving along the leading characteristic one point at a time until the final point (6) is reached.
Point (12) is determined from points (7) and (3).
Point (13) is determined from points (8) and (12).
Point (14) is determined by the jet boundary routine.

3. Special treatment is required when the centreline is reached.

4. Having used the last point on the leading characteristic, the next centreline point is determined. The algorithm now continues until a specified maximum axial co-ordinate is reached.

The presence of a finite external pressure results in a turning of the jet boundary in a downstream direction. This results in a series of weak compression waves forming an internal shock. The outcome of this turning effect leads to the crossing of the characteristic lines, i.e. point (15).

Alternatively, it is possible to calculate the expansion of the jet into a complete vacuum. In this case the boundary Mach number is infinite and the solution procedure is simplified by the absence of compression waves.

2.1.2.1 Prandtl-Meyer Expansion Fan

The calculation of a Prandtl-Meyer fan is valid if it is assumed that the flow is two dimensional at the nozzle lip, and that the expansion is instantaneous. The procedure adopted is to calculate the change in Mach angle α from the exit conditions to those given by the ambient pressure ratio p_∞/p_0. Specifically

$$(\Delta\alpha)_T = \sin^{-1}(Ma_E^{-1}) - \sin^{-1}\left[\left\{\left(\frac{p_\infty}{p_0}\right)^{\frac{1-\gamma}{\gamma}} - 1\right\}\frac{2}{\gamma - 1}\right]^{-0.5} \qquad (2.3)$$

The change in the flow angle may then be calculated using the Prandtl-Meyer angle. The total change in Mach angle is subdivided into an integer number of equal increments. A number of expansion rays at the nozzle lip is thus provided by calculating conditions stepwise through from the exit Mach number to the boundary Mach number.

The ambient pressure ratio for a nominal satellite orbit of 200km is very small, e.g. 10^{-7}. Difficulties were found in the use of such low values in terms of the compression waves resulting from the calculation of the jet boundary points. In such cases, an extremely large number of Prandtl-Meyer expansion rays must be computed. These complications may be overcome by assuming that the jet expands into a hard vacuum which does not require the calculation of such points.

2.1.2.2 Leading Characteristic

The leading characteristic is the Mach line which separates the nozzle flow from the external influence of the ambient pressure. When a uniform Mach number profile is assumed at the nozzle exit plane, simple procedures exist for the calculation of this line.

In the case of a contoured nozzle, the leading characteristic is a straight line with gradient $\tan(\alpha_E)$ where

$$\alpha_E = \sin^{-1}(Ma_E^{-1})$$

and all flow conditions are constant along the line. The spacing of the points is at the discretion of the user, but a concentration of points near the nozzle lip is recommended.

For a conical nozzle, the situation is more complicated. The radial flow properties of such a nozzle result in a curved leading characteristic along which the flow quantities are constantly changing, see Figure 2.4.

The solution technique follows that of Love et al [29] in which the change in Mach number between the nozzle exit and that at the last point on the leading characteristic

is found. The Prandtl-Meyer angle at the centreline, point (6), is given by $\nu_{CL} = \nu_N + 2\theta_N$ where

$$\nu = \sqrt{\frac{\gamma+1}{\gamma-1}}\tan^{-1}\sqrt{\left(\frac{\gamma-1}{\gamma+1}\right)(Ma^2-1)} - \tan^{-1}\sqrt{Ma^2-1} \qquad (2.4)$$

is the Prandtl-Meyer angle and θ_N is the nozzle exit half-angle.

The centreline Mach number is thus determined from Eqn.(2.4) by an iterative procedure. To find the axial co-ordinate along the centreline, the following expressions are then employed

$$R = C\, Ma^{\frac{1}{\gamma-1}}\left(1 + \frac{2}{(\gamma-1)Ma^2}\right)^{\frac{\gamma+1}{4(\gamma-1)}} \qquad (2.5a)$$

$$x = R\cos\theta_N - R_N\cos\theta_N \qquad (2.5b)$$

The constant C is found by substituting the exit conditions into Eqn.(2.5).

The points along the leading characteristic are found by incrementing the Mach number from Ma_E to Ma_{CL} in a stepwise fashion.

For more realistic calculation of the plumes exhausting from small nozzles, it is necessary to introduce a boundary layer velocity profile into the exit plane data [15]. The boundary layer thickness and velocity profile are calculated from the following simple expressions [30] depending on whether turbulent or laminar conditions exist:

$$\delta_T \propto Ma_E^{1.25}Re_E^{-0.14} \;:\; V/V_E = (r/\delta_T)^{\frac{1}{8}}$$

$$\delta_L \propto Re_E^{-0.50} \;:\; V/V_E = (r/\delta_L)^{\frac{1}{2}}$$

where Re_E is the nozzle exit Reynolds number.

In such cases, the Prandtl-Meyer expansion fan is calculated from the Mach number at the nozzle lip rather than that in the isentropic core.

2.1.3 Method of Characteristics Computer Code

The ideas and procedures previously discussed have been incorporated into a programme, MOCJET. The following simple input is required:

(a) nozzle geometry,

(b) gas properties, i.e. γ, T_0, p_0, U_L ,

(c) output options.

One of the major disadvantages of MOC calculations is in the production of useful output. This arises as a consequence of the step-by-step solution procedure which means that it is not possible to identify specific points at which information is required. In the current algorithm, therefore, axial output co-ordinates, contour levels, together with acceptable tolerance levels must be supplied. For each new point, calculations are performed to establish, for example, if the current temperature is acceptably close to a required contour value and that its axial co-ordinate is acceptably close to a specified output station. In this way, the following contours are readily obtained:

(i) temperature, (ii) density, (iii) Pitot pressure, (iv) Mach number,

(v) flow velocity, (v) flow angle, (vi) breakdown parameter P,

(vii) mean free path.

The boundary points of the jet may also be output.

Figure 2.5 shows the effect of ambient pressure on the jet boundary for an exit Mach number of 5. Jet boundaries are shown in Figure 2.6 for contoured and conical nozzles. In Figure 2.7 is shown Mach number contours for a conical nozzle with an exit Mach number of 5. The locus of the leading characteristic is included. These Figures have all been compiled for a jet in which a uniform Mach number distribution in the exit plane is assumed.

2.2 The Simons Model

2.2.1 Introduction

The Simons model is a simple analytic method for determining flow properties in the continuum regime of a rocket or thruster plume. The model assumes that the flowfield is axially symmetric. Several approximations were made by Simons [14] in an effort to reproduce extensive finite difference calculations made by Boynton [31]. A complete description of the theory behind the model, and its implementation into a computer code now follow.

The model provides an expression for the gas density as a function of flowfield position (r,θ). Separation of variables is made such that the density, ρ, is written

$$\rho(r\ ,\ \theta) = g(r)\ f(\theta) \tag{2.6}$$

A farfield assumption is made which states that the gas diverges radially as though from a point source at the nozzle exit. The equation for radial decay is

$$\frac{d\rho}{\rho} + 2\frac{dr}{r} = 0 \tag{2.7}$$

so that g(r) is obtained as

$$g(r)\ \alpha\ \frac{1}{r^2}$$

The angular dependence of the density is calculated by assuming that the plume initially expands through the two dimensional Prandtl-Meyer fan and then continues along straight lines. By making a large Mach number expansion of the Prandtl-Meyer function, and employing the isentropic relationship for density, the following is obtained:

$$f(\theta) = \theta - \theta_\infty$$

which may be approximated by

$$f(\theta) = \left[\cos\left(\frac{\pi\theta}{2\theta_\infty}\right)\right]^{\frac{2}{\gamma-1}} \tag{2.8}$$

where θ_∞ is the limiting angle of the flow. One consequence of the preceding analysis is that the flow velocity is everywhere assumed to be constant and equal to the limiting value.

This particular expression was formulated by Boynton [32] and is for use in the isentropic core of the plume expansion. The full expression for density is usually written in the form

$$\frac{\rho}{\rho^*} = A\left(\frac{r}{r^*}\right)^2 f(\theta) \tag{2.9}$$

where

$$A = \frac{U^*/U_L}{\int_0^{\theta_\infty} f(\theta)\sin\theta\, d\theta} \tag{2.10}$$

is obtained from continuity of the rocket mass flow. A superscript * refers to conditions at the nozzle throat, and U_L is the limiting velocity of the gas. This value may be approximated by the following expression given by Legge & Boettcher [33]:

$$U_L = \left(\frac{2\gamma RT_0}{\gamma - 1}\right)^{\frac{1}{2}} \tag{2.11}$$

where T_0 is the combustion chamber temperature and R is the universal gas constant.

Boynton [31] also made a detailed analysis of the behaviour of the nozzle boundary layer and noted large discrepancies in the angular behaviour of the gas for θ near the limiting value. The decrease in gas density was noted to have an exponential appearance. Simons [14] proposed that the streamline at the edge of the boundary layer is turned through an angle θ_0. For $\theta < \theta_0$ Eqn.(2.8) is valid whilst

$$f(\theta) = f(\theta_0)\exp[-\beta(\theta - \theta_0)] \tag{2.12}$$

is employed in the region defined by $\theta_0 < \theta < \theta_\infty$, i.e. in the boundary layer.

Simons then related the values of the constants β and θ_0 to δ, the thickness of the boundary layer, in the following manner.

The boundary layer mass flow is related to that in the plume which diverges at angles greater than θ_∞ by

$$2\pi r_E U_E \rho_E \delta = \int_{\theta_0}^{\theta_\infty} 2\pi \rho U r^2 \sin\theta \, d\theta \tag{2.13}$$

where subscript E denotes both exit and edge conditions. In obtaining Eqn.(2.13) it was also assumed that the displacement thickness is small compared with δ.

By use of the approximation that $\sin\theta \sim 2\theta_\infty/\pi \sin(\pi\theta/2\theta_\infty)$, substituting into the integral in (2.13) and using Eqn.(2.9) to evaluate the density as if it were inviscid throughout the boundary layer it follows that

$$f(\theta_0) = \cos^{\frac{2}{\gamma-1}}\left(\frac{\pi\theta_0}{2\theta_\infty}\right) = \left(\frac{2\delta}{r_E}\right)^{\frac{(\gamma-1)}{(\gamma+1)}} \tag{2.14}$$

By expanding Eqn.(2.14) for values of θ_0 near θ_∞ the following expression is obtained:

$$\frac{\theta_0}{\theta_\infty} \sim 1 - \frac{2}{\pi}\left(\frac{2\delta}{r_E}\right)^{\frac{(\gamma-1)}{(\gamma+1)}} \tag{2.15}$$

The exponential constant β in Eqn.(2.12) is now related to δ by assuming that the boundary layer mass flow expands inviscidly with the initial conditions specified by the viscous profile, i.e. by employing (2.12) instead of (2.8) and evaluating Eqn.(2.13) leads to

$$\beta = A\left(\frac{\gamma+1}{\gamma-1}\right)^{\frac{1}{2}} \frac{2\bar{U}_L}{U_L}\left(\frac{2\delta}{r_E}\right)^{\frac{(\gamma-1)}{(\gamma+1)}} \tag{2.16}$$

where it has been assumed that $\beta >> 1$, $\sin\theta_0 \sim O(1)$ and $\overline{U}_L$ is the average limiting velocity of the gas in the boundary layer and is given by $\overline{U}_L \sim \alpha U_L$ where $0.5 < \alpha < 1$ for the supersonic part of the flow.

Despite the large number of assumptions employed in this analysis, good agreement was found between the calculations of Simons and Boynton, and the method has achieved some popularity. For example, Legge & Boettcher [33] have applied the Simons model to small hydrazine thrusters. In their paper, the following expressions for boundary layer thickness and Reynolds number at the nozzle exit are adopted:

$$\frac{\delta_E}{l_E} = \frac{6.25}{\sqrt{Re_E}} \tag{2.17}$$

$$Re_E = \frac{\rho_E U_E l_E}{\mu(T_0)} \tag{2.18}$$

where l_E is the length of the nozzle from throat to exit and μ is the viscosity.

From the calculation of the flowfield density at a point, the one dimensional isentropic relationships are then employed to evaluate other properties. Specifically, the quantities of most interest are Mach number, temperature, and pressure. Therefore, the isentropic relationships required are

$$\frac{\rho_0}{\rho} = \left(1 + \frac{\gamma - 1}{2} Ma^2\right)^{\frac{1}{\gamma - 1}} \tag{2.19a}$$

$$\frac{T_0}{T} = \left(1 + \frac{\gamma - 1}{2} Ma^2\right) \tag{2.19b}$$

$$\frac{p_0}{p} = \left(1 + \frac{\gamma - 1}{2} Ma^2\right)^{\frac{\gamma}{\gamma - 1}} \tag{2.19c}$$

In the nonisentropic boundary layer the concept of effective stagnation conditions is introduced [33].

The expansion of the boundary layer is assumed to be isentropic outside of the nozzle. Consider the plume stream tube defined by the angle θ in the boundary layer. The effective stagnation conditions along this tube are determined from the static flow properties in the nozzle exit boundary layer at the radial distance r corresponding to θ in the plume. The following expressions are then used to calculate the effective conditions

$$\frac{U_L(\theta)}{U_{L,CL}} = \exp[-c_u(\theta - \theta_0)] \tag{2.20a}$$

$$\frac{T_{0,eff}(\theta)}{T_0} = \left(\frac{U_L(\theta)}{U_{L,CL}}\right)^2 = \exp[-2c_u(\theta - \theta_0)] \tag{2.20b}$$

$$\frac{p_{0,eff}(\theta)}{p_0} = \exp[-c_p(\theta - \theta_0)] \tag{2.20c}$$

$$\frac{\rho_{0,eff}(\theta)}{\rho_0} = \exp[-(c_p - 2c_u)(\theta - \theta_0)] \tag{2.20d}$$

A suffix CL refers to centreline conditions. The constants c_u and c_p are then calculated from

$$U_L = \frac{U_L}{\theta_\infty - \theta_0}\int_{\theta_0}^{\theta_\infty} \exp[-c_u(\theta - \theta_0)]\, d\theta \tag{2.21a}$$

$$\frac{p_{0,eff}(\theta_\infty)}{p_0} = \frac{p(Ma = \infty)}{p_0}\,\frac{p_0}{p(Ma = 1)} \tag{2.21b}$$

together with Eqn.(2.20c). The value of α is taken as 0.75 in the calculation of U_L. These exponential decay laws are based on experimental and theoretical results [34].

2.2.2 Implementation

The ideas and theory described in the previous Section have been implemented in a computer code, PLUME. The programme requires the following input data:

(i) details of nozzle geometry,

(ii) combustion chamber conditions,

(iii) viscosity, mass and γ for the expanding gas,

(iv) output options.

From such simple data, calculations for density, Mach number, temperature, etc. are readily made. Other properties of interest which are calculated include

(a) Pitot pressure

$$P_{t2} = \frac{\gamma + 3}{\gamma + 1} \frac{1}{2} \rho U^2 \tag{2.22}$$

(b) mean free path

$$\frac{\lambda}{\lambda_0} = \frac{\rho_0}{\rho} \left(\frac{T}{T_0} \right)^{\omega - \frac{1}{2}} \tag{2.23}$$

where ω defines the viscosity temperature exponent,

(c) Bird's breakdown parameter

$$P = \frac{U}{\rho \nu} \left| \frac{d\rho}{ds} \right| \tag{2.24}$$

This expression reduces to

$$P = \frac{2U}{r\nu} \tag{2.25}$$

in the far plume flow field. The contour $P = 0.04$ is found through Eqn.(2.24) whilst that for $P = 2$ is calculated using Eqn.(2.25).

The calculation of a reference mean free path and of the collision rate requires additional molecular input data.

The programme has three modes of operation:

0 : in which contours of flow quantities are calculated

1 : in which flow quantities at specified points are calculated

2 : in which a grid for use in the Direct Simulation Monte Carlo method is calculated.

Temperature contours calculated by PLUME are presented in Figure 2.8 for the expansion of hot nitrogen through a SESSIA nozzle [34]. This nozzle has been used to simulate the larger 22N bipropellant hydrazine thrusters used for radial attitude control onboard the Hughes Intelsat VI spacecraft [35]. The input data required by the programme is shown in Table 2.1. Figure 2.9 shows the calculated axial Mach number distribution compared to experimental data taken from Ref. 34. It may be seen that although the gradients of the two curves are similar, there is a clear quantitative disparity.

Such differences in Mach number result in a factor of 2 when translated into density calculations. The inaccuracy in the calculation may be due to the high exit Mach number of the nozzle [36] which has also posed problems for other continuum methods. Figure 2.10 shows logarithmic plots for density against radius for the experimental data. It is clearly seen that the inverse square behaviour assumed in the Simons model does not become valid until distances of about 20 exit radii are reached. Improvement in the modelling of such plumes has been obtained through modifications to the Simons model which are described in the following Section.

In its attempt to model complex flow phenomena through a simple analytic expression, the Simons model is remarkably successful. Due to the very small computational requirements associated with this prediction method, it is particularly useful

for the determination of basic flow quantities such as γ through the use of parametric studies [5]. The following areas of possible improvement in the model have been outlined by Boettcher [37]:

(i) improved boundary layer modelling through experimental measurement

(ii) treatment of internal shocks for contoured nozzles

(iii) extension to unsteady flow.

The application of the model to a small hydrazine thruster will be discussed in relation to the other flow prediction techniques in Chapter 5.

TABLE 2.1

Stagnation Pressure	3×10^5 Pa
Stagnation Temperature	1100 K
Specific Heat Ratio	1.4
Molecular Weight	28.01 g/mole
Molecular Viscosity	4.47×10^{-6} (N s / m)
Nozzle Throat Radius	0.7 mm
Nozzle Exit Radius	6.5 mm
Nozzle Exit Half Angle	8.5°

2.3 Modified Simons Model

2.3.1 Introduction

The Simons model has been shown to be a useful and inexpensive engineering tool for the calculation of spacecraft impingement effects in the continuum regime although clearly many features of the expansion are not treated. At large distances from the nozzle exit, the flow may be regarded as collisionless. In the region lying between the continuum and freemolecular limits, the gas is no longer in thermal equilibrium and the continuum equations become invalid. Within the transition flow regime impingement calculations may be performed through the use of relationships bridging

the continuum and free molecular flow results. Procedures for the determination of the onset of both the transition and collisionless flow regimes from the Simons model were included in the previous Section.

The Simons model has been adopted by a number of workers. Calia & Brook [38] found good agreement for density measurements made at large angles from the plume centreline. Lengrand [39] has investigated the exhaust plumes for a number of small CNRS thruster nozzles. In this study, excellent agreement is found between theoretical prediction and experimental data for nozzle exit Mach numbers up to $Ma_E \simeq 5$. These comparisons were made with reference to axial density ratio.

The Simons model has also received much attention at DFVLR, Gottingen, F.R.G., where interest has centred on small hydrazine thrusters. In Ref. 40, measurements of Pitot pressure are compared with Simons model predictions and are found to be in error by a factor of 2. In the hypersonic flowfields of such thrusters the Pitot pressure is approximated by

$$P_{t2} = \frac{\gamma + 3}{\gamma + 1} \frac{1}{2} \rho U_L^2 \qquad (2.26)$$

where U_L is the limiting velocity of the expansion. It is clear that any errors found in the calculation of Pitot pressure must arise from the failure of the Simons model formulation to properly describe the density decay.

Errors of a similar magnitude have been found by Lengrand [36] for axial density predictions of the two SESSIA thrusters discussed in Ref. 35. These nozzles, together with those considered at DFVLR, have exit radii of a few millimetres and thus tend to have large laminar boundary layers, e.g. up to 40% of the nozzle exit plane. Lengrand [36] suggested that the poor results were either due to the presence of a finite back pressure acting on very slender expansion plumes, or alternatively due to the failure of the Simons model to adequately deal with the flows produced by these thrusters.

The workers at DFVLR have partially improved the Simons model by the replacement of r by $r-x_0$[41]. The result of such a procedure is to move the effective source of the nozzle a distance x_0 along the plume axis. The experimental derivation of values of x_0 for a number of thrusters and gases is reported in Ref. 41. Rather than

resorting to such expensive undertakings, it is clearly more desirable to obtain an improvement in the model from the particular nozzle and gas under investigation.

An alternative technique for the calculation of plume flowfields is the Method of Characteristics (MOC). The application of MOC to the modelling of expansion plumes has already been described earlier in this Chapter. This method has been used to obtain solutions for the plumes exhausting into vacuum from a number of nozzles including those in which the Simons model gave erroneous results. The expansion of the laminar boundary layer was treated by assuming a typical laminar velocity profile for a flat plate [30]. Whilst such a procedure is rather dubious, variation of this boundary layer velocity profile was found to have no effect on the MOC calculations along the plume axis upon which most of the following analysis is based.

In Figure 2.11 the solutions obtained with both the Simons model and MOC for the density ratio along the plume axis are shown together with experimental data for the SESSIA radial thruster described in Ref. 35. For these studies, the working gas is nitrogen. It is clear that the MOC calculations offer a greatly improved correspondence to the experimental results than do the Simons model predictions. The latter results are consistently found to be in error by a factor of about 2 along the axis. Similar features were observed for the SESSIA axial thruster of Ref. 35. On the basis of these calculations, it was concluded that as the MOC calculations were found to be in good agreement with the experimental data it must be the Simons model formulation itself which is responsible for the poor results obtained with this method.

Contours of constant flow angle were also derived from the MOC calculations and are shown in Figure 2.12. This diagram suggests that the first assumption in the Simons model formulation is valid beyond a few exit radii of the nozzle exit. On extrapolation, these contours are found to converge to points very close to the origin. There is therefore no real evidence to justify the translation of the effective source of the nozzle along the plume axis. It was also apparent from the MOC calculations that the second assumption that the velocity is everywhere constant is valid. It is therefore concluded that the assumption of radial density decay is being violated and is thus responsible for the poor performance of the analytical model.

A comparison of Simons model and MOC solutions of the flow density along the axis of various nozzles has therefore been undertaken. The intention of such a comparison is to indicate the types of nozzle for which the original Simons model is unsuitable, and also to allow the derivation of a modified expression for the density which accounts for the nonradial nature of such plumes.

2.3.2 Analysis

The nonradial nature of a number of flows has been characterised in terms of the exit Mach number Ma_E and the nozzle exit half-angle θ_E . In the present study, the range of exit Mach number investigated is $4.5 < Ma_E < 7$, whilst that for exit angle is $5° < \theta_E < 20°$. The exit Mach number is that calculated from the area ratio reduced by the presence of the boundary layer thickness.

In each configuration for which calculation is made, both Simons model and MOC solutions for the axial density ratio are generated. On the basis of the previous calculations, the MOC results were assumed to provide an accurate solution. The ratio of the MOC and Simons model solutions gives

$$X(r) = \frac{r^2}{g'(r)} \tag{2.27}$$

where g'(r) is the function which will replace the radial decay law normally employed. The function X(r) is plotted in Figure 2.13 for the conditions $Ma_E = 5$ and $\theta_E = 10°$. The nature of this function suggested that an appropriate form for the new model is $g'(r) = r^2 - ar + b$. Therefore, Eqn.(2.9) should be replaced by

$$\rho(r, \theta) = \frac{A}{r^2 - ar + b} f(\theta) \tag{2.28}$$

where the constants a and b are to be derived from the nozzle geometry. It has been assumed that these constants are functions of exit Mach number and nozzle exit half-angle only.

By differentiation of Eqn.(2.27) it is found that the maximum turning point of X(r) occurs at $r/re = 2b/a$. The constants a and b are then determined from this expression

together with Eqn(2.27). The parameters have been determined in this fashion for all the nozzles investigated. By independent variation of first Ma_E and then θ_E, a correspondence between these constants and the nozzle exit conditions has been obtained.

The large number of calculations made in this study are found to be adequately described by the following simple expressions:

$$a = 3\theta_E^{0.5} Ma_E \tag{2.29}$$

$$b = 5\theta_E Ma_E^2 \tag{2.30}$$

where the nozzle exit half angle is expressed in radians. Logarithmic plots of the best-fit constants a, b against nozzle exit half-angle for a number of exit Mach numbers are shown in Figures 2.14 and 2.15. The straight lines represent Eqns.(2.29) and (2.30) for the prescribed exit conditions. The substitution of these Equations into Eqn.(2.28) gives rise to a new flowfield prediction model here termed the Modified Simons model. It is stressed that the single modification made to the procedures described in Ref. 33 is the alteration of the radial density decay behaviour. The performance of this model is now discussed with reference to experimental data for a number of real nozzles.

2.3.3 Discussion

The Modified Simons model has been used to calculate a number of thruster flowfields in order to assess the validity of the assumptions made in deriving the expressions given in Eqns.(2.29,2.30). Figure 2.16 shows calculations for the SESSIA axial thruster of Ref. 35 together with experimental data. It may be seen that the Modified model offers considerable improvements on the original calculations. Such improvements were also found for the SESSIA radial thruster as shown in Figure 2.17. In Figure 2.18 calculations for the exit conditions $Ma_E = 4.63$ and $\theta_E = 10°$ are shown together with experimental data taken from Ref. 39. Lengrand has previously made successful calculations for this nozzle using the original Simons model. Although it is clear that the introduction of the modifications has not greatly altered the theoretical predictions, it is apparent that the original model offers the better

agreement. Procedures for the determination of the preferred model will be described later.

The calculations shown in Figs.2.16-18 show the usefulness of the Modified Simons model, and justify the derivation of the parameters a and b. Although these expressions have been derived from calculations made for nitrogen gas, the new model has also been applied to the MBB/ERNO 0.5N hydrazine thruster which has previously been investigated at DFVLR [40]. In Ref. 40, the value of γ for hydrazine is derived as 1.37 from the matching of transverse Pitot pressure profiles obtained experimentally and with the original Simons model. In Figure 2.19 such a transverse distribution is presented at an axial distance of 24 exit radii. The compression shock due to the presence of a finite background pressure is clearly distinguishable in the experimental data, and cannot be reproduced by the simple analytical models. Calculations using the Modified Simons model are shown for $\gamma = 1.37$ and 1.4. It is clear that for the formulae derived in this study, the analytical predictions near the axis are better described with $\gamma = 1.4$. The calculations made with the new model again show considerable improvement when compared with the original results. Figure 2.20 plots similar calculations made at the axial point 48 exit radii from the nozzle.

The previous calculations have highlighted two important points which depend upon the prevailing exit conditions: (i) that under certain conditions the plume expansion is readily approximated by the assumption of radial density decay and the Simons model is valid, (ii) that under other conditions the plume expansion is found to exhibit a significant degree of nonradial behaviour in which case the Modified Simons model may be employed to obtain more satisfactory density prediction.

In order to determine the conditions under which the Modified Simons model is preferred a further number of nozzle exit conditions has been investigated. The density ratios along the plume axis of these nozzles have been calculated using both of the Simons model formulations. The initial conditions investigated were those for the CNRS nozzle no.1, the solutions for which are shown in Fig. 2.18. Under these conditions, the two solutions agree to within 4%. The exit nozzle angle and Mach number were then varied until the solutions were found to differ by 10%. This is the criterion upon which the recommendation for usage of the Modified Simons model is based. Once again, variation of exit Mach number and of nozzle exit half-

angle was undertaken independently of one another. From this analysis the critical values for the nonradial parameters were found to be given as $a = 8.7$, $b = 32.2$.

In Figure 2.21 the conditions under which the nonradial nature of the expansion plume becomes important is shown graphically. The solid line represents the critical conditions described in the previous discussion. The locations of the four real thrusters investigated in this study are also shown on the Figure. Given a set of nozzle exit conditions, it is possible to identify the most appropriate analytical flow model from Fig. 2.21.

It is interesting to note the form demonstrated by Eqns.(2.28-30) in terms of the physical parameters which characterise the flowfield. It is clear from the Modified formulation that as the nozzle exit Mach number is reduced the flow approaches the radial approximation. This would appear to be physically sound in that since Mach number is the ratio of directed velocity to random thermal velocity, then when the random motion becomes predominant it is to be expected that the flow would approach the effusive, radial condition. Similarly the dependence on nozzle exit half-angle is reasonable: since effusive flow ideally takes place through a thin orifice, the expansion effectively originates from a parallel sided aperture. As the aperture takes an increasing angle of divergence, the bulk flow velocity will gain a significant non-axial component thus reducing the radial nature of the expansion.

In the study described in the above, the experimental and theoretical data considered was that for nozzles with very small dimensions. We must therefore ask ourselves if the observed phenomena is also true for larger rocket engines. As the MOC calculations are all made in dimensionless quantities, it is immediately apparent that these results are independent of the nozzle exit radius. In the case of the Simons model calculations, on close inspection of the derived quantities it is found that the plume constant, together with the newly derived nonradial constants, are dependent only on the nozzle exit area ratio and nozzle exit half-angle. It is therefore concluded that the nonradial effects found in the small nozzles will arise for all nozzles whose exit conditions lie in the Modified Simons model section of Fig. 2.21. This finding may have some implications for DSMC calculations of rocket plumes which employ a radially decaying density point source [42].

The nonradial nature of plumes exhausting from nozzles with large exit Mach number ($Ma_E > 5$) and/or large exit half-angle has been established. The failure of the Simons model to satisfactorily calculate the flow properties of such expansions is therefore explained. By analysing Method of Characteristics solutions of these plumes a new analytical formulation termed the Modified Simons model has been derived. It has been shown that the modifications result in significant improvement in the prediction of density in such nonradial expansion plumes. The critical conditions under which the new model is preferred are presented in graphical format.

Due to the relatively large computational expense of the Method of Characteristics, together with difficulties in effective output of flow properties, the use of the Modified Simons model is recommended for the modelling of the types of nozzle discussed in the present study. The analytical nature of the model allows easy calculation of impingement effects on the complex configurations of modern satellites, so that the improvements introduced in this work increase the usefulness of the Simons model in spacecraft design.

Finally, it is to be noted that the Modified Simons model as developed above should only be expected to provide useful results for gases in which γ is near to 1.4

3. THE DIRECT SIMULATION MONTE CARLO METHOD

3.1 Introduction

For a particular flow problem, it is essential that the different flow regimes present are clearly identified. In this manner, it is possible to identify the fluid equations which are valid and consequently to decide on the most appropriate solution technique to be employed.

The flow regimes are most conveniently characterised by the dimensionless parameter Kn termed the Knudsen number. Its usual definition is:

$$Kn = \frac{\lambda}{l} \quad \alpha \quad \frac{1}{nl} \tag{3.1}$$

where λ is the mean free path of the molecules, n is the number density and l is a length characteristic of the flow.

Figure 3.1 shows a schematic diagram of the validity of various continuum and discrete particle flow equations as a function of Knudsen number. For very small Kn, the flow is in local thermodynamic equilibrium so that the velocity distribution is always the local Maxwellian. These are the basic assumptions prevalent in the Euler equations for inviscid flow. As the Knudsen number is increased, the velocity distribution begins to depart from equilibrium. However, for Kn $<<$ 1 this departure is sufficiently small to allow the derivation of the Navier-Stokes equations from the Chapman-Enskog theory for transport coefficients. As the Knudsen number is further increased to the order of unity and above, the departures from local equilibrium be-

come so large that the continuum equations become invalid. The use of discrete particle methods is now required. The advantage of such methods is that they are valid throughout the full range of Knudsen number. Consideration of Eqn.(3.1) reveals that Kn may be increased by decreasing either the characteristic length or the number density of the flow. Thus, for a particular flow problem, i.e. fixed l, the discrete particle methods may be used throughout the flowfield and do not depend on the number density being of a certain magnitude. A number of such methods are reviewed in Ref. 110.

The two most important discrete particle solution techniques are the Molecular Dynamics method of Alder & Wainwright [43], and the Direct Simulation Monte Carlo method developed by Bird over several years [44 – 46]. In both of these methods, the large number of molecules in a real gas are simulated by a much smaller statistical population of representative particles.

In the Molecular Dynamics method, the simulated molecules have their velocities initially sampled from an equilibrium distribution. Their trajectories are then followed through the region of physical space to be simulated. A collision between two of the simulated molecules is calculated when their distance of separation becomes smaller than the molecular interaction potential field. The computational expense of the method is proportional to the square of the total number of simulated molecules employed. This aspect of the method has seriously limited its application. Nevertheless, the method has achieved some popularity particularly in the high density field of physical chemistry. Recently, the method has been applied to high vorticity rarefied flows by Meiburg [47].

The second discrete particle method is much more computationally efficient and is the method used in the present work. The ideas and concepts behind this method are now described in the following sections.

3.2 Description of the DSMC Technique

3.2.1 General Concepts

As with the Molecular Dynamics method, a large number of molecules are simultaneously followed in the Direct Simulation Monte Carlo method. However, colli-

sions are now based on a probabilistic basis rather than a deterministic one. Again only binary collision are usually considered. These aspects of the method restrict its application to dilute gases in which the mean free path is greater than the molecular diameter. The initial state of the gas is again sampled from equilibrium distributions. The region of physical space to be modelled must be divided into a number of cells to allow the simulation of local collision frequencies, and for calculation of macroscopic quantities. In addition, the cell dimensions should be chosen small enough to avoid smearing of flow properties. Although all calculations are essentially unsteady, a steady time-averaged result is obtained by sampling over a large number of unsteady state results.

Each simulated molecule stores three velocity components and one,two or three space co-ordinates depending on the symmetric nature of the flow. Internal energy may also be included. In addition, each molecule must have an indicator of molecular species and an index which defines its location in the cell network.

The basic assumption of the method is that molecular motion may be decoupled from molecular collisions over a small time step Δt_m. The value of Δt_m should be chosen to be less than the mean time between collisions. All molecules are thus moved a distance v Δt_m and have their positions fixed at the new location. A number of collisions consistent with Δt_m and the local flow conditions are then calculated in each cell of the flowfield. Once all collisions have been completed the locations of the molecules are again altered and more collisions performed. This process is repeated until equilibrium is established in all parts of the flow. Final macroscopic results are then obtained by averaging these converged quantities over a suitable number of loops. The statistical error associated with a population of N data points is approximately given by the square root of the reciprocal, i.e. $N^{-1/2}$. The number of steps over which averaging is performed is therefore specified by the average number of data points provided by each loop, usually about 15, and the required accuracy of the final results. It should be noted that the very nature of the DSMC method implies that statistical fluctuations will always exist. There is thus a limit to the accuracy that can ever be attained with such a method.

The mathematical model which must be simulated in each computational cell is either the Boltzmann equation, or the Kac equation.. Several different solution schemes based on these equations have been devised, and the more important of these are in-

vestigated in terms of implementation and performance in Chapter 4. In the following Sections of this Chapter, details are given of the mechanics of the DSMC algorithm which apply regardless of the particular simulation model employed.

3.2.2 Initial Simulation State

The position at which simulated molecules enter the flowfield is assumed to lie in the near-continuum regime. The thermal properties of these molecules may therefore be sampled from equilibrium distribution functions. The number of molecules entering the flowfield across a unit surface element is given by

$$N_i = \frac{n}{\beta}\left[\exp(-S_n^2\cos^2\theta) + \pi^{1/2}S_n\cos\theta\{1+\mathrm{erf}(S_n\cos\theta)\}\right]/2\pi^{1/2} \qquad (3.2)$$

where S_n is the molecular speed ratio, θ is the angle between the flow vector and the surface element, and β^{-1} is the average thermal speed.

Molecular velocities are sampled from a Maxwellian distribution

$$f(u') = \frac{\beta}{\sqrt{\pi}}\ \exp\ (-\beta^2 u'^2) \qquad (3.3)$$

by the acceptance/rejectance method described in Appendix D, Reference 17. In this method, the distribution function is first divided by its maximum value. Thus Eqn.(3.3) becomes

$$f'(u') = f/f_{max} = \ \exp\ (-\beta^2 u'^2) \qquad (3.4)$$

A value of u' is randomly generated on the assumption that it is uniformly distributed between its limits. In the case of Eqn.(3.4), it is reasonable to assume that $-3 < \beta u' < 3$ which thereby accounts for more than 0.9999 of the distribution. Having generated u' , if $f'(u')$ is greater than the next random number then the value of u' is accepted. Alternatively, if u' is rejected then a new value of u' is generated and the process repeated until acceptance occurs.

When the entering molecules have a stream velocity, the sampling of the velocity component normal to the surface element must be obtained from

$$f(c'_n) = \frac{1}{\beta\pi^{1/2}} (\beta c'_n + S_n) \exp(-\beta^2 c'^2_n) \tag{3.5}$$

The initial internal state of the molecule is again determined from the appropriate equilibrium distribution function, i.e.

$$f\left(\frac{E_i}{kT}\right) = \frac{1}{\Gamma(\zeta)} \left(\frac{E_i}{kT}\right)^{\zeta-1} \exp\left(-\frac{E_i}{kT}\right) \tag{3.6}$$

where ζ is the number of internal degrees of freedom of the molecule.

3.2.3 Molecular Indexing

The physical region to be simulated is divided into a network of reference points. A molecule is said to be in a particular cell when it is nearest the point which defines that cell. The cell dimensions should ensure that the change in flow properties across each cell is small.

The value of time in the simulation is increased in discrete units Δt_m. The choice of the cell dimensions and the value of Δt_m is determined by the available CPU time, the available computer storage, the physical dimensions of the region to be simulated and the density of the real gas: clearly we wish to keep the ratio of simulated molecules to actual molecules as high as possible. Although each application must be treated uniquely, a general guideline is to have at least 10 simulated molecules in each cell, a cell size of 0.1λ, and a value for Δt_m of 0.1 mean collision times.

The construction of a suitable grid is an important part of the successful modelling of any flow. Quadrilateral cells are usually employed in which the centroid of the cell is used as a reference point for indexing the location of collision partners and as a data output point. Bird [48] describes a procedure for the calculation of a grid from the input of data points along the upper and lower boundaries of the simulation region. However, for complex flows it is often easier to calculate the complete set of grid points seperately from the DSMC computation. The process of defining an ef-

fective and efficient grid knowing only the initial flow conditions is a difficult one and has been described as being more of an art than a science. A possible solution would be the idea of a grid which adapts itself as the simulation proceeds [49]. However, for a flow which experiences a large degree of rarefaction, the best grid will only be found after a certain amount of numerical experimentation. One concept which aids this aspect of the DSMC method is the application of weighting factors.

3.2.4 Weighting Factors

As stated previously, the large number of molecules in a real gas is represented by a much smaller number in the simulation procedure. The weighting factor may be regarded as the number of real molecules which each simulated molecule represents. There is no requirement which says that the weighting factors must be constant throughout the flowfield. Major advances in computational efficiency are obtained by variation in the weights which are used to compensate for large variations in density or in cell volume. Indeed, for the examination of the backflow region of a thruster plume in which the density is seen to decrease by several orders of magnitude, the use of weights is absolutely necessary.

The weights may be adjusted in each cell so that the number of simulated molecules remains constant in each cell. For a fixed cell volume, when the flow density decreases then the weighting factor must be increased. Similarly, for a constant flow density, if the cell volumes decrease then the weight is again increased.

By making estimates of the densities in the cells prior to simulation, suitable weighting factors may be calculated for all the flow cells.

A number of schemes exist for the implementation of varying weighting factors in the DSMC technique, and include the following:

(a) removal/duplication of simulated molecules

(b) time-step variation

(c) collisional bifurcation.

Each of these methods is now described and reviewed for application to the simulation of expansion plumes.

3.2.4.1 Removal/Duplication Method

In this method, flux quantities are conserved across cell boundaries in a statistical manner. When a molecule moves from a cell of weight W_1 to one with weight W_2 the probability that the molecule should be removed from the simulation is given by:

$$\text{Prem} = 1 - W_1/W_2 \tag{3.7}$$

If $W_2 < W_1$ then a number of duplicate molecules are created given by

$$\text{Ndup} = \text{INT}(W_1/W_2 - 1) \tag{3.8a}$$

and the probability of the creation of a further duplicate is given by

$$\text{Pdup} = W_1/W_2 - \text{Ndup} - 1 \tag{3.8b}$$

It is desirable to restrain Ndup to zero so that only one duplicate molecule is ever created over each time-step. However, this is not always possible. This method is particularly inappropriate for use in low density flows as the duplicate(s) and original molecules only become statistically decoupled through collision with other molecules. In addition, it is clear that if a number of duplicates are processed, then selection of any two of these will lead to a zero collision probability. In this way, a significant amount of computational time may be wasted in the random selection and inevitable rejection of such molecules. The duplicating aspect of this method is known [50] to give rise to additional statistical fluctuations, and the use of such a procedure should therefore be viewed with caution. The weighting factors should be so arranged such that the need for duplication is a rare event.

3.2.4.2 Time-Step Variation Method

This technique is a rigorous method for handling variation of weighting factors which is only applicable to steady flows. It constitutes an improvement over the previous

scheme in that neither removal nor duplication of molecules is necessary. This is achieved by scaling the computational time-step in each cell to the weight of the cell. In this manner, fluxes are conserved exactly across each cell boundary ($W_1 = W_2$). Evidently, when a molecule passes from a cell employing time-step Δt_1 to one using Δt_2 , this change must be accounted for in terms of translational motion. Problems again arise for application to flows experiencing rapid density decay. In such cases it is necessary to reduce the time-step to such a degree that considerable computational overheads occur as a result of the impeded progress of molecules in these regions. Thus, the results in this part of the flowfield achieve much slower convergence times than those obtained in the less rarefied areas. The latter must be computed unnecessarily after convergence has been reached. This represents a major disadvantage in the simulation of expansion plumes.

3.2.4.3 Collisional Bifurcation Method

This is a new technique proposed by Jan & Guernsey [51] which claims to a overcome the difficulties found with the schemes previously discussed. In this method, each simulated molecule is assigned a molecular weighting factor Wmol. When a molecule enters a new cell its molecular weight is compared to the weight of the cell, Wcell. If Wmol < Wcell the molecule is retained or destroyed using Eqn.(3.7). If the molecule is retained, its molecular weight is changed to that of the current cell. New molecules are created when a "pregnant" molecule, i.e. one in which Wmol > Wcell, is selected for collision. When this occurs the newly created molecule is immediately collided so that it is decoupled from its "mother". A new molecule is therefore only created when sufficient collisions exist. The additional procedures required in the implementation of this scheme are described in Ref. 51. These constitute a significant computational overhead in the collision algorithm. However, the proponents of the method anticipate that for simulations of expansion plumes the collisional bifurcation method will lead to reductions of overall computational requirements of up to a factor of 2. This claim has yet to be validated.

Without direct experience of the scheme, it is difficult to predict its performance. It is intuitively clear that the procedures provide antidotes to the deficiencies of the other schemes. The question remains as to whether the formulation of these new procedures gives rise to fresh problems. One source of error lies in the matching of

fluxes across cell boundaries. This will only be achieved in the Bifurcation scheme if a sufficient number of collisions are calculated to allow an appropriate number of new molecules to be "born". Thus, in the rapid expansion of gas around a nozzle lip, where the density decays rapidly, it may be necessary to increase the time-step to such an extent that proper resolution of flow gradients becomes difficult. It is evident that errors of some magnitude will result if the number fluxes across the cell boundaries are not properly matched. The fact remains that the simulation of expansion plumes still represents one of the greatest challenges to the DSMC technique. Perhaps the most effective way to calculate such flows is to divide the flowfield into several regions which are to be calculated separately with the input of distribution functions from one region to another.

The weighting factors can be varied dynamically throughout the simulation [42] so that the maximum number of simulated molecules may be maintained at some fixed level throughout the flowfield. The ability to vary the weights lays less stress on the initial estimates used to calculate the weighting factors. To a certain extent, the variation of weighting factors overcomes the need for self adaptive grids, provided the initial grid is reasonably appropriate in the first instance.

In the case of a gas mixture, weighting factors may also be applied to different molecular species. When a molecule with molecular weight M_1 collides with a molecule with molecular weight M_2 then the molecule with the lower weight always undergoes change due to the collision. The other molecule has a probability of change given by the ratio of the weights. In this manner, successful simulation of gas mixtures with large differences in partial pressures between its constituents is possible.

The use of varying weighting factors is now widespread and few adverse affects seem to have arisen from their use. The one notable exception, is that Nanbu [52] reports discrepancies in the calculation of heat fluxes in the flow between parallel plates. In the same paper it is confirmed that the density and temperature of the flow are quite unaffected by the use of weights.

3.2.5 Axisymmetric Flow

In two dimensional flow, each cell is assumed to be of unit width so that the cell volume may be calculated from the quadrilateral area. In axisymmetric flow (z,r) the problem is more complicated. In this case, the volume of each cell must be found by rotating the cell through a unit angle. The volumes of cells located at large distances from the axis are therefore much larger than those adjacent to the centreline. These problems are overcome by the use of large weighting factors for cells lying close to the axis of the flow.

If a molecule lies at position (z_0, r_0) having a velocity vector (u_0, v_0, w_0) is moved through a distance Δt_m (u_0, v_0, w_0) in the axisymmetric co-ordinate system, then the new space and velocity vectors are given by the following:

$$z_1 = u_0 \Delta t_m$$

$$r_1 = [(r_0 + v_0 \Delta t_m)^2 + (w_0 \Delta t_m)^2]^{0.5}$$

$$u_1 = u_0$$

$$v_1 = \frac{[v_0(r_0 + v_0 \Delta t_m) + w_0 w_0 \Delta t_m]}{r_1}$$

$$w_1 = \frac{[w_0(r_0 + v_0 \Delta t_m) - v_0 w_0 \Delta t_m]}{r_1}$$

These transformations are required to maintain the radial character of r and v and the azimuthal character of w .

Some problems may occur with the use of weighting factors for axi-symmetric flow near to the axis. Due to the relatively small size of cells at the axis, special attention is required to maintain sufficient sample sizes in such flow regimes.

3.2.6 Collision Dynamics

The manner in which the local collision rate is simulated within the DSMC method has received much attention in recent years. One of the most fundamental concepts

of the method is that motion is treated separately from molecular collisions. This aspect of the method is analysed in detail in the next Chapter with reference to several different DSMC techniques. Here the methods for treatment of collision cross-sections and post collision quantities are described.

3.2.6.1 Collision Model

The collision rate in a simple gas is given by

$$\nu = n\ \overline{\sigma_T\ c_r}$$

where n is the number density, c_r is the relative velocity and σ_T the total collision cross-section. In early applications, an inverse power law potential in which σ_T is given by

$$\sigma_T = \pi\ W_0^2 [\kappa / m_r c_r^2]^{2/\eta - 1}$$

was employed. However, such a model requires the sampling of two impact parameters thus making it numerically inefficient. The special case of hard sphere molecules, i.e. $\eta = \infty$, was normally used as this has a fixed collision cross-section. However, the use of such a model is physically unrealistic. Bird [50] later developed a model which provides an expression for the collision cross-section as a function of the relative velocity of the collision, and which employs the classical scattering law of the hard sphere. The Variable Hard Sphere (VHS) replaces η by $\omega = 2/(\eta - 1)$.

The average translational collision energy in an equilibrium gas at a temperature T is given by [17, Eqn.(4.45)]

$$E_t = < 0.5\ m_r c_r^2 > = \frac{2(\eta - 2)}{\eta - 1} kT = (2 - \omega) kT \qquad (3.9)$$

The collision cross-section in an equilibrium gas is proportional to $T^{-\omega}$. Thus

$$\sigma_T = \sigma_{ref}\ (T/T_{ref})^{-\omega} \qquad (3.10)$$

where σ_{ref} defines a reference cross-section at temperature T_{ref}. In the case of nonequilibrium calculations, use is made of the collision energy to obtain

$$\sigma_T = \sigma_{ref} (c_r^2 / c_{r\,ref}^2)^{-\omega} \tag{3.11}$$

If the reference value of the square of the collision velocity is chosen to be the mean of c_r^2 in an equilibrium gas at the temperature T_{ref} then

$$\sigma_T = \sigma_{ref} [m_r c_r^2 / \{2(2 - \omega)kT_{ref}\}]^{-\omega} \tag{3.12}$$

This is the VHS collision model. To implement the model, T_{ref}, d_{ref} and ω must be provided as input data (d_{ref} is the reference collision diameter, so that $\sigma_{ref} = \pi d_{ref}^2$). Bird [50] provides an expression for d_{ref} as a function of ω, T_{ref} and a reference viscosity. Thus, appropriate values of ω may be calculated for different gases.

One drawback with the VHS model is that ω must have a single constant value, even in the case of gas mixtures. Nonetheless, the VHS model has proved to be an effective and efficient collision model, and its use is highly recommended.

3.2.6.2 Elastic Collisions

Once two molecules have been chosen as collision partners, their post collision properties must be calculated. The procedure for calculating post collision velocities assuming elastic collisions is now outlined.

Conservation of momentum and energy leads to

$$m_1 \underline{c}_1 + m_2 \underline{c}_2 = m_1 \underline{c}_1^* + m_2 \underline{c}_2^* = (m_1 + m_2) \underline{c}_m \tag{3.13a}$$

$$m_1 c_1^2 + m_2 c_2^2 = m_1 c_1^{*\,2} + m_2 c_2^{*\,2} \tag{3.13b}$$

where $\underline{c}_1$, $\underline{c}_2$ are the precollision velocity vectors, $\underline{c}_1^*$, $\underline{c}_2^*$ are the postcollision velocity vectors, $\underline{c}_m$ is the centre of mass velocity vector and m_1, m_2 are the masses of the colliding bodies.

The relative velocity vectors prior to, and following collision are given by

$$\underline{c}_r = \underline{c}_1 - \underline{c}_2 \tag{3.14a}$$

$$\underline{c}_r^* = \underline{c}_1^* - \underline{c}_2^* \tag{3.14b}$$

The following is then obtained by using Eqns.(3.13) and (3.14):

$$\underline{c}_1^* = \underline{c}_m + \frac{m_2}{m_1 + m_2}\underline{c}_r^* \tag{3.15a}$$

$$\underline{c}_2^* = \underline{c}_m - \frac{m_1}{m_1 + m_2}\underline{c}_r^* \tag{3.15b}$$

As the magnitude of the relative velocity is unchanged in an elastic collision we need only determine a vector over the unit sphere to completely specify the post collision velocities of the collision partners. This is achieved by random sampling.

3.2.6.3 Inelastic Collisions

In the modelling of polyatomic molecules internal energy modes i.e. rotational, vibrational and electronic, must be accounted for in collision processes. Relaxation of internal energy occurs through the transfer of energy between the translational and internal modes. Collisions in which transfer of energy occurs are termed inelastic.

Over the years several different methods for simulating internal phenomena have been developed. The most successful in terms of numerical efficiency is the phenomenological model of Larsen & Borgnakke [53]. In this method, a fixed fraction ϕ of all collisions are regarded as inelastic. The remainder of collisions are treated elastically as described in the previous section. This is an aspect of the DSMC technique which could be improved. For flows involving large variations in the temperature field, it is unrealistic to specify a fixed value for the fraction of inelastic collision occurring. Such procedures will inevitably lead to errors in all aspects of the calculations. A method for calculating ϕ as a function of the collision energy has been

suggested by Pullin and reported in Reference 54. However, his expression is valid for nitrogen only, and the method of derivation is not clear.

Energy transfer is treated by sampling post collision properties from equilibrium distributions defined by the total collision energy before collision which is given by

$$E_c = 0.5 m_r c_r^2 + E_{i1} + E_{i2} \tag{3.16}$$

where $m_r = \dfrac{m_1 m_2}{m_1 + m_2}$ is the reduced mass of the collision, E_{i1}, E_{i2} are the internal energies before collision. The total collision energy is conserved in the collision so that the post collision translational energy for a VHS gas is sampled from

$$f_n\left(\frac{E_t^*}{E_c}\right) = \left[\frac{\zeta - \omega}{1 - \omega}\frac{E_t^*}{E_c}\right]^{1-\omega}\left[\left(1 - \frac{E_t^*}{E_c}\right)/\left\{1 - \left(\frac{1-\omega}{\zeta - \omega}\right)\right\}\right]^{\zeta - 1} \tag{3.17}$$

where ζ is the average number of degrees of freedom for the collision pair. The magnitude of the relative velocity of the collision is then given by

$$c_r = \left(\frac{2E_t^*}{m_r}\right)^{1/2}$$

and the vector is again sampled from the unit sphere.

The total internal energy,

$$E_{is}^* = E_{i1}^* + E_{i2}^* = E_c - E_t^*$$

must now be distributed between the colliding bodies. Clearly, if one of the bodies is monatomic then all of the internal energy is associated with the other molecule. Otherwise an internal energy must be sampled from the following VHS gas equilibrium distribution

$$f_n\left(\frac{E_{i1}^*}{E_{is}^*}\right) = [(\zeta - 2)^{\zeta - 2}/[(\zeta_1/2 - 1)^{\zeta_1/2 - 1}(\zeta_2/2 - 1)^{\zeta_2 - 1}]] \ \text{x}$$

$$\times\left(\frac{E_{il}^{*}}{E_{is}^{*}}\right)^{\zeta_1/2-1}\left(1-\frac{E_{il}^{*}}{E_{is}^{*}}\right)^{\zeta_2/2-1} \tag{3.18}$$

where ζ_1, ζ_2 are the individual numbers of internal modes for the two molecules. If either ζ_1 or ζ_2 is equal to 2 then the expression in the first set of square brackets becomes equal to unity. If both ζ_1 and ζ_2 are equal to 2 then the function is evenly distributed between 0 and 1.

In some of the calculations performed, vibrational energy modes were included. The number of vibrational degrees of freedom may be determined from the harmonic oscillator approximation

$$\zeta_v = \frac{2\theta_v}{T} / [\exp(\theta_v/T) - 1] \tag{3.19}$$

where θ_v is the characteristic temperature for vibration.

Separate values of ϕ are employed for the transfer to rotational and vibrational modes. The value for rotational modes is obtained from [55]

$$\phi_R = \frac{1 + 0.5\pi^{3/2}(T_r/T)^{1/2} + (\pi^2/4 + \pi)T_r/T}{(Z_r)_\infty} \tag{3.20}$$

where T_r is the characteristic temperature for rotation and $(Z_r)_\infty$ is the limiting collision number for the molecule.

The value of ϕ for vibrational relaxation is obtained by first calculating the relaxation time τ_v using the formula of Millikan & White [56] whereby

$$\tau_v = \exp[1.16\text{x}10^{-3}\mu^{1/2}\theta_v^{4/3}(T^{-1/3} - 0.015\mu^{1/4}) - 18.42]/\ p \tag{3.21}$$

where θ_v is the characteristic temperature for vibration, μ is half the molecular weight of the molecule, and p is the flow pressure in Atmospheres. The ratio of τ_v to Δt_m may then be regarded as the collision number of the relaxation process.

3.2.7 Macroscopic Flow Quantities

In the DSMC technique, the macroscopic flow quantities are derived by averaging the microscopic behaviour over a sufficiently large sample size. These properties are determined from the conditions existing locally in each of the cells spanning the computational domain. The centroid of the cell is conveniently employed as the output location point.

In a monocomponent gas, the simplest quantity is the number density, n,

$$n = \sum_{i=1}^{N_L} N_i \frac{W}{N_L V} \tag{3.22}$$

where N_i is the number of simulated molecules in the cell after each increment of time in the simulation, N_L is the total number of increments made during the averaging process, W is the weighting factor, and V the volume, of the current cell.

The translational temperature T_{tr} is given by

$$T_{tr} = \frac{m}{3k} \overline{c'^2} = \frac{m}{3k} (\overline{c^2} - \overline{c}^2) \tag{3.23}$$

where m is the molecular mass, and $\underline{c}$ is the velocity vector.

In a similar way, it is also possible to specify seperate translational temperatures for each velocity component, i.e.

$$T_x = \frac{m}{k} \overline{u'^2} = \frac{m}{k} (\overline{u^2} - \overline{u}^2) \tag{3.24}$$

To compute these translational temperatures it is therefore necessary to sample u, u^2, v, v^2, w, w^2 in each cell after every time increment.

For monatomic gases, the total temperature is of course synonymous with the translational temperature. However, for polyatomic molecules, additional energy may be associated with internal behaviour such as rotation, vibration, and electronic activity. It is therefore necessary to define an internal temperature T_{int} given by

$$T_{int} = \frac{2\overline{E}_{int}}{\zeta\, k} = \frac{2}{N_L \zeta\, k} \sum_{i=1}^{N_L} (E_{int})_i \tag{3.25}$$

where E_{int} is the internal energy of each molecule, and ζ is the number of internal degrees of freedom.

An overall temperature in such cases must now be defined by

$$T_{ov} = (3T_{tr} + \zeta T_{int})/(3 + \zeta) \tag{3.26}$$

It is often necessary to determine the vector of the stream velocity in many applications. For flow in two dimensions, the velocity magnitude is defined by

$$U = (\overline{u}^2 + \overline{v}^2)^{1/2} \tag{3.27}$$

and the flow angle by

$$\theta = \tan^{-1}(\overline{v}/\overline{u}) \tag{3.28}$$

For comparison with continuum calculations, it is often useful to derive the Mach number of the flow. The following simple expression uses the results given in Eqns.(3.26) and (3.28):

$$Ma = U/\sqrt{\gamma k T_{ov}/m}$$

where γ is the ratio of specific heats at constant pressure and volume.

Other quantities of interest include the mean collision rate and mean free path. The calculation of these properties requires more careful consideration. Whilst analytical expressions relating these quantities to the total temperature exist, they apply only to equilibrium flows. The proper definition of the mean collision rate is [17, Eqn.(1.6)]

$$\nu = n\, \overline{\sigma_T\, c_r}$$

Therefore, by sampling the quantity $n\,\overline{\sigma_T c_r}$ at the calculation of each collision, the mean collision rate is determined. The mean free path is given by [17, Eqn.(1.8)]

$$\lambda = \overline{c'}/\nu$$

where $\underline{c'} = \underline{c} - \underline{c_0}$, and $\underline{c_0}$ is the stream velocity vector. Thus, it is seen that λ is defined in a frame of reference moving with the flow.

The previous equations apply only to simple, single species gases. Extension to flows involving a mixture of species is straightforward. The following expressions indicate the approach for a gas containing k separate species:

$$n = \sum_{i=1}^{k} n_i \tag{3.30a}$$

$$T_{tr} = \frac{1}{3k} \sum_{i=1}^{k} \frac{n_i}{n} m_i \overline{c'^2_i} \tag{3.30b}$$

$$\nu = \sum_{i=1}^{k} \frac{n_i}{n} \nu_i \quad = \sum_{i=1}^{k} \frac{n_i}{n} \sum_{j=1}^{k} n_j \overline{(\sigma_T c_r)_{ij}} \tag{3.30c}$$

$$\lambda = \sum_{i=1}^{k} \frac{n_i}{n} \lambda_i \quad = \sum_{i=1}^{k} \frac{n_i}{n} \{ \sum_{j=1}^{k} (n_j/\overline{c'_i}) \overline{(\sigma_T c_r)_{ij}} \}^{-1} \tag{3.30d}$$

3.2.8 Numerical Implementation

Many of the theoretical aspects discussed in this Chapter have been implemented in a FORTRAN 77 code called NOZZLE. This programme has been developed on the CRAY-1 at the University of London Computer Centre and on the IBM 3090 at Southampton. The programme has been written in a general way such that it may be readily applied to various flow problems. However, it has been found that improved numerical performance is achieved through the use of customised coding. Thus, for the larger simulations performed in this project, derivatives of NOZZLE have been employed. The programme offers the following options:

(a) 2-d or axially symmetric flow
(b) internal energy exchange
(c) diffuse or specular surface interaction
(d) gas mixtures
(e) choice of simulation method (see Chapter 4)

Output provided at each data point in the cell network include:
(a) number density
(b) translational temperature
(c) internal mode temperature
(d) x and y component temperatures
(e) total temperature
(f) velocity vector
(g) Mach number
(h) mean collision frequency
(i) mean free path.

Input required by the programme include details of the initial state of the gas and specification of the cell network.

The various routines which are comprised in NOZZLE have been extensively validated under the simplest of conditions. Tests on each of the modules were carried out in isolation and in conjunction with each other. Extensive output was used in the checking of each of the microscopic operations undertaken by the programme. In addition, the macroscopic results produced in full operational mode have been

checked. For example, the relaxation of internal energy modes was tested in a heat-bath environment. The testcase chosen to verify the overall implementation of the computer code was the Prandtl-Meyer expansion previously undertaken by Bird [57]. Figure 3.2 shows the flow configuration. Molecules are injected along AB and BC with conditions specified by Prandtl-Meyer continuum theory. In particular the following equations are required:

$$\frac{\rho}{\rho_0} = \cos^{\frac{2}{\gamma-1}} \lambda\theta$$

$$\frac{T}{T_0} = \cos^2 \lambda\theta$$

$$u = U \sin \lambda\theta$$

$$v = \lambda U \cos \lambda\theta$$

$$\lambda = \left(\frac{\gamma - 1}{\gamma + 1} \right)^{\frac{1}{2}}$$

Density contours for the simulation are shown in Figure 3.3 and agree well with the results of Bird. The temperature ratio contours shown in Figure 3.4 show the expected degree of nonequilibrium near the nozzle lip.

Application of NOZZLE to the sonic expansion of hot nitrogen gas will be discussed in the next Chapter, whilst application to a small hydrazine thruster is detailed in Chapter 5.

3.3 Chemical Reactions

3.3.1 Introduction

The governing equations for the rates of chemical change for the reaction

$$A + B \leftrightarrow C + D$$

may be written

$$-\frac{dn_A}{dt} = k_f(T)n_A n_B - k_r n_A n_B \qquad (3.30)$$

where n_A, n_B are the number densities of species A and B, and k_f and k_r are the forward and reverse rate coefficients. The temperature dependence of the rate coefficients is usually expressed in the form

$$k_f(T) = AT^b \exp(-E_a/kT) \qquad (3.31)$$

where E_a is the activation energy for the reaction, k is Boltzmann's constant, A and b are experimentally determined constants. These constants are found by measuring the rate of reaction at different temperatures and fitting the data by a suitable choice of a and b. The process is therefore somewhat arbitrary.

From collision theory the forward rate equation is given by

$$-\frac{dn_A}{dt} = k_f n_A n_B = n_A \nu_{AB} \int_{\frac{E_a}{kT}}^{\infty} f\left(\frac{E_c}{kT}\right) P_r\left(\frac{E_c}{kT}\right) d\left(\frac{E_c}{kT}\right) \qquad (3.32)$$

ν_{AB} is the equilibrium collision rate for species A with species B, $f(E_c/kT)$ is the statistical distribution function for the collision energy E_c, $P_r(E_c/kT)$ is the fraction of those collisions having sufficient energy to react which do react and is known as the steric factor.

The theory and implementation of three DSMC chemical reaction models is now discussed. Two of these involve the inclusion of internal energy modes.

3.3.2 Translational Energy Model

Bird [17, p.191] suggested a theory for chemical reactions which employed only the translational energy in the breaking of chemical bonds. The distribution function for hard-sphere molecules to be used in the integral of (3.32) is

$$f\left(\frac{E_t}{kT}\right) = \frac{E_t}{kT}\ \exp\left(-\frac{E_t}{kT}\right) \tag{3.33}$$

In his translational energy reacting model Bird made his steric factor have the same temperature dependence as k_f. If it is noted that $\nu_{AB} = n_B\overline{\sigma_T c_r}$ and, for hard-sphere molecules

$$\overline{\sigma_T\, c_r} = \left(\frac{8kT}{\pi m_r}\right)^{\frac{1}{2}}$$

then substituting Eqns.(3.31) and (3.33) into (3.32) gives:

$$AT^b \exp\left(-\frac{E_a}{kT}\right) = \left(\frac{8kT}{\pi m_r}\right)^{\frac{1}{2}}\sigma_T\int_{\frac{E_a}{kT}}^{\infty} P_r\left(\frac{E_t}{kT}\right)\frac{E_t}{kT}\ \exp\left(\frac{E_t}{kT}\right) d\left(\frac{E_t}{kT}\right) \tag{3.34}$$

Bird then proposed the following steric factor

$$P_r\left(\frac{E_t}{kT}\right) = \frac{A}{\sigma_T\Gamma(b+\frac{3}{2})}\left(\frac{\pi m_r}{8k}\right)^{\frac{1}{2}}\left(1-\frac{E_a}{E_t}\right)(E_t - E_a)^{b-\frac{1}{2}} \tag{3.35}$$

which when integrated in (3.32) gives the desired result. However, there are two main drawbacks to this model. First the presence of the gamma function in Eqn.(3.35) sets a lower bound on values of b, i.e. b > -1.5. When the implementation of this model was attempted in the modelling of the dissociation of molecular oxygen the rate data for oxygen specified a value of b = -2.0 for one of the reactions. Bird managed to employ a value for of -3.5 [58], but only by assuming that σ_T has a temperature dependence and allowing internal energy contributions to some reactions. This leads us to the second failing of the model, namely that the inclusion of internal energy is not treated which is physically unsatisfactory [59].

3.3.3 Translational/Internal Energy Model

It is certain that the energy stored in the internal modes of a molecule may contribute to the breaking of chemical bonds. Let us consider how such a concept can be implemented into DSMC calculations.

The distribution function for the total internal energy of two colliding molecules is

$$f\left(\frac{E_i}{kT}\right) = \frac{1}{\Gamma(\zeta)}\left(\frac{E_i}{kT}\right)^{\zeta-1}\exp\left(-\frac{E_i}{kT}\right) \tag{3.36}$$

where $\zeta = 0.5(\zeta_A + \zeta_B)$ is the average number of internal degrees of species A and B. Since the total collision energy is the sum of the translational energy and the contributed internal energy then from Eqns.(3.33) and (3.36) it follows that

$$f\left(\frac{E_c}{kT}\right) = \frac{1}{\Gamma(\zeta^* + 2)}\left(\frac{E_i}{kT}\right)^{\zeta^*-1}\left(\frac{E_t}{kT}\right)\exp\left[-\frac{E_i + E_t}{kT}\right] \tag{3.37}$$

where $\zeta^* = 0.5(\zeta_A^* + \zeta_B^*)$ is the average number of internal degrees of freedom allowed to contribute energy to the collision, i.e. the Internal Mode Contribution (IMC). Substituting $E_c = E_t + E_i$ into (3.37) the integral in Eqn.(3.32) becomes

$$\Lambda T^b \exp\left(-\frac{E_a}{kT}\right) = \left(\frac{8kT}{\pi m_r}\right)^{1/2}\sigma_T \int_{\frac{E_a}{kT}}^{\infty}\int_0^{\frac{E_c}{kT}} \frac{1}{\Gamma(\zeta^* + 2)} P_r\left(\frac{E_c}{kT}\right)\left(\frac{E_c - E_t}{kT}\right)^{\zeta^*-1}$$

$$\times \frac{E_t}{kT}\exp\left(-\frac{E_c}{kT}\right) d\frac{E_c}{kT}\, d\frac{E_t}{kT} \tag{3.38}$$

Bird [60] proposed the following expression for the steric factor

$$P_r\left(\frac{E_c}{kT}\right) = \frac{\Gamma(\zeta^* + 2)}{\Gamma(\zeta^* + \frac{3}{2} + b)}\frac{\Lambda}{\sigma_T}\left(\frac{\pi m_r}{8k}\right)^{\frac{1}{2}}\left(1 - \frac{E_a}{E_c}\right)^{\zeta^*-1}\left(\frac{E_c - E_a}{k}\right)^{b-\frac{1}{2}}$$

(3.39)

which gives the temperature dependent result when integrated in Eqn.(3.32).

3.3.4 Simulation Procedure

The model proposed by Bird, described in Section 3.2.3, has been implemented in a FORTRAN 77 programme called REACT. For computational flexibility, Eqn.(3.39) is converted into the format for a VHS gas [50], i.e.

$$P_r\left(\frac{E_c}{kT}\right) = \frac{\Lambda\sqrt{\pi}}{2\sigma_{ref}} \frac{\Gamma(\zeta^* + 2 - \omega)}{\Gamma(2-\omega)\Gamma(\zeta^* + \frac{3}{2} + b)} \left(\frac{m_r}{2k}\right)^{\frac{1}{2}-\omega}$$

$$\times \left[\frac{m_r}{2(2-\omega)kT_{ref}}\right]^{\omega} \left(1 - \frac{E_a}{E_c}\right)^{\zeta^*+\omega-1} \left(\frac{E_c - E_a}{k}\right)^{b-\frac{1}{2}+\omega} \qquad (3.40)$$

From Eqn.(3.40) the steric factor at each collision may be written

$$P_r\left(\frac{E_c}{kT}\right) = \text{const} \frac{(E_c - E_a)^{\zeta^*+\frac{1}{2}+b}}{E_c^{\zeta^*+1-\omega}} \qquad (3.41)$$

where the constant is evaluated at the beginning of the run from the input data.

Consider a typical dissociative reaction

$$M + A \rightarrow M + A + A$$

where M is a diatomic molecule, and A is an atom formed from M. The calculation of post-collision quantities is achieved through a two-step procedure:

The quantities $E'_{i1}, \underline{c}'_1, \underline{c}'_2$ are specified in a VHS format by Eqns.(3.17-18) for the Larsen-Borgnakke energy exchange model. However, it should be noted that for chemical reactions, the total collision energy is given by

$$E_c = \frac{1}{2} m_r c_r^2 + E_{i1} + E_{i2} - E_d = \frac{1}{2} m_r c_r'^2 + E'_{i1}$$

where $E_d = E_a$ is the activation energy of the dissociative reaction. The velocities $\underline{c}''_2, \underline{c}''_3$ are then calculated from $\underline{c}'_2$ by again applying conservation of energy and momentum.

The procedures for calculation of atomic recombination are straightforward and are described in Chapter 12, Ref. 17. The basic assumption made is that a three-body collision may be regarded as two successive binary collisions which occur within a certain collision 'lifetime'.

3.3.5 Application and Discussion

Let us now consider some example calculations made with the steric factors described in the previous Sections. The following three reaction systems have been studied in a heatbath environment.

$$\text{(a)} \quad O_2 + M \leftrightarrow 2O + M \quad ,M = O\,,\, O_2$$

$$\text{(b)} \quad N_2 + M \leftrightarrow 2N + M \quad ,M = N\,,\, N_2$$

$$\text{(c)} \quad N_2 + O_2 \leftrightarrow 2NO$$

These reactions were decided upon because of their importance in the field of spacecraft engineering, and the wide availability of rate data [61,62,63]. Figures 3.5, 3.6, 3.7 show typical simulations for the systems (a),(b),(c). The fraction by number density of the product of the forward reaction in each of the systems is plotted. The statistical error of the calculations is less than 2%.

The main difficulty in the use of this model lies in the determination of suitable values of ζ^*. From a mathematical viewpoint, provided ζ^* satisfies the inequality

$$\zeta^* > \frac{-3}{2} - b \quad \text{(a consequence of (3.32))} \tag{3.42}$$

then there should be no preferred value. Figure 3.8 shows plots of product concentration against ζ^*/ζ for a simulation in which b=-2.5 and $\zeta = 3.2$. The inequality (3.42) gives $\zeta^*/\zeta > 0.3125$, but the plots clearly show that consistent results are not obtained until approximately $\zeta^*/\zeta > 0.5$. This is due to the behaviour of the gamma function as its arguement approaches zero. The first drawback with Bird's model is that the choice of ζ^* is restricted to an unknown extent.

It may also be concluded from Figures 3.5, 3.6, 3.7 that there seems to be values of ζ^* which result in more accurate reaction paths than others, although equilibrium is always reached at some point. In the present work, the intended application of the chemical reaction model is to spacecraft control thruster flows which may become frozen at some unknown point in time. It is therefore imperative that our model is able to predict accurately concentrations of gas species present at all points in time. The second drawback of Bird's model then is that the reaction path followed by the simulation is seen to depend upon the value of ζ^* chosen whilst there is no *a priori* method of obtaining this value. Indeed, the only way to obtain accurate reaction paths is by expensive trial and error testing.

3.3.6 Simplified Chemical Reaction Model

The ideal solution to the problems associated with Bird's model would be the ability to predict beforehand the required value of ζ^*/ζ to give the correct reaction path. Since this does not seem to be possible a simpler version of Bird's model which is independent of the choice of ζ^*/ζ is proposed. The new model simply removes the temperature dependent nature of the steric factor so that the expression may be derived in the following way for a VHS gas:

$$P_r\left(\frac{E_c}{kT}\right) = \frac{k_f}{\exp\left(-E_a/kT\right)} \frac{\sqrt{\pi}}{\sigma_{ref}\Gamma(2-\omega)} \left(\frac{m_r}{2kT}\right)^{\frac{1}{2}-\omega}$$

$$\times \left[\frac{m_r}{2(2-\omega)kT_{ref}}\right]^{\omega} \left(1 - \frac{E_a}{E_c}\right)^{\zeta^*+1-\omega} \tag{3.43}$$

Figure 3.9 shows the variation in steric factor with collision energy for reaction (c) at 3000K.

It seems more logical to employ the value of the rate coefficient in the determination of the steric factor rather than to make it obey a temperature exponent which has been chosen in a somewhat arbitrary way. A review of rate coefficient data [63] reveals a range of values of b for any one reaction, e.g. for the dissociation reaction of nitrogen values for b include -1.5, -0.75, 0.0 and 0.5. While the values of a associated with these temperature exponents are such that the values of k_f are compatible, so that the steric factor given by Eqn.(3.43) is essentially the same for each set of data. However, this is clearly not true for Bird's model.

There are several advantages of this model over that of Bird:

(a) there is no restriction on the choice of ζ^*,
(b) there are no gamma functions present,
(c) the value k_f is the measurement made experimentally rather than an arbitrary combination of Λ and b which happens to give a value close to k_f.

In Figure 3.10, product concentration is again plotted against ζ^*/ζ in a similar fashion to Fig. 3.8. It is evident that the results are self consistent for each value of ζ^*/ζ employed. Hence the choice of ζ^* has indeed been removed from the calculations. Thus it is confirmed that this new model makes the simulation of chemical reactions using DMSC methods more accurate. For simulation in which the temperature is constant throughout the flowfield, e.g. heat bath studies, the new steric factor is found to be as efficient as that proposed by Bird. However, for the investigation of flows in which temperature gradients exist, it is necessary to evaluate the local temperature in each cell of the flowfield every time the collision algorithm is called. It is estimated that such a procedure incurs no more than a 10% computational overhead.

4. ASSESSMENT OF VARIOUS DIRECT SIMULATION SCHEMES

At the development stage of the DSMC code, it was unclear from the literature which of the several existing DSMC methods provided the most realistic simulation of the collision processes in gases. A detailed comparative study of the major methods was therefore undertaken in order to identify the method best suited to the requirements of the project. The findings of this exhaustive study are reported in the following.

4.1 Simulation Schemes for DSMC Calculations

4.1.1 Introduction

The theory and ideas behind the Direct Simulation Monte Carlo method were described in the previous Chapter. The mathematical model which must be simulated in the computational domain is now considered. It is generally recognised that the behaviour of colliding molecules in a dilute gas is best represented by the Boltzmann equation [64]

$$\frac{d(nf)}{dt} + \underline{c}.\frac{d(nf)}{d\underline{r}} = \int_{-\infty}^{\infty}\int_{0}^{4\pi} n^2(f^* f_1^* - f\, f_1)c_r \sigma d\Omega\, d\underline{c}_1 \qquad (4.1)$$

where f, f_1 are the single particle distribution functions in velocity space at $\underline{c},\underline{c}_1$ respectively. When molecules with velocities $\underline{c},\underline{c}_1$ collide, then their postcollision values are given by $\underline{c}^*,\underline{c}_1^*$ which have distributions f^*, f_1^* respectively. The combination of physical space and velocity space gives rise to multidimensional phase space. It should

therefore be noted that nf($\underline{c}$) is the single particle distribution function in phase space when f($\underline{c}$) is also dependent upon $\underline{r}$ and t.

The expression on the right hand side of Eqn.(4.1) is referred to as the collision term. The integral format of this term, in conjunction with the partial differential terms on the left hand side, is the source of much of the mathematical difficulty encountered with the solution of the Boltzmann equation. A limited number of analytical solutions have been found for problems possessing simple boundary conditions. Either by making assumptions about the particular form of the distribution function, or by actual modification of the Boltzmann equation itself, solutions are also found through the use of moment methods or model equation methods. None of these techniques are suited to complex engineering problems.

The DSMC method is therefore found to be the most useful solution technique, but how does it relate to the Boltzmann equation? The left hand side of Eqn.(4.1) shows that in the absence of collisions, nf remains constant when one moves with the molecules in phase space. Therefore, by tracing the paths of the molecules during the uncoupling process over Δt_m, the DSMC method is found to be consistent with this aspect of the Boltzmann equation.

It is in the treatment of the collision term that a degree of uncertainty has arisen. Several DSMC schemes simulating the collisional behaviour now exist and have all been categorised by Nanbu [65,66]. The methods are classified according to the mathematical form of the collision term, i.e. whether the right hand side is specified by (A) the Boltzmann equation, or (B) the Kac Master equation [67]

$$\frac{d\phi}{dt}(t, \underline{c}) = \frac{1}{V}\sum_{l=1}^{N} |\underline{c}_l - \underline{c}_m| \int \phi(t, \underline{c})\, d\sigma_{lm} \qquad (4.2)$$

where $\phi(t,\underline{c})$ is the probability distribution of $\underline{c}(t)$, $\underline{c}_l, \underline{c}_m$ are the post-collision velocities of molecules l, m, and σ_{lm} is the differential cross section for elastic scattering of the pair of molecules $(\underline{c}_l, \underline{c}_m)$. V, in this case, may be interpreted as the cell volume and N is the number of simulated molecules.

The Kac Master equation may be reduced to the Boltzmann equation in the asymptotic limit as N tends to infinity. This assumption is only valid if the N mo-

lecular velocities are independent of each other when time is zero. In DSMC calculations, this is generally true as all simulated molecules have their velocities sampled from the appropriate equilibrium distribution functions. It is therefore possible to derive solutions for the Boltzmann equation through use of the Eqn.(4.2).

Bird's time counter (TC) scheme [17] falls into category (B) [65] , although no conscious effort was made to solve the Kac equation. Instead, the driving force behind this method was the requirement to employ the minimum amount of computational effort whilst still obtaining engineering solutions to complex flow phenomena. In this respect the method has been highly successful. This method is by far the most commonly employed DSMC technique. It is for this reason, together with its superior computational efficiency, that the TC method has been implemented as an example of a method which simulates the Kac Master equation.

Several alternative schemes which simulate the Kac master equation have been developed by Belotserkovskiy & Yanitskiy [68], Koura [69], and Deshpande [70]. These methods propose to treat the collision term in a more rigorous fashion than Bird, thereby incurring additional computational expense. The use of these methods has therefore been limited almost exclusively to their originators. Nevertheless, these alternative schemes are described in the following for the sake of completeness.

The method of Nanbu [71] was the first DSMC method to fall into category (A). He derived the scheme in a mathematical manner directly from the Boltzmann equation. Nanbu's scheme has failed to achieve popularity due to the fact that it is very computationally intensive and also that energy and momentum are not conserved at the collision level. Later, however, Babovsky [72] proved in a strict mathematical sense that Nanbu's method achieves convergence, which has not been proven for the TC method of Bird.

All DSMC methods proceed by uncoupling molecular motion and intermolecular collisions over the small time interval Δt_m. At time t all molecules are moved freely over time Δt_m (Stage I) and then collisions appropriate to the time span Δt_m are calculated by fixing molecular positions (Stage II). It is the treatment of Stage II which has caused the controversy in DSMC methods. The essential differences in the vari-

ous DSMC schemes lie in the selection of collision partners, and in the manner in which post-collision values are assigned.

The various simulation schemes mentioned above are now discussed. In particular, any differences in their concept and implementation will be highlighted.

4.1.2 Bird's Time Counter Scheme

A full description is provided in Reference 17. Bird devised his scheme through the need to simulate (in a classical manner) the physics of molecular collisions in complex flow problems. In this method when the molecular positions of all simulated molecules are frozen in Stage II of the uncoupling process, the number of collisions N_t is then calculated in each of the cells representing physical space. The appropriate number of collisions for a single species gas over time Δt_m is given by

$$N_t = \frac{1}{2} N_m n \Delta t_m \overline{\sigma_T c_r} \tag{4.3}$$

where N_m is the number of simulated molecules in the cell at time t, n is the number density in the flow, c_r is the relative collision velocity of the molecules and σ_T is the total collision cross-section for the collision pair.

The symmetry factor of 1/2 is included because there are two molecules whose properties are recalculated after each collision in the TC method. Hence, if the number of collisions calculated over Δt_m is $1/2N_m$, this means that N_m molecules have experienced a change in state.

The product $\overline{\sigma_T c_r}$ represents the mean collision rate per unit density in the flow. The calculation of $\overline{\sigma_T c_r}$ is clearly time consuming, and so Bird proposed that each collision should have a 'lifetime' given by

$$\Delta t_c = \frac{2}{N_m n \sigma_T c_r} \tag{4.4}$$

Sufficient collisions are then calculated in each cell until the sum of several Δt_c becomes just greater than Δt_m. Thus, time-counters must be kept in each of the cells in the network. Collision partners are sampled from

$$P_{ij} = \frac{(\sigma_T c_r)_{ij}}{(\sigma_T c_r)_{max}} \tag{4.5}$$

by use of the rejection method. The quantity $(\sigma_T c_r)_{max}$ represents the maximum value of the product. The value is initially estimated from equilibrium properties, and updated throughout the simulation if the need arises. When two molecules have been selected, both collision partners have their velocity components recalculated through the application of conservation of energy and momentum as given by Eqns.(3.15a-15b).

The key points in this method are summarised thus:

(i) after each individual collision new statistical populations arise,

(ii) the velocity components of both collision partners are recalculated after each collision,

(iii) one molecule may undergo several collisions in the time interval Δt_m ,

(iv) time-counters are updated in each cell after each collision,

(v) as the method does not require the calculation of $\overline{\sigma_T c_r}$ the computational expense is proportional to N_m.

4.1.3 Alternative Kac Schemes

As mentioned earlier, several other DSMC schemes which simulate the Kac master equation exist. The most important of these is the method developed by Belotserkovskiy & Yanitskiy [68]. In this scheme, the occurrence of molecular collisions is assumed to follow a Poisson distribution, with the rate of occurrence given by

$$\rho(t) = \frac{n}{N_m} \sum_{i=1}^{N_m} \sum_{j=1}^{N_m} (\sigma_T \, c_r)_{ij} \tag{4.6}$$

A collision 'lifetime', τ, is therefore sampled from

$$P = 1 - \exp[- \rho(0 , \tau)] \tag{4.7}$$

The collision pair may be sampled from

$$P_{ij} = (\sigma_T c_r)/\Sigma (\sigma_T c_r)_{ij} \tag{4.8}$$

The efficiency of this procedure may be improved by making use of the rejection method as applied to Eqn.(4.5). Post collision values are assigned in the same manner as in the TC scheme. A number of lifetimes are sampled from Eqn.(4.7), and collisions subsequently calculated, until the sum of the τ is greater than the decoupling time-step Δt_m. The computational expense of the method is proportional to N_m^2 as the collision rate over all molecules must be determined.

Nanbu [65] has shown that Bird's TC method is a variant of the Belotserkovskiy & Yanitskiy scheme whereby a collision pair is first sampled from Eqn.(4.8), and the resulting lifetime is calculated from Eqn.(4.4). Nanbu also shows that the statistical expectation of a collision is the same for both schemes, so that the results they produce should be the same.

The schemes of Koura [69] and Deshpande [70] are very similar to that just described and offer no improvements. Koura again samples collision lifetimes from Eqn.(4.7). However, in his method, $\rho(t)$ is given by an expression involving a multiple integral which is evaluated using the Monte Carlo method, thereby incurring additional computational expense. In the method of Deshpande, it is the number of collisions occurring over Δt_m which is sampled from the appropriate Poisson probability distribution, i.e.

$$P(N_t = k) = \exp(- \rho(0)\Delta t_m)(\rho(0)\Delta t_m)^k/k! \tag{4.9}$$

This method also incurs additional numerical overheads as the sampling from Eqn.(4.9) is not as easy as that from Eqn.(4.7) for the Belotserkovsky & Yanitskiy scheme.

4.1.4 Nanbu's Scheme

A full derivation of the method from the Boltzmann equation is presented in Reference 71. Stage II of the uncoupling process is treated in the following manner.

The number of collisions calculated in each cell over the time-step Δt_m in the Nanbu method is

$$N_t = N_m n \Delta t_m \overline{\sigma_T c_r}$$

When this expression is compared with Eqn.(4.3) it is seen that the factor of 1/2 is here absent. This is due to the fact that in the Nanbu scheme only one of the colliding bodies experiences a change in state.

The collision probability for molecule i in a given cell is

$$P_i = \sum_{j=1}^{N_m} P_{ij} = \frac{n \Delta t_m}{N_m} \sum_{i,j=1}^{N_m} (\sigma_T c_r)_{ij} \qquad (4.10)$$

Thus for each molecule in the cell P_i is calculated to decide whether or not it collides over the time interval Δt_m. If the calculations show that molecule i will collide then a collision partner is chosen in the same way as in the TC scheme. However, only molecule i has its velocity recalculated, from Eqn.(3.15a), and it is not updated until all molecules in the cell have been considered. As each molecule may only collide at most once over Δt_m, this means that the maximum value of N_t is N_m. Hence $n \Delta t_m \overline{\sigma_T c_r}$, and therefore P_i, must be less than unity. If P_i becomes greater than unity then the collision rate will be deformed. The parameters for the simulation must therefore be chosen with care.

The key points in this method are summarised thus:

(i) after each time-step new statistical populations arise,

(ii) the velocity components of molecule i only are recalculated,

(iii) each molecule may undergo at most one collision in the time interval Δt_m ,

(iv) no time-counters are updated,

(v) as the method calculates $\overline{\sigma_T c_r}$ the computational expense is proportional to N_m^2.

Although, when compared to Bird's TC method, Nanbu's simulation scheme appears at first sight to be physically unreal, it should be remembered that it has been derived rigorously from the Boltzmann equation. Finally, it is worth noting that the Nanbu algorithm is partly vectorizable. This is the calculation of each collision probability is dependent on the velocity distribution which exists in each cell at the call of the collision routine. This is different from Bird's algorithm which updates the velocity distribution after each and every collision. Use has therefore been made of the vector facilities available on the CRAY 1-S to improve the performance of the Nanbu calculations. It was found that the application of such techniques speeded the algorithm up by a factor of 2.

4.2 Comparison of the Schemes of Bird and Nanbu

4.2.1 Introduction

The popularity of Bird's TC method has remained unchallenged by the other schemes which are derived from the Kac equation. The reason for this lies in the fact that the methods were found to be much more computationally intensive without offering any improvements in the results calculated. The advent of Nanbu's scheme which directly simulated the Boltzmann equation did not alter this situation. In addition to larger computer overheads, there also existed doubts about the fact that energy and momentum are not conserved at each collision [73]. However, it should always be remembered that the Boltzmann equation describes the behaviour of a single particle distribution function, so that Nanbu's formulation is quite in keeping with this concept. The controversy therefore reduces to the question of which of the two mathematical models best describes the physical properties of rarefied gas flows. It could be argued that any improvements gained through the use of the Nanbu method would merit the increased numerical cost. In addition, the application of vector programming techniques to Nanbu's algorithm had not previously been considered in the literature. It was therefore decided to undertake a thorough comparison of the Nanbu scheme with one which simulated the Kac master equation.

It is clear from the previous discussions that the TC method is the most efficient of those which employ the Kac master equation. As the collision expectation is the same for all of these methods, it seems logical to employ that scheme which offers the

minimal computational expense. A comparison of the Time Counter method of Bird and that developed by Nanbu in the context of an engineering application has therefore been undertaken and is described in the following.

4.2.2 Sonic Expansion of Hot Nitrogen

The flow chosen to be modelled is the sonic expansion of nitrogen gas from a nozzle-lip into a vacuum. The configuration is two-dimensional with a specularly reflecting centreline. The extent of the nozzle modelled is fifteen mean free paths. The nozzle exit plane is taken as $x = 0$.

The gas has exit temperature and pressure of 2000K and 5000Nm^{-2} respectively. The initial input condition was a Maxwellian equilibrium velocity distribution with a superimposed streamwise component. The Variable Hard Sphere (VHS) collision model of Bird [50] has been used throughout and this was the first time to that this model has been used in conjunction with the Nanbu simulation scheme. In the VHS model the total collision cross-section is related to the relative velocity of the collision partners by

$$\sigma_T = \sigma_{ref} \left[m_r c_r^2 / \{(2-\omega) k T_{ref}\} \right]^{-\omega} \qquad (4.11)$$

where σ_{ref} is a reference cross-section calculated at temperature T_{ref}, m_r is the reduced mass of the collision, k is Boltzmann's constant, and ω determines the molecular model and is related to the inverse power law exponent by

$$\omega = \frac{2}{\eta - 1} \qquad (4.12)$$

Thus, $\omega = 0.0$ for hard sphere molecules and $\omega = 0.5$ for Maxwellian molecules. Increasing ω effectively reduces the inverse power law exponent.

Once ω has been chosen a mean free path at temperature T may be defined as

$$\lambda = (T/T_{ref})^{\omega} \left[(2-\omega)^{\omega} \Gamma(2-\omega) \sqrt{2}\, n \sigma_{ref} \right]^{-1} \qquad (4.13)$$

where $\Gamma(x)$ is the gamma function.

The cell system employed in the simulation was rectangular and had cell dimensions chosen such that the majority of molecules collided several times in the process of traversing each cell. For this relatively simple flow, it was possible to use a common weighting factor for all cells, thereby precluding any adverse statistical affects associated with such procedures. The total number of cells employed was about 3000, and on average at least 10 molecules resided in each.

The simulation of internal energy modes was not included at this stage as it was essential that any discrepancies in the resulting calculations should result solely from differences between the two collision algorithms. As the energy exchange model of Larsen-Borgnakke [53] had not previously been used in conjunction with the Nanbu scheme, it was felt that its inclusion might hinder the main aim of the study.

4.2.3 Results and Discussion

The cell network and time interval over which uncoupling occurs were calculated for $\omega = 0.0$,i.e. hard sphere molecules, and subsequently these parameters were kept constant for variations in ω. This was performed so that the physical space modelled in each simulation was the same. For the two simulation schemes three values of ω were initially tested:

(i) $\omega = 0.0$ (hard sphere molecules)
(ii) $\omega = 0.5$ (Maxwellian molecules)
(iii) $\omega = 0.24$ (the value for nitrogen calculated from viscosity data [50])

$\omega = 0.24$ corresponds to an inverse power law exponent of 9.333.

Figures 4.1 and 4.2 show flow contours calculated using Bird's TC method for hard sphere molecules. Figure 4.1 shows density contours and Figure 4.2 shows the velocity vectors of the flow. Results for the same simulation method with $\omega = 0.24$ and $\omega = 0.5$ were consistent with those presented in both Figures.

The relative CPU times and numbers of collisions calculated are included in Table 4.1. It should be remembered that the execution times for the Nanbu method have been reduced through partial vectorization. The number of collisions calculated is seen to decrease with increasing ω for the TC simulation because the mean free

path is increasing while the programme continues to derive the cell network from the hard sphere mean free path.

The same three collision models were then employed with the Nanbu simulation method. For Maxwellian molecules and for molecules having $\omega = 0.24$ the results again agreed with those for the TC simulations. However, the combination of the Nanbu method with hard sphere molecules predicted significantly different flow properties. Figure 4.3 shows the density contours for this simulation.

Comparing the number density predictions of the Nanbu method using the hard sphere molecular model (termed below NHS) shown in Figure 4.3, with typical results from the time counter scheme, reveals immediately that NHS predicts significantly lower flow densities along the plume centre-line. Indeed, the majority of the NHS flowfield is at least a factor of two more rarefied than that produced by the TC simulations. The exception to this trend occurs in the off-axis region immediately following the nozzle exit plane. In this part of the flowfield the NHS density predictions are consistently greater than those given by the TC method. Thus, it can be seen that the NHS simulation predicts a greater amount of backflow than would be expected. The NHS contours resemble those for a collisionless point source expansion rather than those of a sonic gas. Figure 4.4 shows the velocity vectors for the NHS plume scaled with the same velocity as that used in Figure 4.2. It is clear that the NHS velocity vectors are much greater in magnitude than those predicted by Bird's TC method. However, the flow angles show good agreement. The nature of the NHS results are presumed to result from a deficit in the number of collisions calculated. This is suggested by the number density contours and borne out by the contents of Table 4.1. It is therefore appropriate to consider in greater detail the ways in which the simulation schemes differ, and in particular to look at the implementation of both schemes. It should be noted however that *a priori* there is no reason to anticipate a breakdown in the Nanbu method under different collision models, because this method has been shown to solve the Boltzmann equation. Since the Boltzmann equation provides a general kinetic description of gases, no collision model is favoured.

From the equations presented above in Section 4.1.4, it is apparent that the probability of collision is dependent in both schemes on the product $\sigma_T c_r$. The distribution

function for the relative velocity c_r for a gas in equilibrium at temperature T is given by

$$f(c_r) = \frac{4m_r^{3/2}}{\sqrt{\pi}} (2kT)^{3/2} c_r^2 \exp\left(- \frac{m_r c_r^2}{2kT} \right) \qquad (4.14)$$

This function is plotted (solid line) in Figure 4.5 for T = 2000K along with the corresponding distributions taken from the simulations where the hard sphere model was used with each of the simulation schemes. The distribution taken from the TC simulation is a little cooler than the theoretical curve for T = 2000K as would be expected for an expanding gas. In contrast NHS predicts a velocity distribution having a most probable value approximately three times larger than the equilibrium distribution, under the model conditions.

Thus while the number density contours for the NHS method in general resemble those of a free expansion, the NHS relative velocity distribution shows that the collisions are much more energetic than expected. Both phenomena are consistent with a reduced collision rate. This is confirmed in Figure 4.6 where the collision probability distribution functions for both the NHS technique and the Nanbu/Maxwellian molecule scheme are shown. This demonstrates that there is an unacceptably large fraction of NHS collisions whose probability of collision is greater than unity.

Having ascertained that the cause of the spurious NHS results was a reduction in collision rate the question arises as to why the Nanbu method breaks down for hard sphere molecules while it worked perfectly well for the other two values of ω employed. It is therefore appropriate to examine the collision probability of a molecule as a function of ω.

In the Nanbu theory the probability of collision is equal to the sum of $n\Delta t_m \sigma_T c_r / N_m$ over all collision pairs involving the current molecule. For the general VHS model the total collision cross-section is given by Eqn.(4.6). The average probability of collision over the time-step Δt_m in the Nanbu method is

$$P = n\Delta t_m \overline{\sigma_T c_r} \qquad (4.15)$$

As the product $\sigma_T c_r$ is a function of c_r only, for a given gas and collision model, the average value is given by

$$\overline{\sigma_T c_r} = F = \int_{-\infty}^{\infty} \int_{-\infty}^{\infty} \sigma_T c_r f_1 f_2 d\underline{c}_1 \, d\underline{c}_2 \tag{4.16}$$

where f_1, f_2 are the two single-particle distribution functions, $\underline{c}_1, \underline{c}_2$ are the velocity vectors of the collision partners.

The Maxwellian equilibrium distribution function is

$$f(c) = \frac{\beta^3}{\pi^{\frac{3}{2}}} \exp(-\beta^2 c^2) \tag{4.17}$$

so that (4.16) becomes

$$F = \int_{-\infty}^{\infty} \int_{-\infty}^{\infty} \sigma_T c_r \exp\left[- \frac{m_1 c_1^2 + m_2 c_2^2}{2kT} \right] d\underline{c}_1 \, d\underline{c}_2 \tag{4.18}$$

By a change of variables from $\underline{c}_1$ and $\underline{c}_2$ to $\underline{c}_r$ and $\underline{c}_m$, where $\underline{c}_m$ is the velocity vector in the centre of mass frame, this integral may be evaluated. Using

$$\underline{c}_r = \underline{c}_1 - \underline{c}_2 \tag{4.19a}$$

$$\underline{c}_1 = \underline{c}_m + \frac{m_2}{m_1 + m_2} \underline{c}_r \tag{4.19b}$$

$$\underline{c}_2 = \underline{c}_m - \frac{m_1}{m_1 + m_2} \underline{c}_r \tag{4.19c}$$

$$m_1 c_1^2 + m_2 c_2^2 = (m_1 + m_2) c_m^2 + m_r c_r^2 \tag{4.19d}$$

the Jacobian of the transformation is found to be equal to one.

Since the integrand is not dependent on the directions of $\underline{c}_r$ and $\underline{c}_m$, it is apparent from integrating over all azimuth and polar angles that:

$$d\underline{c}_r = 4\pi^2 c_r^2 dc_r \; : \; d\underline{c}_m = 4\pi^2 c_m^2 dc_m$$

Substituting into Eqn.(4.18) gives:

$$F = K\frac{2(m_1m_2)^{3/2}}{\pi(kT)^3}\int_0^{\infty}\int_0^{\infty} c_r^{3-2\omega}c_m^2\exp\left[-\frac{(m_1+m_2)c_m^2+m_rc_r^2}{2kT}\right]$$

$$x \qquad dc_m\,dc_r \tag{4.20}$$

where

$$K = \sigma_{ref}\{m_r/[2(2-\omega)kT_{ref}]\}^{-\omega}$$

Evaluating this integral yields

$$F(\omega, T) = \frac{2\sigma_{ref}}{\sqrt{\pi}}\left[(2-\omega)\frac{T_{ref}}{T}\right]^{\omega}\Gamma(2-\omega)\left(\frac{2kT}{m_r}\right)^{1/2} \tag{4.21}$$

Hence for the specific cases of a hard sphere collision model ($\omega = 0$) and Maxwellian molecules ($\omega = 0.5$), the value for $F(\omega,T)$ has the specific form:

$$F(0.0, T) = \frac{2\sigma_{ref}}{\sqrt{\pi}}\left(\frac{2kT}{m_r}\right)^{1/2} \tag{4.22a}$$

$$F(0.5, T) = \frac{2\sigma_{ref}}{\sqrt{\pi}}\left(\frac{2kT}{m_r}\right)^{1/2}\Gamma(1.5)\left(1.5\frac{T_{ref}}{T}\right)^{0.5} \tag{4.22b}$$

For the Nanbu method to reproduce accurately the theoretical collision rate, the probability of collision given by Eqn.(4.10) must always be less than unity. However, Eqns.(4.22) show that if a time-step is chosen such that the probability of collision has an upper limit of unity for the Maxwellian molecules, i.e. $\omega = 0.5$, then the corresponding upper limit for hard sphere molecules is given by

$$\{(1.5T_{ref}/T)^{0.5}\Gamma(1.5)\}^{-1}$$

Table 4.1

CHARACTERISTICS OF INITIAL CALCULATIONS

METHOD	BIRD		NANBU		BIRD/NANBU	
Model (ω)	CPU	Collisions	CPU	Collisions	CPU	Collisions
0.0	1.000	1.000	1.116	0.345	0.896	2.899
0.24	0.773	0.689	5.848	0.632	0.132	1.090
0.5	0.612	0.451	6.011	0.457	0.102	0.987

Table 4.2

CHARACTERISTICS OF CALCULATIONS FOR VARIATIONS IN ω

METHOD	BIRD		NANBU		BIRD/NANBU	
Model (ω)	CPU	Collisions	CPU	Collisions	CPU	Collisions
0.00	1.000	1.000	1.116	0.345	0.896	2.899
0.05	0.977	0.918	1.873	0.360	0.522	2.550
0.10	0.910	0.848	2.182	0.385	0.417	2.203
0.15	0.866	0.799	3.434	0.504	0.252	1.585
0.20	0.816	0.737	5.670	0.686	0.144	1.074
0.25	0.768	0.675	5.890	0.655	0.130	1.031

Table 4.3

CHARACTERISTICS OF CALCULATIONS FOR VARIATIONS IN Δt_m

METHOD	BIRD		NANBU		BIRD/NANBU	
Time-step Factor (Φ)	CPU	Collisions	CPU	Collisions	CPU	Collisions
1.00	1.000	1.000	1.116	0.345	0.896	2.899
0.90	0.966	0.894	1.053	0.311	0.917	2.875
0.80	0.954	0.801	1.208	0.333	0.790	2.405
0.70	0.906	0.696	1.276	0.317	0.710	2.120
0.65	0.899	0.641	3.158	0.571	0.285	1.122
0.60	0.855	0.593	3.581	0.548	0.239	1.082
0.50	0.831	0.493	3.606	0.483	0.230	1.021

At the operational temperature of 2000K this upper limit is equal to 2.5. Thus it can be seen that the choice of ω leads to very appreciable differences in the number of collisions calculated in each cell.

It is thus apparent that a coupling exists between the time-step chosen and the molecular model for the Nanbu method. Further, since the function F(ω ,T) given by Eqn.(4.21) is also a function of temperature, a dynamic time-step may be required for the maintenance of an appropriate collision probability. This result implies that the Nanbu method is significantly more complex to implement than had hitherto been anticipated.

Returning to the specific flow simulation results noted above, it is possible to evaluate expression (4.21) for F(ω,T) as a function of ω and temperature. This is demonstrated graphically in Figure 4.7. It can be clearly seen that the choice of ω greatly affects the collision probability for fixed density and time-step. It is seen that there is a reduction in the average collision probability by increasing ω. It should be noted that the family of curves are seen to nearly converge around the reference temperature used in the VHS collision model, in this case 273K.

To determine the exact effect of collision model the programme was run for both the Time Counter and Nanbu simulation schemes for several values of ω and the results compared. The ratio of number densities along the plume centreline for the two methods are plotted for various values of ω in Figure 4.8. The very large disagreement in results for the hard sphere simulations is seen to be dramatically reduced by increasing ω to a value of 0.25 whereafter no appreciable difference in output is observed. These calculations agree with the results described above which used ω = 0.24 which was coincidentally just on the threshold of being able to provide reasonable results. Table 4.2 contains details of these simulations. The results in the Bird/Nanbu column show that as ω is increased to 0.25 the collision rates for the two simulation methods become compatible. When the results finally begin to converge, the Bird method is seen to be over seven times more efficient than the Nanbu scheme.

If Eqn.(4.21) is evaluated at 2000K, with Δt_m set by the hard sphere model and using parameters appropriate to nitrogen, then

$$P_{\omega=0} = n\Delta t_m F(0\ ,\ 2000) = 0.231$$

$$P_{\omega=0.5} = n\Delta t_m F(0.5\ ,\ 2000) = 0.148$$

as the average value of the collision probability.

The number density taken for these calculations was the value at the nozzle exit plane. The maximum value of both number density and temperature occur at the nozzle exit, so that these probabilities may be regarded as maximum values of the average collision probability. Hence it may be seen that an average collision probability of ~0.148 will provide a suitable probability distribution function having only the smallest fraction of probabilities greater than unity.

An alternative way of reducing the collision probability, without changing the collision model, is to decrease the time-step Δt_m. For employment of the same cell network then a reduction in time-step will result in an increased number of simulated molecules in each cell. This will then lead to much increased execution times. This build-up of molecules may be counteracted by reconstructing a grid with smaller cell dimensions. This would obviously require an increased number of cells to cover the same flowfield. It is clear that this course of action requires additional storage space in addition to an increase in computational expense. In the present work, the cell dimensions were reduced although this is irrelevant as the same procedure was applied to both simulation schemes.

The ratio of F(0.25,2000)/F(0.0,2000) ~0.64 so that it would be anticipated that convergence of results would be achieved in the two methods for a reduction in the time-step by this factor. The results of a series of simulations for both schemes varying Δt_m is shown in Figure 4.9. The hard sphere collision model was used throughout. The results are seen to converge for a Δt_m factor of between 0.6 and 0.65 as expected. Relative velocity distributions taken from the Nanbu simulations for several values of Δt_m are plotted in Figure 4.10 and confirm the convergent trend of the results with decreasing Δt_m .

Details of these runs of the programme are reported in Table 4.3. Again the most important results are obtained from the Bird/Nanbu calculations. As the time step factor is reduced to 0.6 the collision rates are found to have converged with the Bird simulation operating some four times more effectively. Thus, by comparison with Table 4.3, it can be seen that reducing the time-step is a more efficient method of

achieving convergence than increasing the value of ω. Indeed it is more appropriate to modify Δt_m on the basis that ω is a parameter which should be specified for a particular molecular species.

It would also appear that by decreasing the density of the flow it is also possible to obtain a reduced collision probability. However, this would have the effect of increasing the mean-free path of the flow with a corresponding need to increase the cell dimensions. This, in turn, would require an increase in Δt_m that would of course exactly counteract the effect of decreasing the number density.

The effect of temperature on the convergence of the two methods was tested by running simulations at 1000K, 3000K and 4000K. In each case the results began to agree for $\omega = 0.25$. To estimate the time-step factor required to produce satisfactory NHS results the following function is introduced

$$\Phi(T) = \frac{F(0.25, T)}{F(0.00, T)} = \left(1.75 \frac{T_{ref}}{T}\right)^{0.25} \Gamma(1.75)$$

This function is plotted in Figure 4.11 together with time-step factors successfully used in the simulations at various temperatures. It was concluded that once a set of parameters given by the gas type and ω has been shown to provide accurate results at one temperature, these parameters may subsequently be used for any temperature. However, this merely highlights the difficulty in using the Nanbu scheme effectively. There seems to be no *a priori* method of determining a set of parameters which will enable the Nanbu method to function correctly. This makes it a much less useful tool than the Bird scheme which adapted its collision rate to each different parameter set for all the runs undertaken.

Finally, the question arises as to whether problems similar to those experienced with the Nanbu scheme will occur in any of the other simulation methods. In all the methods considered earlier, time-counters and/or probability distribution functions are employed to reproduce the correct collision rate so that deformation cannot occur. It is anticipated that any of these methods would produce the required collision rates for all molecular models in the flow study presented above.

Nanbu has also proposed an approximate simulation method [74]. In this scheme, $\overline{\sigma_T c_r}$ is approximated by the local equilibrium distribution function. When this approximation is applied to the Nanbu simulation scheme the CPU time expense is certainly reduced, but the same problems concerning collision rate deformation still occur.

When faced with a practical problem to be solved using the Nanbu Direct Simulation scheme there are two possible courses of action. Either an analysis similar to that described above must be followed, or the time-step Δt_m must be taken so small that it is certain that the collision probability never approaches unity. The first course is time consuming for the engineer and the second is computationally expensive both in terms of the CPU time and computer storage required to perform the simulation. The overheads of the second course are caused by a necessary shrinking of the cell network which therefore requires an increase in the number of cells employed.

By comparison, Bird's TC method offers none of these difficulties. This method is able to adapt the collision rate in each cell to the prevailing conditions and gave self-consistent results in all the modes of operation investigated. In addition the method gave a ratio of CPU times with the Nanbu method of up to ~8 when the Nanbu method was producing favourable results.

It is concluded that despite advances in computer hardware that make it possible in theory to use of the Nanbu simulation scheme for complex flow problems, in practise the method is less flexible and more difficult to implement than the time counter scheme proposed by Bird.

4.3 Assessment of the Modified Nanbu Scheme

At about the same time as the completion of the work on the Nanbu method, the work of Babovsky [72] and Ploss [75] appeared in the literature. Babovsky proved convergence of the Nanbu scheme by splitting the decoupling time-step Δt_m into an integer number of equal intervals. This seemed to suggest that the difficulties encountered with the initial choice of Δt_m could be eliminated. In addition, a further modification to Nanbu's scheme which was again suggested by Babovsky, and implemented by Ploss, claimed to reduce the computational expense of the method. The paper by Ploss was not published until after the completion of the author's assessment of the Nanbu scheme. The renewed interest being shown in Nanbu's work as a result of the progress made by Babovsky highlights the timeliness of the work reported in the previous Section. The form of the modifications suggested to the author that the improvements made to the Nanbu scheme could possibly overcome the difficulties discussed previously. The application of a Boltzmann solving DSMC scheme would therefore become more desirable. This scheme which has been designated the Modified Nanbu method has therefore been investigated under the same test conditions as those applied to the original Nanbu method. The implementation of the Modified Nanbu scheme is now described.

4.3.1 Description of Method

In the original scheme of Nanbu the collision probability for molecule i is given by

$$P_i = \sum_{j=1}^{N} P_{ij} = \sum_{j=1}^{N} \frac{n}{N} \Delta t_m (\sigma_T c_r) \qquad (4.23)$$

where n is the number density in the cell, N is the number of simulated molecules in the cell and the total collision cross section is a function of the relative velocity c_r of molecules i and j.

Over the decoupling time-step Δt_m, each particle is considered in turn as a candidate for collision so that each molecule may only collide once at most over each time-step.

This aspect of the Nanbu scheme gave rise to the adverse effects reported in the preceding sections and made the choice of Δt_m difficult.

The first modification made to the method was to split the time-step Δt_m into L equal intervals $\Delta\tau$. The collision algorithm is then called L times before molecular motion is again computed. This concept was introduced to prove convergence of Nanbu's method, but it has the additional result of allowing each molecule to collide up to L times over the decoupling time-step Δt_m. This clearly allows the initial choice of Δt_m to be made in a less stringent manner although the choice of L still has to be dealt with.

The second modification leads to the expense of the method becoming proportional to the number of simulated molecules rather than to the square of this quantity. An explanation of the modifications may be found in [75]. It is sufficient here to confine ourselves to a description of the implementation.

In Nanbu's scheme the quantity P_i, which is the sum of all the P_{ij} terms, must be less than one for each molecule i, see Figure 4.12(a). On the line [0,1] the subsection defined by $[P_i,1]$ is the probability that the i-th molecule does not collide. The manner in which $[P_i,1]$ is distributed is unimportant and so for convenience each of the P_{ij} are distributed at N identical intervals in [0,1] as shown in Figure 4.12(b). A random number $R \in [0,1]$ is generated and used to define the possible collision partner in the following way:

(i) if $R \in [\frac{j-1}{N}, j/N]$ then j is the possible collision partner.

P_{ij} is then computed using $\Delta\tau$ instead of Δt_m and using the same random number

(ii) if $R > j/N - P_{ij}$ a collision between molecules i and j is calculated.

The calculation of the collision then proceeds in the same manner as for the original method of Nanbu, i.e. only molecule i undergoes change and the molecular properties are updated at the end of each call of the collision algorithm.

Whilst in the original scheme Δt_m must be chosen with care so that P_{ij} is always less than unity, in the Modified method L must be chosen to satisfy

$$n\Delta t_m(\sigma_T c_r)_{ij} \leq L \qquad (4.24)$$

for all i and j. This is clearly a more desirable criterion as the value of L will not affect the motion of the molecules whilst the choice of Δt_m has a direct effect.

Only one P_{ij} calculation is made for each molecule, so that it may be seen that the expense of the Modified Nanbu method is proportional to N thus making it considerably more efficient than the original scheme. However, the increased parallel nature of the Modified algorithm results in a further powerful reduction in computational expense through the application of vector computers. A full description of the vectorization procedure for part of the algorithm is included in Ref. 75.

This new DSMC scheme has been implemented and tested on a CRAY 1-S and utilizes the vectorization facilities available. When analysing a new computational method the choice of test case is important. In order to gain some experience in using the Modified Nanbu method, and to validate the new collision algorithm, the scheme was first applied to the one-dimensional Rayleigh problem. Having established confidence in both the method and the vectorized code, the sonic expansion of nitrogen through a small nozzle was then calculated. With the experience gained from these simulations, a simple method for estimating the number of subdivisions, L, of the time-step Δt_m was subsequently developed.

4.3.2 The Rayleigh Problem

The Rayleigh problem is a well known, theoretical, one-dimensional, unsteady flow problem. A semi-infinite volume of homogeneous gas of density ρ_∞ and temperature T_∞ is at rest above the diffusely reflective plane y = 0. This plane instantaneously acquires a temperature T_w and a velocity in the positive x direction U_w at time t = 0. In the present case T_w and U_w are chosen to coincide with the finite-difference solution of Chu [76] who solved the non-linear Krook equation for the problem. Specifically, U_w is taken as twice the most probable thermal speed of the stationary gas and T_w is taken as 1.6 times the gas temperature.

Results are presented at $t\nu_0 = 5$ and $t\nu_0 = 10$ where ν_0 is the collision rate in the undisturbed gas. The simulation region extends to $20\lambda_0$, where λ_0 is the mean free path

before displacement occurs, and the number of cells employed is 80. As the flow is unsteady, each set of results is averaged by running the simulation from the initial conditions through to $tv_0 = 10$ over a large number of repetitions (typically 200). In this study hard-sphere molecules have been employed and the initial configuration follows that of Bird [17, Appendix G] .

In this problem the surface properties at the diffusely reflecting plate are also of interest. Bird [17, p.152] calculated a number of time independent collisionless properties and claimed that his DSMC results could be extrapolated to these values. Specifically, number flux, pressure, shear stress and heat flux are investigated. However, due to the relatively small number of cells employed, the resolution of Bird's calculations near to the wall were not conclusive. To investigate this phenomena in more detail a larger number of flow cells has been employed in these simulations.

Calculations were made with both Bird's time counter method and the Modified Nanbu simulation scheme. The most efficient value for L in the Modified method was found to be three. Employing larger values gave consistent results with increasingly longer execution times. Smaller values gave unsatisfactory results. The Modified Nanbu calculations required about 20% more processing time than that for the TC method.

Flowfield results for number density, temperature, and the velocities in the shear and normal directions are shown for the two methods together with Chu's calculations in Figures 4.13-4.16. Excellent agreement exists for the two DSMC techniques. The main deviation of the Monte Carlo results from Chu's calculations occur for the normal velocity. It is interesting to note in this respect that the results obtained with the Modified Nanbu method seem to show an improved correspondence with the finite difference solution than do those obtained with the TC scheme.

It is certainly true that the Modified Nanbu method produces results which are consistent with Bird's calculations, thus indicating that the violation of conservation of energy and momentum at the molecular level does not seem to have an adverse effect on the results. In addition, the calculated surface properties agreed well with those of Bird and the increased number of cells confirmed Bird's extrapolations.

4.3.3 Sonic Expansion

Having established confidence in the Modified method through the one-dimensional experiments it was decided to re-investigate the two-dimensional flow discussed previously. It would then be possible to assess the Modified method against both Bird's TC and Nanbu's original schemes. In addition, these calculations include the transfer of energy between internal modes using the Larsen-Borgnakke [53] phenomenological model. It is of great importance that such aspects of the DSMC method are proved to function correctly within the structure of the new scheme. This model is implemented in the usual manner in that the total collisional energy of the colliding molecules is used to sample post-collision values from local equilibrium distribution functions. In keeping with the general concept of the Nanbu algorithm, only one molecule undergoes change as a result of each inelastic collision calculated. In the present study, the collision number is assumed to be constant throughout the flowfield and has a value of 5. Calculations including transfer of internal energy using the original Nanbu method have also been generated for a true comparison.

Once again the effect of different collision models was investigated using the Variable Hard Sphere (VHS) formulation of Bird [50]. In the present work it was of particularly interest to discover the relationship between the value of L and that of ω. In particular, for direct comparison with the results presented in the previous Section, the values of ω investigated were $\omega = 0$, 0.24, and 0.5. An efficient value of L was discovered through a series of numerical experiments. For each value of ω chosen an estimate of the initial value for L was found. The Modified algorithm was run and results averaged over the same number of loops as for the simulation which employed the TC method. The calculations for the two methods were then compared. In particular number density and translational and rotational temperature contours together with the collision rates in the various regions of the flowfield were analysed.

If good agreement in the results was found then the value of L was reduced until the calculations for the two methods began to diverge. Alternatively, if the results for the initial value for L did not agree then L was increased until satisfactory results were obtained. In this manner a correspondence between L and ω was obtained. In addition, the collision probability distribution function was extracted from the Modified Nanbu calculations. A typical plot is shown in Figure 4.17. It should be noted that

a run which incurred a significant fraction of collisions whose probability exceeded unity also gave poor agreement with the time counter calculations.

Results for density and translational temperature contours are shown in Figures 4.18 and 4.19 for typical calculations. It can be seen that good agreement exists for the two methods. The rotational temperature contours are plotted in Figure 4.20. It is clear that the energy exchange model has been successfully incorporated into the Modified Nanbu scheme. The large degree of thermal nonequilibrium in the expansion is highlighted in Figure 4.21 where both the translational and rotational temperature contours obtained from the Modified Nanbu simulation are plotted.

In addition to providing good agreement, it was found that the computational cost of the new method was up to eight times faster than the original Nanbu scheme, and just 25% more expensive than the TC method of Bird. The relative CPU times required for these calculations using the TC, Nanbu, and Modified Nanbu schemes, for the three values of ω investigated are shown in Table 4.4. These findings appeared to support the claim of Nanbu [66] that the Modified method should be considered seriously as an alternative simulation method to the TC scheme of Bird.

It is clear that the ability to choose L rather than having to alter Δt_m is much preferable. It is concluded that the Modified Nanbu Direct Simulation method may be used to solve engineering problems providing a suitable value of L is determined. To avoid unnecessary computational cost it is clear that a method of determining L from the initial flow conditions is desirable. Such a method is now described.

4.3.4 Approximate Method for Calculating L

The determination of an effective value for L in the Modified Nanbu scheme through numerical experimentation is a very expensive procedure. It is clearly desirable that a value for L should be predicted from the initial flow properties prior to simulation. A description of a simple method developed by the author for prescribing L now follows.

Consider the form of Eqn.(4.23) for the VHS collision model

$$L \geq n\Delta t_m \sigma_{ref} c_r^{1-2\omega} [m_r/\{2(2-\omega)kT_{ref}\}]^{-\omega} \qquad (4.24)$$

The number density may be replaced by N / V where V is the volume of the current cell. For a particular flow problem, an estimate of the maximum value of the expression in Eqn.(4.24) is required. In particular the maximum value of

$$nc_r^{1-2\omega} \equiv \frac{N}{V} c_r^{1-2\omega} \tag{4.25}$$

must be found. In the range of operation of ω, i.e. $\omega \in [0, 0.5]$ the expression $1 - 2\omega > 0$ so that the maximum value of c_r coincides with that of $c_r^{1-2\omega}$. When $1 - 2\omega = 0$, the expression in (4.25) is constant, so that in this case the following analysis is unnecessary.

The thermal velocities u′ of colliding molecules are assumed to have a Maxwellian distribution given by the temperature T in each cell, i.e.

$$f(u') = \frac{\beta}{\sqrt{\pi}} \exp(-\beta^2 u'^2) \tag{4.26}$$

where $\beta^{-1} = \sqrt{2kT/m}$ is the most probable thermal velocity and m is the molecular mass. Hence the maximum value for the total velocity in any one direction may be approximated by

$$u_{max} = U + 3\beta^{-1}$$

and the minimum velocity by

$$u_{min} = U - 3\beta^{-1}$$

where U is the component of the stream velocity.

It should be noted that in a Maxwellian distribution an argument of 3 accounts for 99.99% of probable velocities and is the usual cut-off value used when sampling from such a distribution.

The maximum value for the relative velocity between two colliding molecules in any one direction is then given by

$$(u_r)_{max} = (U + 3\beta^{-1}) - (U - 3\beta^{-1}) = 6\beta^{-1}$$

An approximate value for the maximum relative velocity calculated over all three components is now

$$(c_r)_{max} = [(6\beta^{-1})^2 + (6\beta^{-1})^2 + (6\beta^{-1})^2]^{1/2} = (108)^{1/2}\beta^{-1} \qquad (4.27)$$

Substituting into expression (4.25) reveals that the maximum collision probability occurs at the maximum value of

$$\frac{N}{V}[\sqrt{108}\,\beta^{-1}]^{1-2\omega} \equiv \frac{N}{V}[\sqrt{108}\,(2kT/m)^{1/2}]^{1-2\omega} \qquad (4.28)$$

It is therefore essential that the maximum values of N and T be estimated before commencing the Monte Carlo simulation. In the case of the Rayleigh problem these parameters may be obtained from Chu's solutions. The other necessary values may be obtained from initial conditions and substitution into Eqns.(4.28) and (4.24) results in $L > 2.1$ which is in good agreement with the value of $L = 3$ obtained by experiment.

In the calculations for the sonic expansion the conditions at the nozzle exit are used to determine L as both N and T have their maximum values at this part of the flowfield. The full expression for the determination of L is

$$L \geq \Delta t_m \frac{N}{V}\left(\frac{216kT}{m}\right)^{0.5-\omega}\sigma_{ref}[m_r/\{2(2-\omega)kT_{ref}\}]^{-\omega} \qquad (4.29)$$

Thus it can be seen that the choice of ω will directly affect the value of L required to ensure that the Modified algorithm functions correctly.

The calculations made at the nozzle exit using this equation together with the values of L found by numerical experiment are shown in Table 4.5. The expression is plotted as a function of ω in Figure 4.22.

It is clear that excellent agreement exists between the values, so that it is felt that an effective value for L may be obtained using this simple method for any given conditions. It has been suggested to the author that a better approximation for the

maximum relative velocity may be obtained from the following equilibrium distribution function

$$f(c_r) = \frac{4m_r^{3/2}}{\sqrt{\pi}} (2kT)^{3/2} c_r^2 \exp\left(- \frac{m_r c_r^2}{2kT} \right) \qquad (4.30)$$

This function is also plotted in Fig. 4.22. It is immediately obvious from this plot that the expression given by Eqn.(4.29) gives a much better correspondence to the results of the numerical experiments.

For large engineering problems in which there are large differences in local mean free path at different points in the flowfield it is necessary to employ different decoupling time-steps. In such problems it will also be necessary to calculate different values of L for each of these flow regions.

It should be noted that the large values of L required for when $\omega < 0.25$ suggests that in many cases the particles should collide several times over Δt_m. This emphasizes the improvement made to the Nanbu method by the subdivision of the decoupling time-step.

The usefulness of the Modified Nanbu Direct Simulation Monte Carlo method has been illustrated in the preceding Sections. This method offers great improvements on the original scheme of Nanbu both in terms of performance and implementation by allowing the decoupling time-step to be split into a number of L equal subdivisions.

The method has successfully predicted results for one and two-dimensional flows with additional computational costs of less than 25% compared with those incurred with the TC method of Bird. It should be noted, however, that the parallel nature of the Modified algorithm may lead to further reductions in computational effort. Results for diffuse reflection from a hot surface and for internal energy transfer are found to be consistent with those of Bird.

The statistical fluctuations inherent in the two methods should also be considered. In the comparative studies discussed above it is always assumed that each of the DSMC schemes converges towards a steady state in the same identical fashion. This aspect of the schemes is previously unproven. The next step in the assessment of the DSMC

techniques therefore involved a detailed analysis of the statistical fluctuations associated with the various methods.

Table 4.4

Problem	Coll. Model (ω)	CPU Relative to Bird		
		Bird	Nanbu	Mod. Nanbu
1-d	0.00	1.000	-	1.193
2-d	0.00	1.000	4.341	1.235
2-d	0.24	1.000	7.565	1.260
2-d	0.50	1.000	9.822	1.245

Table 4.5.

Problem	Coll. Model (ω)	L calcd	L exprmt
1-d	0.00	2.10	3
2-d	0.00	55.60	50
2-d	0.05	42.64	41
2-d	0.15	24.87	24
2-d	0.24	15.16	15
2-d	0.35	8.17	9
2-d	0.50	3.55	5

4.4 Statistical Fluctuations in DSMC Calculations

Having established the fact that the Modified Nanbu and TC schemes produce consistent macroscopic flow solutions, an investigation into the process by which these averaged solutions are seen to settle has been undertaken. In the previous comparisons, the sample size from which the final results are obtained is assumed to be the same for each technique. This assumption is unqualified. As the Modified Nanbu method calculates the collision probability of each and every simulated molecule in the flowfield, the scheme may be regarded as more deterministic in nature than that of the Time Counter method. This attribute of the scheme may then be expected to

produce results exhibiting less statistical scatter. If this is observed to be true then the use of this scheme would be preferred as acceptable error margins would be attained over a reduced statistical sample size. However, additional fluctuations may be associated with the Modified Nanbu method since energy and momentum are not conserved at the calculation of each individual collision. The investigation reported here was made with reference to such variables as translational and rotational temperature, and flow velocity which are sampled at several points in the flowfield. Both macroscopic averages and molecular distribution functions were analysed.

4.4.1 Results Along the Plume Axis

The flowfield modelled is the sonic expansion of hot nitrogen into a vacuum and is similar to that considered in Sections 4.2 and 4.3. In the following, all distributions and macroscopic values are obtained by sampling the flow quantities over a suitable sample size once equilibrium has been established in the flowfield. Later, the manner in which equilibrium is achieved will also be considered.

Good agreement between the methods for such macroscopic quantities as translational and rotational temperature, density, and velocity vectors has been found in the preceding Sections. In addition to predicting comparable macroscopic properties, it is essential that detailed agreement exists for the molecular properties simulated by the two schemes. Therefore, in the present study, distribution functions for velocity and rotational energy have been calculated at various points in the flowfield. The manner in which these distributions are seen to converge to a steady state is also investigated.

In Figures 4.23(a) and 4.23(b) transverse velocity distributions are shown at two separate points in the flowfield for the two simulation schemes. The first is at a point near to the nozzle exit which is characterised by high density and thermal equilibrium. The distribution in Fig. 4.23(b) was derived at the point near the axis at a distance of 20 exit mean free paths (20 λ_0) downstream of the nozzle exit plane. Significant rarefaction effects are present in this region of the flowfield. The macroscopic velocities are found to be in good agreement for the two methods at both of these flowfield sampling locations. However, it is clear that in the case of Fig.

4.23(b) the distribution provided by Bird's TC method is smoother and more closely resembles those shown in Fig. 4.23(a). The profile derived from the Modified Nanbu scheme indicates that significant statistical fluctuations exist. It is to be noted that all distributions are calculated from identical sample sizes, and that a large number of collisions were calculated before sampling was commenced.

The manner in which the Modified Nanbu method converges to a final distribution at $20\lambda_0$ is shown in Figure 4.24 for rotational energy. The solid line represents the final distribution obtained after completion of the averaging process, whilst the other data was derived at the halfway point of this procedure. Similar results for the TC method are plotted in Figure 4.25 and show a smaller degree of scatter and greater agreement exists for the two cases.

In Figure 4.26, the convergence to steady state of translational temperature is plotted for the two methods. Once again it is clear that the calculations made with the TC scheme are more satisfactory in that the values calculated throughout the averaging process are clustered around the final value.

Figures 4.23-26 indicate that the Modified Nanbu scheme exhibits an increased amount of statistical scatter when compared with calculations made with the TC method. In order to quantify such observations, a series of simulations has been undertaken in which the decoupling time-step Δt_m and the average number of simulated molecules per cell, N, were varied. In the case of the Modified Nanbu calculations, the number of times which the collision algorithm is called over each Δt_m, i.e. L, was also varied. Table 4.6 contains details of the 11 different sets of conditions analysed.

In Figure 4.27 are shown values of translational temperature derived at the same point in the flowfield as used in Fig. 4.23(b) for each of the runs listed in Table 4.6. The results obtained from run 2 are assumed to represent the best DSMC predictions. This assumption is based on a number of previous investigations all of which were found to be consistent with the calculations resulting from the use of these particular parameters. The translational temperature provided by the results of run 2 are bounded both above and below by the generally accepted margin of 1σ error for DSMC calculations, i.e. the percentage error is given by the inverse of the square

root of the sample size. These errors are represented by the two horizontal, broken lines. Each point in Figure 4.28 is generated by storing the value of translational temperature obtained in every cell after each time-step increment throughout the averaging procedure. Then, using the final value obtained at the end of the simulation, the deviation of these interim temperatures about the final mean value is calculated. The horizontal line represents the theoretical value.

TABLE 4.6

Run	Method	N	$\Delta t_m(L)$	Symbol
1	Time Counter	10	0.5	*(1)
2	"	20	0.5	*(2)
3	"	20	0.6	*(3)
4	"	20	0.7	*(4)
5	Mod. Nanbu	10	0.5(2)	+(1)
6	"	20	0.5(2)	+(2)
7	"	20	0.6(2)	+(3)
8	"	20	0.7(2)	+(4)
9	"	20	0.7(4)	O
10	"	20	0.7(8)	X
11	"	20	0.7(16)	⊠

Several important features of the calculations are immediately discernible from these Figures. Firstly, as expected, more accurate results are obtained by increasing the average number of simulated molecules per cell for a given time-step. It should be noted that all results reported are extracted from the same sample size, so that by doubling the number of molecules in each cell, the total number of time increments is thereby halved. This result is supported by Figure 4.28 where the observed statis-

tical scatter about the mean value is also reduced as the number of molecules in each cell is increased. These trends are observed for both simulation schemes. It is also apparent that under the same conditions, the Modified Nanbu scheme shows a larger standard deviation about the mean. In addition, it may be seen that by assuming that run 2 provides the true solution also provides us with the value showing the least statistical scatter.

Examination of Fig. 4.27 for runs 2-4 reveals that for the Bird method, as Δt_m is increased, the results obtained begin to depart from the "true" value. The amount of statistical instability in these solutions is confirmed by the increases observed in the standard deviation, shown in Fig. 4.28.

Let us now consider the results obtained with the Modified Nanbu technique. The study of runs 6-8 allows analysis of the effect of the choice of Δt_m for a fixed value of L. The results obtained in runs 6 and 7 may be regarded as self consistent. However, a further increase in time step leads to a poor value in run 8.

From the previous investigations of the Nanbu schemes it would be expected that smaller collision probabilities would lead to better calculation of the collisional processes. This expected behaviour is assessed in runs 8-11. In these investigations Δt_m is fixed whilst L is increased. It should be remembered that the collision probability in the Modified Nanbu scheme is given by

$$P = \frac{\Delta t_m}{L} \frac{n}{N} \sigma_T c_r \qquad (4.31)$$

Thus it is seen that a lower collision probability is associated with a large value of L.

In run 8, a high deviation about the mean is coupled with a largely inaccurate value for the translational temperature. The margin of these errors indicates that it is necessary to employ a larger value of L in order to improve the Modified Nanbu calculations, i.e. the collision probability has been allowed to exceed unity. Hence, as L is increased, the accuracy and scatter of the calculated results would be expected to improve. Whilst this is immediately observed in the cases where L is increased to values of 4 and 8, a further rise to 16 leads to a higher degree of scatter and a less accurate result. From these results it becomes clear that increased statistical errors

are associated with the Modified Nanbu method for both very high and very low collision probabilities.

It is concluded that L should be chosen such that at least two molecules undergo change over each reduced time step $\Delta\tau$. Such a procedure then increases the opportunity for exact conservation of energy and momentum, i.e. if molecule j is chosen to collide with molecule i, then for conservation of energy and momentum it is required that molecule i is subsequently chosen to collide with j. If the value of L is too large, such that one molecule at most collides over each $\Delta\tau$, then a large degree of scatter will result.

Finally, it should be noted that the standard deviations about the mean of the values obtained with Bird's TC method are certainly lower than those for the Modified Nanbu scheme. The sample size employed in each of the investigations 1-11 was 5000 giving a statistical fluctuation level of about 1.4%. This value is very close to that exhibited by the calculations performed in run 2. The smallest fluctuation level observed with the Modified Nanbu scheme is 1.9% for run 6. If it is assumed that the deviation about the mean may be expressed as a single power of the sample size, then it may be deduced that

$$\sigma = N^{-0.465} \tag{4.32}$$

With this expression, the sample size required to give a deviation of 1.4% is found to be about 9700, i.e. almost double that required for the TC method. In a further investigation, it was found that for a sample size of 10000, the deviation about the mean for the Modified Nanbu scheme had only been reduced to 1.7%. It is therefore concluded that an increased amount of statistical noise is always present in the Modified Nanbu calculations.

Other flow properties examined in this study include rotational temperature and flow velocity. In the case of the internal mode temperature, the trends observed were consistent with those reported above for the translational mode. When the velocity distributions such as that shown in Fig. 4.23(b) were analysed in detail it was found that despite differences in higher moments, excellent agreement existed for the mean

value and the deviation about the mean. Even under the worst conditions, the mean values were found to differ by no more than 4%.

4.4.2 Results Throughout the Entire Flowfield

Having established the existence of differences in statistical fluctuations for the different DSMC schemes at one point, the investigation is completed with an analysis of the entire flowfield. Such a study will inevitably produce a very large volume of data. The interpretation of such data has been greatly helped by the application of simple computer graphics techniques.

Of particular interest are the manner in which equilibrium is first established in the flowfield, i.e. the point at which steady state averaging commences, and also the process by which acceptable macroscopic results are attained. In the previous results, an unnecessarily prolonged period was allowed before the sampling of data was commenced. This procedure was adopted in order to avoid any effects resulting in differences between the two schemes during the approach to the point of equilibrium. The set of parameters chosen for the following more exhaustive comparison are those listed in Table 4.6 for runs 2 and 9. These are the conditions which gave the best performance in terms of statistical fluctuations for the TC and Modified Nanbu methods respectively.

Of the numerous flow properties which may be examined with the DSMC technique, the most relevant in terms of statistical fluctuations are number density and translational temperature. For this study, comparison is made of both unsteady and steady contours for the two DSMC techniques considered.

In DSMC calculations initial equilibrium in the flowfield is usually detected through the number of simulated molecules present in the computational domain. Simulated particles are introduced into the flowfield at a point lying inside the nozzle. When a particle passes out of the region of interest it is removed from the simulation. At each time increment there is therefore a net flux of particles either into or out of the computational domain. At some point of time in the calculation a point is reached at which the effective flux of particles becomes equal to zero, i.e. the number of

molecules entering the simulation is equal to the total number removed over each time increment. This is the stage at which sampling of flow properties is usually begun.

To analyse the manner in which the Time Counter and Modified Nanbu DSMC methods approach equilibrium the unsteady calculations of number density and temperature have been output at several time stations up to the point at which sampling of data commences. The statistical significance of these results is improved by averaging over several complete runs of the simulation.

Once the particle flux number has reached equilibrium the sampling of flow quantities is begun. The degree of statistical fluctuations found in the calculation of number density and translational temperature has also been analysed through the use of computer graphics output. It is commonly accepted that fluctuation levels in DSMC calculations are inversely proportional to the square root of the sample size. The aim of the present study is to investigate the validity of this assumption in the various regions of the flowfield and to establish any differences inherent in the two simulation methods. In addition, the manner in which steady results are reached is of interest.

Thus the calculation of number density and translational temperature are output at several points through the averaging process. In addition, output showing the actual statistical fluctuations at all points of the flowfield are processed. This is achieved by calculating the percentage error between the intermediate and the final values of both density and temperature. Once again, any apparent differences in the results observed for the two simulation schemes are of particular interest.

4.4.3 Use of Computer Graphics

The large amount of data calculated in the present study is conveniently examined through the use of computer graphics raster images which have been developed at the IBM UK Scientific Centre, Winchester, England. The results from the DSMC calculations are initially output onto the irregular mesh which encompasses the computational domain. These data points are then mapped onto a regular 256x256 array using a simple interpolation scheme. Each point in this array is then colour-coded to produce a raster graphics image which may be displayed on an IBM 5080 output device. Linear scaling is employed for the temperature contours whilst the rapid

density decay is best examined through use of a logarithmic scale. The output of the statistical fluctuations is again achieved through the use of linear scaling laws.

In the Figures which follow, results are shown at various time stations throughout the simulation. These values indicate the number of times over which collisions have been calculated and, in the case of the steady flow results, indicate the size of the statistical sampling population. As a general rule each time step provides 20 new values in each computational cell throughout the flowfield.

Figure 4.29 shows the unsteady density contours produced as the gas expands into a complete vacuum. Similar plots are found for temperature and these are compared for the two DSMC methods in Fig. 4.30. In the legend, B denotes calculations performed with Bird's TC technique whilst MN indicates the use of the Modified Nanbu scheme. It is clear that the MN contours are less smooth. This indicates that the calculations contain a higher degree of statistical scatter. In addition it was found that the MN contours converged to those produced by the TC method by extending the sampling population.

In terms of the unsteady approach of both density and temperature towards equilibrium, the TC method was found to be noticeably more stable and converged in a smaller number of computations. Thus, the Modified Nanbu method is found to incur additional expense even before the averaging process is undertaken.

Similar phenomena is again observed on examination of the results obtained throughout the averaging procedure. In Fig. 4.31 temperature contours obtained with the two DSMC methods are compared. It is stressed that as time is progressing the statistical sample size is also increasing. The calculations made with the TC method of Bird become smooth over a smaller statistical population than do those obtained with the Modified Nanbu scheme.

This observation is confirmed by the values of the variances calculated for the two methods. Figure 4.32 shows the density variances calculated on the basis of the final values throughout the flowfield for the TC technique. The colour scheme employed is such that as the variances are reduced the images are transformed from blue to dark red. This is clearly observed in Fig. 4.32.

The variances at several time stations are compared for density in Fig. 4.33 and for temperature in Fig. 4.34. It is quite apparent from both these Figures that the variances associated with the TC technique are smaller than those for the Modified Nanbu calculations.

It should be noted that the limited number of results displayed in the preceding Figures are representative of those obtained throughout the simulations.

The application of computer graphics techniques is found to be well suited to the interpretation of the data processed in the present comparative study. The contour images obtained for density and temperature show an increased amount of detail when compared with traditional cartesian graphics output. This allows for better understanding of the phenomena occurring in the simulation methods investigated.

This aspect of the data presentation techniques is of particular importance in the present study. The behaviour of the unsteady flow as the gas expands towards a steady state is better understood through the colour images presented. The differences between the DSMC results are clearly identified from these contour maps. In addition, the relative smoothness of the contours calculated throughout the averaging procedure indicates the increased amount of statistical fluctuations found in the Modified Nanbu results.

The images displaying the actual degree of statistical scatter of the results in the various parts of the flowfield are found to be invaluable in the interpretation of such data. The reduction in the level of statistical fluctuations with the increase in the sample size is vividly indicated through the use of colour contours. It is difficult to conceive of a more suitable medium for the analysis of these important results.

It is concluded that the use of computer graphics in the present application has been a valuable aid in the reduction and understanding of the large amount of data considered. The graphics techniques are particularly useful in the identification of the degree of statistical scatter exhibited by the simulation results.

4.4.4 Discussion

It has been observed with reference to number density, and translational and rotational temperature, that the Time Counter DSMC method of Bird shows less statistical scatter than that found with the Modified Nanbu simulation scheme. Nanbu [77] has previously shown that in his original method the statistical fluctuations are indeed inversely proportional to the square root of the sample size. However, these investigations were carried out in a model cell environment with a large number of simulated molecules and not in the more demanding context of a practical application. It is important to note that in the TC scheme, the fluctuation level is maintained within the theoretical limit. The fluctuations associated with both methods increase as the time-step Δt_m is increased, and decrease as the average number of simulated molecules per cell is increased.

It has also been noted that large statistical fluctuations are associated with the Modified Nanbu scheme when the number of subdivisions of the decoupling time-step is taken to be too large. This is a previously unexpected result. The unsatisfactory fluctuations exhibited by the Modified Nanbu scheme are associated with the regions of the flow where the collision rate is low. Better correspondence to the results obtained with the TC method are achieved in the less rarefied regions close to the nozzle exit.

The different fluctuation levels observed must result from differences between the two simulation schemes. They must therefore originate either in the manner in which collision partners are selected, or in the way in which post-collision values are assigned. It is unlikely that the selection procedure for colliding molecules will have a large effect. In general, it is the pairs of molecules having the largest collision probabilities which will actually be chosen for collision in both simulation schemes.

The fact that energy and momentum are only conserved in the Nanbu schemes for the single particle system will be unimportant when the number of simulated molecules is large. In such cases, a large number of collisions will be calculated and the fluctuations in energy and momentum will be damped out. However, for smaller numbers of simulated molecules, giving rise to only one or two collisions over each $\Delta\tau$, failure to conserve these quantities will become significant.

There are therefore two limitations on the practical use of the Modified Nanbu scheme. If the flow parameters are such that the collision probability of a significant number of molecules exceeds unity, then the type of poor result observed in Section 4.1 may occur. Alternatively, if the collision probability is too small (small Δt_m or large L) then increased fluctuations occur in the calculations due to the lack of conservation of energy and momentum. Bird [78] suggests that the penalty for failing to conserve energy and momentum in Nanbu simulations where the number of simulated molecules is small manifests itself in increased random walk effects.

It is inferred that a minimum number of collisions must be performed to reduce the scatter observed in the Modified Nanbu calculations. This aspect of the DSMC technique has already been noted by Hermina [42] with reference to the TC method. However, it appears that the problem is more acute in the case of the Modified Nanbu scheme. It is therefore concluded that use of the Modified Nanbu method in the solution of large scale problems is quite impracticable. When the complexity of the flow problem is such that a relatively small number of simulated molecules per cell must be employed, as for the sonic expansion calculations presented in this Chapter, then unsatisfactorily large statistical fluctuations occur for the Modified Nanbu scheme. If the available computational resources allow use of larger numbers of molecules per cell then the results produced will be satisfactory for both methods. However, it is evident that the same results can be obtained with the Time Counter method in a fraction of the time by successfully employing fewer molecules. The Modified Nanbu scheme seems therefore to be better suited for use in problems of a more fundamental nature. For example, in cases where a solution of the Boltzmann equation is required and cannot be found using other methods.

On the basis of the investigations reported in this Chapter, the use of the Time Counter method is recommended for engineering applications. The computational penalty that must be payed in obtaining a solution to the Boltzmann equation cannot be justified. In the first place, a flow problem has yet to be found in which a Nanbu-type solution is preferred to that provided by the TC method. Secondly, it should be remembered that it is the molecular gas dynamics of the flow which should govern the solution procedure rather than preference for a particular mathematical model. It is therefore the Time Counter method which is employed in the calculations of plume expansions presented in the following Chapter.

Finally, let us briefly consider the future status of simulations methods. Work on Molecular Gas Dynamics simulation schemes continues most notably at the Universities of Kaiserslautern [79] and Stanford [80]. The group involved in this research at Kaiserslautern are hopeful that it will be possible to develop a completely deterministic scheme. However, for the use of such schemes to become widespread, they must at least compete with the Time Counter method in terms of computational efficiency, and be able to simulate internal energy transfer, chemical reactions, ionization, etc.

For the present, the arguements in favour of Bird's TC scheme are strong, and it is clear that this technique will retain its current level of popularity in the foreseeable future. Indeed, the fact that such a simple algorithm has achieved such a level of success begs the question that perhaps further approximations can be made which will further reduce the computational requirements of the DSMC technique for application to simple flows which do not require simulation of internal energy modes, gas mixtures, and so forth. An example of such a scheme solves the Discretised Boltzmann Equation first examined by Broadwell [81] and recently reexamined at the California Institute for Technology [82]. In this method, large savings can be made both in terms of computer processing and storage requirements by using only integer quantities in the computer code. The errors associated with such procedures are yet to be assessed.

5. APPLICATION OF METHODS TO A SMALL HYDRAZINE THRUSTER

5.1 Physical Considerations

The use of monopropellant hydrazine, which has the chemical formula N_2H_4 , has been widespread now for a number of years. The detailed modelling of the nozzle and plume flowfields produced by hydrazine has however been limited [83,84] until recently. At the DFVLR Experimental Institute for Experimental Fluid Mechanics, Gottingen, F.R.G., a series of workpackages on hydrazine thruster systems has been carried out. This research takes the form of European Space Agency contract work. The modelling of these plumes has previously been restricted to the analytic Simons model described previously. It is therefore the aim to improve our knowledge of such flowfields through the use of both the Method of Characteristics and the Direct Simulation Monte Carlo method which may be regarded as more sophisticated solution procedures.

The application of each of the solution techniques to the isentropic core of a particular hydrazine thruster is described. The DSMC technique has also been applied to flow in the nozzle lip and backflow regions of the flowfield where the use of the continuum methods is not practicable, and experimental investigation difficult. However, let us begin with a discussion on the physical properties of the hydrazine thruster presently considered.

5.1.1 Combustion Chamber

The particular thruster chosen to be modelled in the present work is that manufactured by the German Aerospace company MBB/ERNO with a nominal thrust of 0.5N. The fuel used in this thruster is mono-propellant hydrazine. Under normal conditions, anhydrous hydrazine is a liquid which decomposes in the following manner: [85]

$$N_2H_4 \rightarrow 4NH_3 + N_2 \qquad +336kJ \tag{5.1a}$$

$$4NH_3 \rightarrow 2N_2 + 6H_2 \qquad -184kJ \tag{5.1b}$$

The degree of dissociation of ammonia is a function of the chamber temperature. In terms of the degree of dissociation of ammonia, α, the complete reaction scheme is conveniently written as

$$3N_2H_4 \rightarrow 4(1-\alpha)NH_3 + (1+2\alpha)N_2 + 6\alpha H_2 + (336 - 184\alpha)kJ \tag{5.2}$$

The degree of dissociation for ammonia and the molecular weight of the gas mixture may be given by the following expressions [5]:

$$\alpha = \frac{1649 - T_0}{782} \tag{5.3a}$$

$$M = \frac{96.14}{5 + 4\alpha} \tag{5.3b}$$

where T_0 is the combustion chamber temperature.

The molecular weight and species composition of the gas are plotted as a function of α in Figure 5.1. The degree of dissociation may also be used to determine the ratio of specific heats γ_0 in the combustion chamber. For $\alpha > 0.3$ it is possible to employ the following approximation:

$$\gamma_0 = 1.14 + 0.23\alpha \tag{5.4}$$

The exothermic decomposition of hydrazine in the MBB/ERNO thruster is achieved catalytically. The expansion of the resulting hot gas mixture through a nozzle leads to a specific impulse in the range 200-250s. The propellant is normally stored on board the satellite as a liquid in tanks under the pressure of an inert gas such as helium.

5.1.2 Nozzle Flow

The MBB/ERNO 0.5N thruster is one of the three hydrazine thrusters investigated at DFVLR. The other two are also manufactured by MBB/ERNO and have effective thrust levels of 2N and 5N respectively. The geometries of the three MBB/ERNO thrusters are shown in Figure 5.2. The low thrust level of the 0.5N engine leads to the dimensions of the nozzle being very small, e.g. the exit radius is less than 2.5 millimetres. To aid manufacturing simplicity, and because contouring is not necessary for such a small nozzle, this thruster has a conical nozzle-wall. As the flow has a small characteristic dimension, the Knudsen number is relatively large, (see Eqn.(3.1)). This aspect of the nozzle makes calculation of its exhaust plume more amenable to the DSMC technique.

It may be seen that the other two MBB/ERNO thrusters have contoured nozzles. Such nozzles produce internal shock waves thus complicating the modelling of the flowfield. The contouring of nozzles is undertaken in order to reduce the length, and consequently the weight, of the nozzle by first increasing the expansion of the flow from the throat, and then by turning the exhaust in the axial direction. The bell-shaped nozzle which is the result of such procedures is the shape most commonly used for both rockets and thrusters [86]. Such nozzles may certainly be considered in the future, but for the present the aim is to understand in a better way the simpler conical thruster.

The ratio of the exit to throat cross sectional areas is critical in the performance characteristics of the nozzle. In the design of the nozzle geometry the influence of the boundary layer which forms along the nozzle wall must be considered. In Section 2.2, Eqns.(2.7,2.8) give the thickness of the boundary layer as

$$\delta_E \propto (Re_E)^{-1/2} \tag{5.5}$$

The nozzle exit Reynold's number, Re_E, associated with this thruster is small, i.e. about 2400, thus giving rise to a thick laminar boundary layer. Indeed, the boundary layer accounts for about 30% of the nozzle exit plane. Clearly, the boundary layer is particularly influential in such small thrusters.

The modelling of relaxation and chemical phenomena in the thruster has been undertaken by Kewley [87]. In these calculations one dimensional flow is assumed. A detailed examination of the thermal decomposition of both hydrazine and ammonia is made, with the inclusion of up to 24 separate chemical reactions. Vibrational relaxation is treated through the application of a sudden freeze criterion. The calculations of Kewley show that the chemical state of the gas may be regarded as being effectively frozen throughout the nozzle flow, and presumably in the subsequent plume expansion. In the case of vibration, this is shown to be frozen at a point just beyond the throat of the nozzle. It is therefore concluded that the initial conditions assumed are of great importance. These calculations also found the value of the ratio of specific heats at the nozzle exit to be about 1.37. It should be stressed that Kewley's analysis applies only to the isentropic core of the plume. Investigation of the chemical and vibrational behaviour in the laminar flow near to the nozzle wall, which is at a much greater temperature, may therefore be necessary.

Basic nozzle flow quantities for the 0.5N thruster have been calculated using the one dimensional chemical equilibrium programme of Gordon & McBride [88]. This programme has been extensively modernized by the author to run in FORTRAN 77 on the IBM 3090 at Southampton. The calculations assumed frozen composition during expansion and some typical results are plotted as a function of distance from the throat along the nozzle axis in Figure 5.3.

5.1.3 Expansion Plume

Due to the near zero ambient pressure, p_∞, experienced in orbit, most satellite thrusters operate in underexpanded mode, i.e. the ambient pressure is less than the pressure of the jet at the nozzle exit. In theory, it is clearly possible to reduce the exit

plane pressure of the nozzle by increasing the exit area ratio. From a practical viewpoint, however, a limitation is placed on the mass of the thruster. Whilst operation in underexpanded mode results in non-ideal performance of the nozzle, achieved when the the ambient and exit pressures are equal, such effects are off-set by the increased thrust which results from the pressure difference $p_E - p_\infty$.

Whilst the plume produced by such the 0.5N thruster is certainly simpler than those produced by engines burning solid propellants [18] or bi-propellants [89], the decomposition of hydrazine into ammonia, nitrogen and hydrogen does allow some investigation of any species separation effects. In a similar fashion to the nozzle flow, it is assumed that the collision rates are sufficiently slow to ensure that the chemical and vibrational states are frozen throughout the plume flowfield.

Condensation effects in the expanding gas should also be considered. Due to the large exit area ratio of the 0.5N thruster, very low temperatures are soon experienced in the plume. Figure 5.4 shows saturated vapour pressure curves as a function of gas temperature for the constituent gases. The Figure has been taken from Ref. 39 which employs data from Reference 90. Also included is the pressure curve for an isentropic gas with $\gamma = 1.39$.

In the case of hydrogen, it is clear that condensation will never occur. However, condensation of nitrogen will begin at temperatures lower than about 40K, whilst for ammonia the onset commences at about 150K. It should be noted that the partial pressure of ammonia in the mixture is expected to be of the order of 15% and thus any condensation effects will be minimal. The exit temperature of the nozzle is about 160K, with an exit pressure of 0.012bar, so that it is safe to assume that no condensation occurs in the nozzle flow. However, it is also clear that a finite amount of condensation will occur in the plume flowfield. This phenomena is beyond the scope of the present work.

Finally, the concept of viscosity is considered. The calculation of the viscosity of the gas mixture as a function of the temperature is important in the determination of an effective temperature exponent ω for use in the VHS collision model in the Direct Simulation calculations. The method adopted is that developed by Brokaw [90] and results are plotted in Figure 5.5 for a particular gas composition given by $T_0 = 1100$K. Once again the plot is taken from Ref. 39 and the viscosity behaviour of ni-

trogen is included. As the gradients of the two curves are similar the temperature exponent of the mixture is taken to be equal to that for nitrogen, i.e. ω is 0.24.

In the expansion plume, three distinct areas are identified:

(i) the isentropic expansion of the core,

(ii) the non-isentropic expansion of the boundary layer,

(iii) the nozzle lip flow and consequent expansion into the backflow region.

In the following Sections, calculations made in regions (i) and (iii) are presented for the MBB/ERNO 0.5N hydrazine thruster. Unfortunately, due to restrictions on computational resources, the expansion of the boundary layer could not be adequately treated.

5.2 Analysis of the Isentropic Core

5.2.1 Introduction

Three different techniques commonly employed in the calculation of rocket and thruster expansion plumes are assessed. These techniques vary both in computational expense and in the accuracy and detail of the solutions which they provide. The assessment is made with reference to the plume expanding from a small monopropellant hydrazine thruster and includes comparison with experimental data.

The Method of Characteristics has been applied to a variety of thrusters by Hoffman et al [92,93] using the CONTAM computer programme. Whilst this code has achieved some success for large bi-propellant and solid propellant engines, its boundary layer estimates, particularly for small nozzles, have caused concern. Figure 5.6 shows density contours for the SESSIA 0.5N thruster (described in Chapter 2) which have been calculated by CONTAM. Included in the Figure is experimental data provided by SESSIA. It is clear that whilst in the isentropic core the prediction is consistent, the boundary layer density is about an order of magnitude in error. This plot has been provided by C. Koeck of MATRA Espace, Toulouse, France, to whom

the author extends his thanks. Therefore, in the present work, the Method of Characteristics is only applied to the isentropic expansion of the hydrazine thruster plume.

The Direct Simulation Monte Carlo method is finding increased application to various flow problems, although only a limited amount of calculations have been performed on nozzle and plume flowfields. It is widely accepted that, due to the strong rarefaction effects observed in plume expansion, such problems may be considered amongst the most challenging for this or any other solution technique.

The DSMC method has been applied to the boundary layer expansion of large solid propellant engines by Hueser et al [18,94]. The continuum breakdown parameter is found to be a function of the nozzle dimensions. A plot of the continuum breakdown contour $P=0.04$ for a nozzle exit Mach number of 5 is shown in Figure 5.7 as a function of the nozzle exit radius. The engines simulated by Hueser have a nozzle exit of 0.6m whilst that for the MBB 0.5N thruster is 2.38mm. It is clearly seen that the nonequilibrium problems for large and small nozzles are very different. Whilst in the work of Hueser it is sufficient to calculate only the backflow region, in the smaller nozzle continuum breakdown is seen to occur at a few exit radii along the plume axis. Indeed, it is due to the fact that the MBB/ERNO thruster is so small which enables us, for the first time, to analyse the isentropic core expansion with a realistic DSMC calculation. In previous DSMC calculations of rocket plumes [95], a point source approximation must be made to initiate the flow. These calculations are primarily interested in plume enhancement, which is a far-field phenomenon, rather than detailed impingement analysis.

The method has also been applied by Nanbu [96] and Doo & Nelson [97] to the problem of nozzle flows. In Nanbu's calculations, investigation is made for a nozzle throat varying from 25 to 0.005 times the chamber mean free path, λ. For the 0.5N thruster, the nozzle throat is several thousand times λ so that it is clear that Nanbu's calculations are not of a very practical nature. It should be remembered that the 0.5N thruster has a particularly small throat, so that for larger nozzle throats, the situation is even more problematic.

In the work of Doo & Nelson, the large number of mean free paths throughout the nozzle flow are modelled by employing cells whose dimensions are in hundreds of mean free paths. The errors associated with such assumptions are not discussed, but

cannot be ignored. The DSMC results are compared with a Navier-Stokes solution of the flow, and large disparities noted. The authors report an increased degree of convergence when the cell dimensions in the DSMC calculations are reduced. This phenomena clearly implies that the modelling of nozzle flows is only possible when the cell dimensions are of an appropriate value, i.e. 10λ at the most. As this criterion implies that at least tens of thousands of cells are required for proper modelling, it is impossible for such investigations to be undertaken with current computational resources.

The primary reason for undertaking the calculation of the isentropic core expansion is to assess the validity in employing continuum methods in the flowfield between the continuum and free molecular limits, i.e. in the transition flow regime. It is noted that the more computationally intensive DSMC solution method is the proper technique in this region of the expansion plume. Additional results provided solely by the DSMC calculations such as thermal nonequilibrium effects may also be considered. The consequences arising from the apparent differences in the results obtained with the continuum and discrete particle methods at the free molecular limit are to be assessed in terms of impingement effects.

Before undertaking any calculations, the degree of detail required from the investigation should be balanced against the computational cost involved in processing the results. In the present work, the modelling of combustion processes and the expanding nozzle flow is undertaken in a simplistic manner. The primary focus of the investigation is the expansion of the thruster plume.

The exhaust plume prediction techniques considered in the present work may be regarded as the most popular in common usage. The implementation of these techniques has been described in previous Chapters. The Simons model provides an analytic expression for the density as a function of the position in the flowfield, and therefore incurs little computational expense. To obtain results of good spatial resolution using MOC calculations necessitates a moderate amount of CPU time by comparison. Both these techniques rely on continuum equations so that their use in the transition regime is incorrect.

Although it is certainly the most expensive of the three techniques considered, the DSMC method is the proper technique for calculating flow in the transition regime. In addition the calculations may provide information concerning thermal nonequilibrium and species separation effects. These properties cannot be investigated using continuum methods.

In previous work [15,33], continuum calculations have been used throughout the transition regime and are used to identify the "freezing" surface, i.e. the point at which $P=2$. As stated already, this is quite incorrect. It is the aim of the present work to investigate the errors associated with such procedures by carrying out DSMC calculations throughout the transition regime. In particular, errors encountered with continuum calculations near the free molecular limit are analysed, and the subsequent effects on impingement calculations assessed. It is stressed that calculation is made of free-stream quantities only. Whilst such quantities are generally distorted in the presence of a spacecraft surface, they do provide a useful indicator of the likely impingement effects.

Whilst the Simons model and the Method of Characteristics solution techniques have sufficiently low computational requirements to allow parametric investigations, the same can hardly be said to be true of the Direct Simulation Monte Carlo method. The solution corresponding to the available experimental data is therefore the only solution presented for each of the three modelling methods.

5.2.2 Simons Model Calculations

Details of the prevailing combustion chamber conditions together with the plume gas properties are given in Table 5.1 and have been obtained through the procedures described in Ref. 40. Table 5.1 is on pp. 114-115.

As already stated, a series of experiments on real hydrazine thrusters has been carried out under the auspices of the European Space Agency by DFVLR. The experiments reported to date involve the measurement of heat transfer [98] and Pitot pressure [40] in the isentropic core of the plume. The three MBB/ERNO thrusters described previously have all been investigated. In a recent publication [99], the first

results obtained in the boundary layer expansion of pure gases have been reported. These consist of velocity measurements made with a time-of-flight technique.

For the moment, let us concentrate on the isentropic core of the 0.5N thruster. Direct comparison between experimental and model calculations will be made in the following Sections. It should be noted that modelling of the plumes is made difficult through the inability of the experimentalists to obtain the chamber temperature of the flows investigated. As explained in the previous Section, the chamber temperature effectively determines the gas composition and therefore the ratio of specific heats. In Reference 40 the following constants required by the Simons model calculations have been derived from experimental data for the 0.5N thruster:

Stagnation Pressure, p_0	15.7bar
Stagnation Temperature, T_0	1170K
Viscosity, μ	4.03×10^{-5}Ns/m
Ratio of Specific Heats, γ	1.37
Plume Constant, A	3.0
Limiting Velocity, U_L	2450m/s

For a stagnation temperature of 1170K, the following quantities may be calculated for use in the Simons model:

Dissociation of Ammonia, α	0.613
Mass of Mixture, M	12.904
Plume Constant, A	2.71
Limiting Velocity, U_L	2363m/s

It may be seen that discrepancies occur in the estimation of both U_L and the plume constant. However, these errors are quite small. Results have been obtained with the PLUME code by inputting the experimental constants.

Figure 5.8 shows Mach number contours for the complete flowfield. The outer contour is for a Mach number of 45, and the contour increment is five. The streamline separating the expansion of the isentropic core from that of the boundary layer is clearly discernible. Further results obtained with PLUME will be presented in the

next section where comparison is made with both experimental data and Method of Characteristics calculations.

5.2.3 MOC Calculations

Transverse calculations have been made at the following axial stations: (a) 8 exit radii, (b) 24 exit radii, (c) 32 exit radii, (d) 48 exit radii, and are presented in Figures 5.9(a-d). Included in these Figures are experimental results obtained at DFVLR [40]. The results obtained near the nozzle exit are observed in Fig. 5.9(a) to be unsatisfactory for both calculation procedures. These profiles are obtained in that part of the flowfield where the limiting velocity has not yet been reached. This area is designated the near-field of the expansion and extends to a distance no greater than 20 exit radii along the plume axis [40]. In the remaining three sets of profiles it is clear that the MOC solutions offer greater correspondence to the experimental data. Table 5.2 lists the differences observed between the calculated and experimental data found at the plume axis as a function of axial distance. Two important features become apparent from this analysis. First, it is clear that the MOC and Simons model solutions are found to converge as we proceed along the axis. Simultaneously it is found that the agreement between the experimental data and the MOC calculations diverges further downstream.

The barrel shock observed in the experimental data is a consequence of the presence of a finite background pressure in the laboratory and indicates the influence of the boundary layer.

The primary object in obtaining the solutions to expansion plumes is to enable prediction of possible impingement effects. In particular, the calculation of the forces resulting from the interaction of the plume with a spacecraft surface is of interest. The flow quantities relevant to such analysis are density, velocity and to a lesser extent temperature. The results presented in the isentropic core of the plume expansion for the MBB/ERNO 0.5N thruster show that the important properties are predicted by the MOC calculations to be within about 13%. The results obtained with the Simons model do not correspond so well to the experimental data. However, the fact that the Simons model is more readily and efficiently applied to the calculation of the

effects of impingement with complex spacecraft structures suggests that it is a useful design tool.

Calculation of the two contours identifying the beginning and the end of the transition flow regime has also been undertaken. As the Simons model is found to be less accurate, the contours were found using MOC calculations and are displayed in Figure 5.10. The point at which the continuum breakdown contour intersects the plume axis is found to lie at a distance of 22 exit radii downstream of the nozzle and is thus beyond the near-field. Also, the MOC calculations which best correspond to the experimental data, Fig. 5.9(b), are observed to lie close to the continuum regime. We may therefore be confident that the continuum limit has been accurately identified.

Figure 5.10 also demonstrates that the experimental investigation of Ref. 81 which reaches a maximum point downstream of 48 exit radii, covers a small fraction of the total transition flow regime. The trends observed in Figs. 5.9 and Table 5.2 for the correspondence between calculated and experimental data indicate that significant errors may be associated with the determination of the location of the free-molecular limit. This aspect of the calculations is investigated using the discrete particle approach.

Although temperature contours for the flow may be obtained with both methods, the nonequilibrium effects associated with the breakdown of continuum flow cannot be evaluated with either. In addition, species separation effects cannot be investigated. The Direct Simulation Monte Carlo method is the only solution technique which provides such information. It should also be stressed that it is the most appropriate method for modelling the transition regime. It is also assumed that the DSMC method will model the nonequilibrium effects expected at the nozzle lip, thereby solving the boundary layer expansion in a more accurate way. The application of this method is discussed in the following section.

5.2.4 Application of the DSMC Method

In the calculation of the hydrazine thruster plume, the flow is taken to be axisymmetric. As the chemical and vibrational states of the flow are assumed to be

frozen, these phenomena are not included. Exchange of energy between translational and rotational energy modes is simulated through the use of the Borgnakke-Larsen phenomenological model [53]. Details of the initial species concentrations of hydrogen, nitrogen, and ammonia, together with their relevant molecular properties, are listed in Table 5.1.

The flow domain to be simulated is described by the flow limits shown graphically in Fig. 5.10. Having identified the transition regime the construction of a suitable computational grid must be considered. This has been accomplished by using the continuum MOC calculations to make local estimates of mean free path. The grid employed is shown in Figure 5.11 and spans the isentropic core of the expansion plume as predicted by the Simons model. This region of the flowfield was also found to be unaffected by variations in the laminar velocity profile assumed for the MOC calculations. Molecules are released into the simulation region across both the continuum breakdown locus and the upper boundary of the grid. The initial flow properties are sampled from the equilibrium distribution functions appropriate to the local flow conditions provided by the continuum solutions. The upper boundary flow conditions, initially provided by the MOC solution, are periodically updated from the DSMC calculations. The distributions of number density and total temperature which are initially input into the DSMC calculation are shown in Figures 5.13 and 5.14 respectively.

The large differences in mean free path and collision rate in the extremities of the flowfield are treated through the use of different physical scaling factors in accordance with the Removal/Duplication method described in Section 3.1.4.1. Molecular weighting factors are also employed to improve the statistics of the collisions involving nitrogen and ammonia which appear in smaller quantities than the more dominant hydrogen. Procedures enabling the variation of all weighting factors were at first included in the simulation. These were to be implemented if the number of simulated molecules of a particular species was found to exceed a specified number. However, in preliminary investigations, it was found that the initial grid was adequate enough to dispense with the need for any adjustment to the original weights.

The DSMC results are obtained from large sample sizes (in excess of 10,000 molecules for each data point) which are regarded as large enough to make statistical fluctuations negligibly small.

5.2.5 Results and Discussion

In Figure 5.14, the number densities obtained with the DSMC and MOC techniques along the plume axis are plotted. A logarithmic scale is used for the density whilst the grid cell number is employed along the abscissa for better plotting resolution. It is seen that small differences in the results are discernible once we move away from the near-continuum flow. Figure 5.15 shows the temperature calculations which are again taken along the plume axis. The degree of thermal nonequilibrium in the expansion may be observed in the DSMC results which manifests itself in the divergence of the translational and rotational energy modes. This behaviour is to be expected in the transition flow regime in which the collision rate is too slow to maintain equilibrium. The rotational temperature cools at a slower rate than that for the translational mode and is observed to "freeze". The translational temperature initially experiences a large degree of cooling before freezing occurs. The DSMC total temperature is initially observed to agree with the MOC result. Up to the point at which the rotational temperature freezes, the DSMC total temperature is cooler than the corresponding continuum result. Thereafter, the discrete particle result experiences little further cooling and thus becomes significantly larger than the MOC predictions.

Let us now consider the angular flow property distributions at various radial distances from the nozzle exit plane. In Figure 5.16 the ratio of the number densities calculated with the two techniques (MOC/DSMC) is shown as a function of polar angle at a distance of 48 exit radii. The difference between the two sets of results varies from about 13% at the axis to 9% at the upper boundary. The DSMC densities are larger than those obtained with MOC. For direct comparison with the experimental data, these density calculations have been converted into Pitot pressure and are plotted in Figure 5.17. It is clear that the DSMC results more closely resemble those obtained in the laboratory. It is therefore concluded that differences observed in the continuum and DSMC calculations are due to inaccuracies associated with the MOC solutions in the transition flow regime.

It is seen that the DSMC solution gives better correspondence to the experimental data than does MOC. As regards temperature prediction, the DSMC calculations are presumed to be more accurate. This is reasonable as the freezing of the energy

modes is accounted for whereas the MOC solutions have assumed that equilibrium exists even in the most rarefied regions of the plume. The behaviour of the various temperatures along the same radius is plotted in Figure 5.18. The point on the axis at 48 exit radii is close to that at which the rotational temperature is observed to freeze. It is clear from Fig. 5.18 that the rotational temperature is frozen for all polar angles. The same is not true for the translational mode which undergoes significant cooling before freezing occurs at a polar angle of about 180. The cooling of the translational mode results in the total temperature solution obtained in the DSMC calculations being cooler than that predicted in the MOC results.

The MOC and DSMC results for number density and temperature are again compared in Figures 5.19 and 5.20 for a radial distance of 150 exit radii. In this case, the difference between the densities predicted remains constant at about 15%. Figure 5.20 clearly demonstrates that both the rotational and translational modes are now frozen for all angles. There is no region of translational cooling, and the DSMC total temperature remains significantly greater than the MOC results.

For the small dimensions of the MBB/ERNO thruster, most impingement studies will involve the use of flow properties derived at the free molecular limit. This is located at about 68 centimetres from the nozzle exit. The ratio of number densities and total temperature obtained with the two solution techniques are plotted in Figure 5.21 as a function of polar angle. It is evident that significant differences exist in the flow properties themselves, but we are more interested in how such differences relate to the calculation of impingement quantities.

As an illustrative example, let us consider the heat transfer and total drag force on a flat plate in free molecular flow. Schaaf & Chambre [100] give the heat transfer as

$$Q \;\alpha\; \rho\, U\, St' \tag{5.6}$$

where the modified Stanton number for a diffuse plate at angle of attack θ is given by

$$St' = \frac{1}{4\sqrt{\pi}\,S}\{\exp[-(S\sin\theta)^2] + \sqrt{\pi}\,S\sin\theta[1 + \mathrm{erf}(S\sin\theta)]\} \tag{5.7}$$

In the same reference, the following expression for total drag force is given as

$$D \alpha \rho U^2 C_D \tag{5.8}$$

where the drag coefficient is

$$C_D = \frac{2}{\sqrt{\pi} S} \{\exp[-(S\sin\theta)^2] + \sqrt{\pi} S\sin\theta(1 + 0.5S^{-2})\mathrm{erf}(S\sin\theta) + \pi S/S_w \sin^2\theta\} \tag{5.9}$$

In Eqns.(5.7) and (5.9), the molecular speed ratio is

$$S = \frac{U}{(2kT/m)^{1/2}} \tag{5.10}$$

and S_w is that determined by the surface temperature. Thus, it may be seen that both the heat transfer and total drag are effectively functions of velocity, density, and total temperature. Equations (5.7) and (5.9) are plotted for the MOC results at the free molecular locus in Figures 5.22 and 5.23 respectively.

Close scrutiny of the MOC and DSMC calculations reveals that differences in the predicted flow velocities are negligible. From Eqns.(5.6) and (5.8) it is clear that any differences in the density solutions are directly translated into differences in both heat transfer and drag force. Therefore, along the free molecular locus, there is a 20% error in the MOC estimates of both these quantities due to the application of this continuum technique in the transition flow regime.

Let us now turn our attention to the effect of the observed differences in total temperature. Figure 5.24 shows the ratio of calculated Stanton number as a function of impingement angle for the two methods. It is evident that significant differences of greater than 50% arise at very small angles. For angles larger than about 60, the errors associated with the MOC calculations have a negligible effect. A similar trend is observed in Figure 5.25 in which the ratio of the two drag coefficients is plotted. Once again the largest disagreement occurs at small angles of attack. It is worth noting that the most significant errors found for the impingement properties occur for the smallest values of these quantities. Nevertheless, it is evident that important errors arise through the use of the continuum results. These are particularly evident

close to the plume axis where the differences exceed 50%. It should be noted that such impingement angles are likely to occur on typical spacecraft configurations, e.g. along solar arrays.

Such errors have important implications in the assessment of onboard fuel budgets and arise as a direct consequence of applying continuum equations in the transition flow regime. It is concluded that careful consideration should be given to the use of the more expensive DSMC technique where accurate assessment of thruster plume impingement is required by the design specifications of the spacecraft.

The local flow angle is another quantity which directly affects the calculation of impingement effects. The small disagreement found for the two sets of solutions was again found to have a negligible effect on both heat transfer and drag calculations. Species separation effects may also be investigated with the DSMC technique. In the present application, these were found to be minimal due to the fact that the stream velocity is very much larger than the thermal velocities associated with the molecular species present in the flowfield.

For completeness, the solutions of the Simons model and Direct Simulation have also been compared at the free-molecular limit. The results are found to be similar to those shown in Fig. 5.22. The disagreement in number density is calculated at about 28%. The values for temperature and mean free path are very close to those obtained in the MOC calculations. These results are to be expected from the trends observed in Table 5.2. They show that at the point where the flow becomes collisionless, little additional error is incurred by adopting the more economical Simons model instead of the Method of Characteristics.

Table 5.1

Stagnation Conditions		Exit Plane Properties	
Pressure (Pa)	1.57×10^{6}	Mach Number	5.78
Temperature (K)	1170	Specific Heat Ratio	1.37
Viscosity (Ns/m)	4.03×10^{-5}	Molecular Weight	12.90

Gas Properties

Molecular Species	Mole Fraction	Molecular Weight	Collision Diameter	Degrees of Freedom
H_2	0.4933	2	2.98×10^{-10}m	2.00
N_2	0.2987	28	4.07×10^{-10}m	2.00
NH_3	0.2080	17	4.86×10^{-10}m	3.25

Table 5.2

Axial Station (exit radii)	Ratio of Results (MOC/Experiment)	Ratio of Results (Simons/Experiment)
8	0.9142	0.6223
24	0.9925	0.7490
32	0.8973	0.7538
48	0.8712	0.7664

5.3 Analysis of the Nozzle Lip Region and Backflow Expansion

5.3.1 Introduction

An increasing amount of interest is being shown in the accurate determination of the backflow regions exhausting from small satellite thrusters. This interest has partly arisen as a result of the growing requirement for improved budgeting of on-board satellite resources, and partly as a consequence of the deleterious effects of thruster plume impingement encountered on several missions. Both experimental [10,15] and theoretical [15,97] investigations have been undertaken. In the prediction of possible

impingement occurring between the plume backflow and the surfaces of the spacecraft, the flow near the nozzle lip has been shown to be of great importance. In References 10 and 97, it is reported that the flow properties near the nozzle lip do not correspond to those predicted using conventional Navier-Stokes boundary layer techniques. It is therefore necessary to calculate the flow in greater detail.

In the previous Section, the results of calculations in the isentropic core were discussed, and it was found that little species separation occurred. Whilst the differences provided by the various techniques considered were clearly of some importance in the isentropic core, larger and more significant departures between discrete particle and continuum calculations are to be expected in the boundary layer expansion and backflow regions of the plume where thermal nonequilibrium effects are predominant. Indeed, the use of continuum methods in such flows has been shown to be inappropriate [94]. In the following Section, the calculations made in the laminar boundary layer and in the region around the nozzle lip of the MBB/ERNO 0.5N hydrazine thruster. Similar flowfields have been examined previously for a large solid rocket motor [94] and for the flow of argon out of a small tube [101]. The present application differs in that a large, multi-species, laminar boundary layer must be tackled.

In this study calculations are made solely with the DSMC technique. Whilst the Simons model has been reformulated, in Section 2.3, to cater for nozzles such as that presently considered which have large exit Mach numbers, the simplifying assumptions inherent in the method are such that no backflow beyond a limiting angle of about 56° for the 0.5N thruster is to be expected. This is certainly not the case and evidently represents a serious limitation on the use of this solution technique. As the MOC technique is derived from the Euler equations, its application to viscous flow should always be viewed with extreme caution. MOC calculations of nozzle boundary layers are usually performed by assuming a characteristic velocity profile at the nozzle exit [15]. The errors associated with such a procedure may be acceptable for large thrusters which exhibit small turbulent boundary layers at the nozzle exit. However, it can be stated with some certainty that for small nozzles possessing large laminar boundary layers the technique is particularly inappropriate.

It is now generally recognized that the DSMC method is the most reliable solution technique for calculation of plume expansion around a nozzle lip and into the back-

flow region. It is the only method which properly deals with the thermal nonequilibrium and species separation effects which are so important in such flows. The application of this technique to the boundary layer of the hydrazine thruster is now considered.

5.3.2 Calculations

In the current work the calculation of the boundary layer is begun inside the nozzle lip. In Figure 5.26 the computational domain is shown. Due to the dramatic rarefaction effects experienced by the gas as it expands around the nozzle lip (it is anticipated that the density will decrease by several orders of magnitude), the domain is divided into a number of separate regions. In each of these regions, separate physical scaling factors and decoupling time-steps are employed. The flux of molecules across cell boundaries is always exactly matched. The exact grid structure, together with the various time-steps and weighting factors employed, have been obtained through a number of preliminary numerical experiments.

Whilst these procedures have previously been successfully applied to similar flows [94], they are found to be extremely inefficient. The number of simulated molecules entering the backflow region is small. In order to accumulate sample sizes large enough to reduce the statistical fluctuations always encountered with the DSMC method a large number of calculations of the entire flowfield must be performed. This means that a significant amount of computational effort is wasted in unnecessary recalculation of the more dense regions of the flowfield. An alternative set of procedures which proposes to improve the computational efficiency of such flows has recently been suggested by Jan & Guernsey [51] and has been described in Section 3.1.4.3. Unfortunately, their method has not yet been validated.

One of the primary aims of the present work is to assess the influence of several basic assumptions pertinent to the calculation of the flow. In Refs. 94 and 101, the initial velocity, density and temperature distributions inside the nozzle are provided by continuum calculation methods. Whilst the effect of nozzle geometry is considered in Ref. 101, the sensitivity of the results presented to the assumptions initially made is not analysed in these publications. In the work reported herein, the effect of the initial distributions together with the gas/surface interaction model assumed, are in-

vestigated with reference to the flowfield properties. For such flows, where experimental investigation is expensive if not altogether impractical, it is felt that greater understanding of the physically occurring processes is gained through such parametric examinations.

The chamber conditions for the thruster and the relative species concentrations in the boundary layer are identical to those considered in Section 5.2 and are listed in Table 5.1. In the following calculations, both the vibrational and chemical states of the gas are assumed to be frozen. The effect of such assumptions are not considered in the present analysis.

As a suitable boundary layer code was not available to us, a flat plate velocity profile, a uniform temperature profile, and a typical laminar boundary layer density profile were initially assumed for input into the DSMC code. The nozzle wall was taken to be a diffusely reflecting surface with complete energy accomodation corresponding to the boundary layer flow temperature at the surface.

A number of solutions to the flowfield were then generated in which the initial assumptions were varied. Details of the conditions considered are listed in Table 5.3. The nonuniform profiles assumed for velocity, density and temperature are shown in Figures 5.27-29. The results are plotted such that a boundary layer position of 1 corresponds to the nozzle wall, whilst position 0 lies at the inviscid edge of the boundary layer. The sensitivity of the solutions has then been characterised by examination of the flow properties in the nozzle exit plane and along lines AB and CD of Figure 5.26. In the exit plane, we are interested in all of the basic flow effects such as thermal nonequilibrium and velocity profile. In the outer regions of the flowfield, attention is confined to those quantities which affect impingement analysis. The properties of most significance in terms of impingement potential are dynamic pressure, relative species abundance, and flow angle.

5.3.3 Results in the Nozzle Exit Plane

The flow conditions in the nozzle exit plane are first considered. Figure 5.30 shows the exit plane velocity profiles obtained with the six initial conditions investigated. The profiles obtained for Runs 1, 2, and 3 are similar. The result taken from Run 4

indicates that some influence exists for the diffuse wall temperature assumed. The use of specular wall reflection (Run 5) leads to higher flow velocities in regions close to the nozzle. Finally, it may be observed that the relationship between the profile obtained in Run 6 and that from Run 3 is similar to that found between the initial velocity input conditions plotted in Fig. 5.30. In general, it is found that the influence of the assumed wall conditions extends some 60% from the nozzle wall into the laminar boundary layer.

The degree of thermal nonequilibrium in the nozzle exit plane may be assessed by examination of Figure 5.31 in which the temperatures of the various thermal modes obtained in Run 3 are plotted. It is found that close to the inviscid boundary, the modes are in thermal equilibrium. However, as we proceed towards the nozzle wall, significant departure between the translational and rotational modes is observed. At the same time, good agreement is found between the axial and radial translational modes for most of the exit plane.

The relative concentrations by number density of the various species remains invariant throughout the majority of the boundary layer for five of the runs investigated. The exception occurs in Run 4, the results for which are shown in Figure 5.32. The condition investigated sets the wall temperature lower than that of the gas (see Table 5.3). At small distances a rather unexpected phenomenon is observed. The concentration of the lightest constituent (hydrogen) is seen to fall whilst those for ammonia and nitrogen both increase. This result is presumed to arise from thermal diffusion effects which have recently been discussed by Bird [102]. The trend of this effect is similar to that first noted in the calculations of Moss, Cuda & Simmonds [103]. In their calculations, the concentration of heavier species was observed to unexpectedly increase at a small distance from a cold surface suffering impingement from a hot gas.

5.3.4 Results in the Region Forward of the Nozzle Lip

Let us then turn our attention towards the flow properties along CD. This part of the flowfield originates in the expansion of the boundary layer. Thus as we move along CD the effect of the nozzle wall should decrease. In Figure 5.33 dynamic pressure is plotted along this line for each of the simulations undertaken. It is clear that whilst

Runs 3,4,5 and 6 give quite good agreement, the results of Runs 1 and 2 are markedly different. Such trends are hardly surprising as the introduction of a temperature profile at the nozzle wall would certainly be expected to influence the flowfield structure. It may be concluded from this Figure that larger impingement forces are associated with a boundary layer having a temperature profile which gives rise to high values near the nozzle wall.

It is interesting to note that the introduction of specular reflection (Run 5) at the nozzle wall seems to have little impact on the dynamic pressure calculated. However, examination of Figures 5.34(a)-(c) in which the relative species concentrations by number density are shown, suggests that this is not in fact the case. In these Figures it is evident that the results of Run 5 more closely resemble those given under the conditions initially prevailing in Runs 1 and 2. Careful scrutiny of the calculations revealed that the assumption of specular reflection altered both the density and velocity fields in such a way that these effects were cancelled out in the determination of dynamic pressure.

Inspection of Figs. 5.33 and 5.34 reveals that the assumed velocity profile has a limited effect on those properties analysed along CD. In Figure 5.35, the relative abundance of each species is plotted from the calculations of Run 3. It is noted that as the nozzle lip is approached, moving from D towards C, the fraction of hydrogen present in the gas increases rapidly. In addition, the concentration of ammonia is seen to rise above that of nitrogen. Thus it is clear that, unlike the calculations performed in Section 5.2, separation effects are found to be of great significance in the expansion of the boundary layer. The trends of these calculations are as would be expected and reflect those found by Hueser et al [94].

The distribution of flow angle along CD is plotted in Figure 5.36. As little difference in any of the solutions was discernible, the result from Run 3 only is shown. Thus it is found that the flow angle is unaffected by the initial conditions assumed. For completeness, the degree of thermal nonequilibrium is considered by examination of Figure 5.37 in which the translational, rotational, and total temperatures are plotted as a function of distance along CD. The results shown are those obtained in Run 3. By comparison with Fig. 5.31 it is clear that in expanding around the nozzle lip the translational and rotational modes have experienced significant departure. Indeed, the region just in front of the nozzle wall is characterised by strong rarefaction effects

which give rise to the observed nonequilibrium phenomena. Whilst the contours in Fig. 5.37 are relatively flat, the flow should not be regarded as frozen. In the direction normal to CD, significant temperature gradients exist .

5.3.5 Results in the Backflow Region

Finally, let us consider the properties along AB which lies in the backflow region of the plume expansion. In Figure 5.38 the dynamic pressure is again plotted. It is evident that each set of initial conditions gives rise to a unique profile, at small distances from the nozzle lip. These plots demonstrate that the introduction of a temperature profile leads to an increased amount of backflow. The results suggest that the temperature specified for the diffuse wall is relatively unimportant except in the immediate vicinity of the nozzle lip. Once again the assumption of specular wall reflection has a dramatic effect on the flowfield. Also, in the region of backflow, the velocity profile seems to have more significance.

Figures 5.39(a)-(c) show the relative species concentrations. The results are observed to be much more sensitive to the initial conditions than those obtained along CD. Nevertheless, it is possible to group together the solutions from Runs 3,4, and 6, which are quite different from the others. However, the convergence of dynamic pressure observed for Runs 3 and 4 is not mirrored in these Figures.

In Figure 5.40, the relative abundance of the various species is shown for Run 3. Once again as we approach the nozzle lip the fraction of hydrogen increases, whilst the amount of ammonia present exceeds that of nitrogen. The mixture of gas found in this part of the flowfield is far removed from that given initially in Table 5.1. In Figure 5.41 the flow angle distribution is plotted. Once again the values obtained were invariant for all the conditions investigated, and the results shown were obtained from Run 3. Finally, the thermal nonequilibrium in this part of the flowfield is evident from Figure 5.42 which is again derived from Run 3. It should be noted that the translational and rotational modes have undergone further separation in comparison with Fig. 5.37. In addition, it is evident from the flowfield calculations that the thermal modes are effectively frozen due to the very low collision rates occurring in the backflow region.

5.3.6 Discussion

A number of interesting results have been generated in the present study. These are now considered first in terms of the initial conditions assumed, and then in terms of the flow properties at the various locations chosen for particular examination.

The laminar boundary layer temperature profile assumed has a direct bearing on the backflow potential of the thruster considered. In particular, the degree of backflow obtained is effectively specified by the gas temperature at the nozzle wall. The higher the gas temperature near to the wall, the greater the mass flow around the nozzle lip. These trends are also observed in the region forward of the lip. Such phenomena is to be expected as the flow in this region mainly arises as a result of the backscattering of molecules. This finding may have some impact on the design of nozzles in which some effort in reducing the flow temperature at the nozzle lip would certainly reduce the impingement effects associated with the thruster.

For a given temperature profile there are large differences in flowfield properties depending on whether specular or diffuse reflection is assumed along the nozzle wall. However, much smaller departures are found for variation in the wall temperature used in the diffuse reflector model. The reliance of the amount of backflow upon the wall interaction modelling within the DSMC technique highlights the requirement for improvement in this aspect of the simulation scheme. It is generally recognized that both the diffuse and specular reflectors are over-simplified models with physical reality lying somewhere between these two extremes. It is found that the influence of the conditions specified at the nozzle wall extends to about 60% of the boundary layer at the nozzle exit.

The velocity profile assumed has a limited effect on the flow in front of the nozzle lip. Larger differences are noted in the backflow region. The input of different velocity profiles is found to directly affect the flow velocity in the nozzle boundary layer flow right up to the nozzle exit plane.

A large degree of species separation is found, and is most pronounced in the regions close to the nozzle lip. As expected, it is the lighter species which predominate in the backflow area. When the nozzle wall temperature was taken to be cooler than that for the gas, the fraction of heavy molecules present was observed to rise at small

distances from the surface. This result seems to offer further support in favour of the need to properly account for thermal diffusion in such flows.

The flow angle is generally found to be insensitive to the initially prescribed conditions in both the forward and backward flow regimes. The large flow angle found in the calculations was about 140^{o}.

Thermal nonequilibrium, in which the various thermal modes of the gas are seen to depart, exists to a varying degree in most of the flowfield. In the nozzle exit plane, a small amount of departure of the translational and rotational modes is observed as we proceed towards the nozzle wall. In the region in front of the nozzle lip these modes are found to have separated to a larger degree. In the backflow region, further separation is then followed by temperature freezing caused by the very low collision rate. As expected, the energy in the translational modes is seen to relax at a greater rate than that for the rotational degrees of freedom.

It is generally found that the calculations in the backflow region are much more sensitive to the initial conditions specified, and show significant variation when compared with those in front of the nozzle lip. This aspect of the calculations reinforces the need for parametric study such as that reported here, and for verification of such predictive methods through comparison with reliable experimental data.

5.3.7 Experimental Implications

The sensitivity of the DSMC calculations emphasizes the need for experimental investigation of such flows. In the following, the measurement of various flow properties in the different regions considered is discussed. Special attention is given to the determination of the proper initial starting conditions input into the DSMC code.

Before commencing the calculations it is intuitively clear that the distributions initially assumed for temperature, velocity, and number density, would have a significant impact on the results obtained in the exit plane. What then are the prospects that these initial conditions can be prescribed by matching calculations such as those presented in Figs. 5.32-5.34 against experimental data? Bailey [10,104] has made Pitot pressure measurements in the exit planes of a number of nozzles. Some of these

have been compared with a Navier-Stokes code [104] and good agreement found. However, these investigations were made using pure gases in nozzles which have an exit radius one order of magnitude larger than that found in the MBB/ERNO 0.5N thruster.

In the region in front of the nozzle lip it may be possible to use nonobtrusive diagnostic techniques such as electron beam fluorescence. This technique allows measurement of the flow density which is proportional to the intensity of the fluorescence induced in the flow. In addition, rotational temperature may be inferred from the detailed vibrational-rotational band structure. Unfortunately, the calculated results are such that little conclusive information could be derived from such data. The most that could be attained would be the confirmation of a temperature profile in the boundary layer. It should however be noted that whilst the general appearance of the rotational temperature profiles generated by the DSMC are correct, they may be inaccurate in detail. The use of the Larsen-Borgnakke energy exchange model [53] implies that the relaxation rate must be modelled by assuming a collision number which is constant and therefore independent of the local flow temperature. This represents a limitation on the model, with which an unknown error must be associated.

The results obtained in the backflow region for dynamic pressure seem to offer the best opportunity for determination of the correct initial flow conditions. In Fig. 5.38 it is seen that each set of conditions investigated gives rise to a unique solution. The differences are particularly noticeable at small distances from the nozzle lip. The measurement of the degree of species separation would also be of great benefit. Unfortunately, experimental investigation of the backflow region presents several problems. Firstly, the flow properties in this region will clearly be very sensitive to the background pressure obtained in the vacuum chamber. Secondly, in Bailey's measurements of flow angle [10] an effect is sometimes found whereby backscattering of molecules from the measuring device occurs. However, provided that both of these possible sources of error are overcome, it should be possible to accurately determine the required quantities from probe and Quartz Crystal Microbalance (QCM) measurements. The free-molecular probe employed by Bailey has an accuracy of $1.3x10^{-3}$Pa which is well within the range of pressures encountered in Fig. 5.38. QCMs are used to measure the mass flux of the different species, although it should be noted that detection of hydrogen is usually impossible. It is therefore proposed that

it is possible to determine the correct nature of the initial flow conditions by appropriate measurement of pressure and species concentrations in the backflow region.

TABLE 5.3

Run	Density	Velocity	Temperature	Surface
1	Laminar	Flat Plate	Uniform(197K)	Diffuse(197K)
2	Laminar	Flat Plate	Uniform(197K)	Diffuse(855K)
3	Laminar	Flat Plate	Laminar	Diffuse(855K)
4	Laminar	Flat Plate	Laminar	Diffuse(300K)
5	Laminar	Flat Plate	Laminar	Specular
6	Laminar	Power Law	Laminar	Diffuse(855K)

6. CONCLUSIONS

In the work undertaken in the project, a number of separate work areas have received attention. The initial aim of the research was to calculate the plumes from satellite thruster plumes as they exhaust into the vacuum of space. This has been achieved through the development of three separate computer codes which utilize different solution techniques. These prediction methods vary both in the complexity of the coding required for implementation, and in the soundness of their mathematical basis.

A significant portion of the work has concentrated on the performance of one of these techniques. This is the Direct Simulation Monte Carlo method, which may be regarded as the best solution technique in the rarefied flows associated with much of the plume exhausting from a typical satellite thruster. In the DSMC technique, a number of simulation schemes exist for the treatment of the collision term, which must be solved locally throughout the computational domain. Several of these schemes have been assessed in terms of suitability for application to engineering problems. The first investigation undertaken compared the scheme developed by Nanbu with the Time Counter (TC) method of Bird. The results of this study showed, for the first time, that in addition to increased numerical costs (despite vectorization of the collision algorithm), the Nanbu method is also more restrictive in the choice of initial flow parameters.

After the completion of the assessment of the Nanbu method, a number of improvements made to Nanbu's scheme appeared in the literature. The so called Modified Nanbu DSMC method seemed to merit consideration as it was claimed that both the efficiency and the flexibility of the method were improved as a consequence of the modifications suggested. A further comparison between this new technique and the Time Counter method was therefore completed. It was found that the Modified Nanbu method did indeed overcome the difficulties encountered with the original Nanbu scheme. It was concluded that as the new method was found to require just

25% additional resources that it should be seriously considered as an alternative method to that of Bird.

The question of the degree of statistical fluctuations observed in the TC and Modified Nanbu schemes was then considered. Quantitative analysis of such fluctuations in an engineering application had not previously been undertaken and it had been generally assumed that they were similar for all DSMC schemes. The results of this investigation showed that increased statistical scatter is associated with the Modified Nanbu scheme. These fluctuations are such that up to 100% additional resources may be required to achieve the same error margin with the two methods. The cause of the increased degree of fluctuation in the Modified Nanbu calculations lies in the fact that energy and momentum are not conserved at each collision. This feature of the Modified Nanbu algorithm becomes important when the number of collisions calculated in each cell is small. It is concluded that as Bird's TC method offers results which are in agreement with the Modified Nanbu calculations at a much reduced computational cost, it is the simulation method most suited to the extensive calculations required in the modelling of thruster exhaust plumes, and most other complex rarefied flows. The Modified Nanbu method is better suited to theoretical studies for which a solution of the Boltzmann equation is required.

The modelling of a particular hydrazine thruster plume has been undertaken. In particular, the expansion of the isentropic core, and the flow around the nozzle lip into the backflow area were treated. In addition to the DSMC technique, the Simons model and the Method of Characteristics were also applied to the isentropic core. As the latter two methods are derived from continuum equations, their previous application to the noncontinuum transition flow regime of the plume must involve some degree of error. The assessment of such errors formed the primary aim of these calculations.

It was found that errors of up to 20% for number density occurred in the MOC calculations. The MOC calculations are found to be consistently smaller than both the DSMC results and the available experimental data. Such inaccuracies are directly translated into the calculation of heat transfer and aerodynamic forces on the spacecraft surface. Large differences also exist for the total temperature results produced by the DSMC and continuum methods. The MOC calculations are invalid

as the the technique assumes that the gas is in thermal equilibrium thereby failing to take account of the separation and freezing of the translational and rotational energy modes which actually occurs in the expansion process. The errors associated with the MOC temperature calculations of drag coefficient and Stanton number are significant at small angles, near to the plume axis, and may be greater than 50%. Once again it is found that the MOC calculations underpredict the extent of the impingement effects. In all cases, larger errors are associated with use of the Simons model. The extent of the errors incurred by applying the less expensive continuum methods to such flows had not been previously realized.

In the nozzle lip and backflow regions, results were obtained solely with DSMC calculations. The large degree of thermal nonequilibrium and species separation effects observed show that the use of continuum methods in such flows is quite difficult. In order to assess the influence of some of the initial assumptions made in the DSMC calculations, a sensitivity analysis was undertaken for these flowfields. In particular, the effect of the temperature and velocity profiles in the laminar boundary layer, together with the gas-surface interaction assumed at the nozzle wall, were investigated. It is found that the temperature profile assumed at the nozzle wall effectively governs the amount of backflow found for a particular thruster. It is concluded that impingement potential in this region would be significantly reduced if it were possible to reduce the flow temperature near to the nozzle wall. The solutions in the backflow region are found to be quite sensitive to the assumptions initially made. Large differences are noted between the assumption of diffuse and specular reflection at the nozzle wall. The results of these investigations show that it is important to assess the influence of the initial flow conditions assumed. Greater confidence in any set of calculations will only emerge as a result of direct comparison with experimental data. It has been shown that the initial flow conditions could be determined by measurement of pressure in the backflow region of the plume where the DSMC calculations are particularly sensitive.

It is found that the modelling of satellite control thruster plumes should not be regarded as a trivial undertaking. The accurate determination of all possible impingement effects resulting from such thusters is becoming increasingly important as the proper determination of onboard fuel resources becomes more critical. Design engineers should be aware of the errors associated with the application of the simpler

and less expensive solution techniques. The errors found for prediction of impingement quantities along the plume axis for the hydrazine thruster are not insignificant. It is concluded that proper consideration should be given to the use of the more computationally expensive DSMC technique when the design specifications require accurate prediction of the plume flow quantities.

The fact that backflow angles of up to 140° are found for the thruster shows that it is impossible to avoid contamination effects on the complex geometries of modern spacecraft. Whilst the flow in this region is of a highly rarefied nature, it is evident that a large total flux will accumulate over a typical satellite lifetime which runs into a number of years. The findings of this work study clearly show that the prediction of such effects can be achieved with the DSMC technique.

7. FURTHER WORK AREAS

As the current project has progressed, many challenging problems associated both with the physical problem considered, and with the solution techniques employed, have presented themselves. Due to time limitations, it was not possible to investigate every avenue. Several of these problem areas are therefore briefly outlined as suggestions for future research.

One improvement to the Simons model has been made by the author and is described in Chapter 2. Another area which may yield further improvement is in the treatment of the boundary layer expansion. The main obstacle to the modification of this aspect of the model is the lack of both experimental and theoretical data. Perhaps it may be possible to use the results of DSMC calculations to develop a suitable extension to this analytical model. However, it is felt that the simplistic assumptions made in the formulation of the model will ultimately limit the amount of useful information that can be supplied on the complex phenomena occurring in real exhaust plumes.

The Method of Characteristics programme developed in the project is of the most simple kind in that the variation in the ratio of specific heats (real gas effects) is not accounted for. Such procedures, involving numerical integration, have been developed by Reis et al [105] and incorporated into a MOC algorithm.

As an alternative to the Method of Characteristics, it may be possible to extend the finite difference solution of the nozzle flow into the plume expansion region. Such a procedure is currently under review at MATRA Espace, Toulouse, France [106]. Once again, such calculations could be employed in the improvement of the Simons model.

The Direct Simulation Monte Carlo method is a flow solution technique which has grown in status in recent years. The method is being applied by an increasing number of scientists to many different flow phenomena. However, the need to prove the theoretical basis of the method should not be overlooked. The Modified Nanbu method developed at the University of Kaiserslautern is the first simulation method to rival that of the Time Counter method of Bird in terms of numerical efficiency. As the research on this subject advances, it is probable that new gas dynamics methods will eventually overtake the Bird method. The need for the testing of these methods in the context of simple, well understood flows is an essential requirement to their application to complex flows in which Direct Simulation proposes to find the 'exact' solution.

Recent advances in computer hardware technology have given greater computing power to the engineer. Whilst the current trend seems to use these resources in the application of the DSMC technique to increasingly complex flow problems, there is a more urgent requirement for the improvement of several aspects of the method. This can only be achieved through direct comparison with experimental data. One of the most urgent needs is for the development of a proper scheme for the determination from local flow conditions of the fraction of inelastic collisions occurring throughout the flowfield. This aspect of the DSMC technique is particularly important for flows in which large degrees of thermal nonequilibrium exist. In such flows, errors in the calculation of internal energy transfer will inevitably lead to large uncertainties in all flow properties.

There is also a need for the consideration of advanced computer programming techniques by the engineering community. Recently, both parallel computing [107] and vectorization [108] techniques have been applied to DSMC algorithms. As the DSMC technique is so expensive, it is imperative that a large degree of optimization is achieved in the computer coding. In addition, proper consideration should be given to the type of hardware required for particular applications. Whilst large super computers such as the CRAY-2 may offer the best answer to flows involving complex three-dimensional geometries, chemical reactions, internal energy exchange, etc., for more straightforward problems it is often more economical to employ a dedicated minicomputer system.

The results presented in Chapter 5 show that large errors in the prediction of impingement properties are found by the application of continuum methods. However, this result has only been found for one particular thruster, and a more general analysis would be of great value. At the end of Section 5.3 proposals for the experimental validation of the DSMC calculations in the backflow region are considered.

There is also a great need for the undertaking of a full finite difference calculation of the nozzle flow of small thrusters such as those manufactured by MBB/ERNO and SESSIA. In particular, a solution for the laminar boundary layer must be found. In addition, the calculations should allow prediction of the internal shocks produced by contoured nozzles. Such a solution would allow the initial flow conditions used in Direct Simulation of the boundary layer and backflow regions to be better defined. Due to the expense of the Monte Carlo method, parametric studies are limited in scope. It is therefore of great importance that the specification of the initial flow quantities should be as accurate as possible. A finite difference scheme such as that developed by MacCormack [109] might be employed. With such a scheme, investigation of any relaxation and chemical effects may also be investigated in two dimensions for the first time. Analysis of the MBB/ERNO 2N and 5N contoured thrusters would also then be made possible.

8. REFERENCES

1. Mayer, E., Hermel, J. & Rogers, A.W.
"Thrust Loss Due to Plume Impingement Effects", J. Spacecraft & Rockets 23(6), pp. 554-560, 1986.

2. Trinks, H.
"Experimental Exhaust Plume Investigation with MBB 1o N Thruster", AIAA 19th Joint Propulsion Conference, Seattle, 1983.

3. Trinks, H. & Bindemann, I.
"Experimental Investigation of Exhaust Plume Flow Field of MBB 4N Bipropellant Thruster", MBB Contract Rep., No. TU HH-TRI-JPL-84-2, 1984.

4. Trinks, H. & Bindemann, I.
"Bipropellant Plume Measurements 22N Marquardt Thruster R6C", Vol. I, INTELSAT Contract No. 511A, 1986.

5. Dettleff, G., Boettcher, R.-D., Dankert, C., Koppenwallner, G. & Legge, H.
"Attitude Control Thruster Plume Flow Modelling and Experiments", AIAA 20th Thermophysics Conference, Williamsburg, Virginia, 1985.

6. Legge, H. & Dettleff, G.
"Pitot Pressure and Heat Transfer Measurements in Hydrazine Thruster Plumes", J. Spacecraft & Rockets 23(4), pp 357-362, 1986.

7. Lengrand, J.-C., Allegre, J. & Raffin, M.
"Interaction of Underexpanded Jets with Adjacent Flat Plates", Rarefied Gas Dynamics, Vol.51 of Progress in Astronautics & Aeronautics, pp.447-458, 1977.

8. Lengrand, J.-C., Allegre, J. & Raffin, M.
"Heat Transfer to a Surface Impinged upon by a Simulated Underexpanded Rocket Exhaust Plume", Rarefied Gas Dynamics, Vol.74 of Progress in Astronautics & Aeronautics, pp.980-993, 1981.

9. Allegre, J., Raffin, M. & Lengrand, J.-C.
"Investigation of Freejets Issued from Small Solid-propellant Rocket Engines", J. Spacecraft & Rockets 21(2), pp. 131-135, 1984.

10. Bailey, A.B.
"Flow-Angle Measurements in a Rarefied Nozzle Plume", AIAA J. 25(10), pp. 1301-1304, 1987.

11. Bird, G.A.
"Breakdown of Translational and Rotational Equilibrium in Gaseous Expansions", AIAA J. 8(11), pp.1998-2003, 1970.

12. Bird, G.A.
"Breakdown of Continuum Flow in Freejets and Rocket Plumes", Vol. 74 of Progress in Astronautics & Aeronautics, Part II, AIAA, New York, pp. 681-694, 1980.

13. Cattolica, R., Robben, F., Talbot, L. & Willis, D.R.
"Translational Nonequilibrium in Free Jet Expansions", Phys. Fluids 17(10), pp.1793-1807, 1974.

14. Simons, G.A.
"Effect of Nozzle Boundary Layers on Rocket Exhaust Plumes", AIAA J. 10(11), pp. 1534-1535, 1972.

15. Hoffman, R.J., Kawasaki, A., Trinks, H., Bindemann, I. & Ewering, W.
"The CONTAM 3.2 Plume Flowfield Analysis and Contamination Prediction Computer Program", AIAA 20th Thermophysics Conference, Williamsburg, Virginia, 1985.

16. Boyd, I.D. & Stark, J.P.W.
"Modification of the Simons Model for Calculation of Nonradial Expansion Plumes", 16th International Symposium on Rarefied Gas Dynamics, Pasadena, California, 1988.

17. Bird, G.A.
'Molecular Gas Dynamics', Oxford, Clarendon Press, 1976.

18. Hueser, J.E., Melfi, L.T., Bird, G.A. & Brock, F.J.
"Analysis of Large Solid Propellant Rocket Engine Exhaust Plumes Using the Direct Simulation Monte Carlo Method", AIAA Paper 84-0496, 22nd AIAA Aerospace Sciences Meeting, Reno, Nevada, 1984.

19. Boyd, I.D. & Stark, J.P.W.
"Direct Simulation of Chemical Reactions", submitted to J. Thermophysics & Heat Transfer.

20. Boyd, I.D. & Stark, J.P.W.
"Comparison of Monte Carlo Techniques for Nozzle Lip Expansion", presented at Euromech 225, Cranfield, England, 1987.

21. Boyd, I.D. & Stark, J.P.W.
"A Comparison of the Implementation and Performance of the Nanbu and Bird Direct Simulation Monte Carlo Methods", Phys. Fluids 30(12), pp. 3663-3668, 1987.

22. Boyd, I.D. & Stark, J.P.W.
"On the Use of the Modified Nanbu Direct Simulation Monte Carlo Method", to appear in J. Comput. Phys..

23. Boyd, I.D. & Stark, J.P.W.
"Statistical Fluctuations in Monte Carlo Calculations", 16th International Symposium on Rarefied Gas Dynamics, Pasadena, California, 1988.

24. Boyd, I.D.

"Discrete Particle Simulation of an Expanding Gas", presented at Graphics Techniques for Simulation, British Computer Society Conference, London, 1988.

25. Quarendon, P., Boyd, I.D. & Burridge, J.M.
"A System for the Display of Three-Dimensional Images", in Proceedings of the 2nd Image Symposium, CESTA, Paris, 1986.

26. Boyd, I.D. & Stark, J.P.W.
"Modelling of Small Hydrazine Thruster Plumes Using Discrete Particle and Continuum Methods", AIAA Paper-88-2631, presented at AIAA Thermophysics, Plasmadynamics and Lasers Conference, San Antonio,Texas, 1988.

27. Ferri, A.
'Elements of Aerodynamics of Supersonic Flows', MacMillan, New York, 1949.

28. Vick, A.R., Andrews, E.H., Dennard, J.S. & Craidon, B.
"Comparisons of Experimental Free-jet Boundaries with Theoretical Results Obtained with the Method of Characteristics", NASA TN D-2327, 1964.

29. Love, E.S., Grigsby, C.E., Lee, L.P. & Woodling, M.J.
"Experimental and Theoretical Studies of Axisymmetric Jets", NASA TR R-6, 1959.

30. Schlichting, H.
'Boundary Layer Theory', McGraw-Hill, New York, 1960.

31. Boynton, F.P.
"Exhaust Plumes from Nozzles with Wall Boundary Layer", J. Spacecraft & Rockets 5(10), pp. 1143,1147, 1968.

32. Boynton, F.P.
"Highly Underexpanded Jet Structure: Exact and Approximate Solutions", AIAA J. 5(9), pp. 1703-1704, 1967.

33. Legge, H. & Boettcher, R.-D.

"Modelling Control Thruster Plume Flow and Impingement", 13th Int Symp on Rarefied Gas Dynamics, Novosibirsk, USSR, 1982.

34. Allegre, J., Raffin, M. & Lengrand, J.-C.
"Intelsat VI Plume Impingement - Final Report", SESSIA Report 110/84.458, 1984.

35. Rogers, A.W., Allegre, J., Raffin, M. & Lengrand, J.-C.
"Plume Impingement Heat Transfer Measurements on Model Simulated Intelsat VI Configurations and Conversion to Real Flight Conditions", AIAA 22nd Thermophysics Conference, Honolulu, Hawaii, 1987.

36. Lengrand, J.-C.
Private Communication.

37. Boettcher, R.-D.
Private Communication.

38. Calia, V.S. & Brook, J.W.
"Measurements of a Simulated Rocket Exhaust Plume Near the prandtl-Meyer Limiting Angle", J. Spacecraft 12(4), pp. 205-208, 1975.

39. Lengrand, J.-C.
"Calculs de Jets Sous-etendus Issus de Tuyeres Supersoniques", CNRS Rapport 75-4, Meudon, France, 1975.

40. Dettleff, G. & Legge, H.
"Hydrazine Thruster Near Field Plume Profile Measurements: Part2: Pitot Pressure Measurements", DFVLR IB 222-85, A15, 1985.

41. Legge, H., Dankert, C. & Dettleff, G.
"Experimental Analysis of Plume Flow from Small Thrusters", in Proceedings of the 14th International Symposium on Rarefied Gas Dynamics, Vol. 1, University of Tokyo Press, Japan, pp. 279-286, 1984.

42. Hermina, W.L.
"Monte Carlo Simulation of High Altitude Rocket Plumes with Nonequilibrium Molecular Energy Exchange", AIAA/ASME 4th Thermophysics and Heat Transfer Conference, Boston, Massachusetts, 1986.

43. Alder, B.J. & Wainwright, T. Proc. Int. Symp. on Transport Processes in Statistical Mechanics, Interscience, New York, p. 97, 1958.

44. Bird, G.A.
"Approach to Translational Equilibrium in a Rigid Sphere Gas", Phys. Fluids 6, pp. 1518-1519, 1963.

45. Bird, G.A.
"Aerodynamic Properties of Some Simple Bodies in the Hypersonic Transition Regime", AIAA J. 4(1), pp. 55-60, 1966.

46. Bird, G.A.
"Direct Simulation and the Boltzmann Equation", Phys. Fluids 13(11), pp. 2676-2681, 1970.

47. Meiburg, E.
"Comparison of the Molecular Dynamics Method and the Direct Simulation Monte Carlo Technique for Flows Around Simple Bodies", Phys. Fluids 29(10), pp. 3107-3113, 1986.

48. Bird, G.A.
"Near Continuum Impact of an Underexpanded Jet Plume on a Wall" Proc. AIAA Compuational Fluid Dynamics Conf., AIAA, New York, pp. 103-108, 1973.

49. Olynick, D.P., Moss, J.N. & Hassan, H.A.
"Grid Generation and Adaptation for the Direct Simulation Monte Carlo Method", AIAA Thermophysics, Plasmadynamics and Lasers Conference, San Antonio, Texas, 1988.

50. Bird, G.A.

"Monte Carlo Simulation In an Engineering Context", Vol.74 of Progress in Astronautics & Aeronautics, AIAA, New York, pp. 239-255, 1980.

51. Jan, D.L. & Guernsey, C.S.
"Implementation of the Direct Simulation Monte Carlo Method on the Hypercube Concurrent Processor", 17th JANNAF Plume Technology Meeting, NASA Langley, Virginia, 1988.

52. Nanbu, K.
"Heat Transfer Between Parallel Plates in Continuum to Free Molecular Regime", Report 364, Inst. High Speed Mechanics, Tohoku University, Japan, 1983.

53. Borgnakke, C. & Larsen, P.
"Statistical Collision Model for Monte Carlo Simulation of Polyatomic Gas Mixtures", J. Comp. Phys. 18, pp. 405-420, 1975.

54. Davis, J., Dominy, R.G., Harvey, J.K. & MacRossan, M.N.
"An Evaluation of Some Collision Models Used for Monte Carlo Calculations of Diatomic Rarefied Hypersonic Flows", J. Fluid Mech. 135, pp. 355-371, 1983.

55. Parker, J.G.
"Rotational and Vibrational Relaxation in Diatomic Gases", Phys. Fluids 2(4), pp. 449-462, 1959.

56. Millikan, R.C. & White, D.R.
"Systematics of Vibrational Change", J. Chem. Phys. 39(12), pp. 3209-3213, 1963.

57. Bird, G.A.
"Prandtl-Meyer Flow of a Finite Knudsen Number Gas", in Proc. 7th Australian Conf. on Hydraulics and Fluid Mechanics, pp. 306-308, 1980.

58. Bird, G.A.
"Direct Simulation of a Dissociating Gas", J. Comp. Phys. 25, pp. 353-365, 1977.

59. Hinshelwood, C.N.

'Kinetics of Chemical Change', Clarendon, Oxford, 1940.

60. Bird, G.A.
"Simulation of Multi-dimensional and Chemically Reacting Flows", Rarefied Gas Dynamics, CEA, Paris, pp. 365-388, 1978.

61. Vincenti, W.G. & Kruger, C.H.
'Introduction to Physical Gas Dynamics', Wiley, New York, 1965.

62. Baulch, D.L., Drysdale, D.D. & Horne, D.G.
'Evaluated Kinetic Rate Data for High Temperature Reactions Vol.2 Homogeneous Gas Phase Reactions of the H_2-N_2-O_2 System', CPC Press, Cleveland, Ohio, 1973.

63. Park, C.
"Problems of Rate Chemistry in the Flight Regimes of Aeroassisted Orbital Transfer Vehicles", AIAA Paper 84-1730, 1984.

64. Boltzmann, L.
Sber. Akad. Wiss. Wien Abt. II, 66, p. 275, 1872.

65. Nanbu, K.
"Interrelations Between Various Direct Simulation Methods for Solving the Boltzmann Equation", J. Phys. Soc. Jpn. 52(10), pp. 3382-3388, 1983.

66. Nanbu, K.
"Theoretical Basis of the Direct Simulation Monte Carlo Method", in Proceedings. 15th Int. Symp. on Rarefied Gas Dynamics, Grado, Italy, 1986, edited by V.Boffi & C.Cercignani (Teubner, Stuttgart, 1987), pp. 369-383.

67. Kac, M.
'Probability & Related Topics in Physical Science' (Interscience, London, 1959).

68. Belotserkovsky, O.M. & Yanitskiy, V.Ye.
Zhurn. Vych. Mat. i Mat. Fiz. 15, p. 1195, 1975 ffl in Russian ".

69. Koura, K.
"Transient Couette Flow of Rarefied Binary Gas Mixture", Phys. Fluids 13(6), pp. 1457-1466, 1970.

70. Deshpande, S.M., Subba Raju, P.V. & Ramani, N.
"A Comparative Study of the Time Counter and Random Collision Number Strategies Used in Monte Carlo Simulation", 'Rarefied Gas Dynamics', C.E.A., Paris, 1978, pp.435-440.

71. Nanbu, K.
"Direct Simulation Scheme Derived from the Boltzmann Equation. I. Monocomponent Gases", J. Phys. Soc. Jpn. 49(5), pp. 2042-2049, 1980.

72. Babovsky, H.
"On a Simulation Scheme for the Boltzmann Equation", Math. Meth. Appl. Sci. 8, pp. 223-233, 1986.

73. Koura, K.
"Comment on 'Direct Simulation Scheme Derived from the Boltzmann Equation. I. Monocomponent Gases'", J. Phys. Soc. Jpn. 50(11), pp. 3829-3830, 1981.

74. Nanbu, K.
"Speedup of the Direct Simulation Methods for Solving the Boltzmann Equation", J. Phys. Soc. Jpn. 53(9), pp. 2996-2999, 1984.

75. Ploss, H.
"On Simulation Methods for Solving the Boltzmann Equation", Computing 38, pp. 101-115, 1987.

76. Chu, C.K.
"The High Mach Number Rayleigh Problem for Solving the Boltzmann Equation", in Proc. 5th Int. Symp. on Rarefied Gas Dynamics, Oxford, England, 1966, edited by C.L.Brundin (Academic Press, London, 1967), p.589-605.

77. Nanbu, K.

"Direct Simulation Scheme Derived from the Boltzmann Equation. V. Effects of Sample Size, Number of Molecules, Step-Size, and Cut-off Angle, upon Simulation Data", Report 348, Institute for High Speed Mechanics, Tohoku University, Japan, 1981.

78. Bird, G.A.
Private communication.

79. Babovsky, H.
"Low Discrepancy Methods for Solving the Boltzmann Equation", 16th International Symposium on Rarefied Gas Dynamics, Pasadena, California, 1988.

80. McDonald, J.D. & Baganoff, D.
"Vectorization of a Particle Simulation Method for Hypersonic Rarefied Flow", AIAA Thermophysics, Plasmadynamics and Lasers Conference, San Antonio, Texas, 1988.

81. Broadwell, J.E.
"Study of Rarefied Shear Flow by the Discrete Velocity Method", J. Fluid Mech. 19, pp. 401-414, 1964.

82. Goldstein, D., Sturtevant, B. & Broadwell, J.E.
"Investigations of the Motion of Discrete-Velocity Gases", 16th International Symposium on Rarefied Gas Dynamics, Pasadena, California, 1988.

83. Sansevero, V.J., Garfinkel, H. & Archer, S.F.
"On-orbit Performance of the Hydrazine Reaction Control Subsystem for the Communications Technology Satellite", AIAA/SAE 14th Joint Propulsion Conference, Las Vegas, Nevada, 1978

84. Genovese, J.E.
"Rapid Estimation of Hydrazine Exhaust Plume Interaction", AIAA/SAE 14th Joint Propulsion Conference, Las Vegas, Nevada, 1978.

85. Dadieu, A., Damm, R. & Schmidt, E.W.

'Raketentreibstoffe', Springer-Verlag, Vienna, 1968.

86. NASA Space Vehicle Design Criteria (Chemical Propulsion)
Liquid Rocket Engine Nozzles, NASA SP, July 1976.

87. Kewley, D.J.
"Predictions of the Exit Conditions, Including Species Concentrations and the Ratio of Specific Heats, of Hydrazine Decomposition Thrusters", DFVLR IB 222-85, A05, 1985.

88. Gordon, S. & McBride, B.J.
"Computer Program for Calculation of Complex Chemical Equilibrium Compositions, Rocket Performance, Incident and Reflected Shocks, and Chapman-Jouguet Detonations", NASA SP-273, 1968.

89. Doo, Y.C. & Nelson, D.A.
"Analysis of Small Bipropellant Engine Internal Flows by the Direct Simulation Monte Carlo Method", AIAA 22nd Thermophysics Conference, Honolulu, Hawaii, 1987.

90. Handbook of Chemistry & Physics
46th Edition, The Chemical Rubber Co., Cleveland, Ohio, 1966.

91. Brokaw, R.S.
"Viscosity of Gas Mixtures", NASA TN D-4496, 1968.

92. Hoffman, R.J.
"TC-1 AKM Plume Characterisation, Heat Transfer and Contamination Analysis Study", Report prepared for MATRA, Science Appl. Inc., California, 1981.

93. Hoffman, R.J.
"Evaluation of Plume Impingement Effects on L-sat 1", Report prepared for British Aerospace, Science Appl. Inc., California, 1983.

94. Hueser, J.E., Melfi, L.T., Bird, G.A. & Brock, F.J.

"Rocket Nozzle Lip Flow by Direct Simulation Monte Carlo Method", J. Spacecraft & Rockets 23(4), pp. 363-372, 1986.

95. Hermina, W.L.
"Monte Carlo Simulation of Rocket Plume Enhancement Regions", 15th JANNAF Plume Technology Meeting, San Antonio, Texas, 1985.

96. Nanbu, K.
"Rarefied Flows Through A Convergent-Divergent Nozzle", in Preprints from International Symposium on Computational Fluid Dynamics, Tokyo, pp. 91-100, 1985.

97. Doo, Y.C. & Nelson, D.A.
"Direct Monte Carlo Simulation of Small Bipropellant Engine Plumes", AFRPL TR-86-100, 1987.

98. Legge, H. & Dettleff, G.
"Hydrazine Thruster Near Field Plume Profile Measurements: Part 1: Heat Transfer Measurements", DFVLR IB 222-84, A48, 1984.

99. Dankert, C.
"Velocity Measurements in Rarefied Rocket Plumes", AIAA Thermophysics, Plasmadynamics and Lasers Conference, San Antonio, Texas, 1988.

100. Schaaf, S.A. & Chambre, P.L.
"Flow of Rarefied Gases", High Speed Aerodynamics and Jet Propulsion, Vol. III, Sec. H, Princeton University Press, Princeton, pp. 687-739, 1958.

101. Campbell, D.H. & Weaver, D.P.
"Nozzle Lip Effects on Gas Expansion into Plume Backflow Region", AIAA 26th Aerospace Sciences Meeting, Reno, Nevada, 1988.

102. Bird, G.A.
"Thermal and Pressure Diffusion Effects in High Altitude Flows", AIAA Thermophysics, Plasmadynamics and Lasers Conference, San Antonio, Texas, 1988.

103. Moss, J.N., Cuda, V. & Simmonds, A.L.
"Nonequilibrium Effects for Hypersonic Transitional Flows", AIAA Paper 87-0404, 1987.

104. Cooper, G.K., Jordan, J.L. & Phares, W.J.
"Analysis Tool for Application to Ground Testing of Highly Underexpanded Nozzles", AIAA/SAE/ASME/ASEE 23rd Joint Propulsion Conference, San Diego, California, 1987.

105. Reis, R.J., Aucoin, P.J. & Stechman, R.C.
"The Prediction of Rocket Exhaust Flow Fields with Embedded Shocks and Nozzle Boundary Layers", AIAA 5th Propulsion Joint Specialist Conference, Colorado, 1969.

106. Koeck, C. & Petitjean, L.
"Numerical Simulation of Plume Effects", Euromech 225, Cranfield, England, July 1987.

107. Furlani, T.R. & Lordi, J.A.
"Implementation of the Direct Simulation Monte Carlo Method for an Exhaust Plume Flowfield in a Parallel Computing Environment", AIAA Thermophysics, Plasmadynamics and Lasers Conference, San Antonio, Texas, 1988.

108. Usami, M., Fujimoto, T. & Kato, S.
"Monte Carlo Simulation on Mass-Flow Reduction by Roughness Through a Slit Surface", 16th International Symposium on Rarefied Gas Dynamics, Pasadena, California, 1988.

109. MacCormack, R.W.
"A Numerical Method for Solving the Equations of Compressible Viscous Flow", AIAA J. 20(9), pp. 1275-1281, 1982.

110. Yen, S.M.
"Numerical Solution of the Boltzmann Equation for Nonequilibrium Flow Properties", Ann. Rev. Fluid Mech. 16, pp. 67-97, 1984

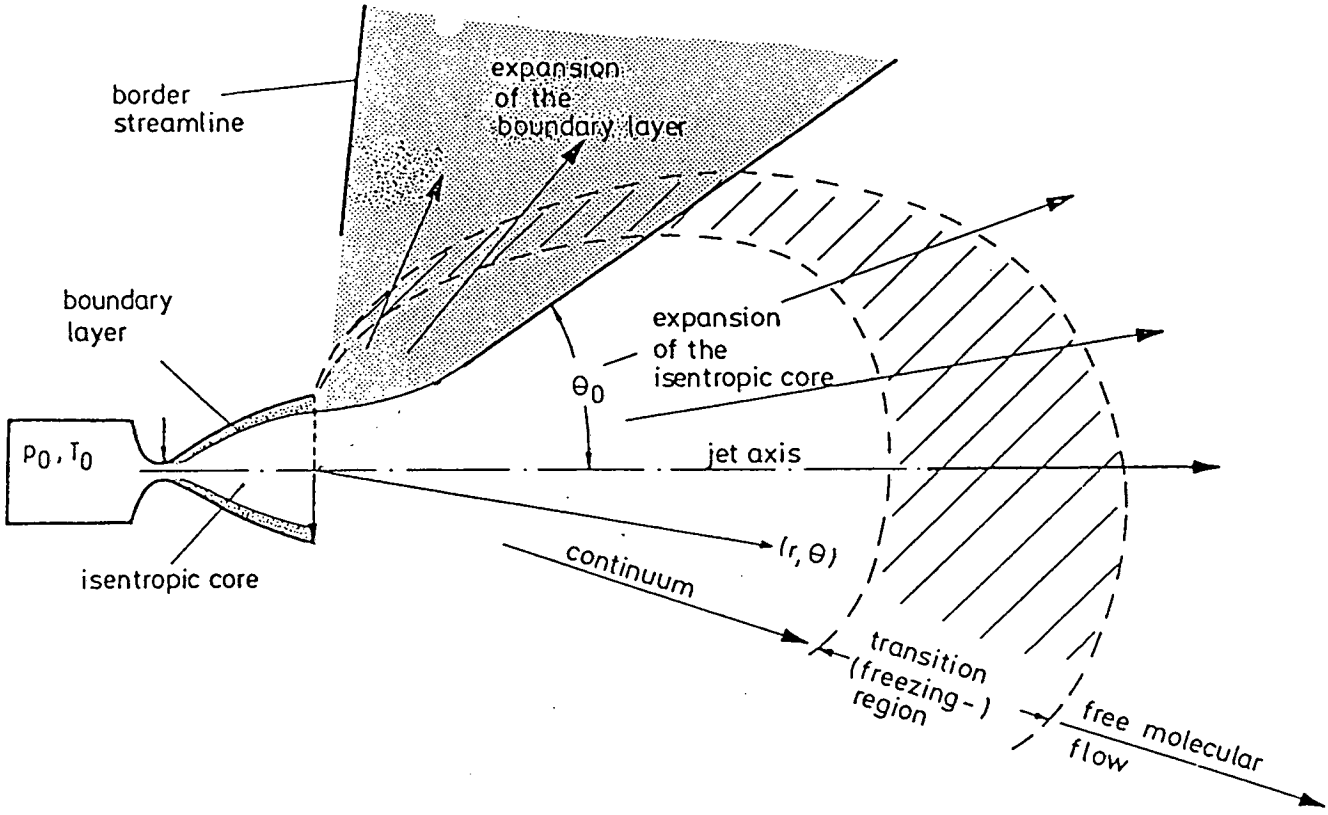

Fig. 1.1 Different flow regions in a plume.

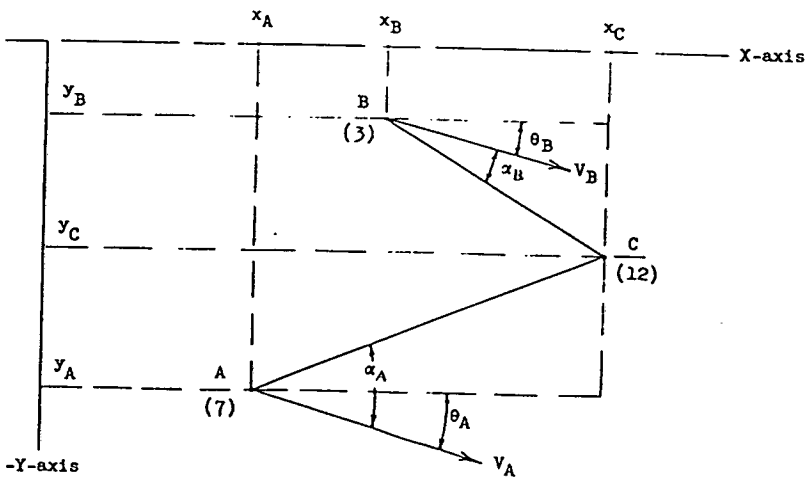

Fig. 2.1 General point MOC solution.

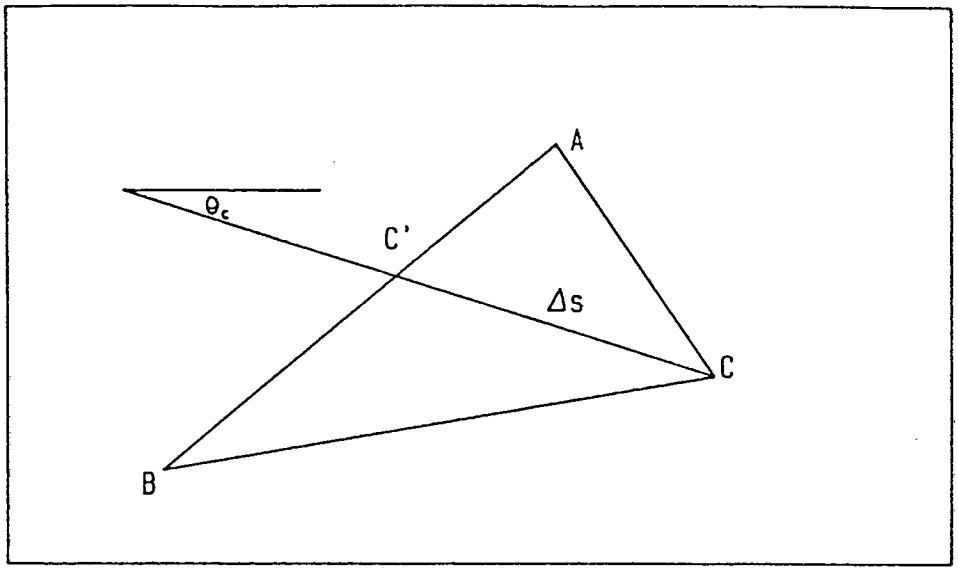

Fig. 2.2 MOC procedure for derivation of breakdown parameter.

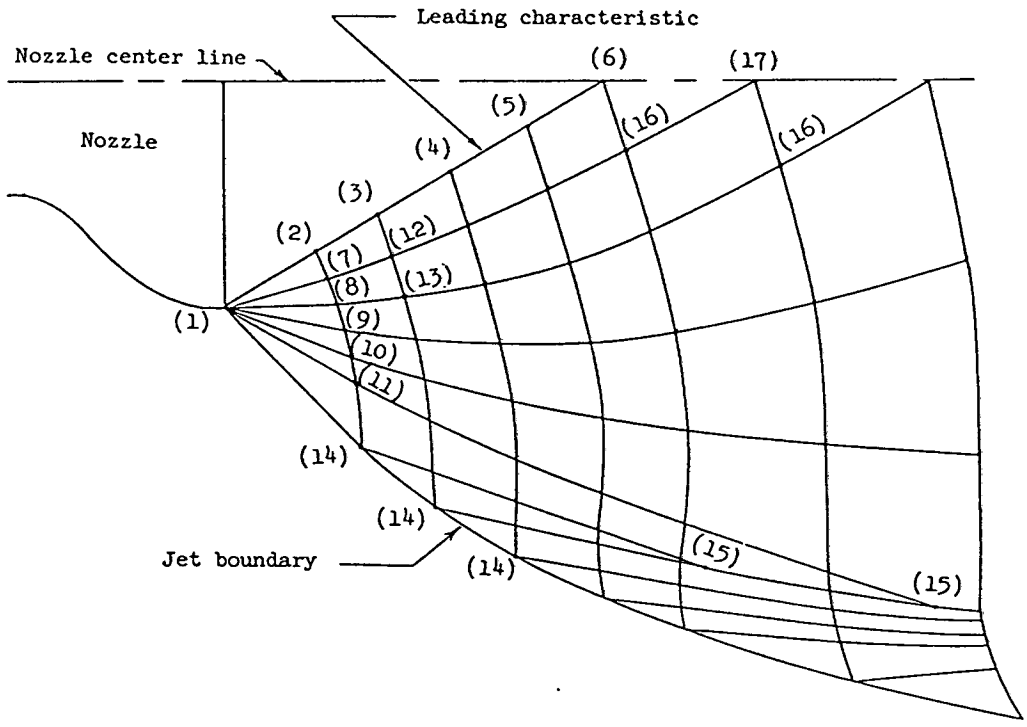

Fig. 2.3 Schematic diagram of MOC solution procedure for an expanding jet.

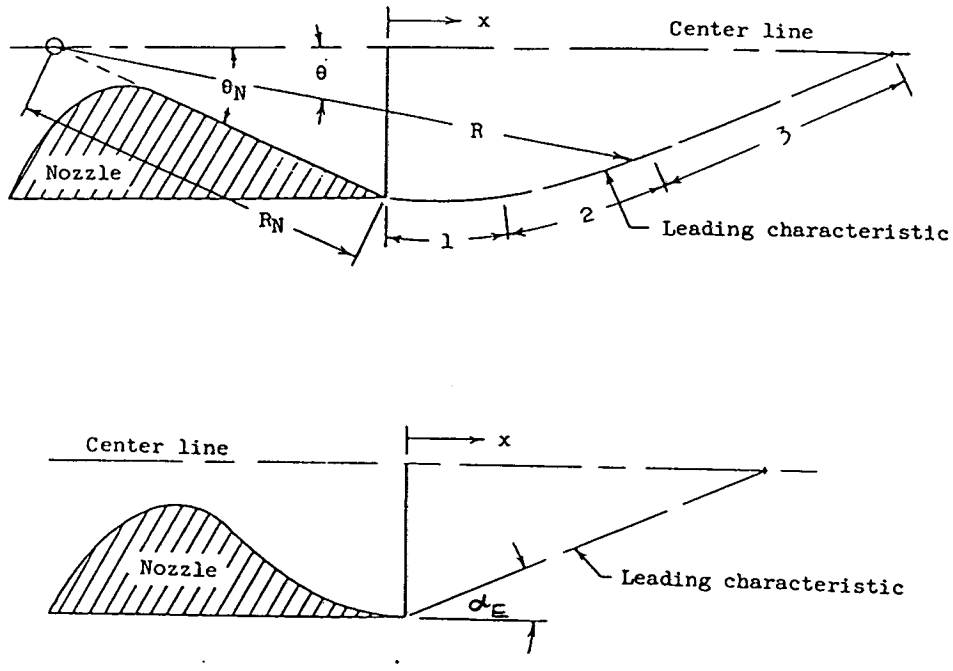

Fig. 2.4 Leading Characteristic for a conical nozzle.

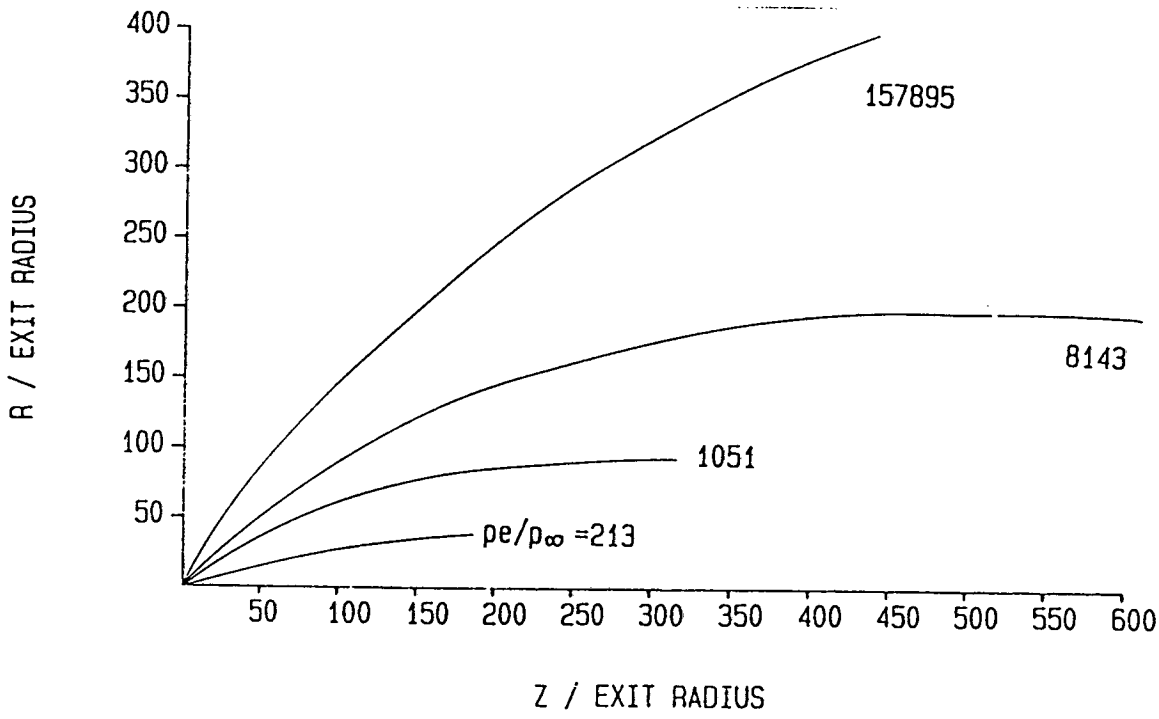

Fig. 2.5 Jet boundaries calculated with MOC as a function of ambient pressure.

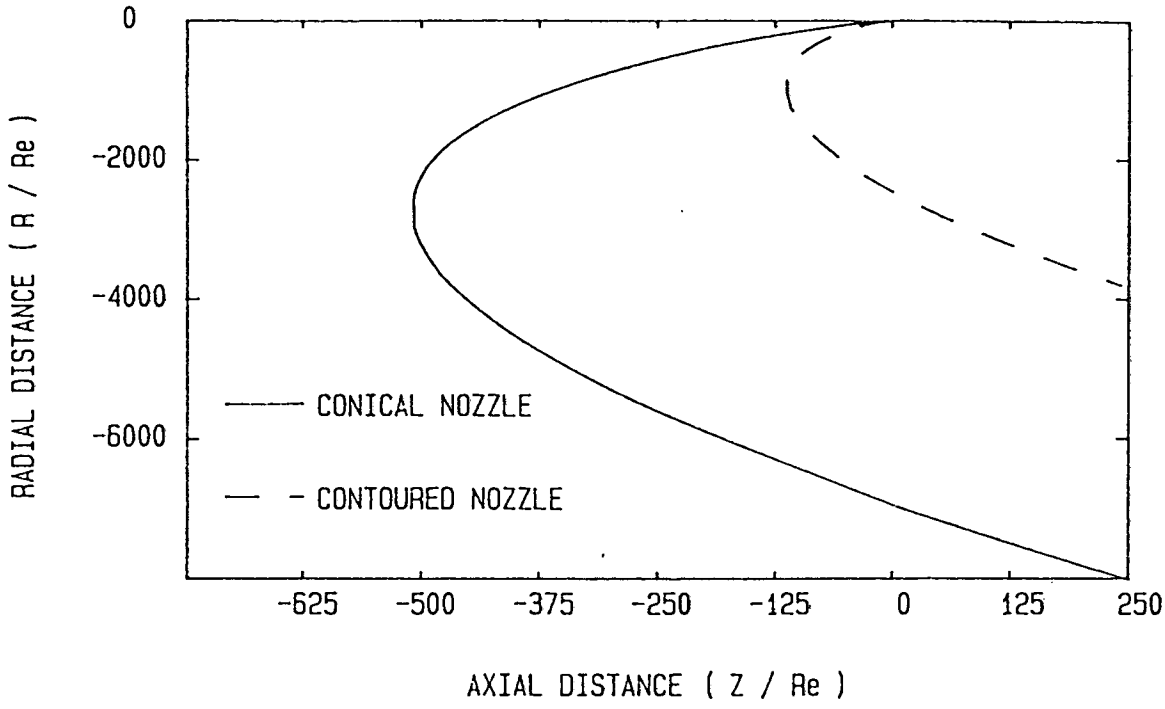

Fig. 2.6 Jet boundaries for sonic nozzles having conical and contoured walls.

The curved nature of these plots indicates the failure of the algorithm in regions of very low density, ie. high Mach number.

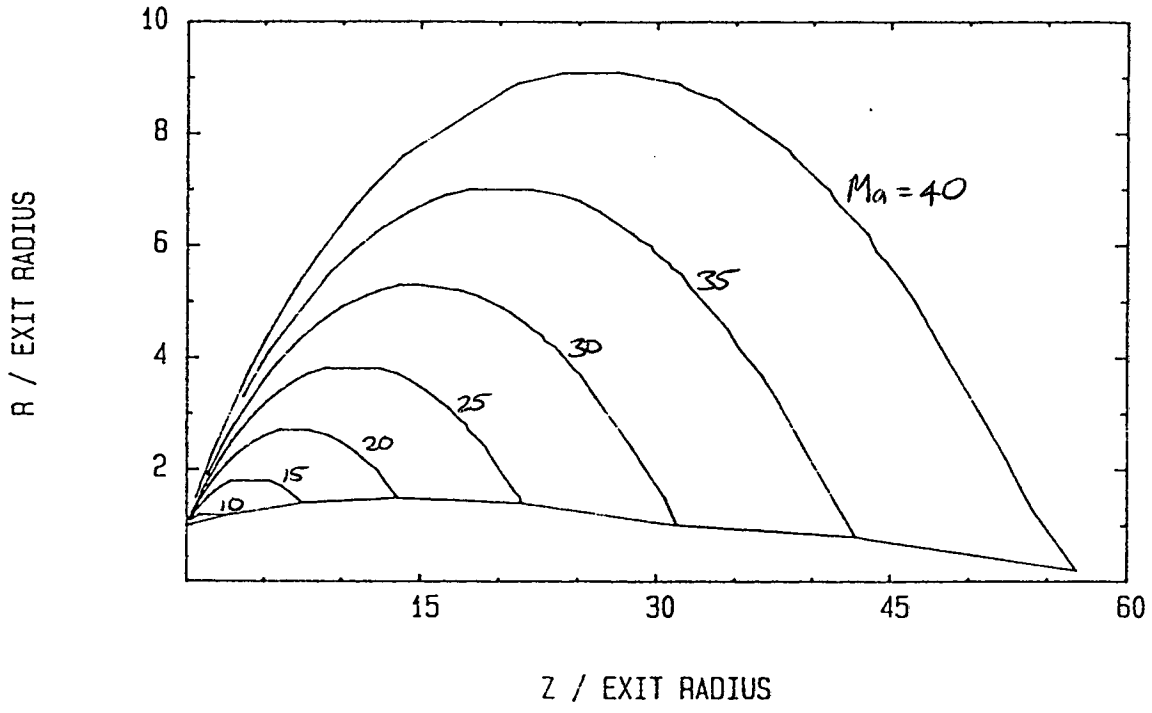

Fig. 2.7 Mach number contours obtained with MOC for exit Mach number of 5.

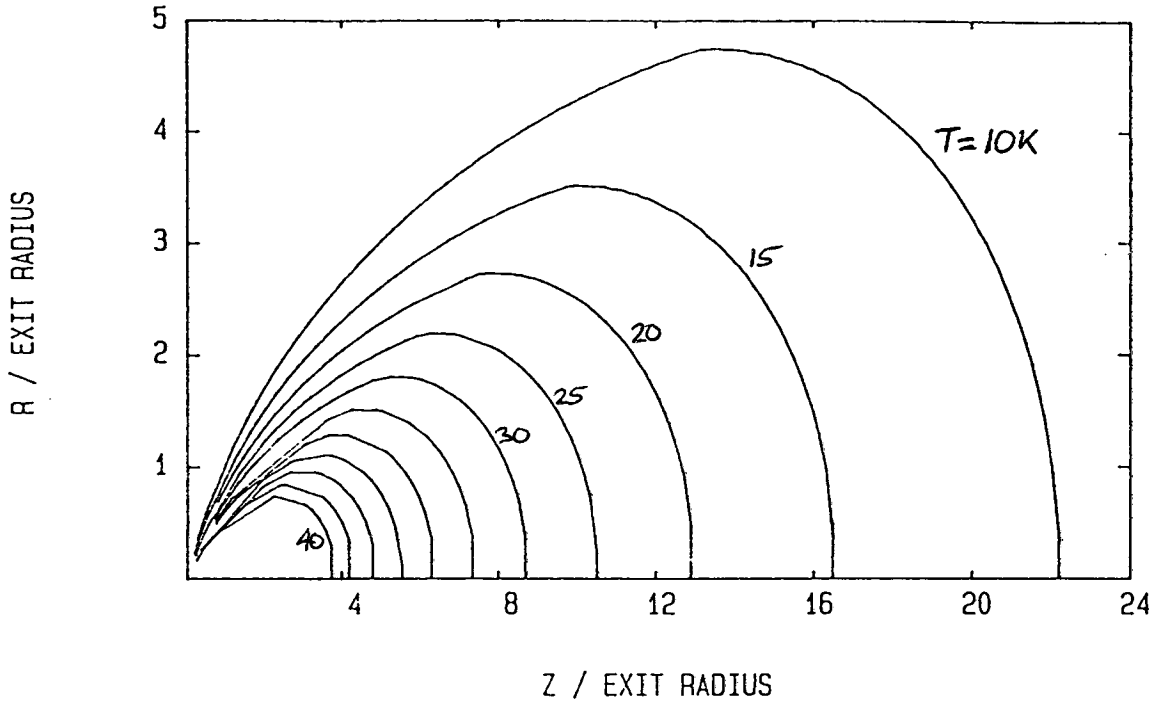

Fig. 2.8 Temperature contours for SESSIA nozzle obtained with Simons model.

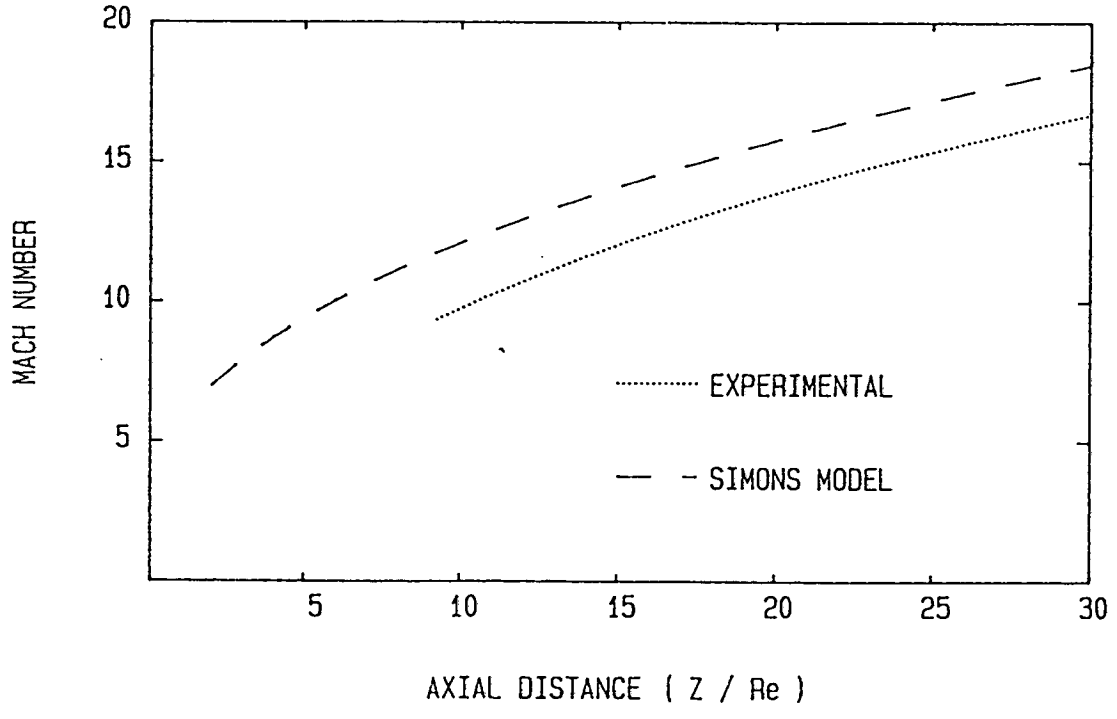

Fig. 2.9 Axial Mach number distributions for SESSIA radial thruster.

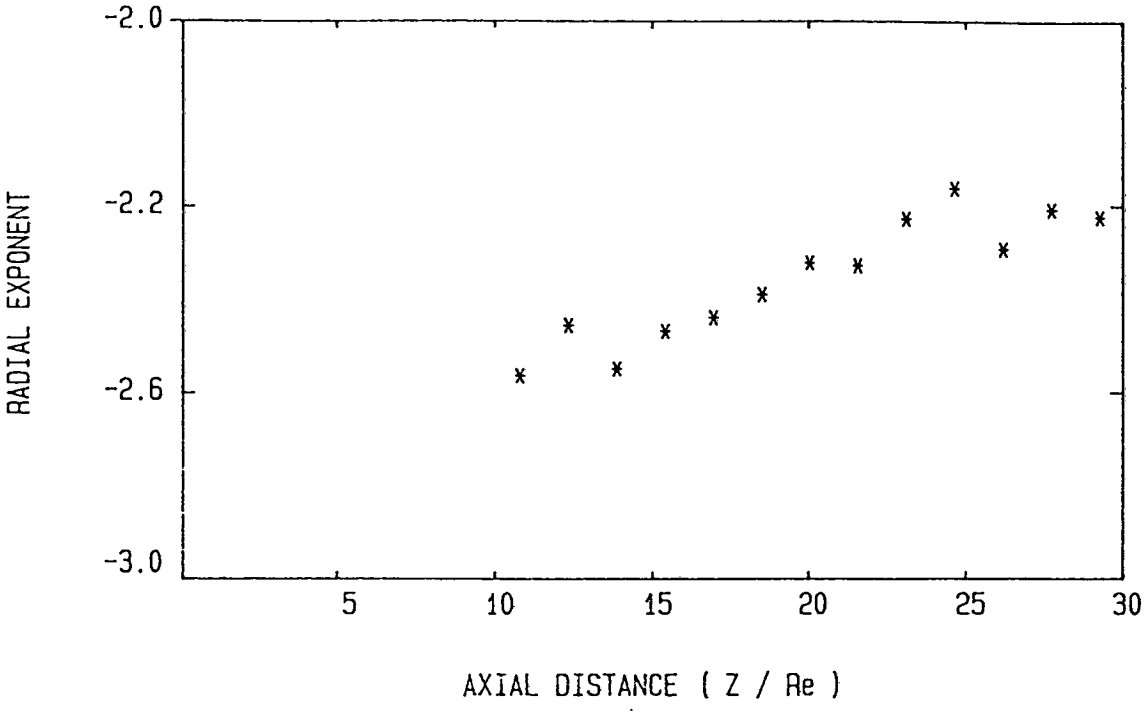

Fig. 2.10 Nonradial nature of experimental axial number density.

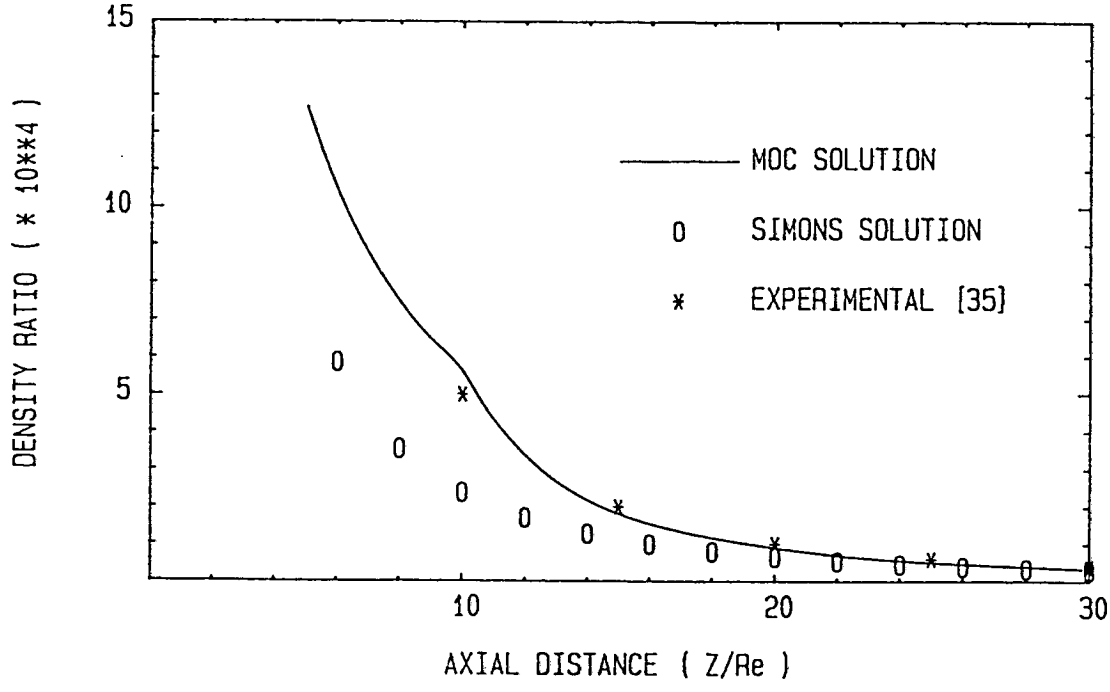

Fig. 2.11 Density ratio on the plume axis for the SESSIA radial thruster [35] .

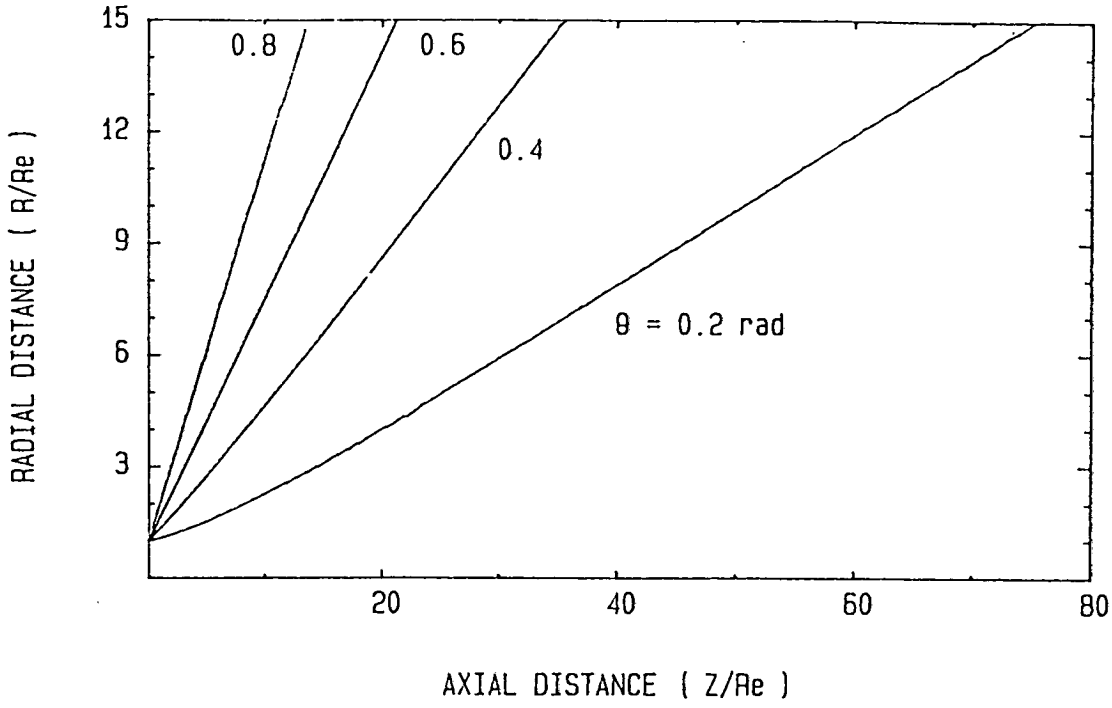

Fig. 2.12 Contours of constant flow angle for the SESSIA radial thruster [35] .

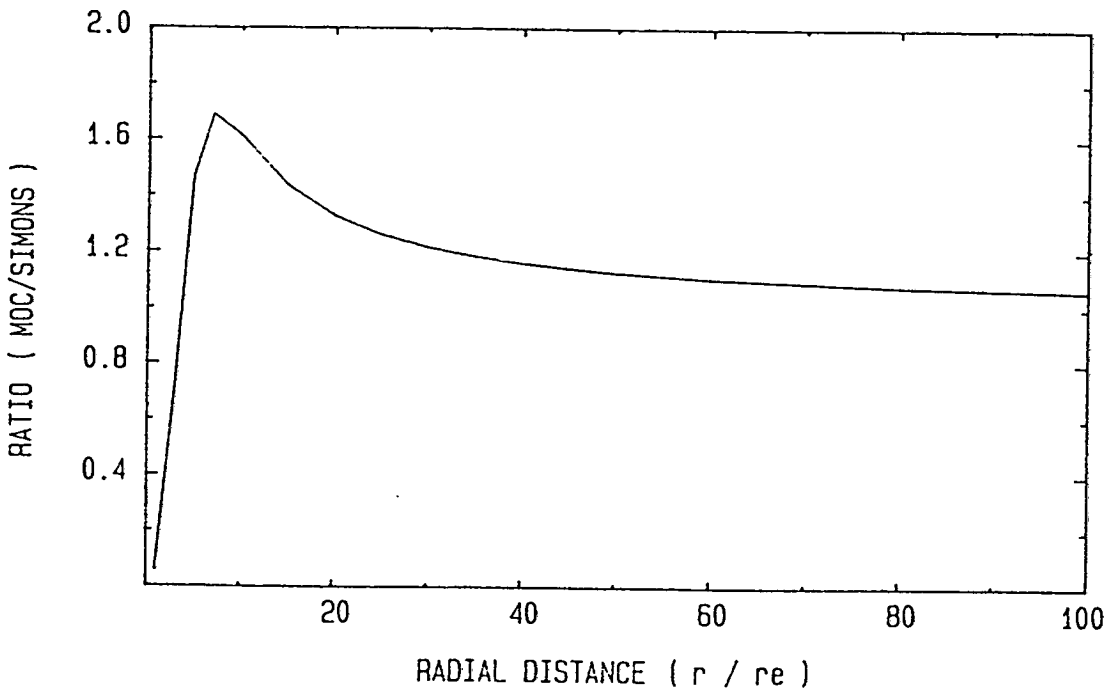

Fig. 2.13 The function defined by the ratio of MOC and Simons model solutions for density along the plume axis.

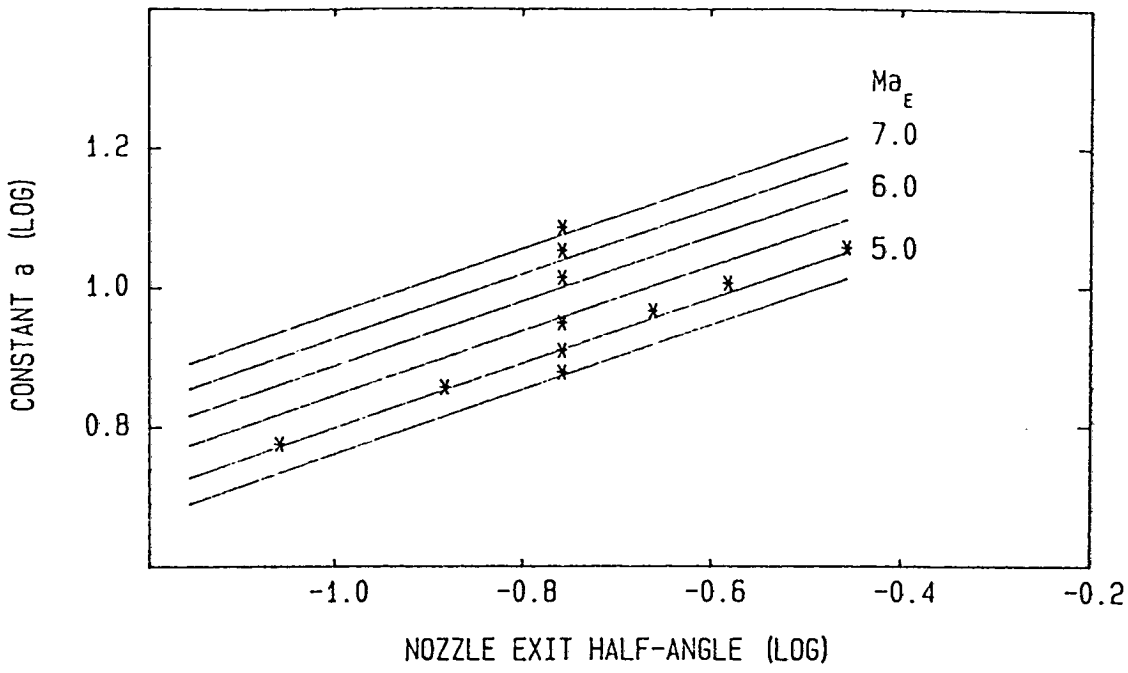

Fig. 2.14 Best-fit constant a plotted as a function of θ_E and Ma_E.

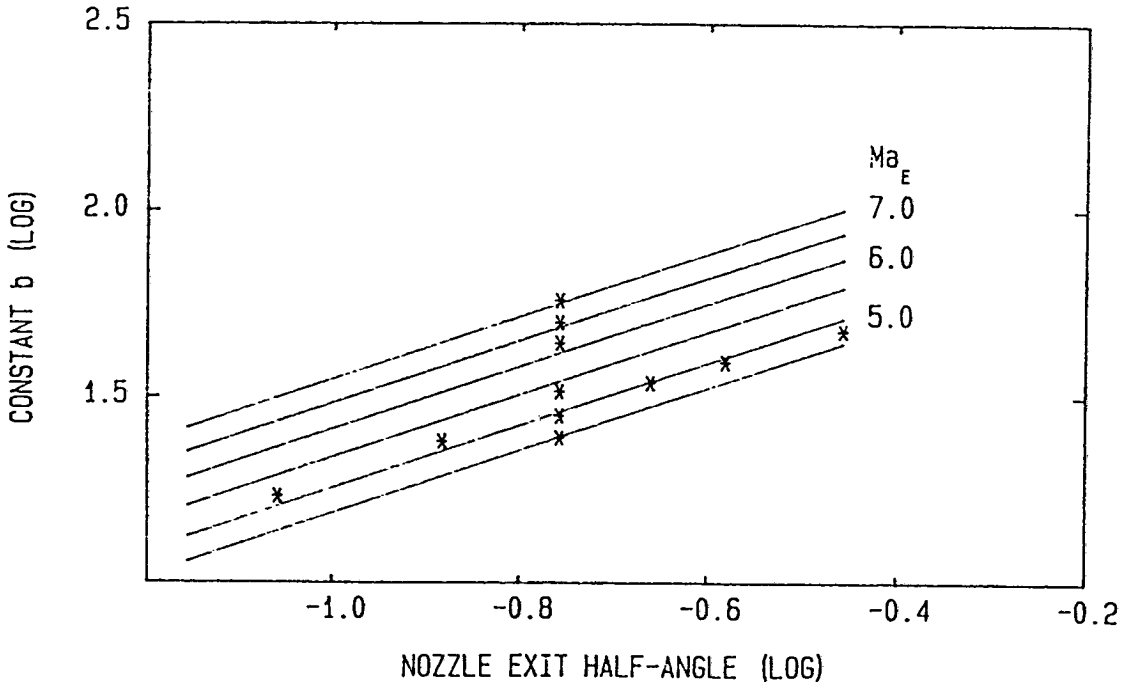

Fig. 2.15 Best-fit constant b plotted as a function of θ_E and Ma_E.

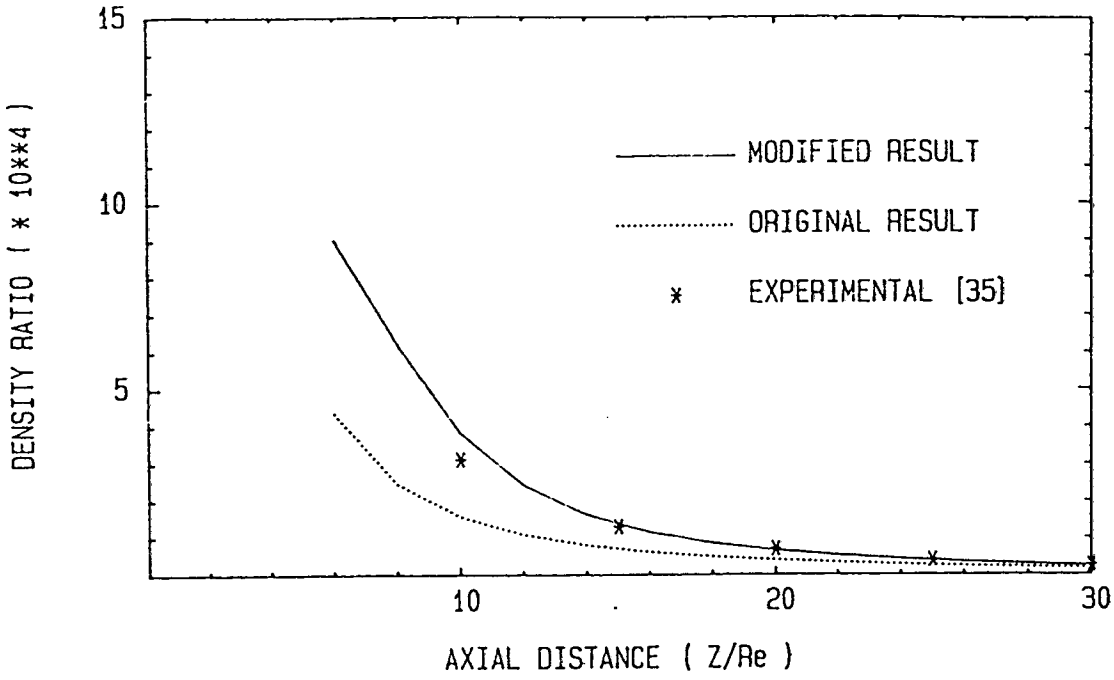

Fig. 2.16 Density ratio on the plume axis for the SESSIA axial thruster [35] .

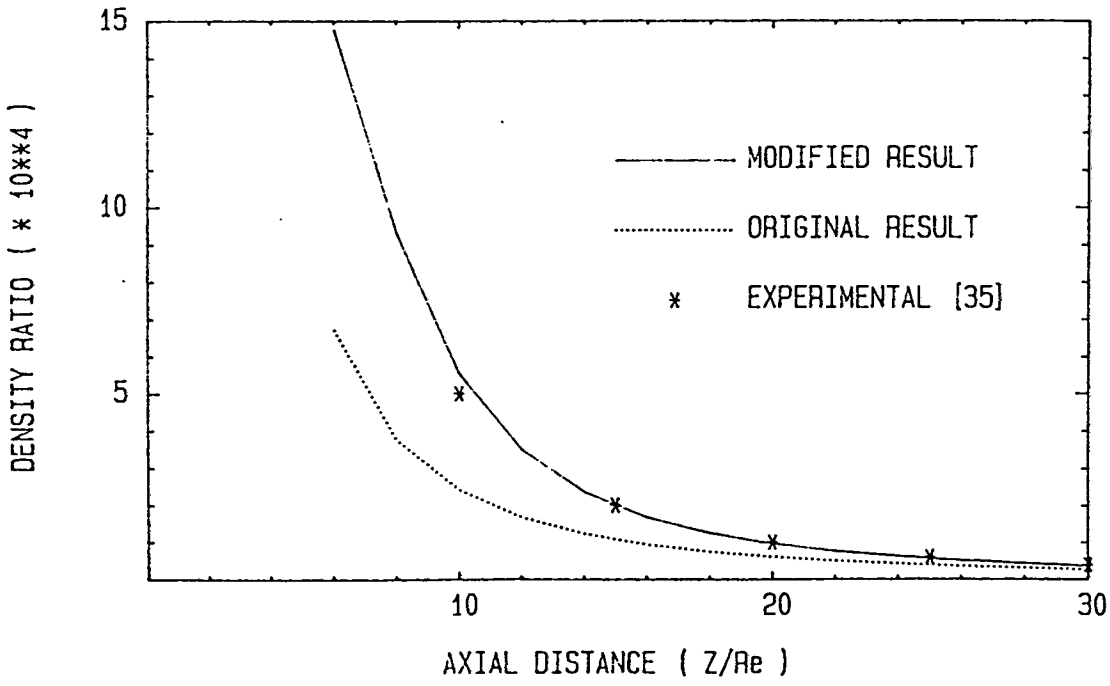

Fig. 2.17 Density ratio on the plume axis for the SESSIA radial thruster [35] .

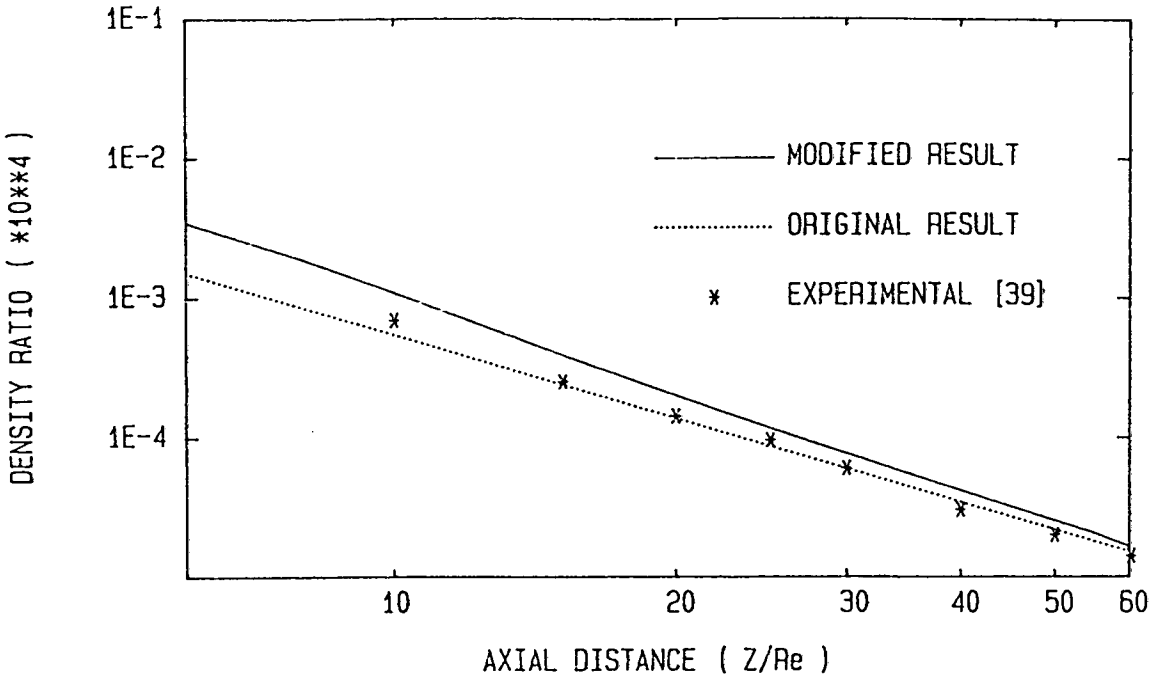

Fig. 2.18 Density ratio on the plume axis for CNRS nozzle no. 1 [39].

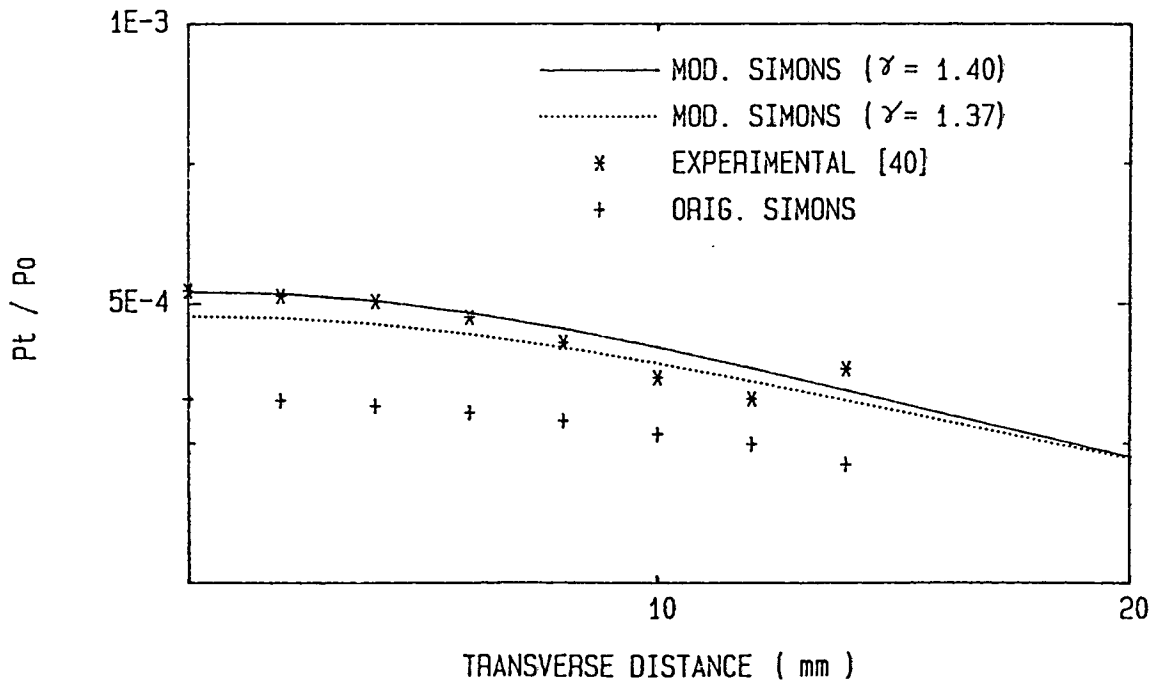

Fig. 2.19 Transverse Pitot pressure profile at an axial distance of 24 exit radii for MBB thruster.

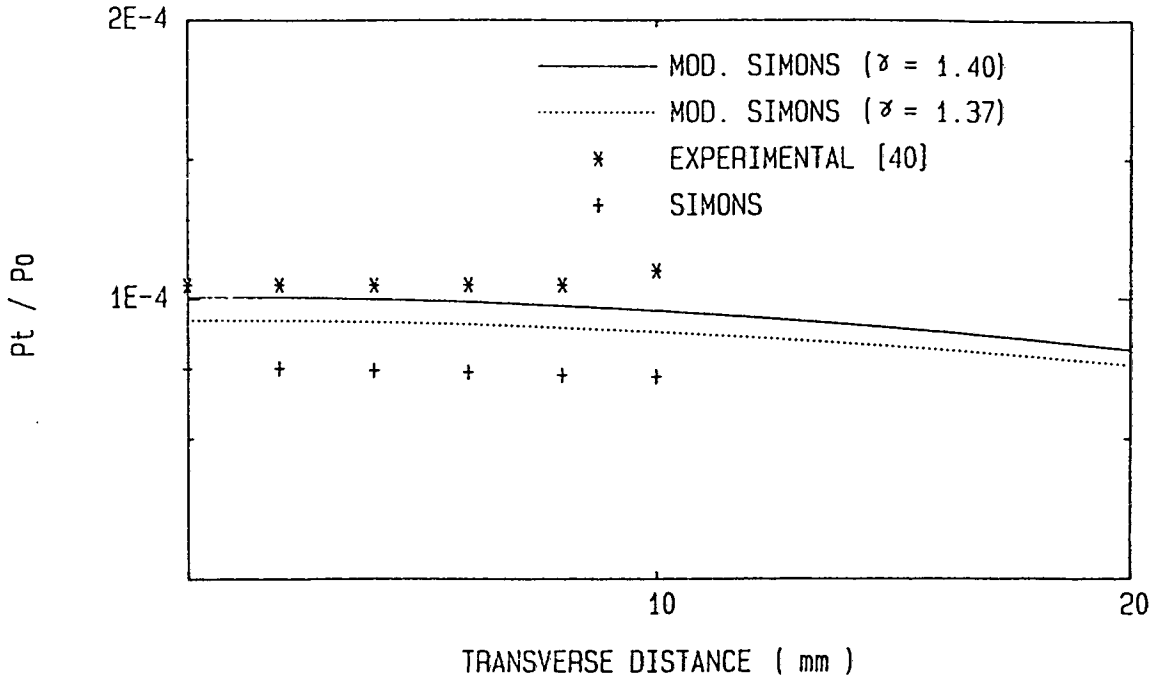

Fig. 2.20 Transverse Pitot pressure profile at an axial distance of 48 exit radii for MBB thruster.

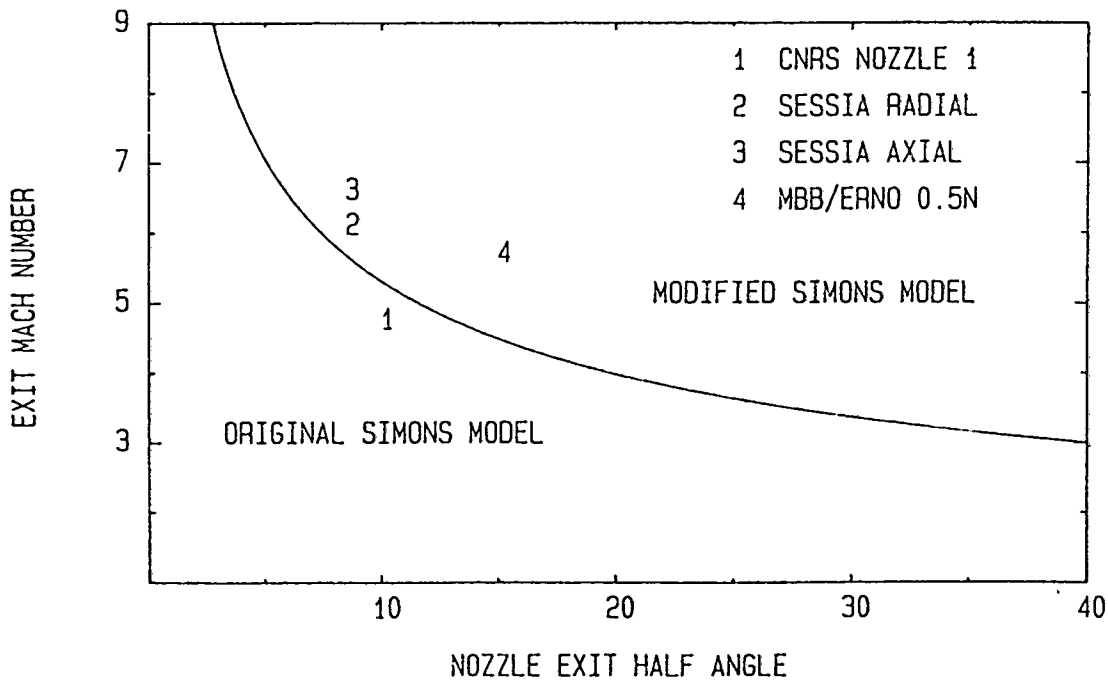

Fig. 2.21 Critical nozzle exit conditions for nonradial plume expansion.

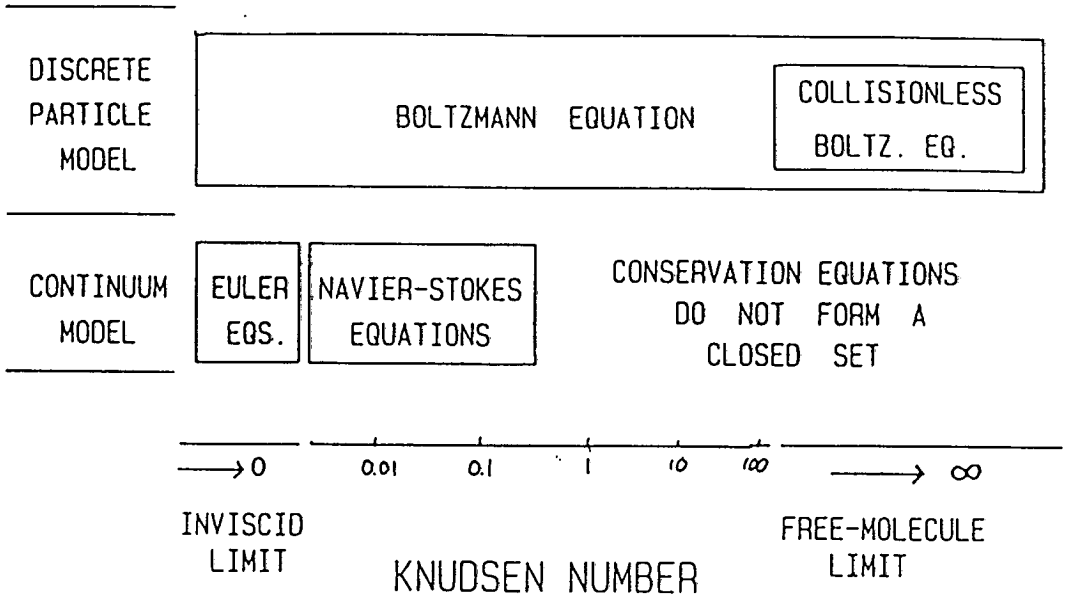

Fig. 3.1 Validity of flow equations as function of Knudsen number.

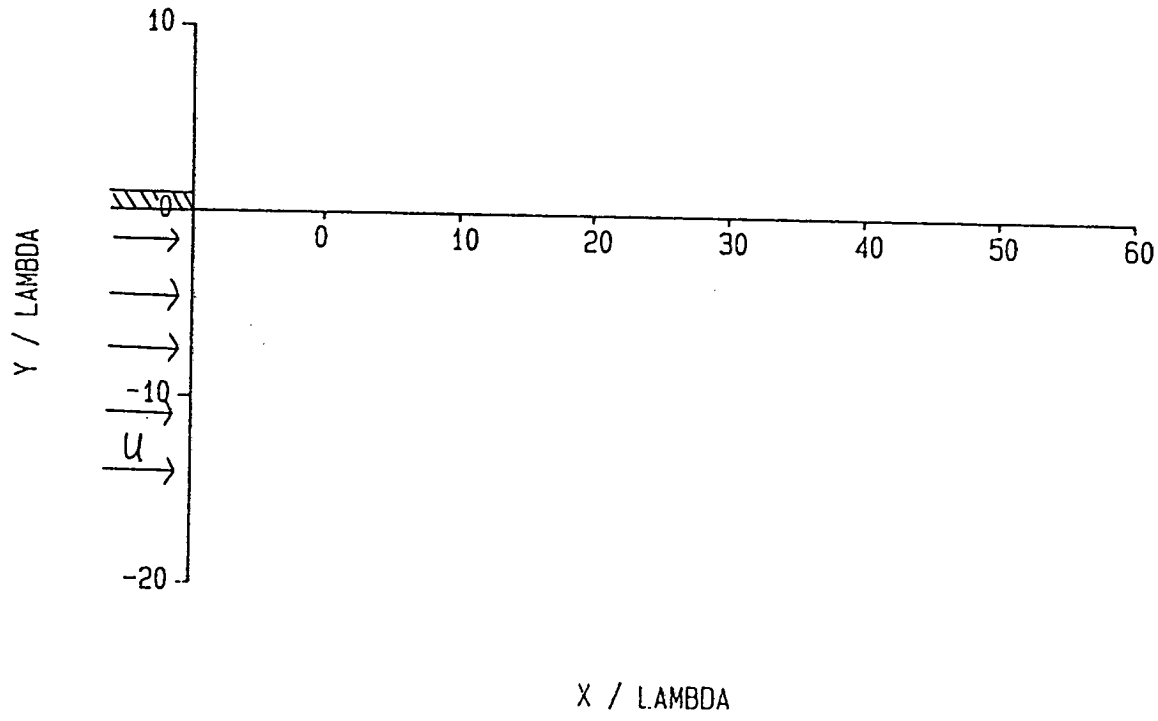

Fig. 3.2 Flow configuration for Prandtl-Meyer expansion.

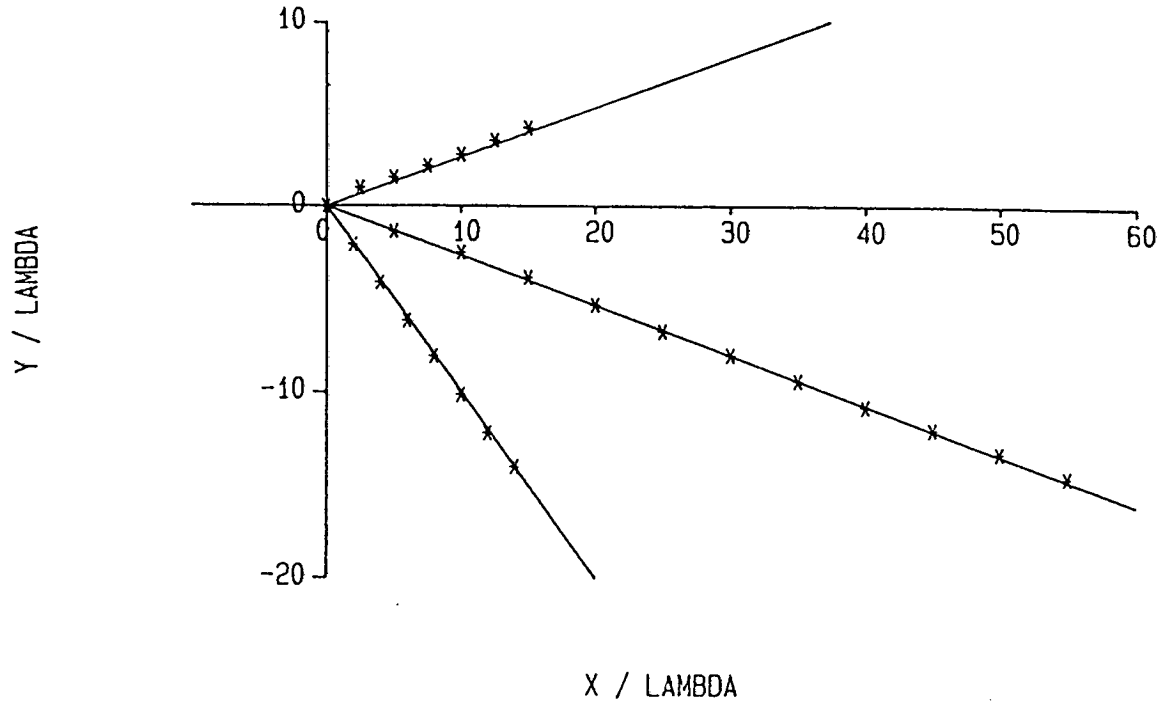

Fig. 3.3 Continuum (———) and DSMC (*) density calculations for Prandtl-Meyer expansion.

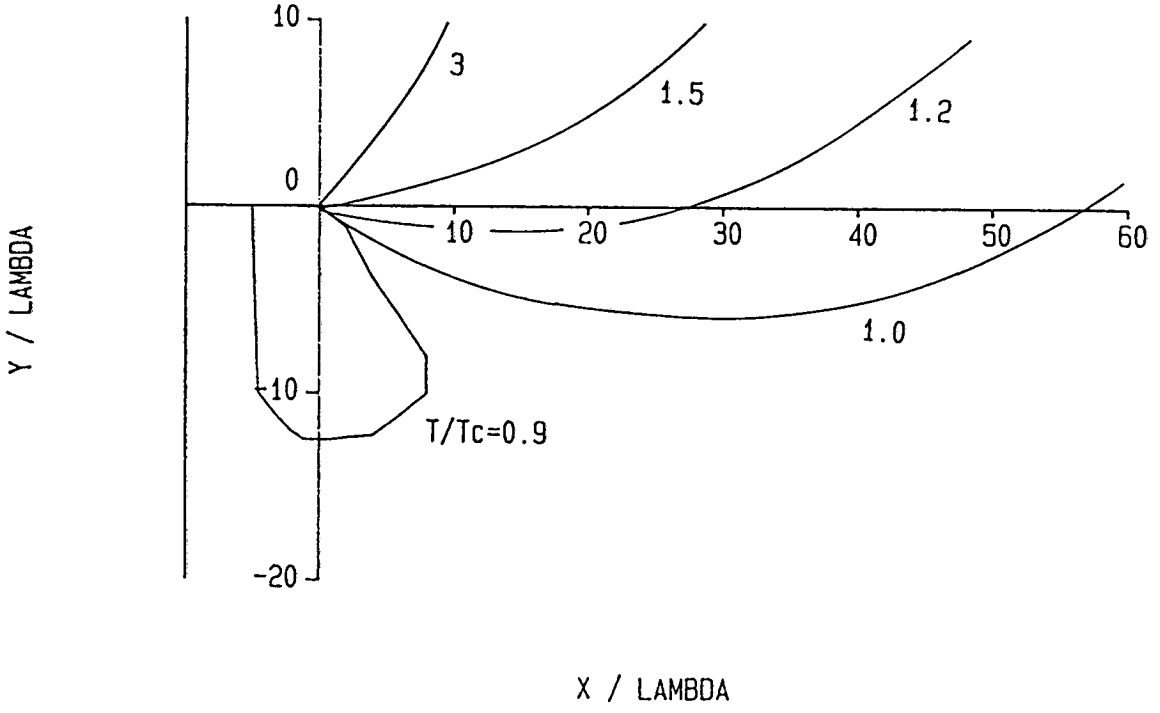

Fig. 3.4 Ratio of DSMC to continuum temperature contours for Prandtl-Meyer expansion.

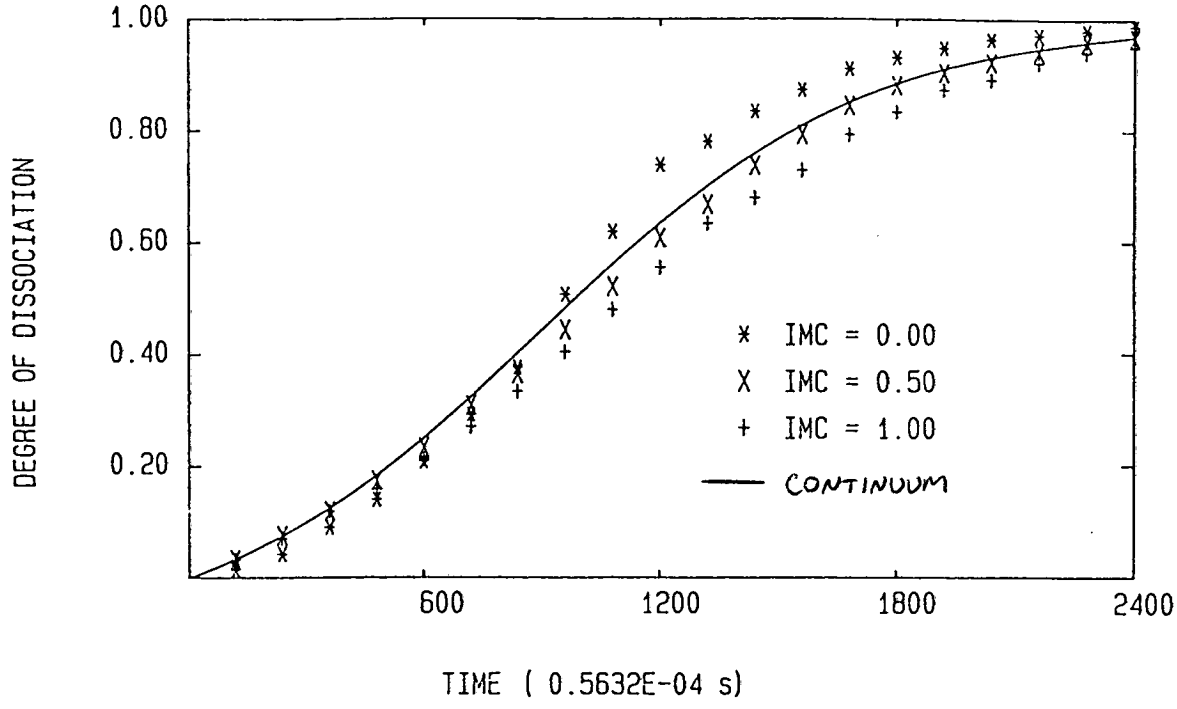

Fig. 3.5 Reaction path for dissociation of oxygen at 5000K and 0.001 Atm.

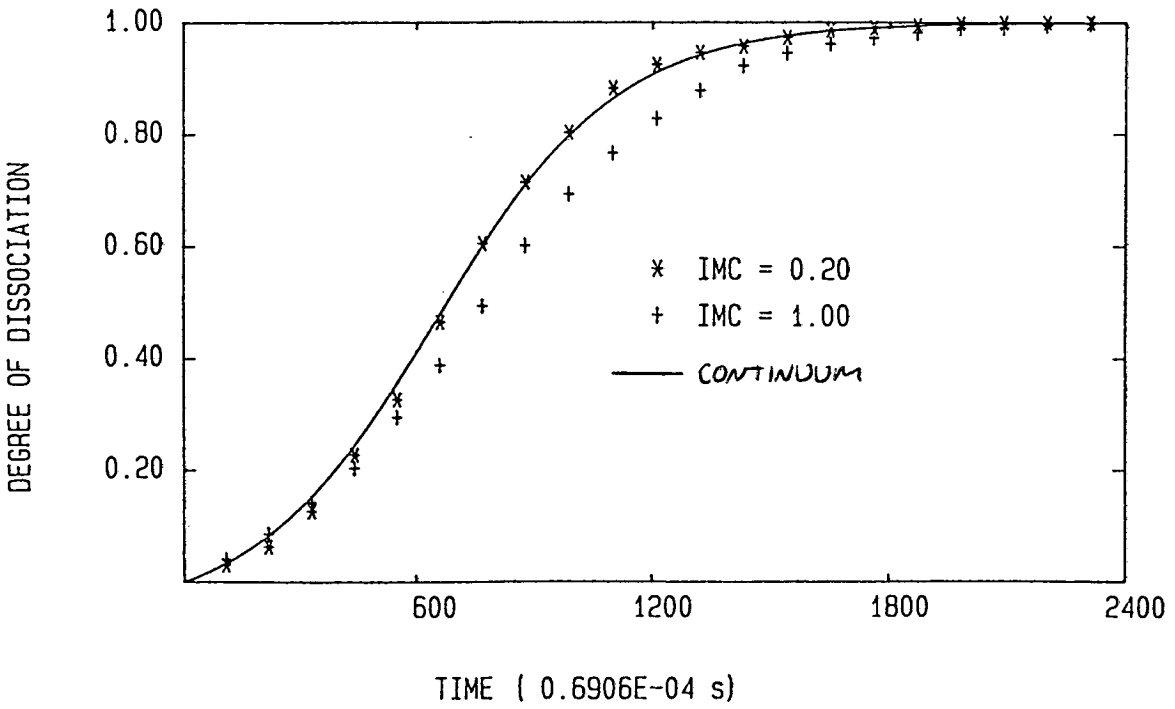

Fig. 3.6 Reaction path for dissociation of nitrogen at 10000K and 0.001Atm.

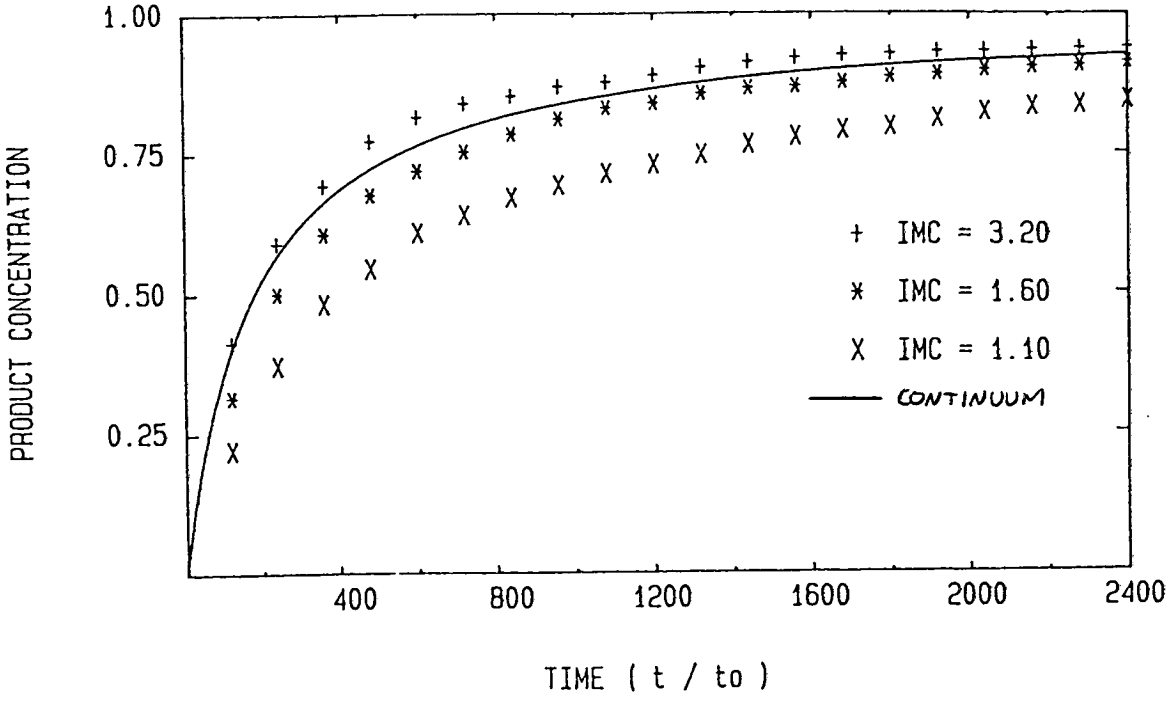

Fig. 3.7 Reaction paths for several values of IMC using Bird's steric factor.

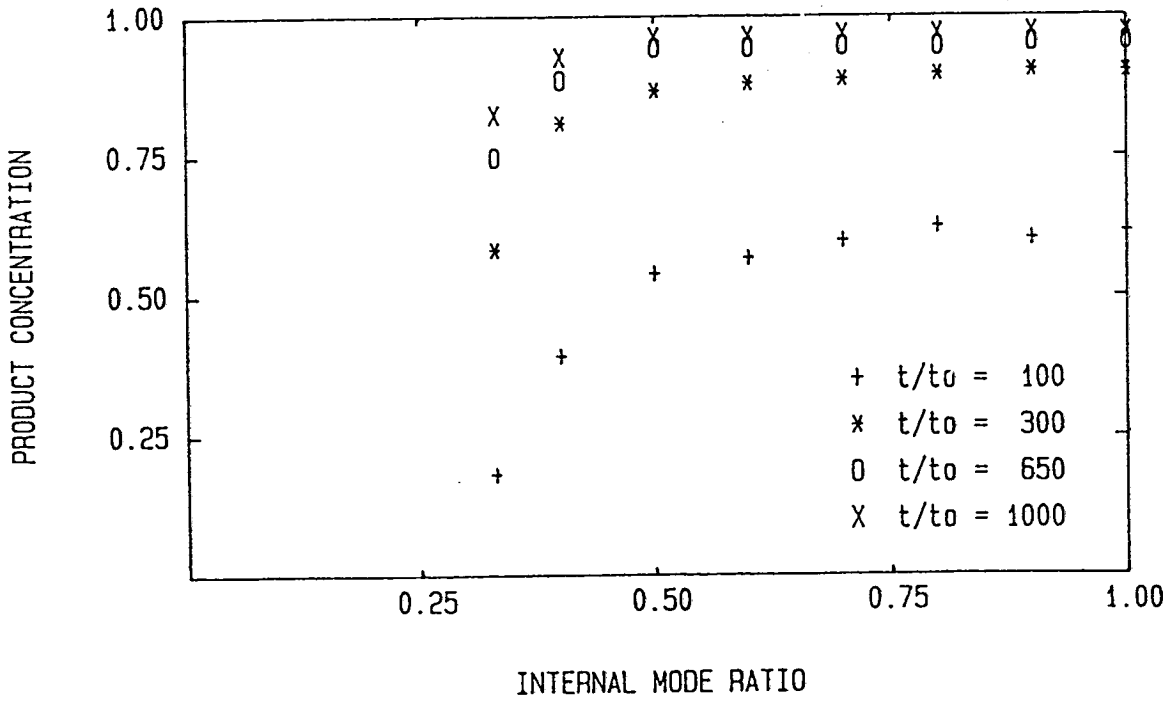

Fig. 3.8 Concentration of NO at various time stations for several values of IMR using Bird's steric factor.

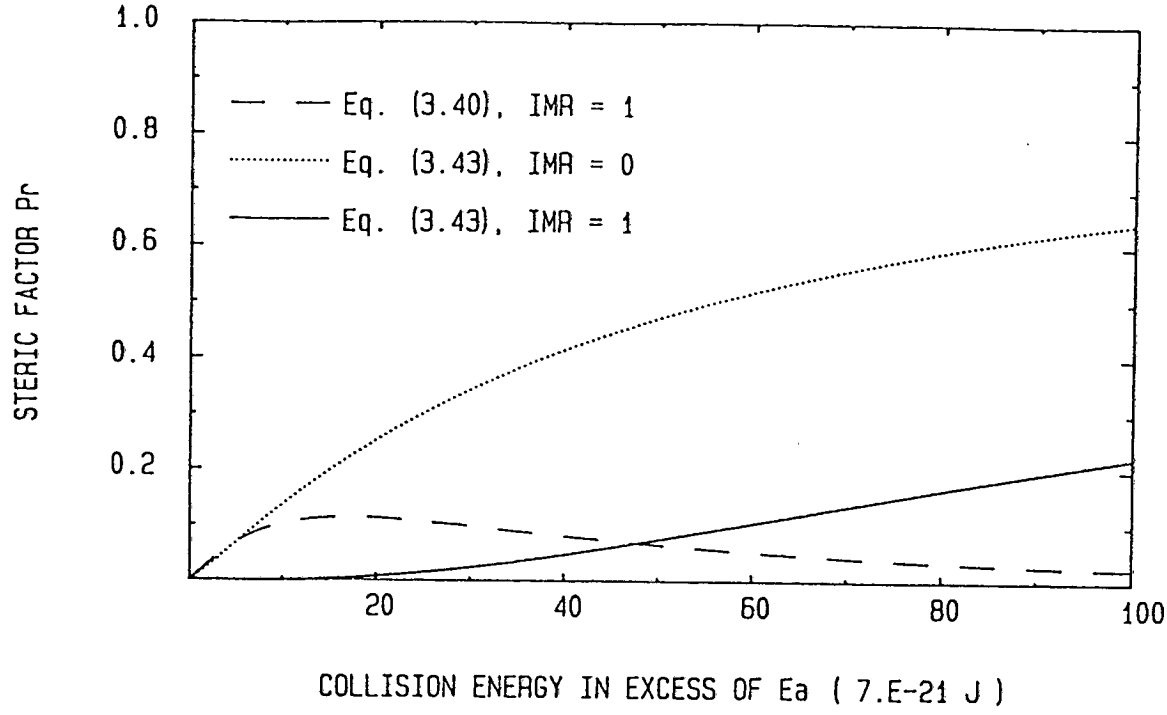

Fig. 3.9 The steric factors as a function of collision energy in excess of the activation energy E_a.

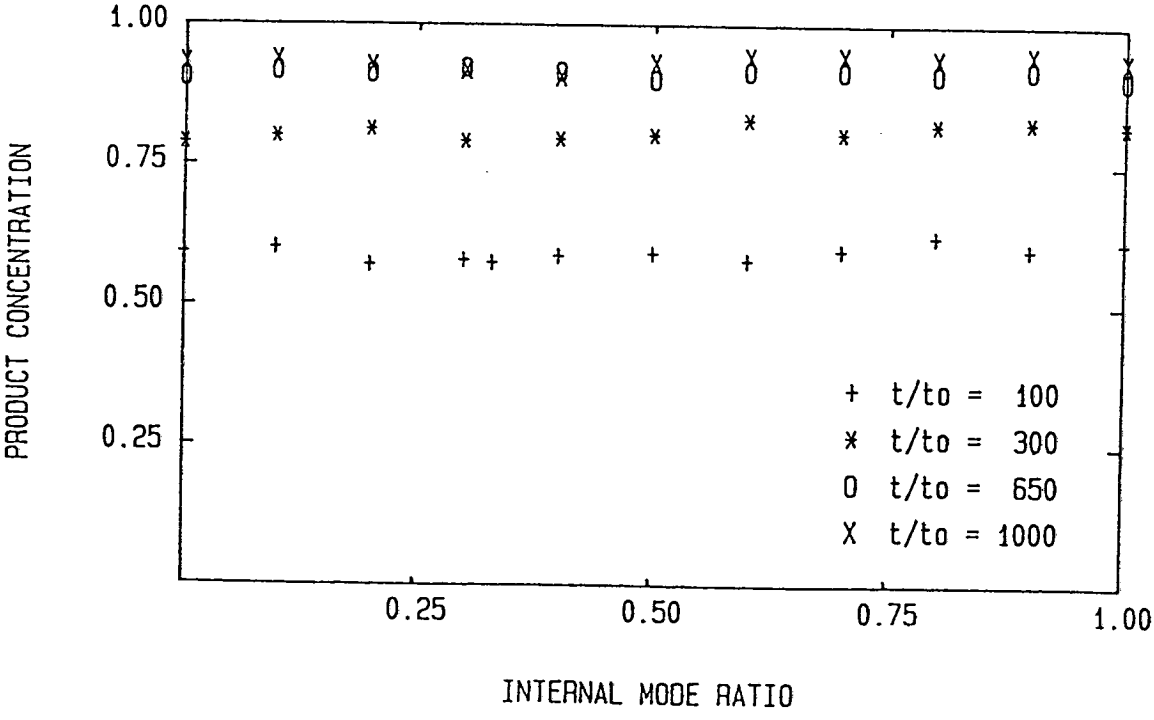

Fig. 3.10 Concentration of NO at various time stations for several values of IMR using the new steric factor.

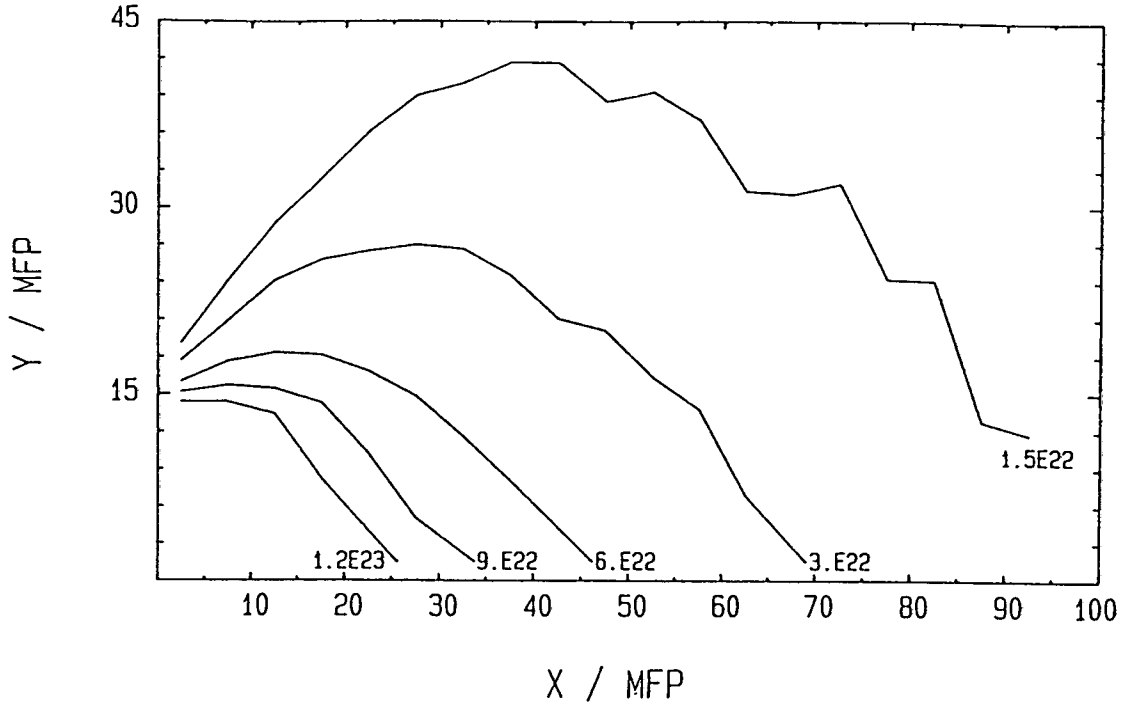

Fig. 4.1 Number density contours with hard-sphere molecules using Bird's Time Counter method.

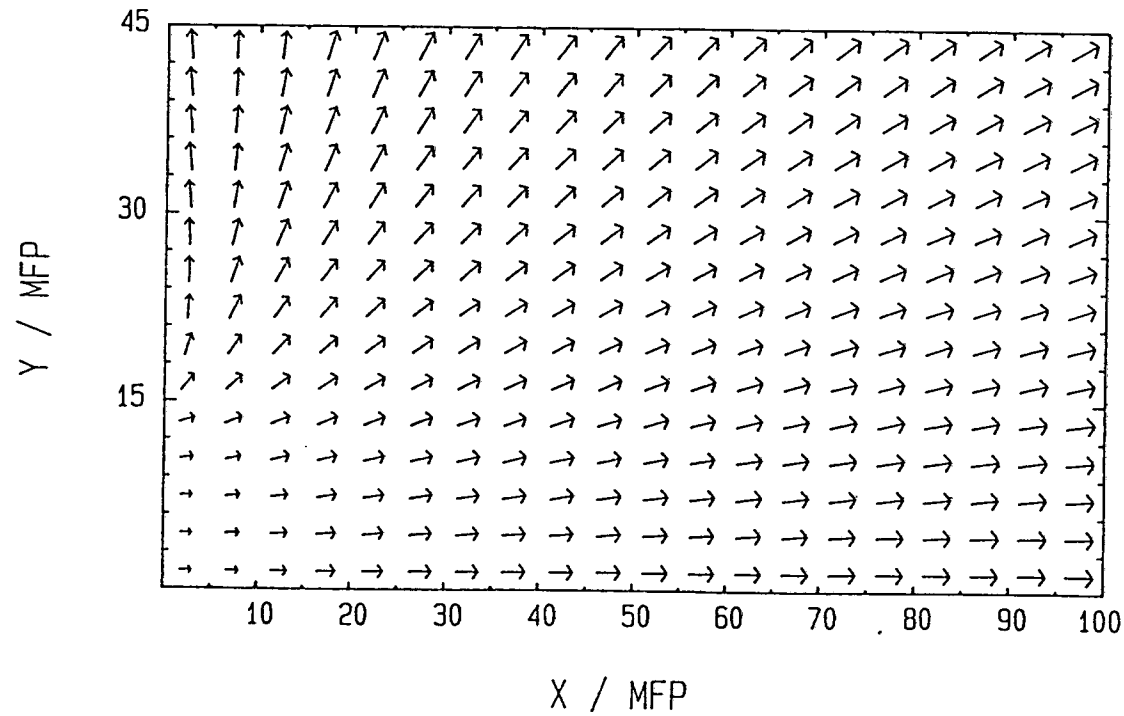

Fig. 4.2 Velocity vectors with hard-sphere molecules using Bird's Time Counter method.

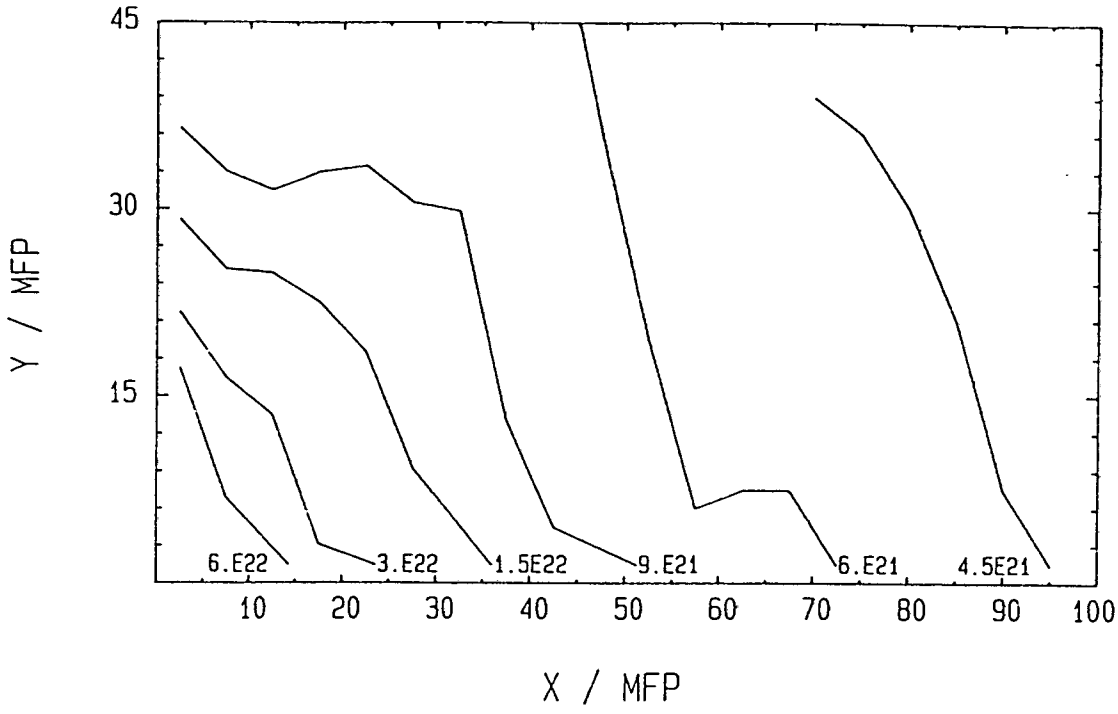

Fig. 4.3 Number density contours with hard-sphere molecules using Nanbu's method.

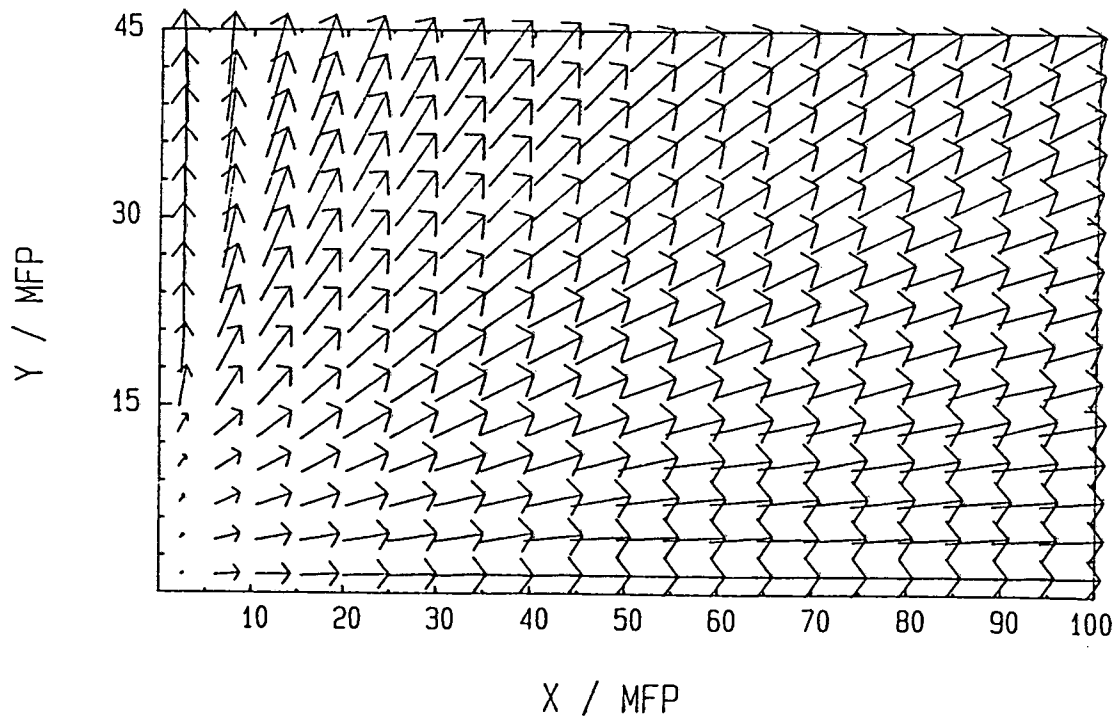

Fig. 4.4 Velocity vectors with hard-sphere molecules using Nanbu's method.

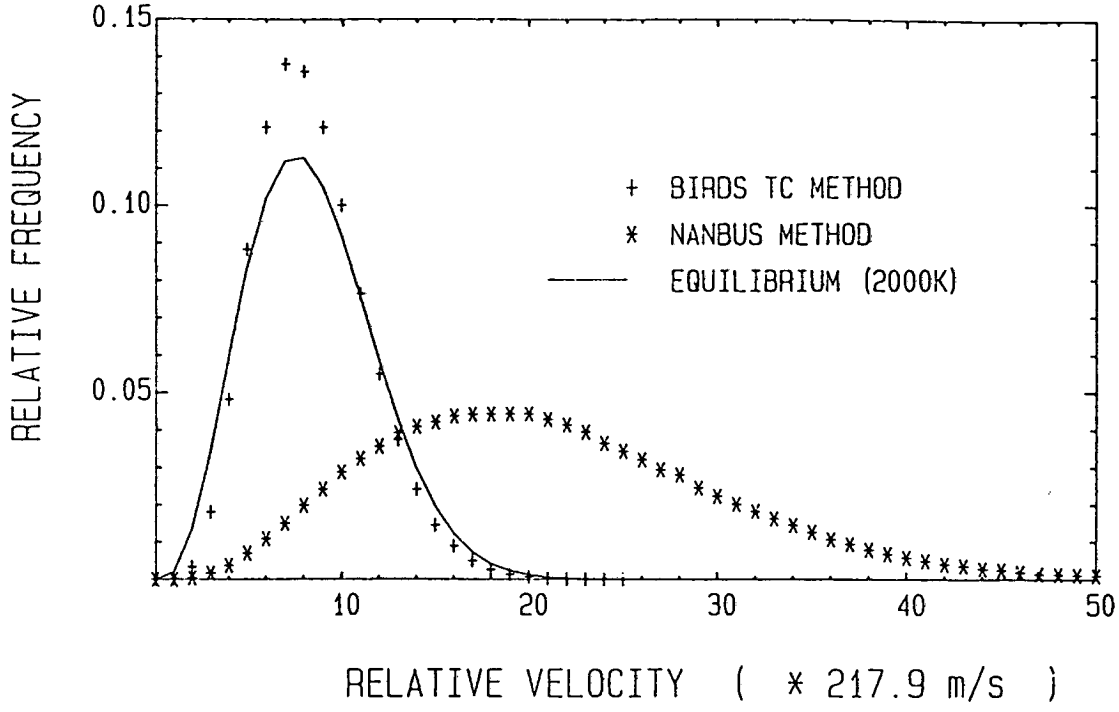

Fig. 4.5 Relative velocity distribution functions for the entire flowfield.

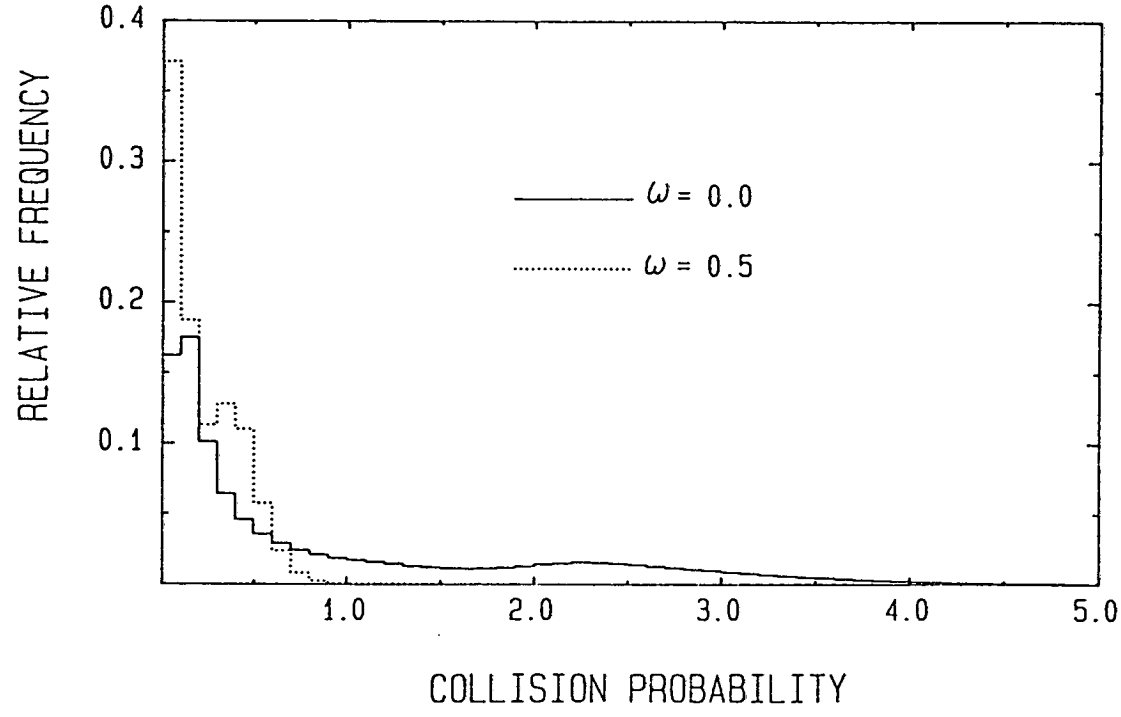

Fig. 4.6 Collision probability distribution functions from two Nanbu simulations.

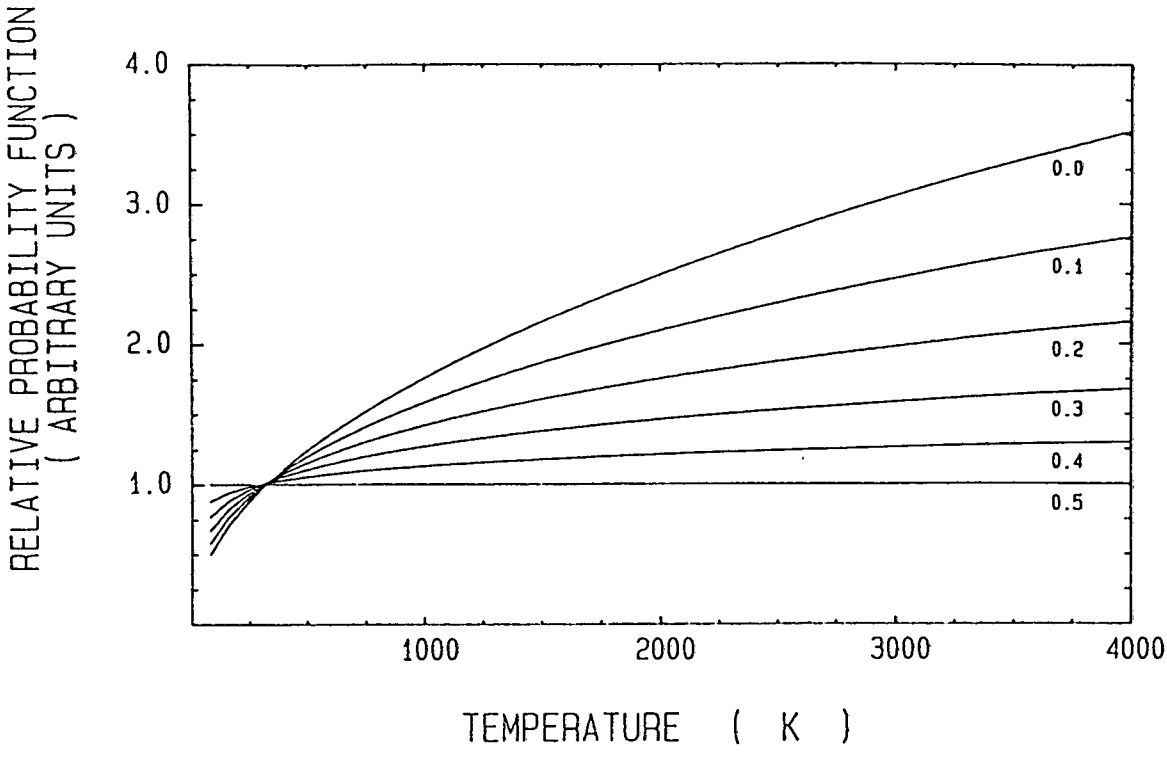

Fig. 4.7 The average collision probability F(ω,T) as a function of temperature for several values of ω.

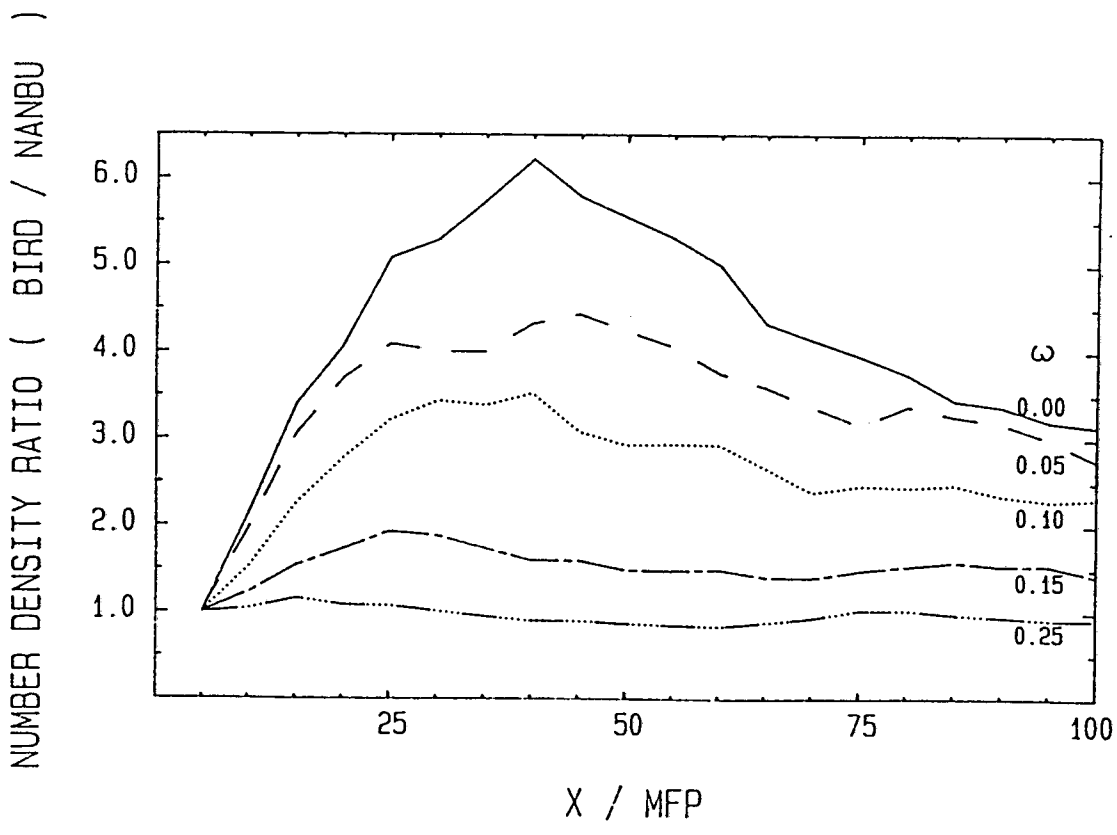

Fig. 4.8 Number density ratios (Bird/Nanbu) along the centreline for several values of ω.

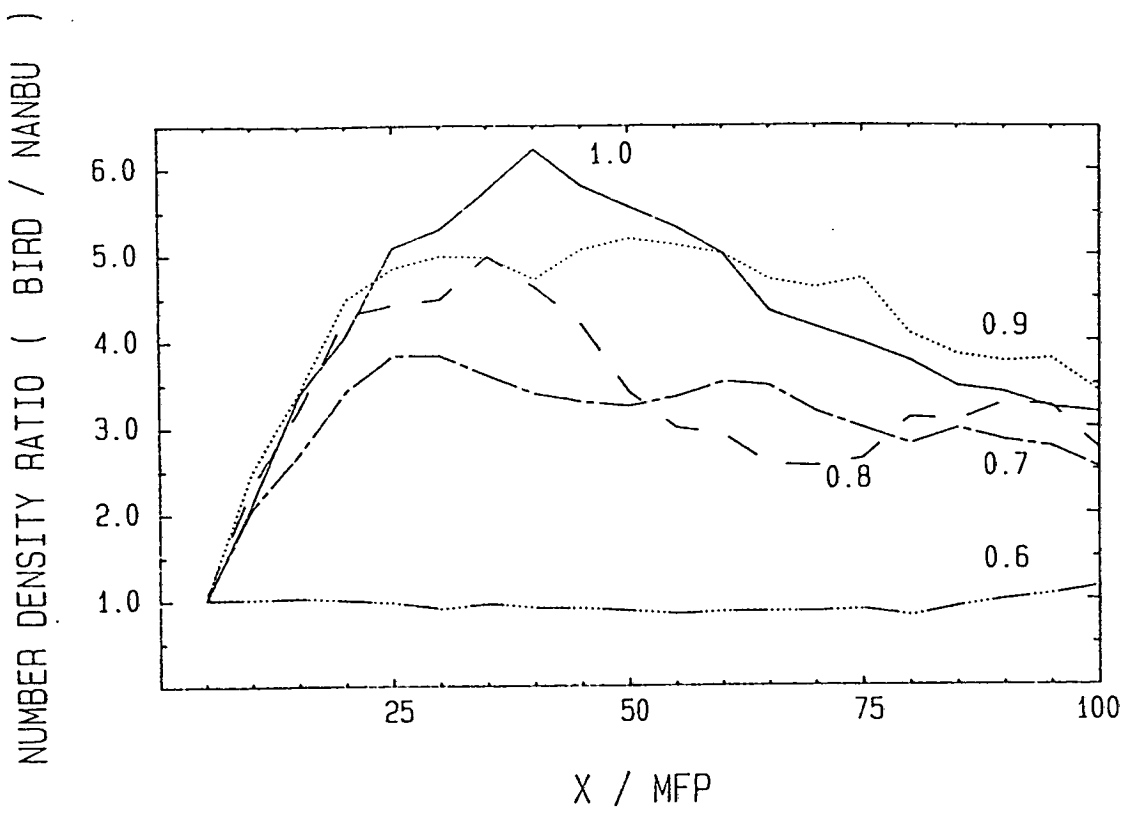

Fig. 4.9 Number density ratios (Bird/Nanbu) along the centreline for several values of Δt_m.

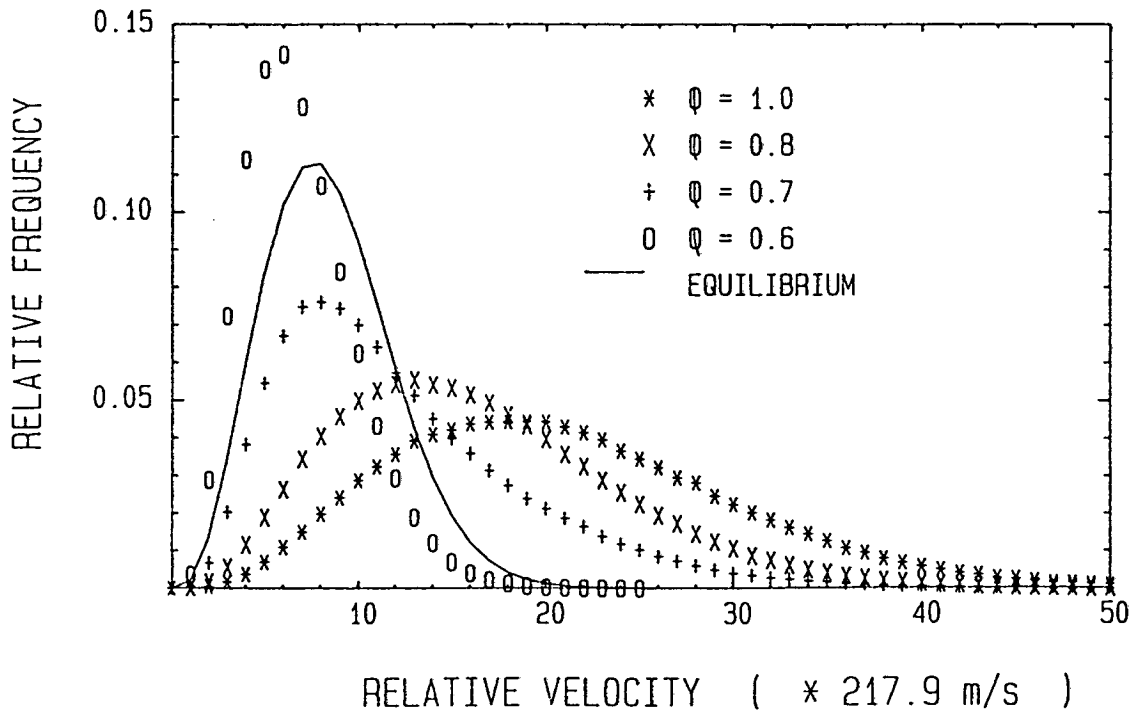

Fig. 4.10 Relative velocity distribution functions taken from Nanbu simulations for several values of ω.

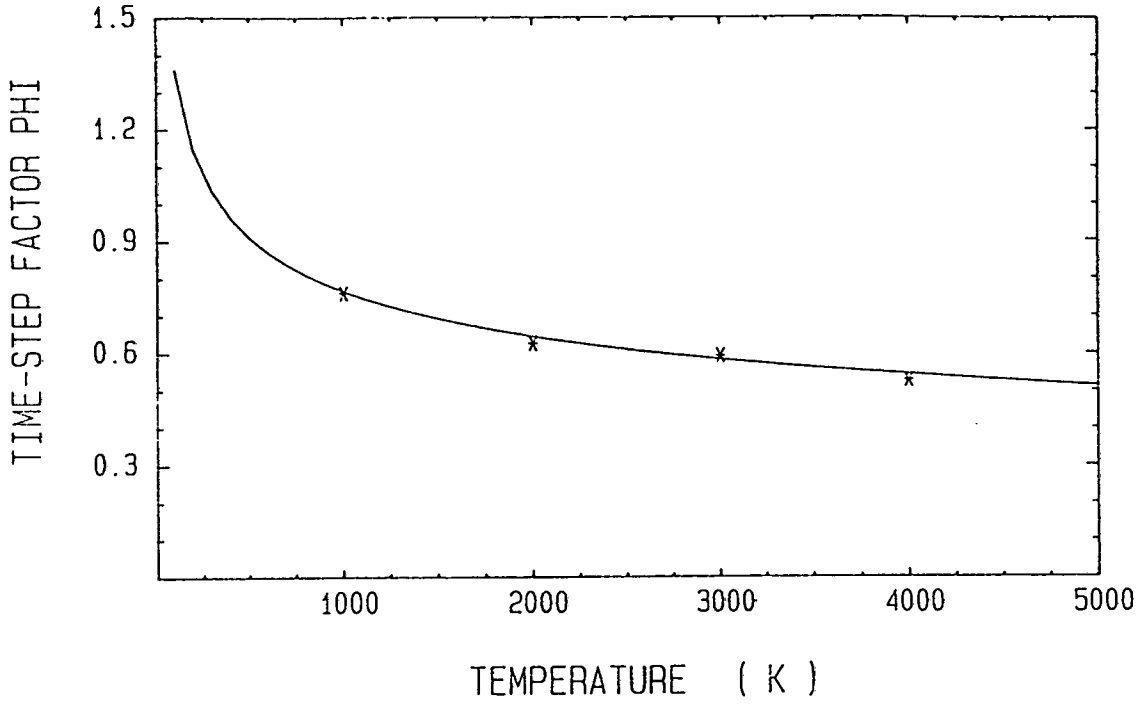

Fig. 4.11 Time-step estimate as a function of temperature, together with time-step values employed successfully in Nanbu simulations.

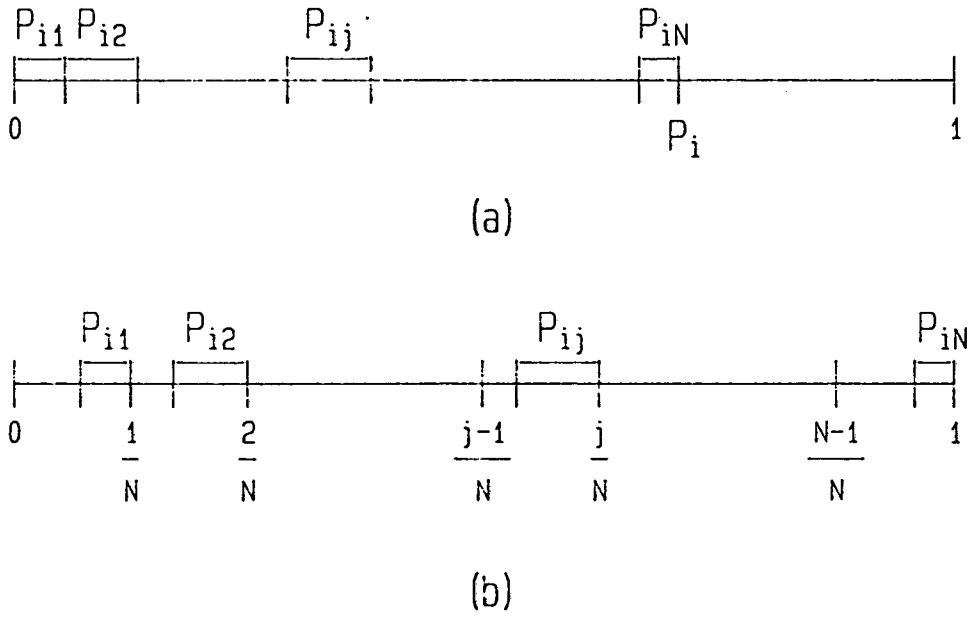

Fig. 4.12 Distributions of the probabilities P_{ij} over the unit interval for (a) the original Nanbu scheme and (b) the Modified Nanbu scheme.

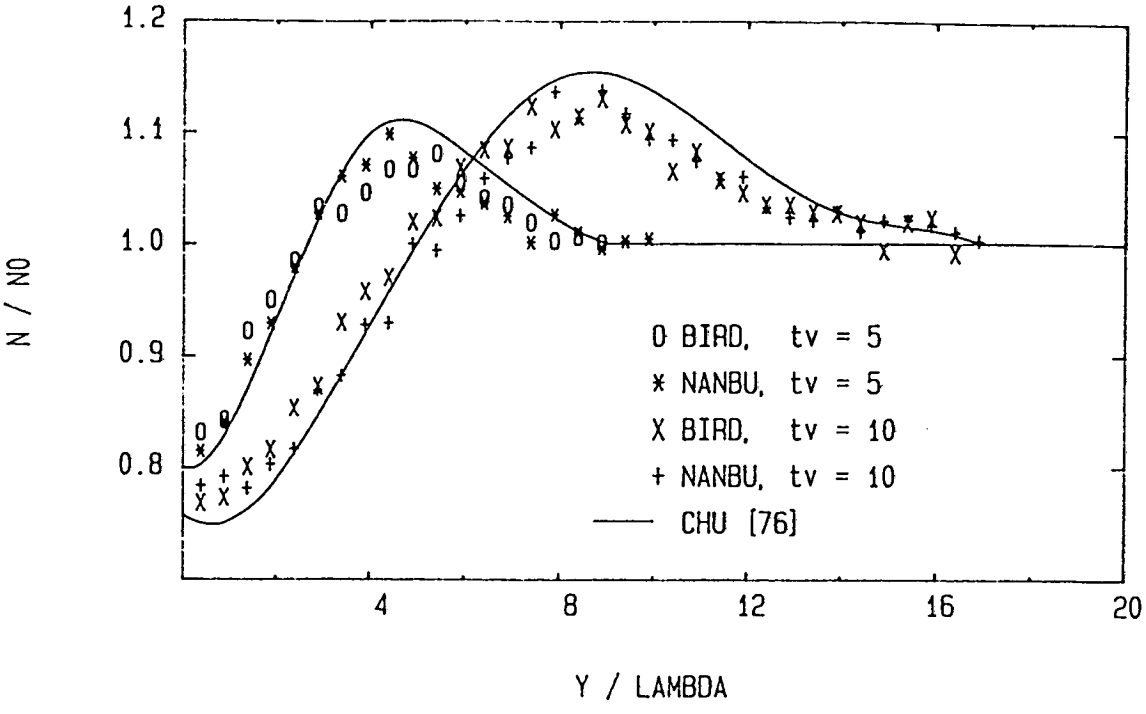

Fig. 4.13 Number density plots for the Rayleigh problem.

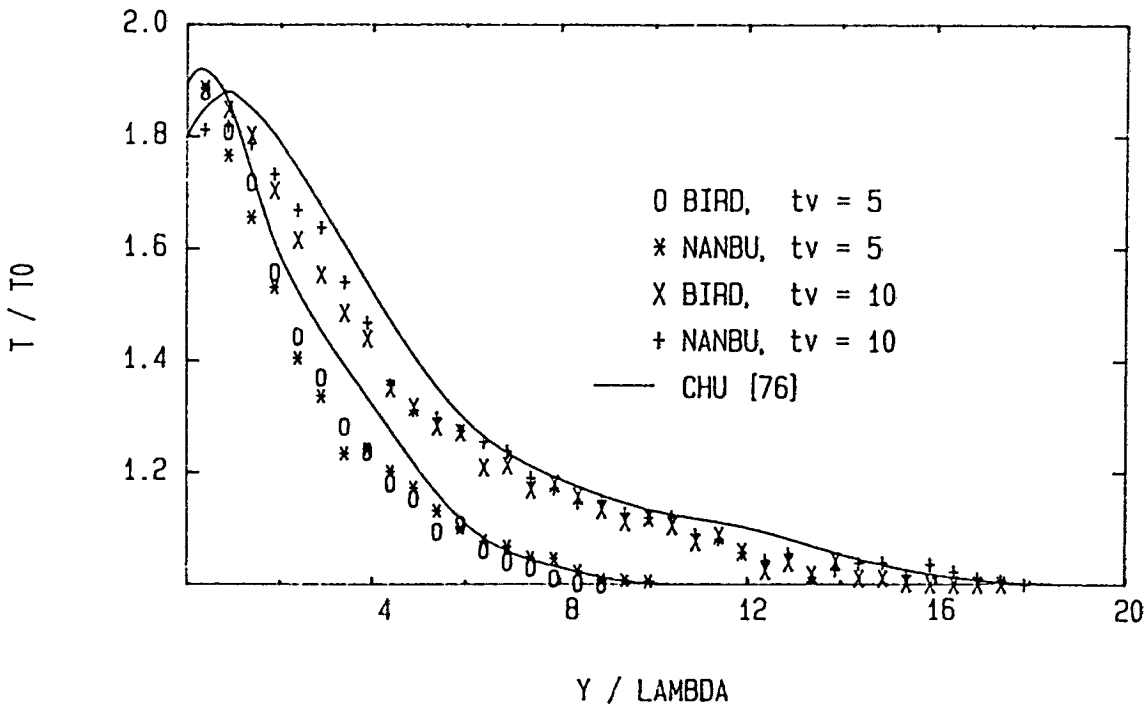

Fig. 4.14 Temperature plots for the Rayleigh problem.

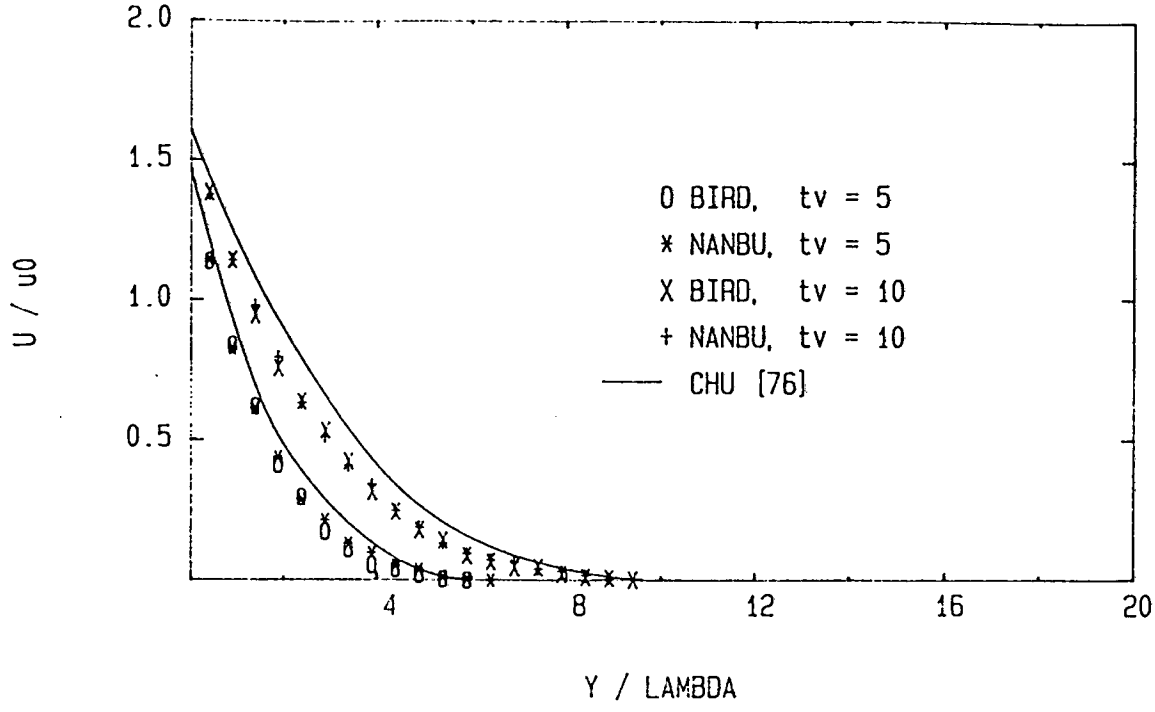

Fig. 4.15 Shear velocity plots for the Rayleigh problem.

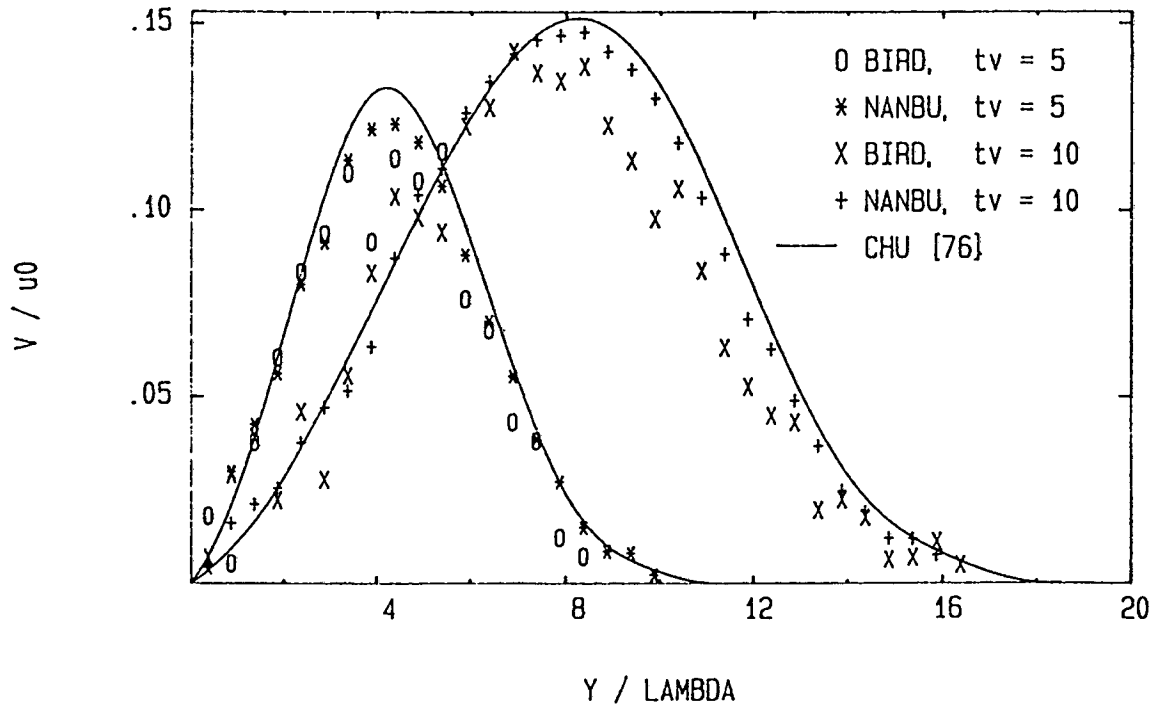

Fig. 4.16 Normal velocity plots for the Rayleigh problem.

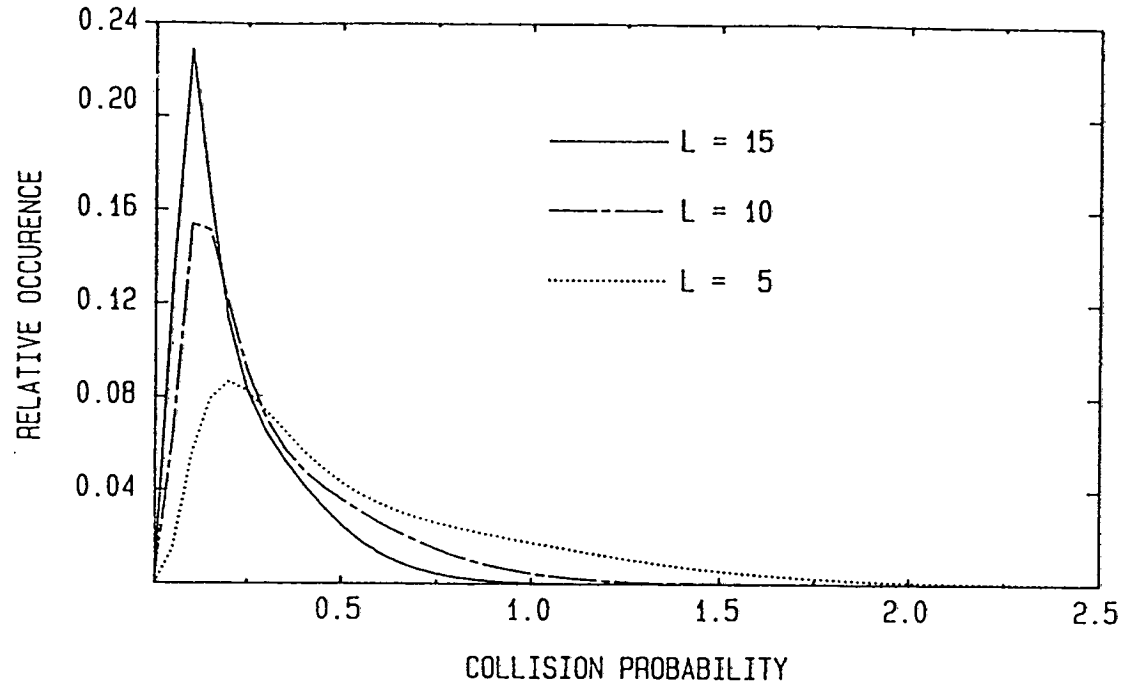

Fig. 4.17 Collision Probability distribution functions for different L.

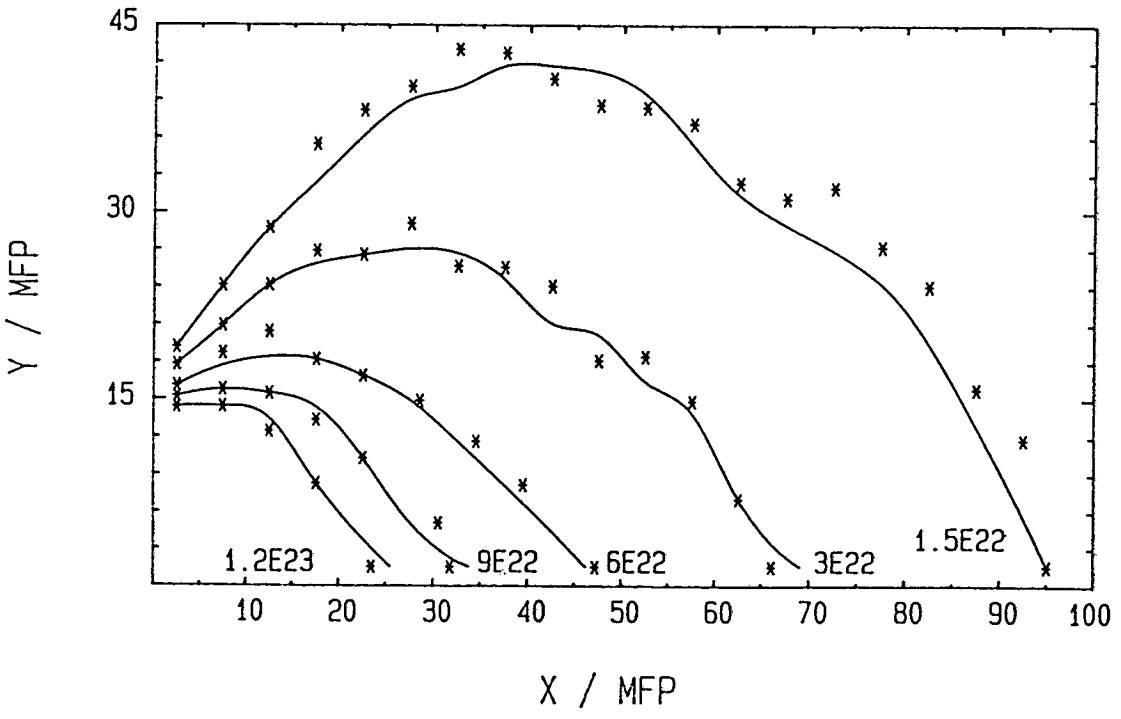

Fig. 4.18 Density plots for the sonic expansion of hot nitrogen.
———— , Bird method; *, Modified Nanbu method.

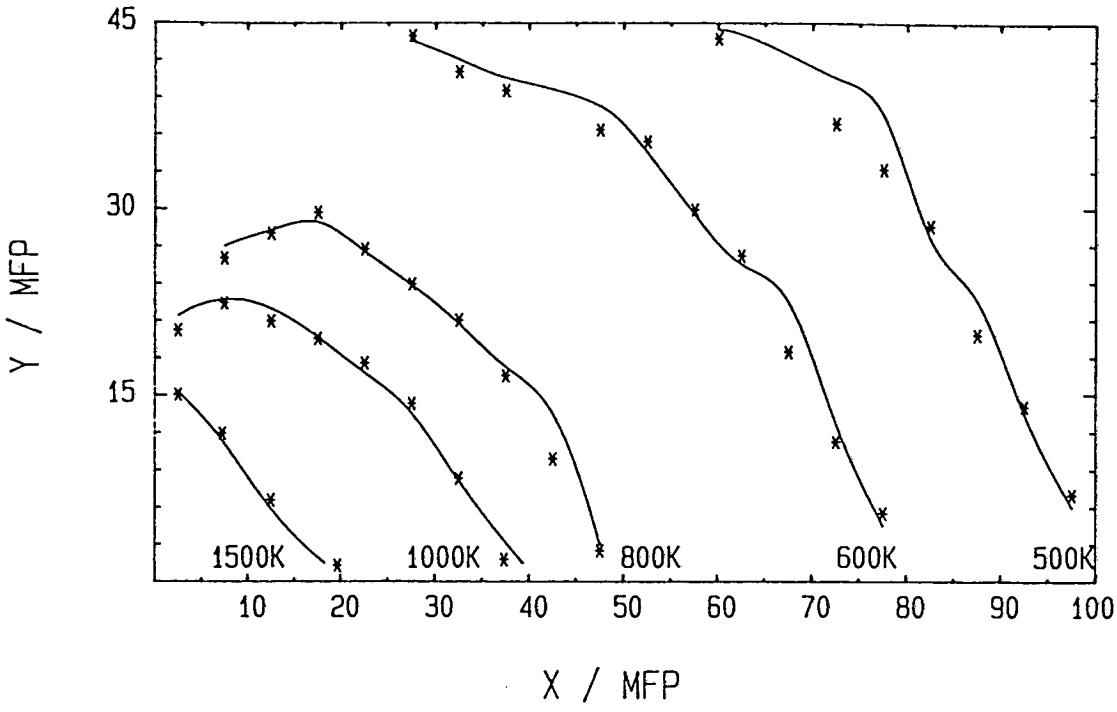

Fig. 4.19 Temperature plots for the sonic expansion of hot nitrogen. ——— , Bird method; *, Modified Nanbu method.

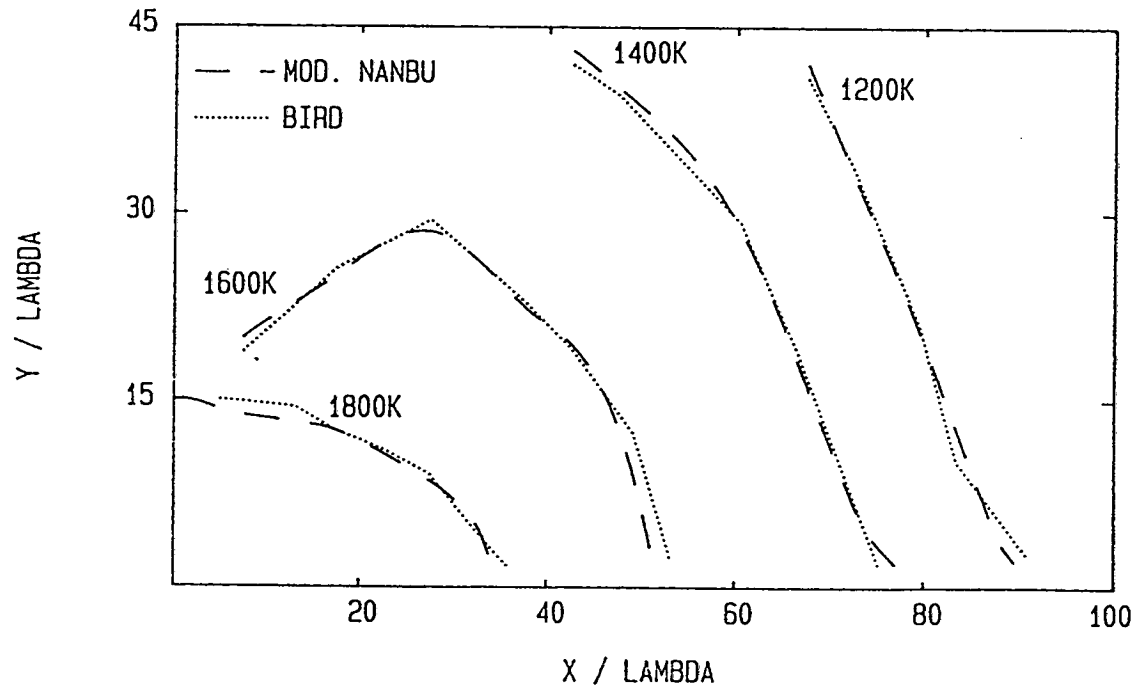

Fig. 4.20 Rotational temperature contours for sonic expansion of nitrogen.

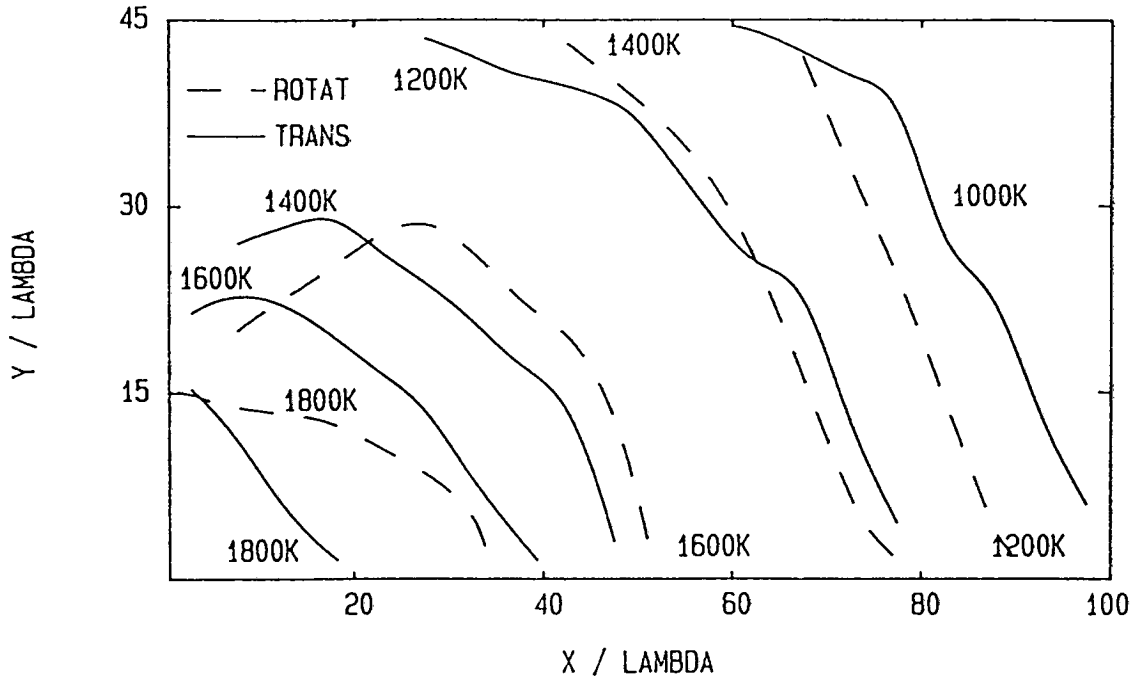

Fig. 4.21 Comparison of translational and rotational temperature contours.

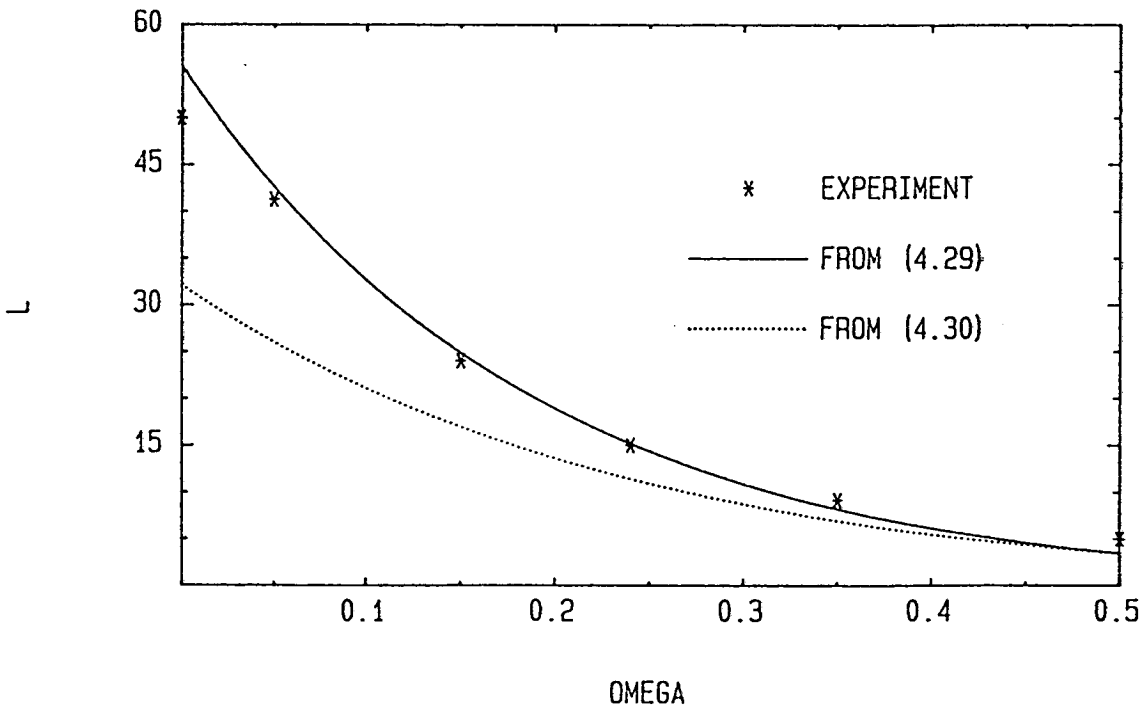

Fig. 4.22 Number of subdivisions of the time-step Δt_m in the Modified Nanbu scheme as a function of the VHS collision model parameter ω.

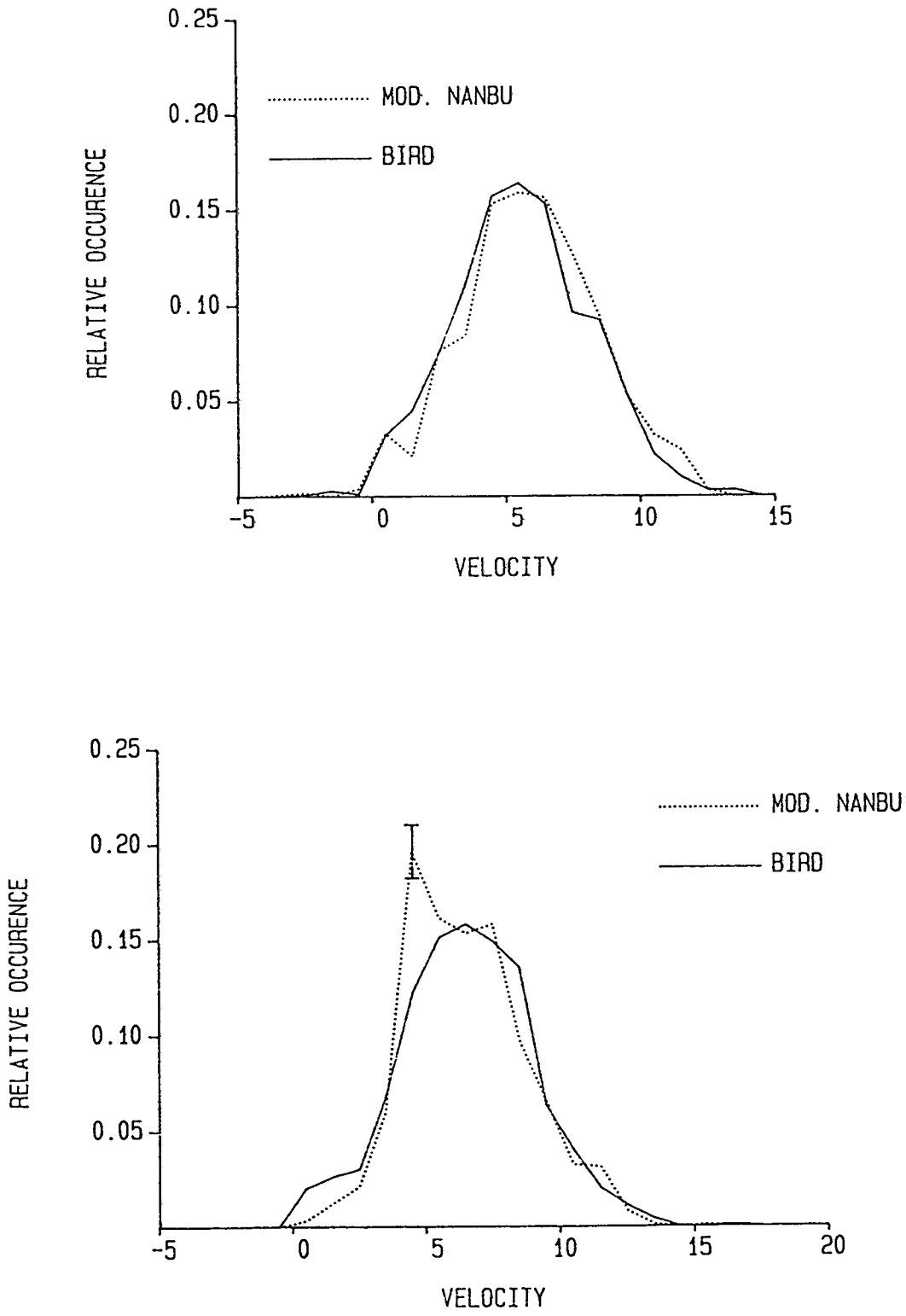

Fig. 4.23 Transverse velocity distributions, (a) at $x = 3\lambda_0$ and (b) at $x = 20\lambda_0$.

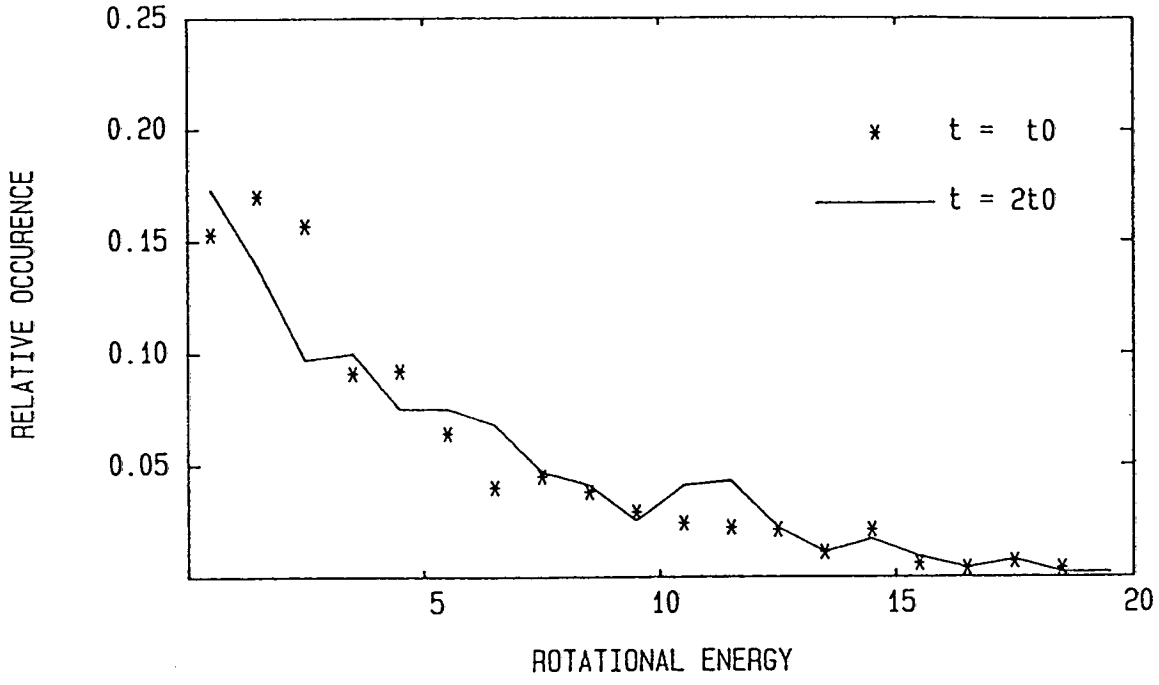

Fig. 4.24 Rotational energy distributions for the Mod. Nanbu method, $x = 20\lambda_0$.

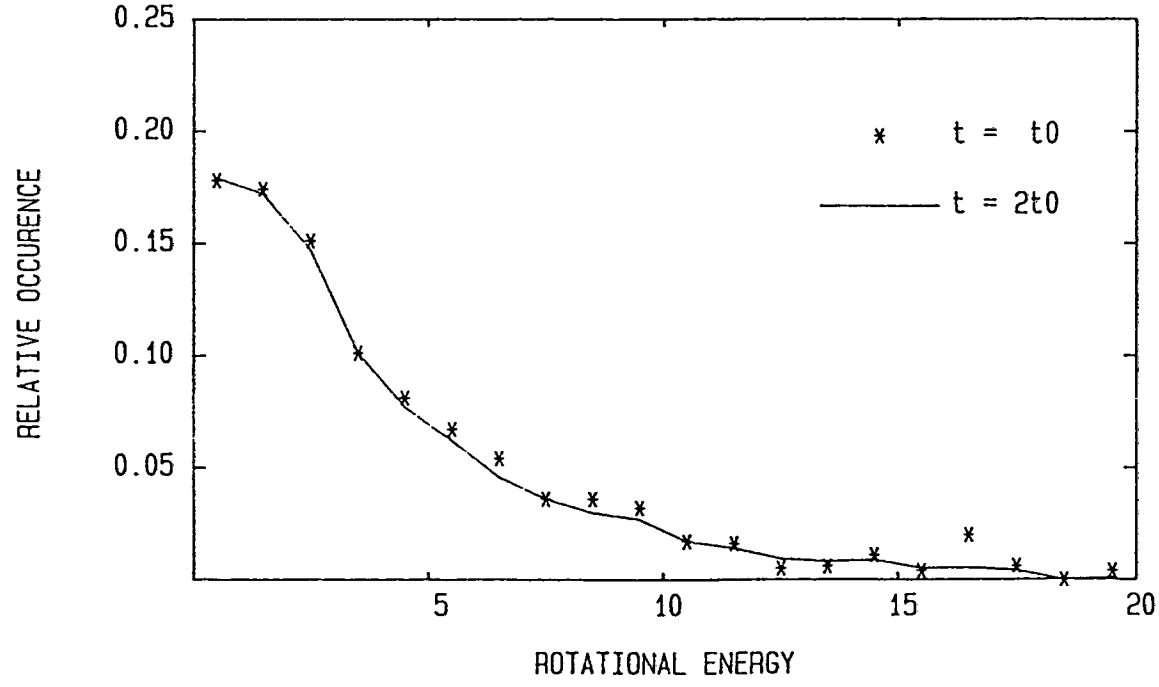

Fig. 4.25 Rotational energy distributions for the Bird method, $x = 20\lambda_0$.

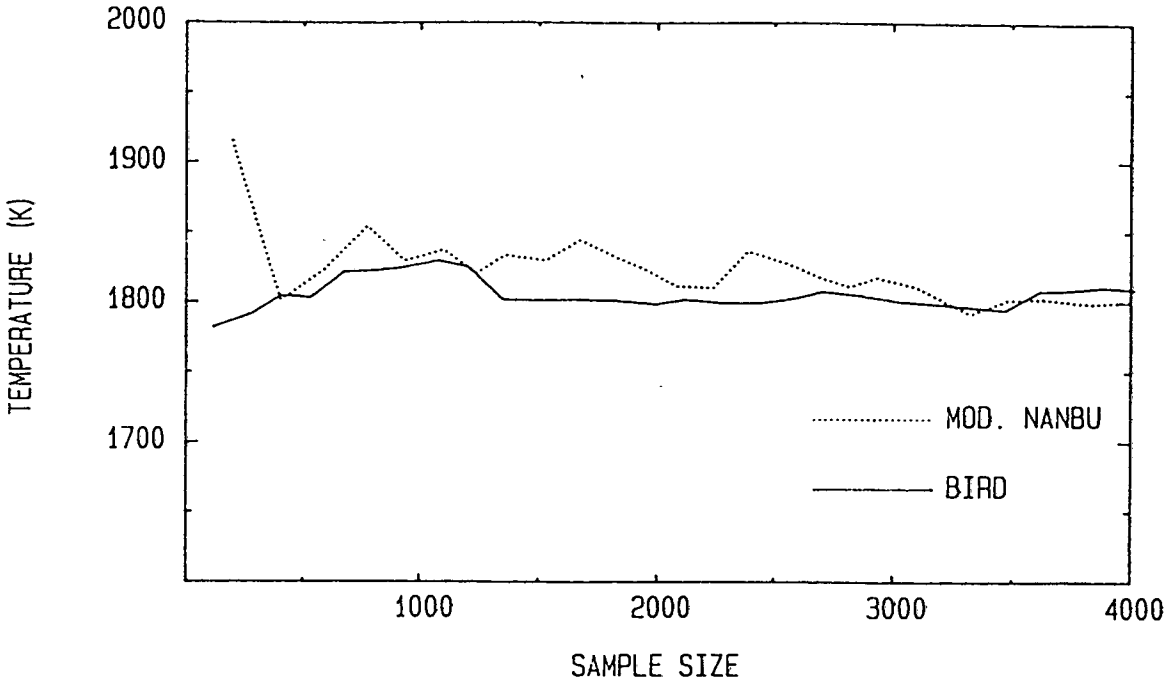

Fig. 4.26 Convergence of translational temperature to a steady state, $x = 20\lambda_0$.

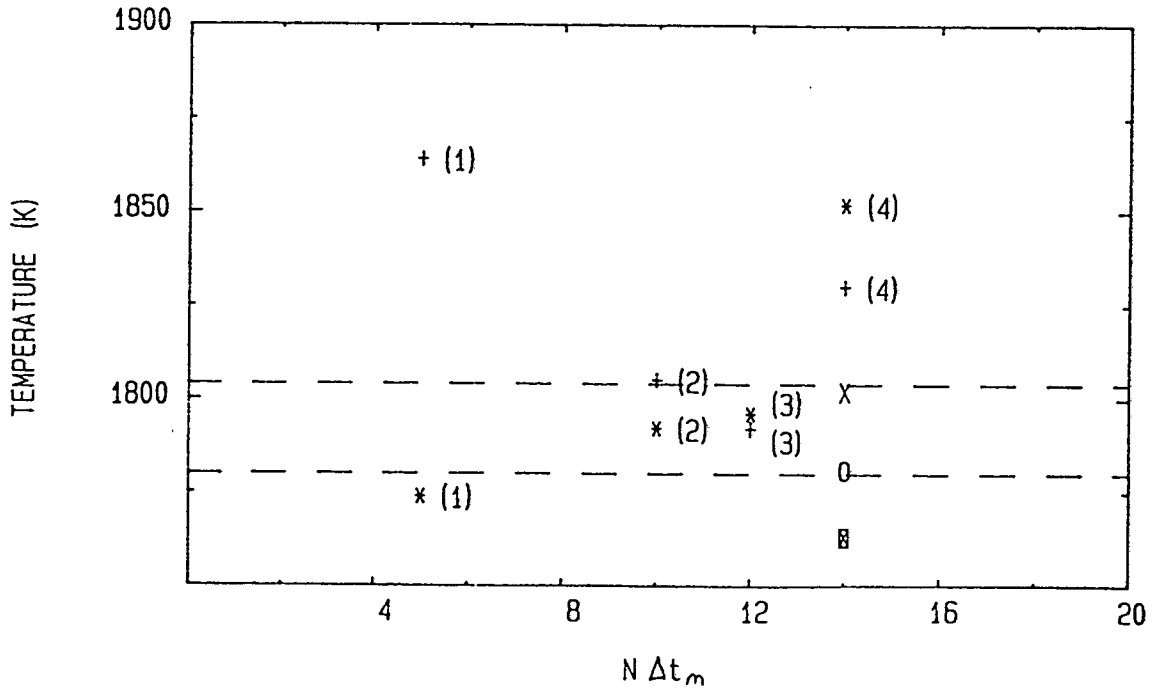

Fig. 4.27 Translational temperature values at $x = 20\lambda_0$.

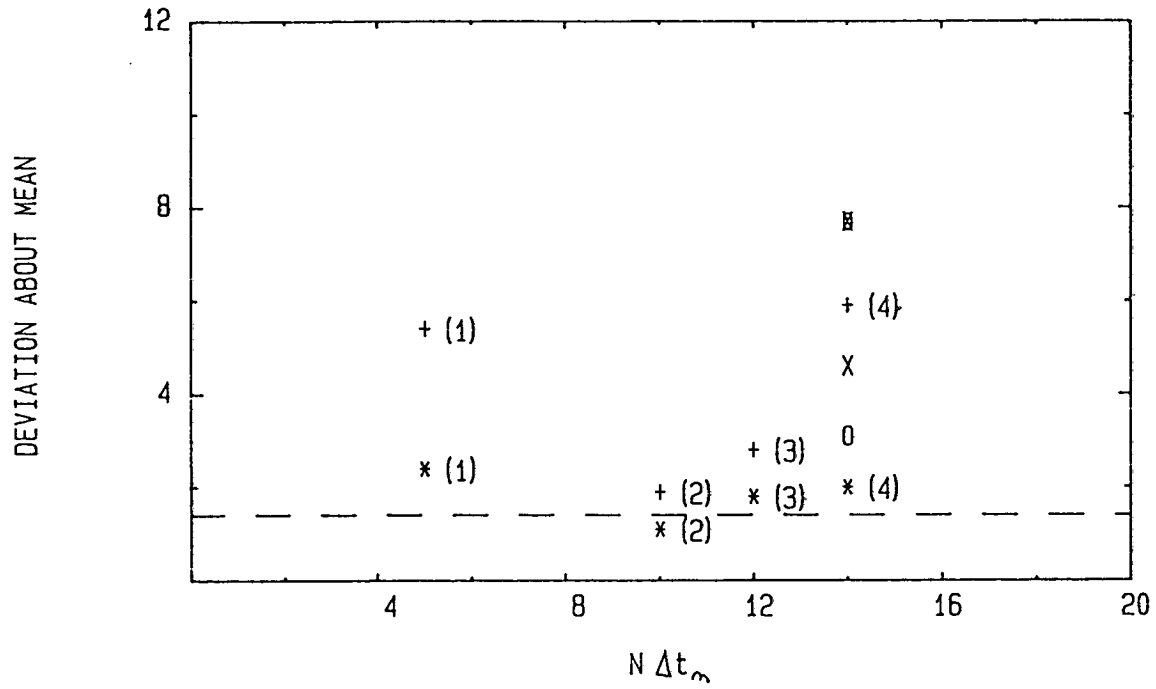

Fig. 4.28 Percentage deviation about the mean translational temperature, $x = 20\lambda_0$.

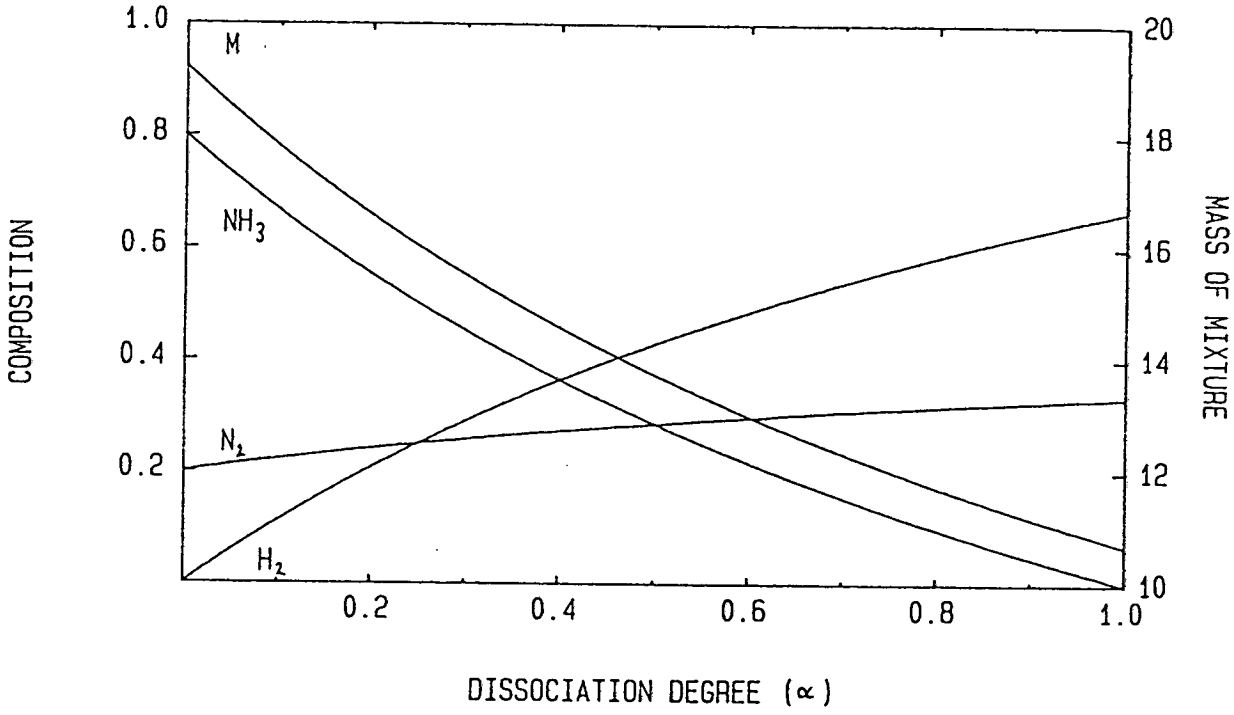

Fig. 5.1 Gas composition of a function of α, the degree of ammonia dissociated.

Fig. 4.29 Unsteady density contours at several time stations calculated with Bird's (B) Time Counter method.

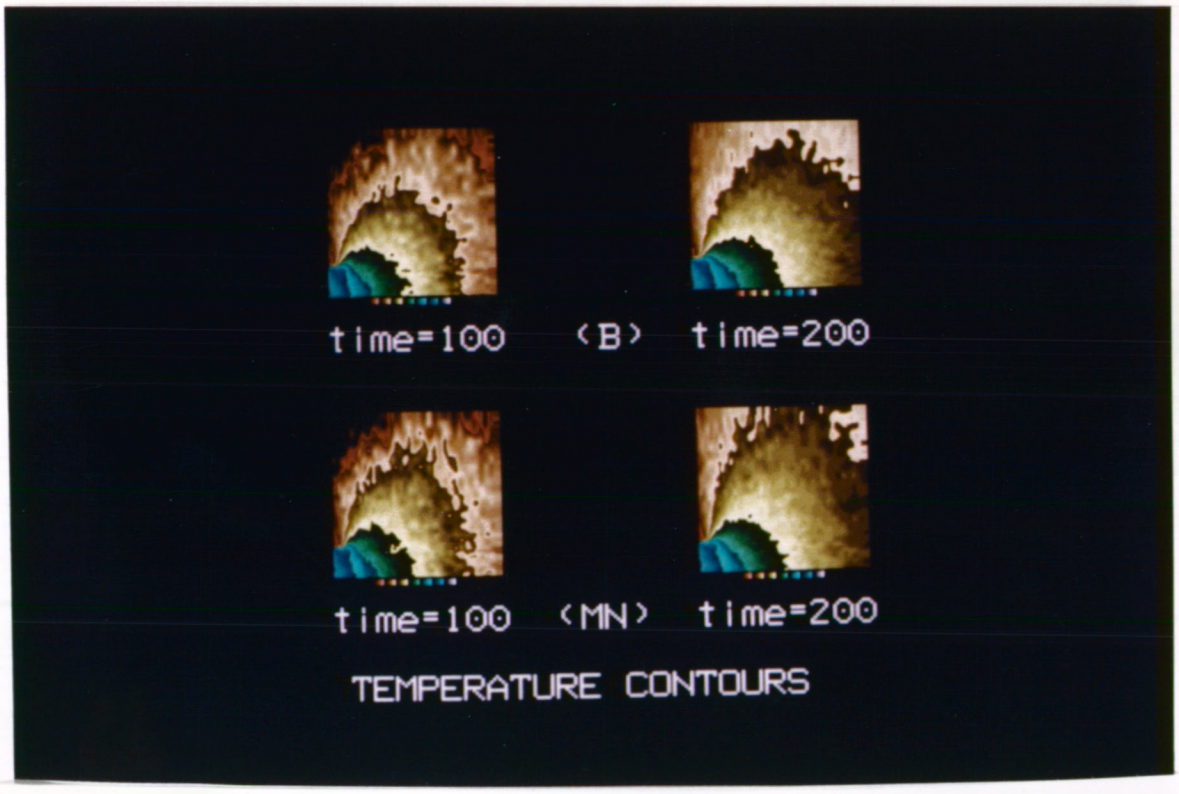

Fig. 4.30 Comparison of unsteady temperature contours.

Fig. 4.31 Comparison of steady temperature contours.

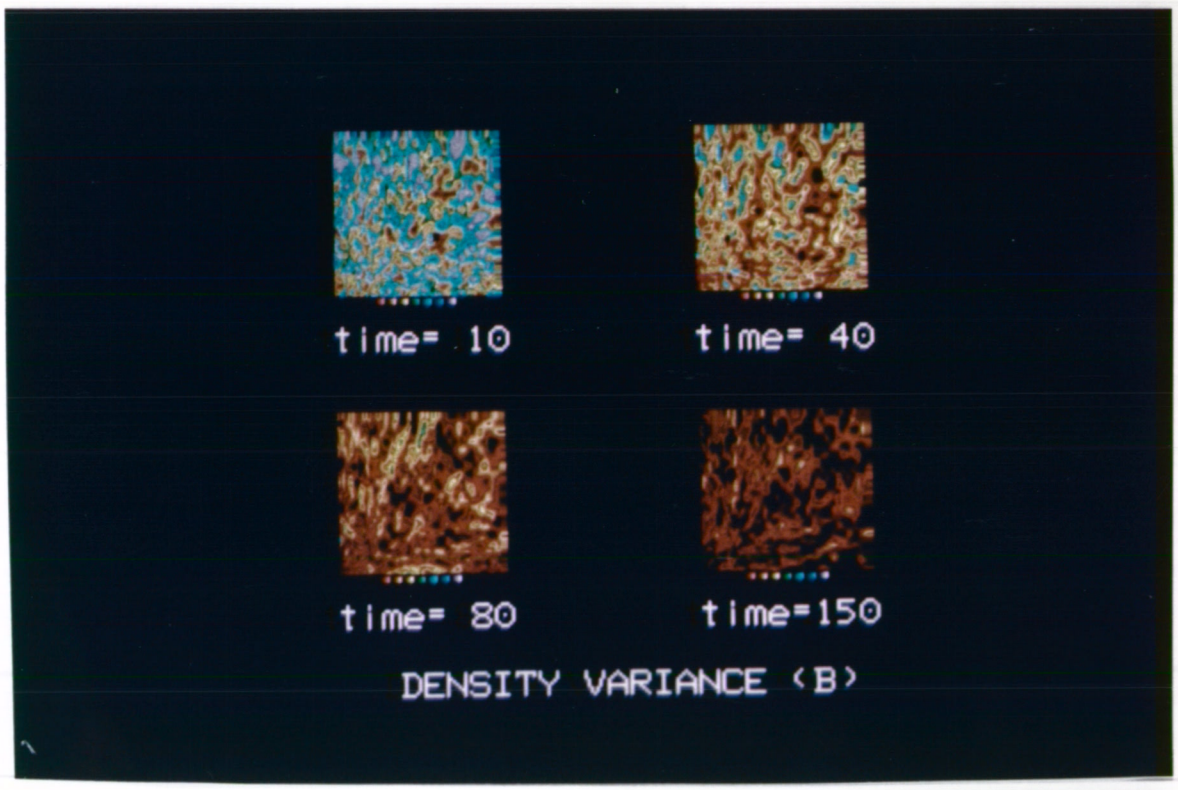

Fig. 4.32 Variance of steady density calculations showing the reduction of fluctuations as sample size is increased.

Fig. 4.33 Comparison of steady density variances.

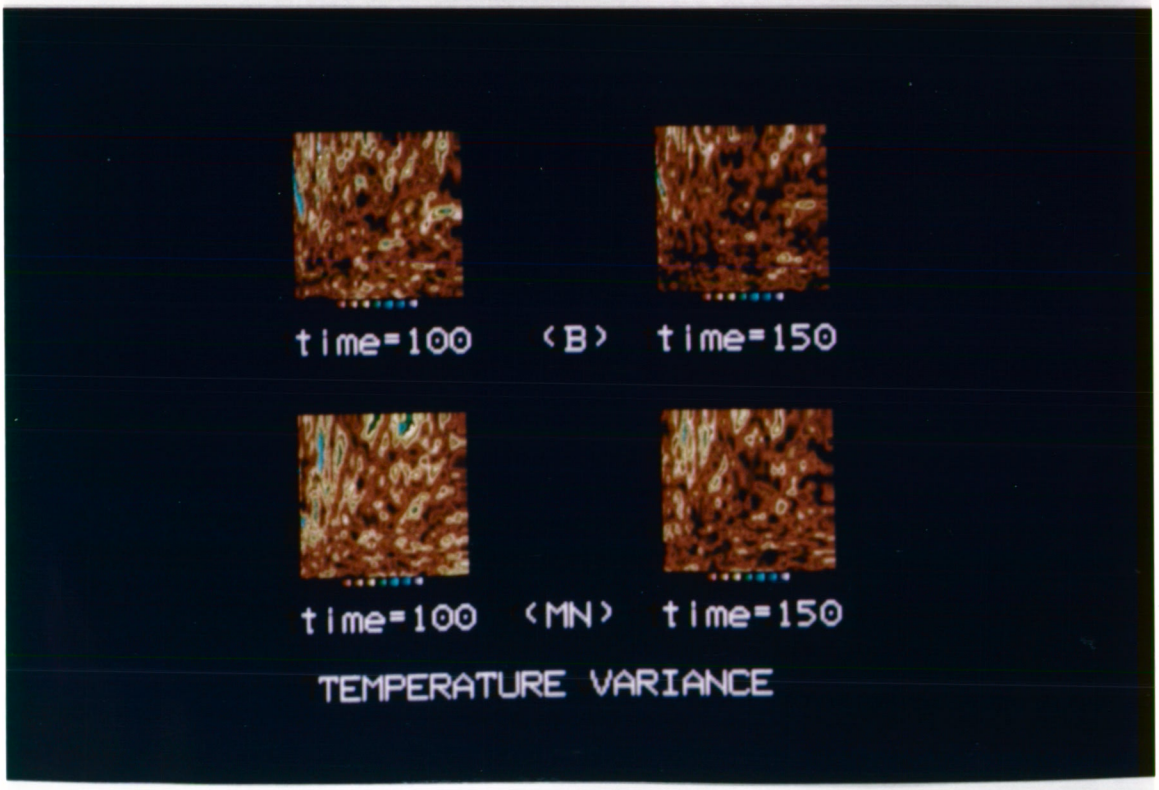

Fig. 4.34 Comparison of steady temperature variances.

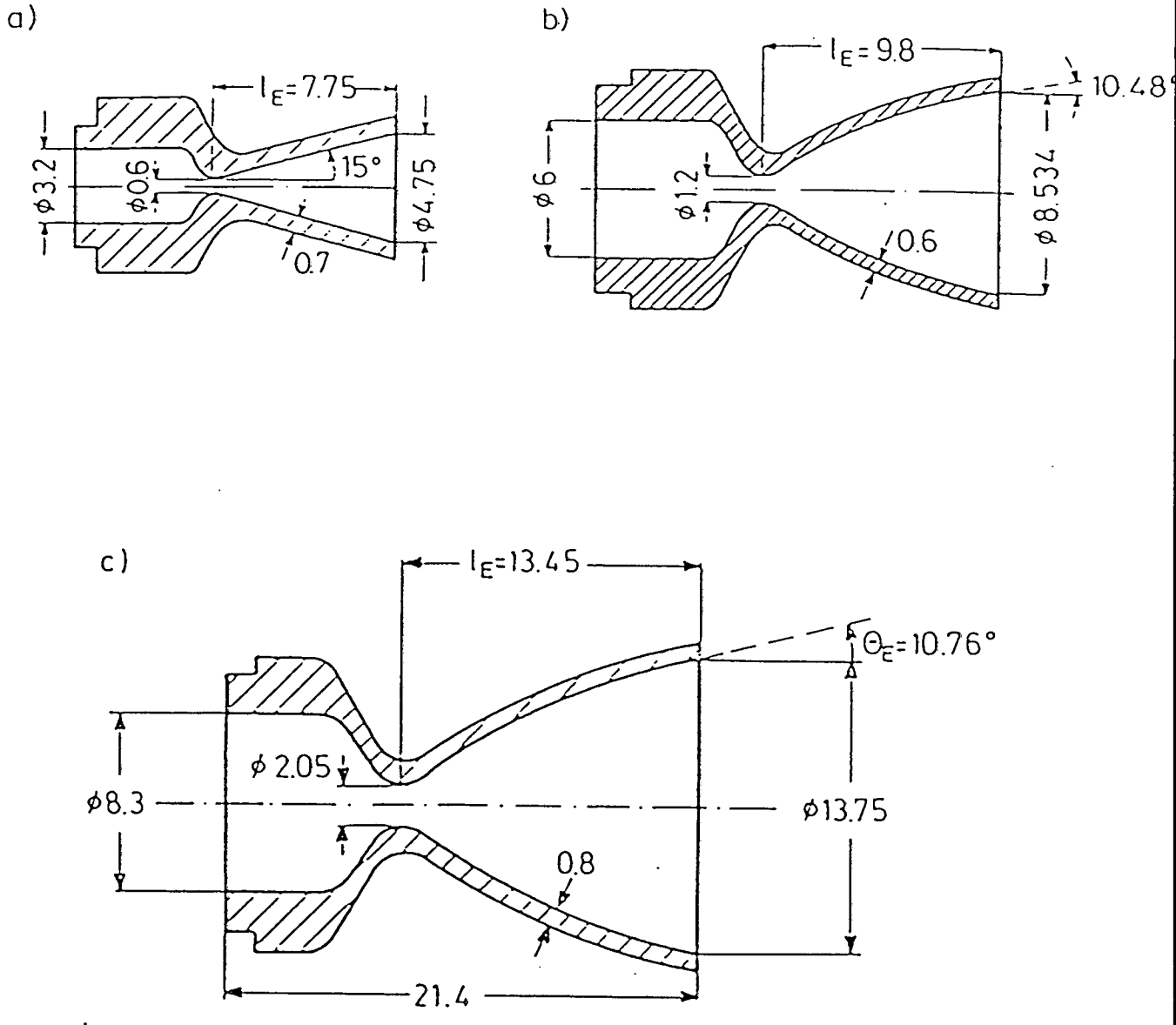

Nozzle geometries·

a) ERNO 0.5 N

b) ERNO 2 N

c) ERNO 5 N

Linear dimensions in mm.

Fig. 5.2 The geometries of three hydrazine thrusters manufactured by MBB/ERNO.

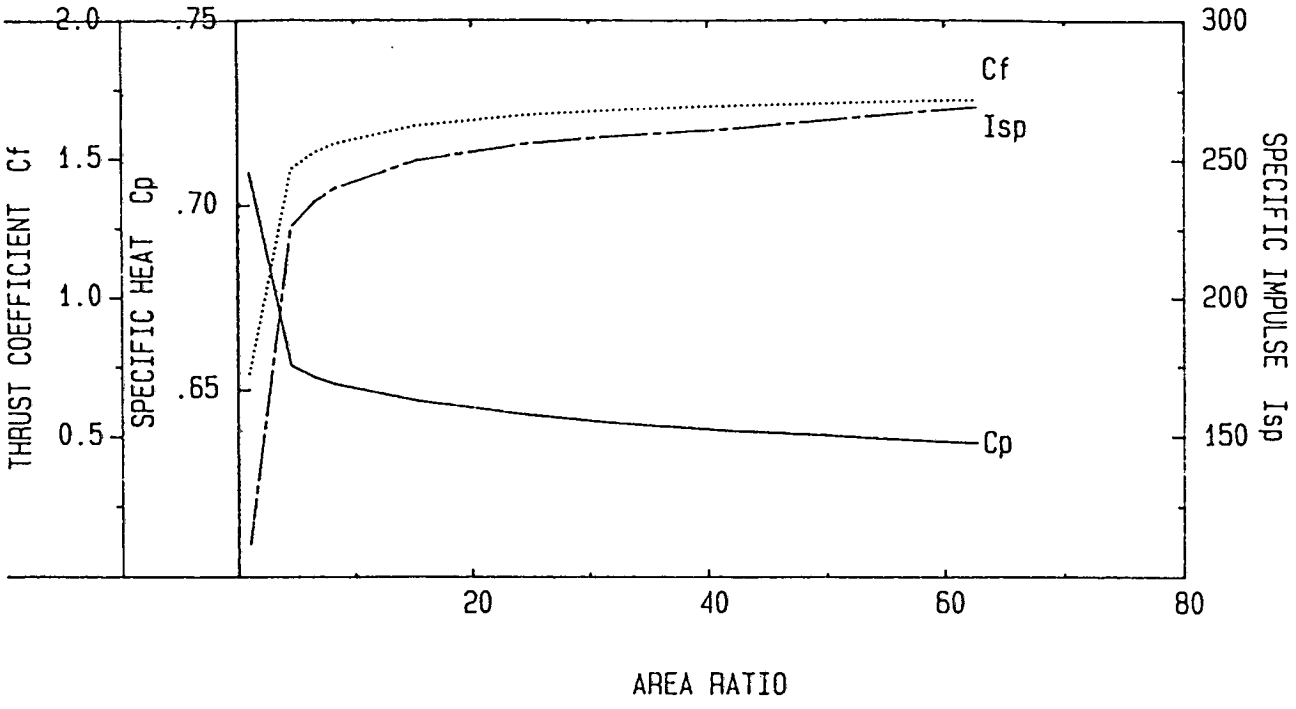

Fig. 5.3 Nozzle flow characteristics for the MBB/ERNO 0.5N thruster.

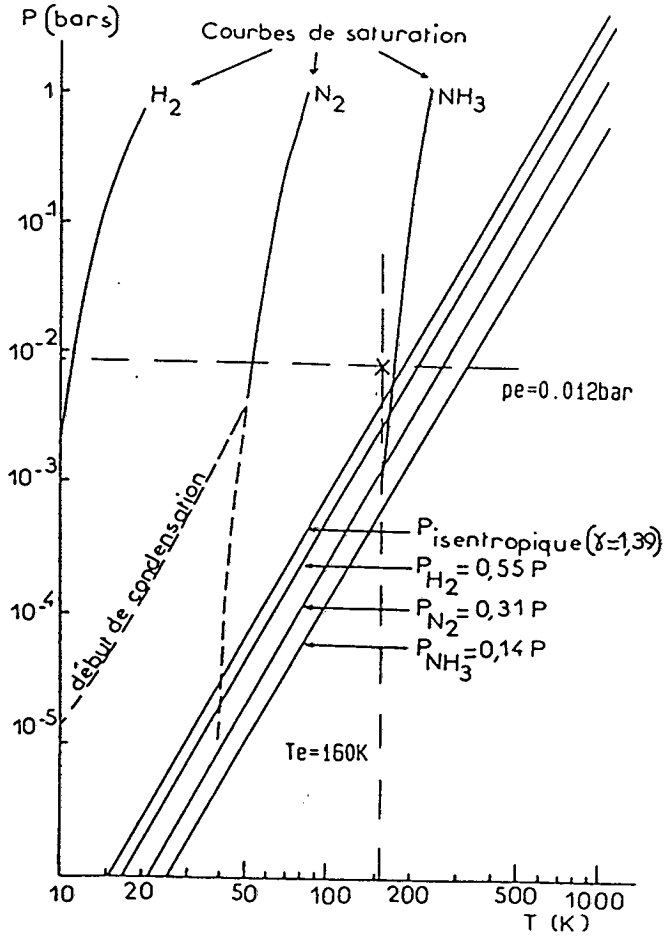

Fig. 5.4 Saturated vapour pressure as a function of temperature, taken from Ref. 39.

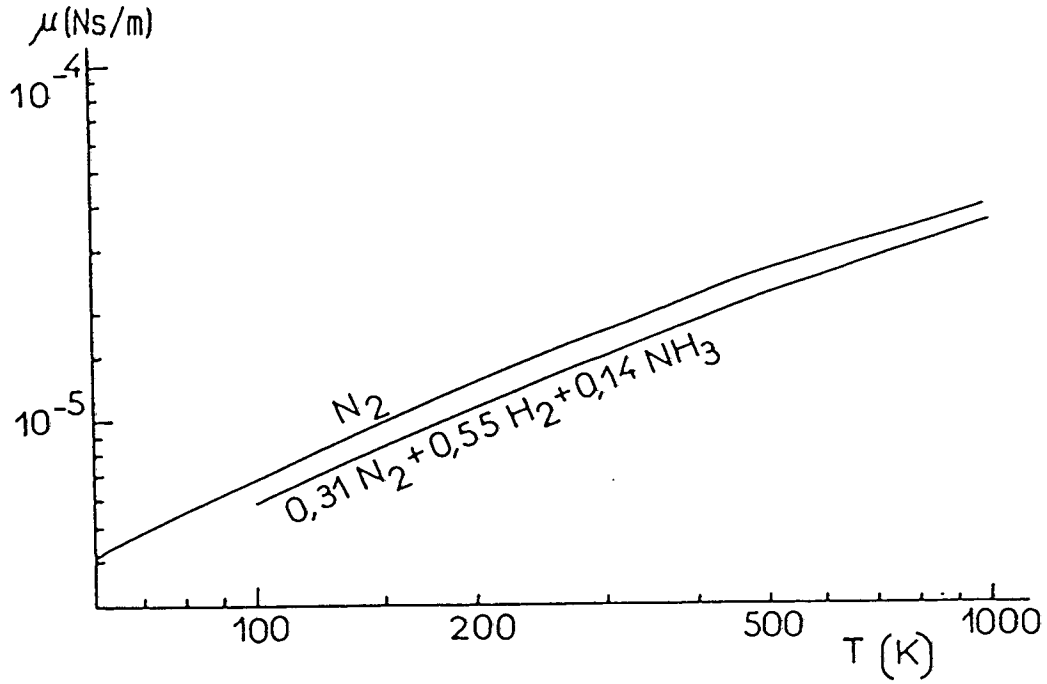

Fig. 5.5 Viscosity as a function of temperature, taken from Ref. 39.

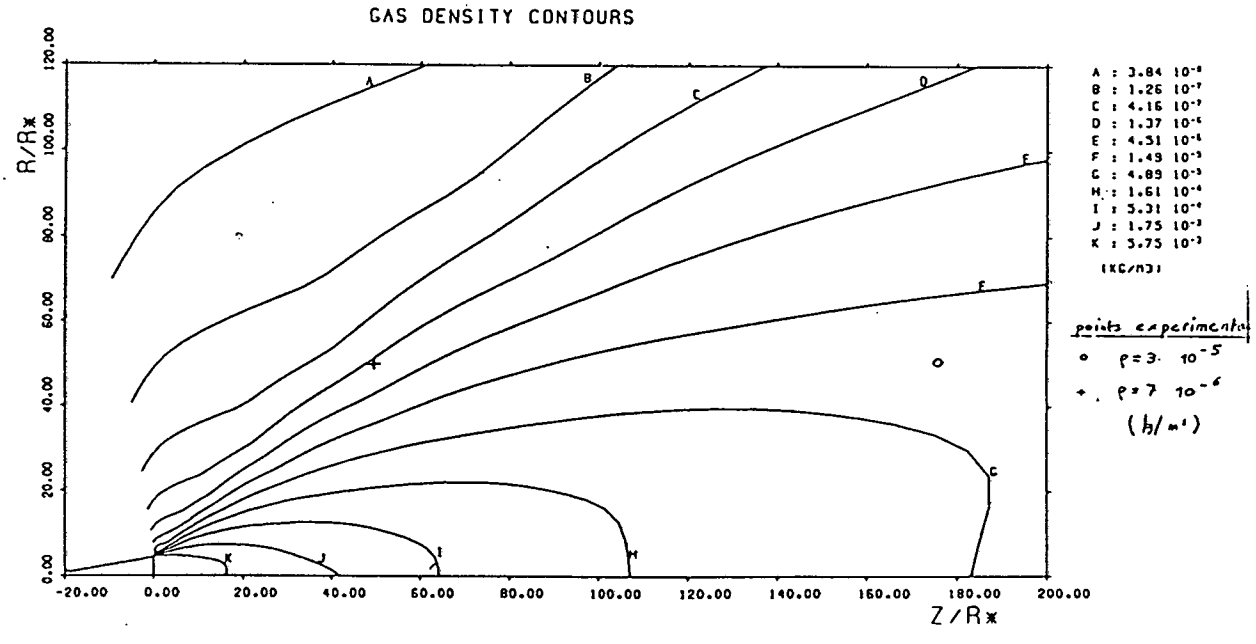

Fig. 5.6 CONTAM calculations of SESSIA thruster showing poor results in the boundary layer expansion.

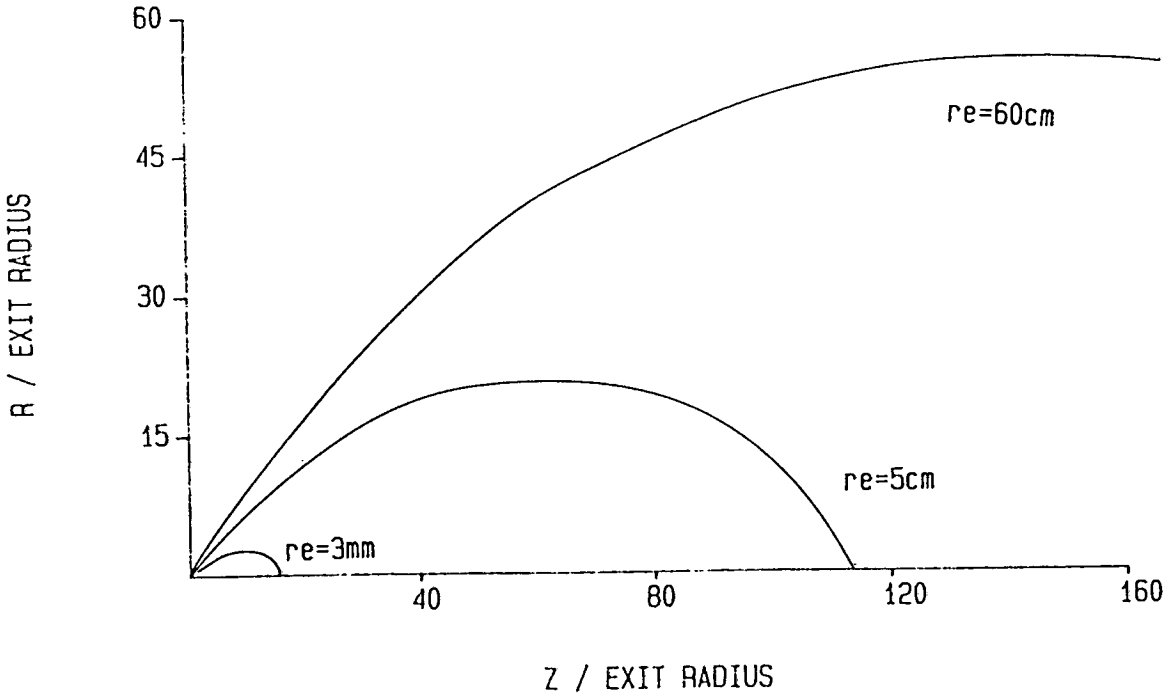

Fig. 5.7 Continuum Breakdown contours as a function of nozzle exit radius.

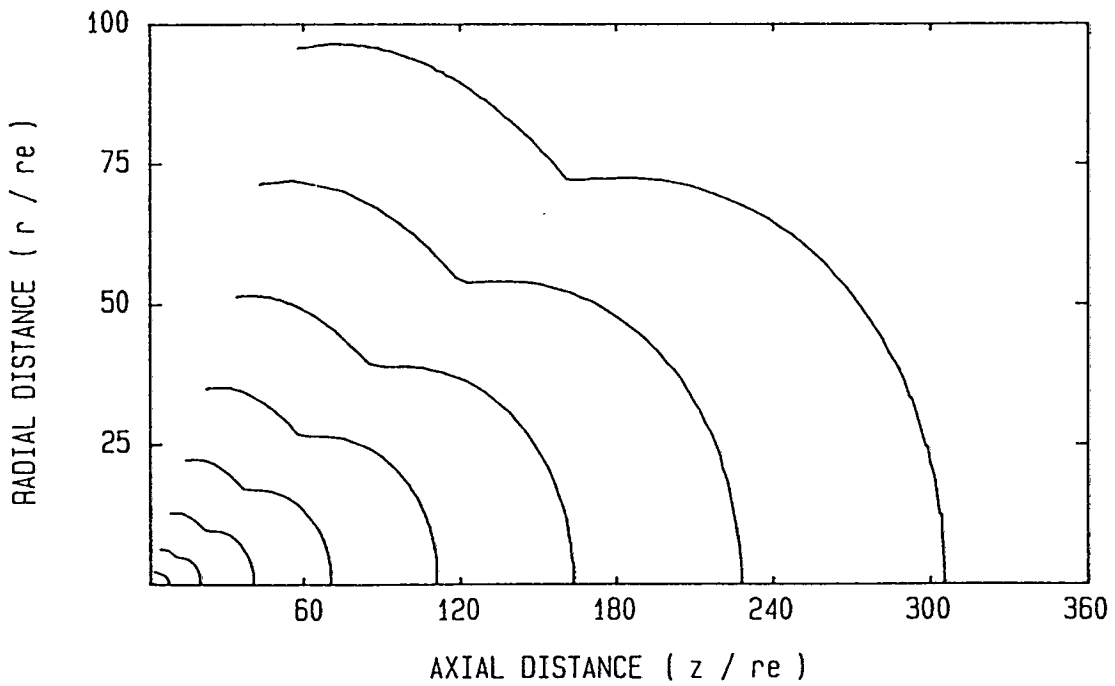

Fig. 5.8 Mach number contours for MBB/ERNO 0.5N thruster using the Simons model.

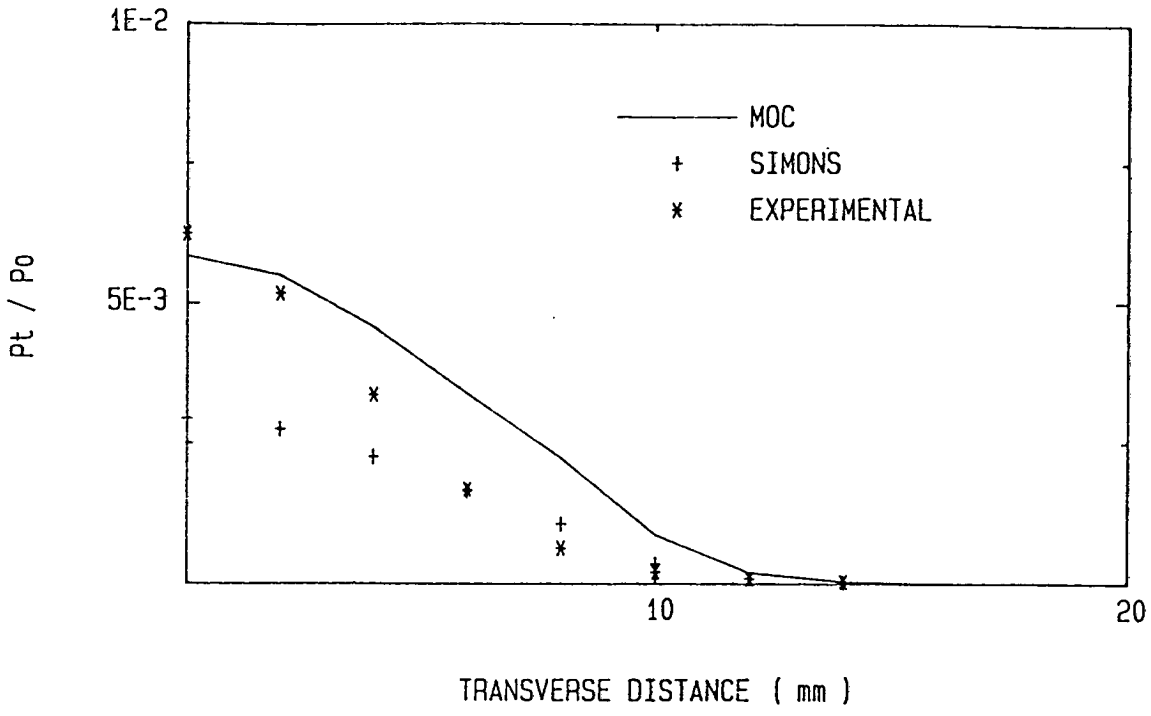

Fig. 5.9(a) Transverse Pitot pressure distributions at z = 8 exit radii.

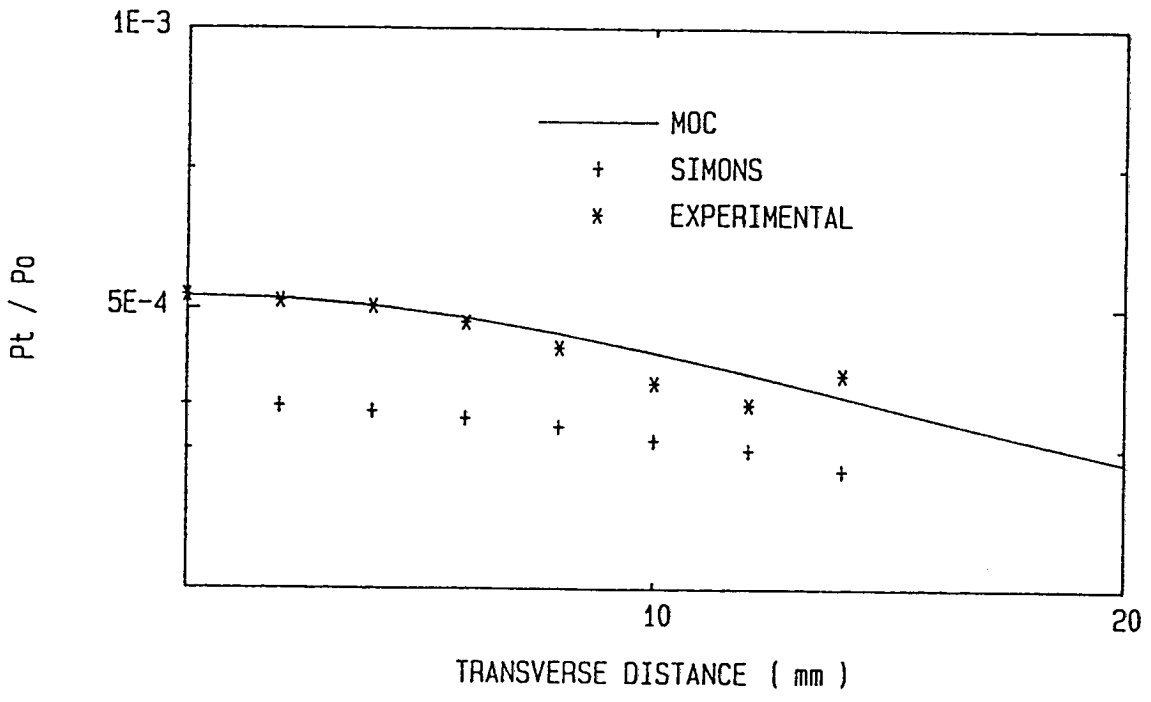

Fig. 5.9(b) Transverse Pitot pressure distributions at z = 24 exit radii.

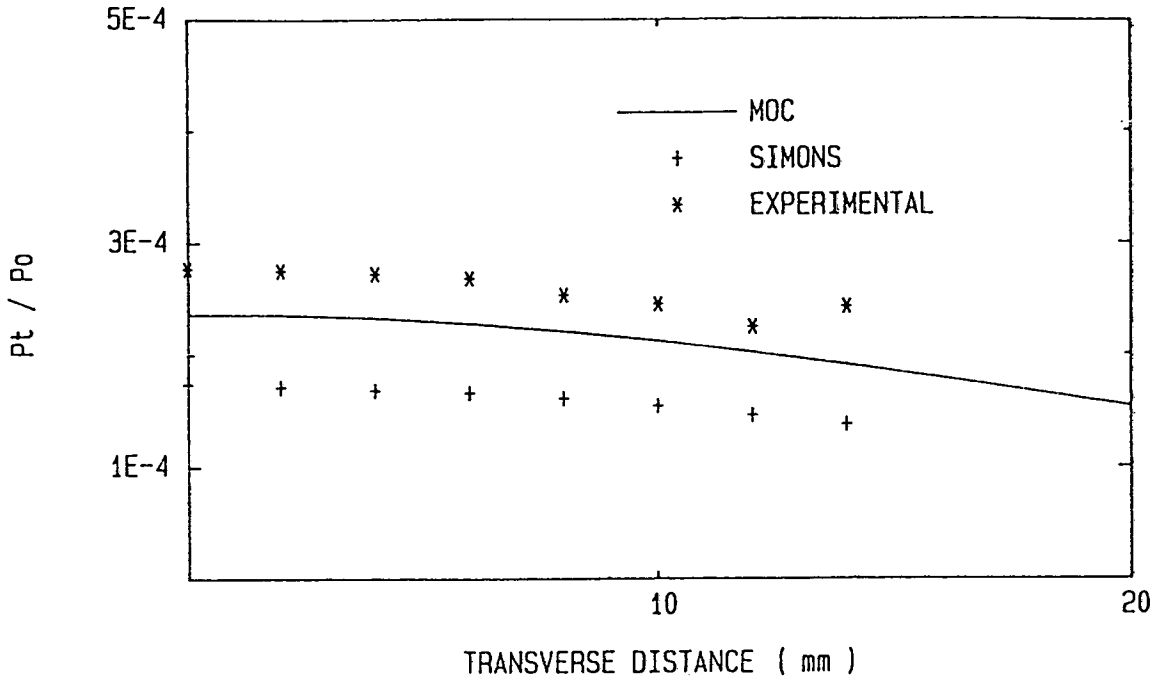

Fig. 5.9(c) Transverse Pitot pressure distributions at z = 32 exit radii.

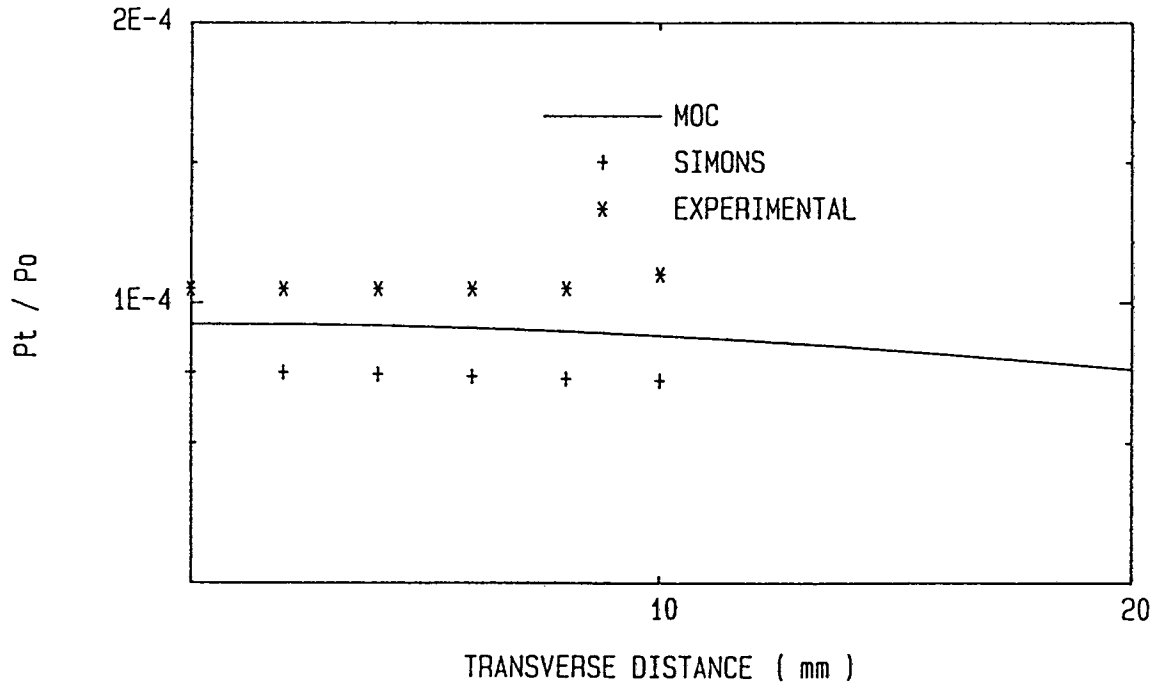

Fig. 5.9(d) Transverse Pitot pressure distributions at z = 48 exit radii.

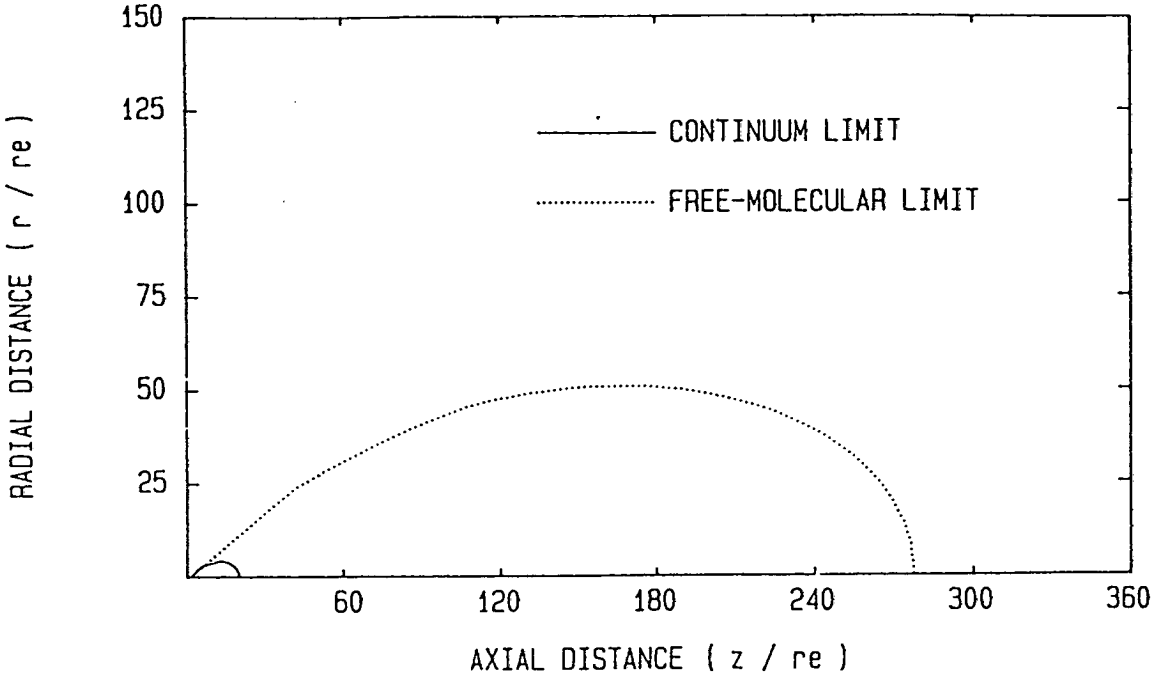

Fig. 5.10 Breakdown contours defining the transition flow regime.

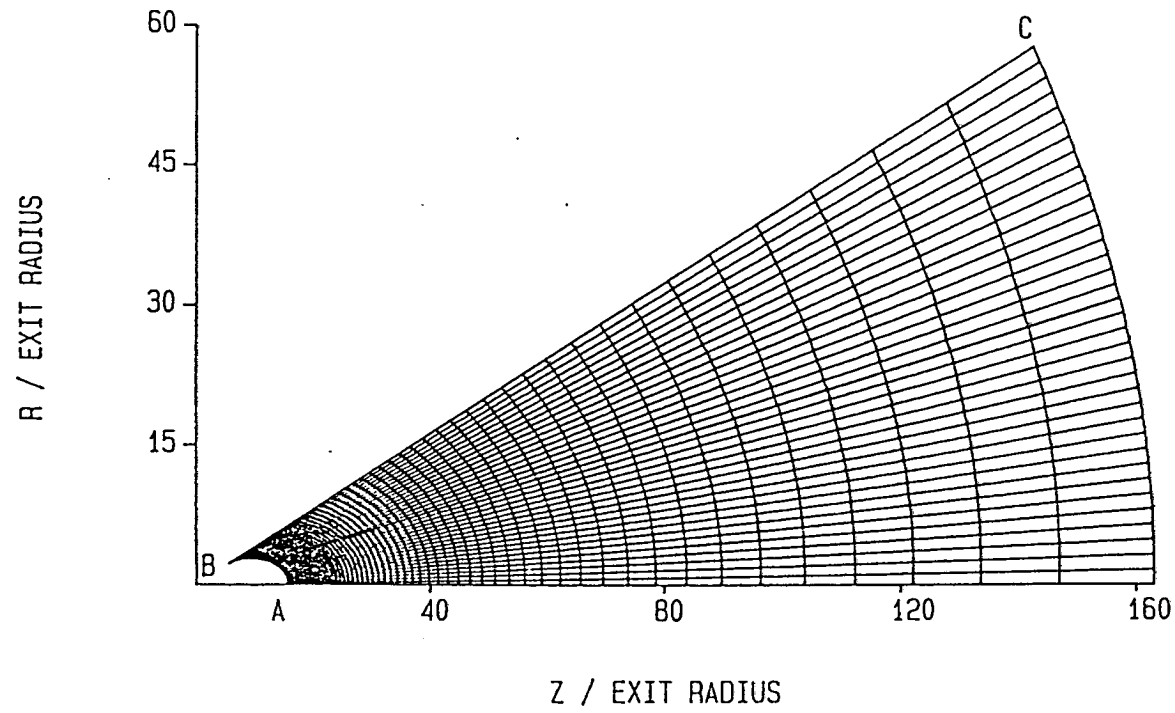

Fig. 5.11 Computational grid for DSMC calculation of isentropic core.

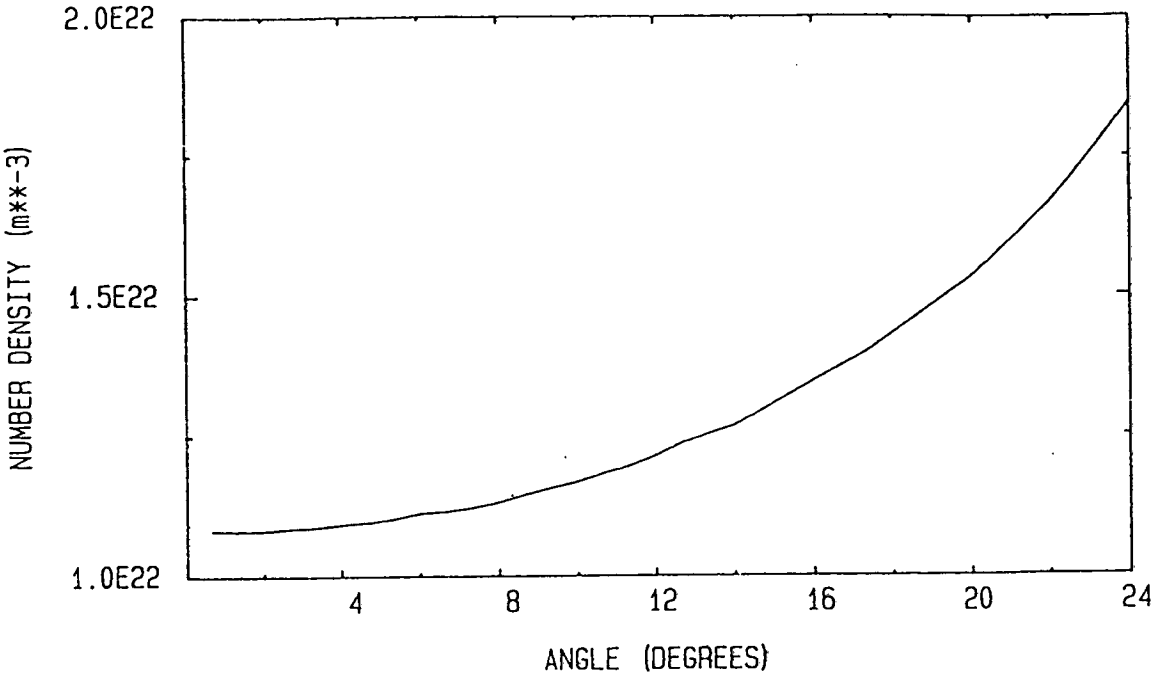

Fig. 5.12 Density profile input into DSMC calculation.

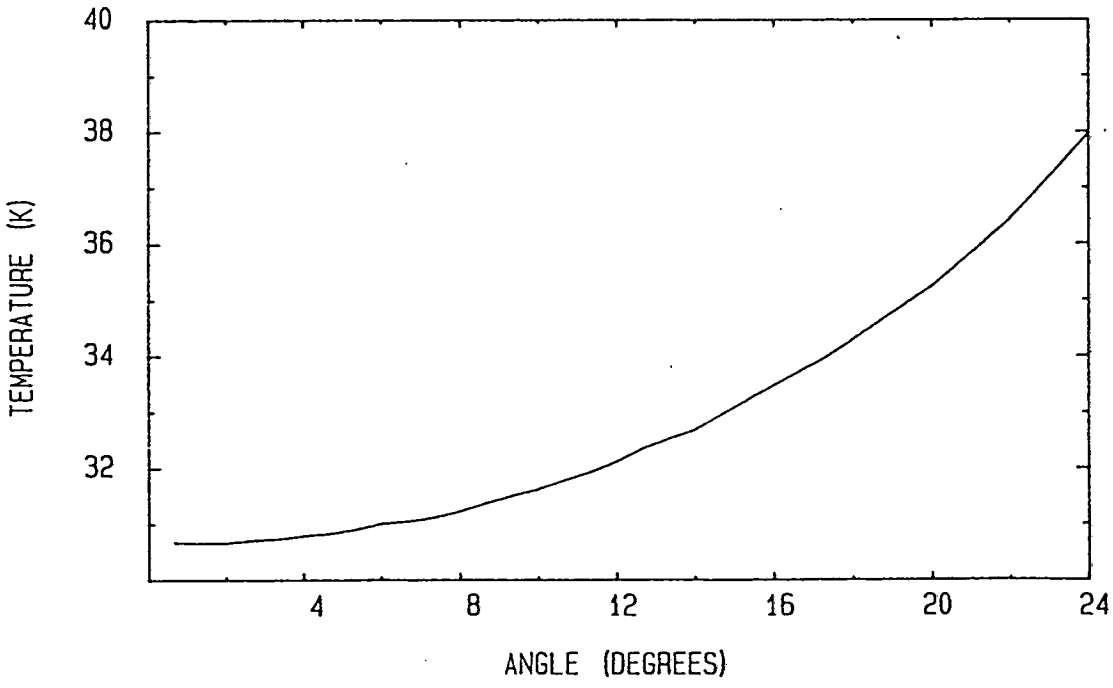

Fig. 5.13 Temperature profile input into DSMC calculation.

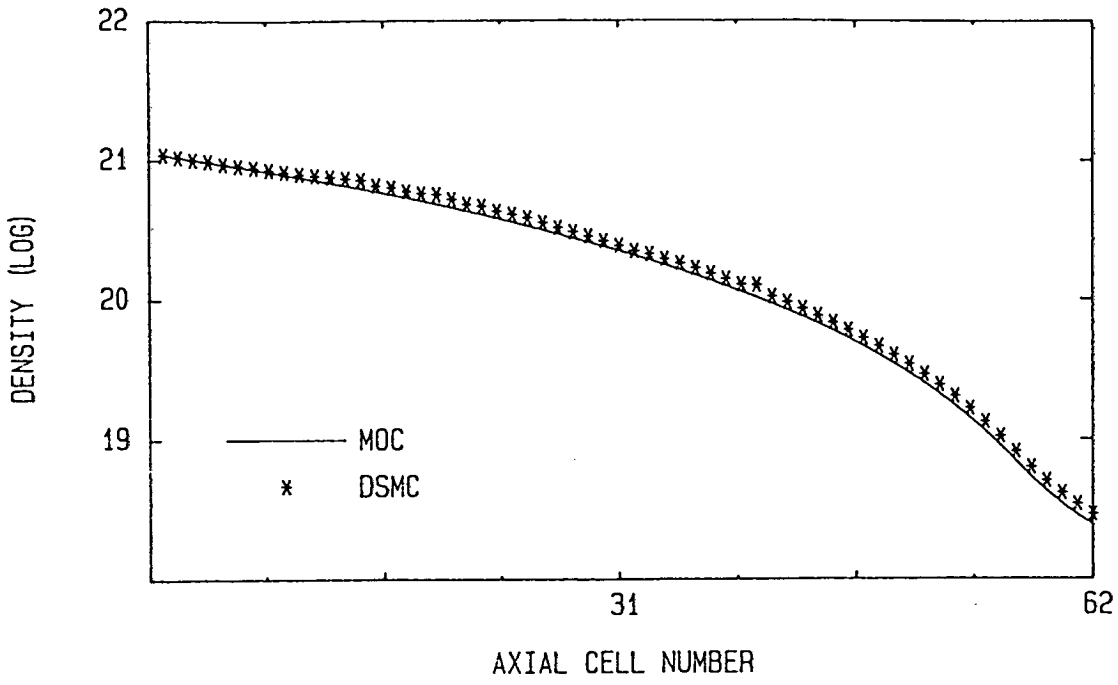

Fig. 5.14 Comparison of MOC and DSMC solutions for density along the plume axis.

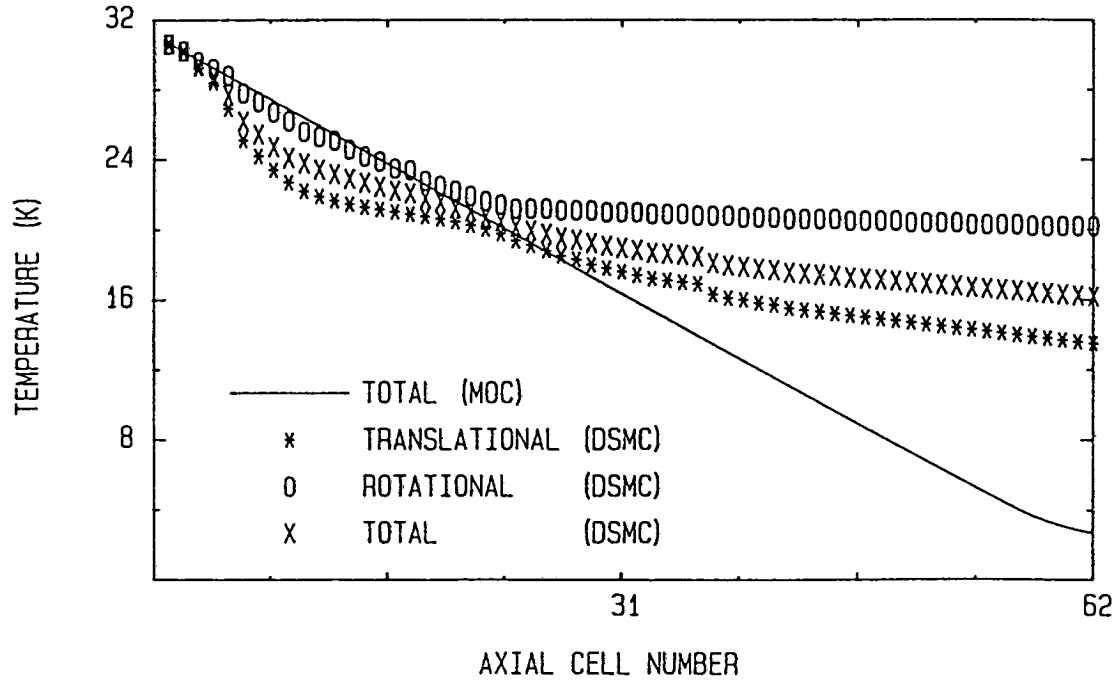

Fig. 5.15 Comparison of MOC and DSMC solutions for temperature along the plume axis.

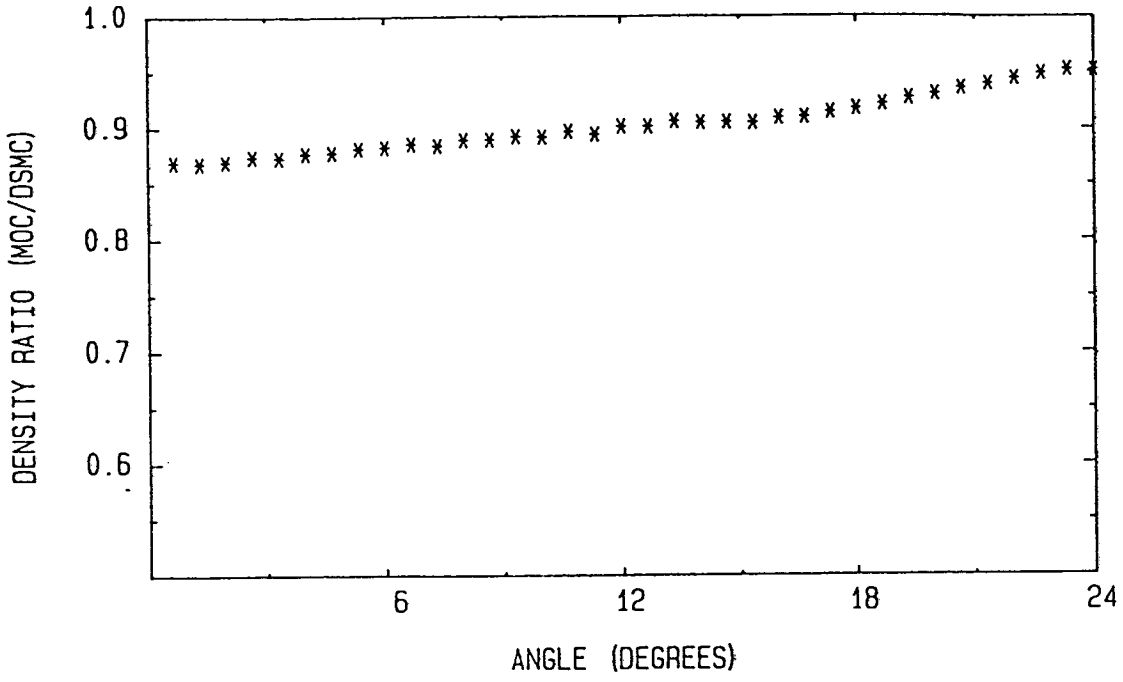

Fig. 5.16 Ratio of MOC and DSMC densities along the radius r = 48 exit radii.

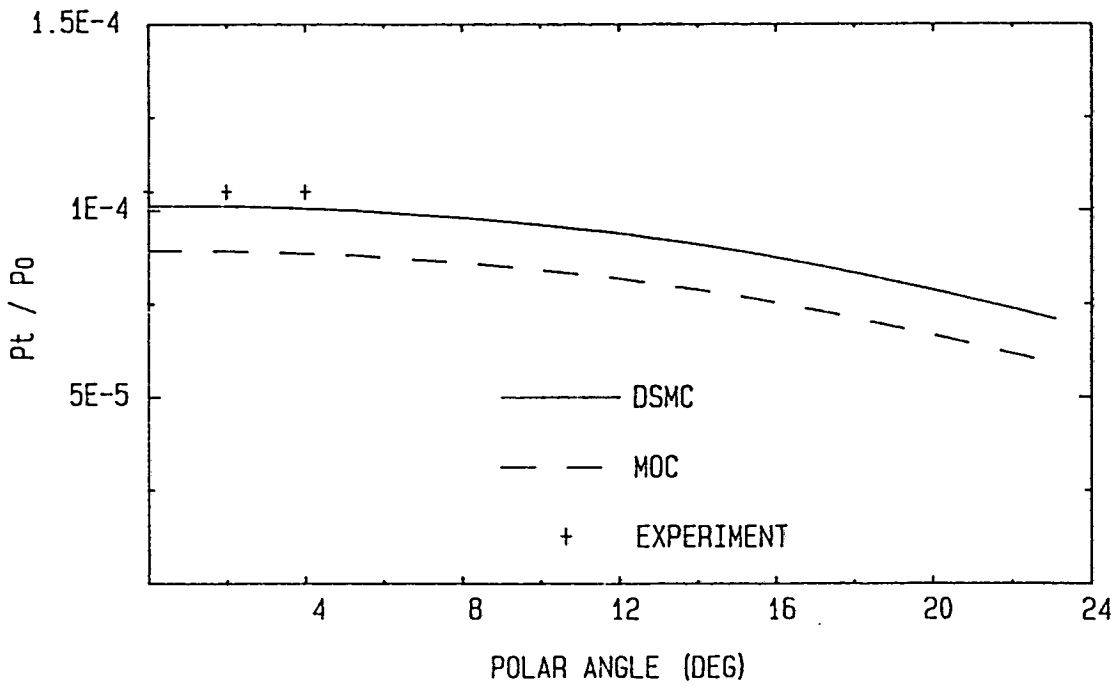

Fig. 5.17 Pitot pressure solutions along the radius r = 48 exit radii.

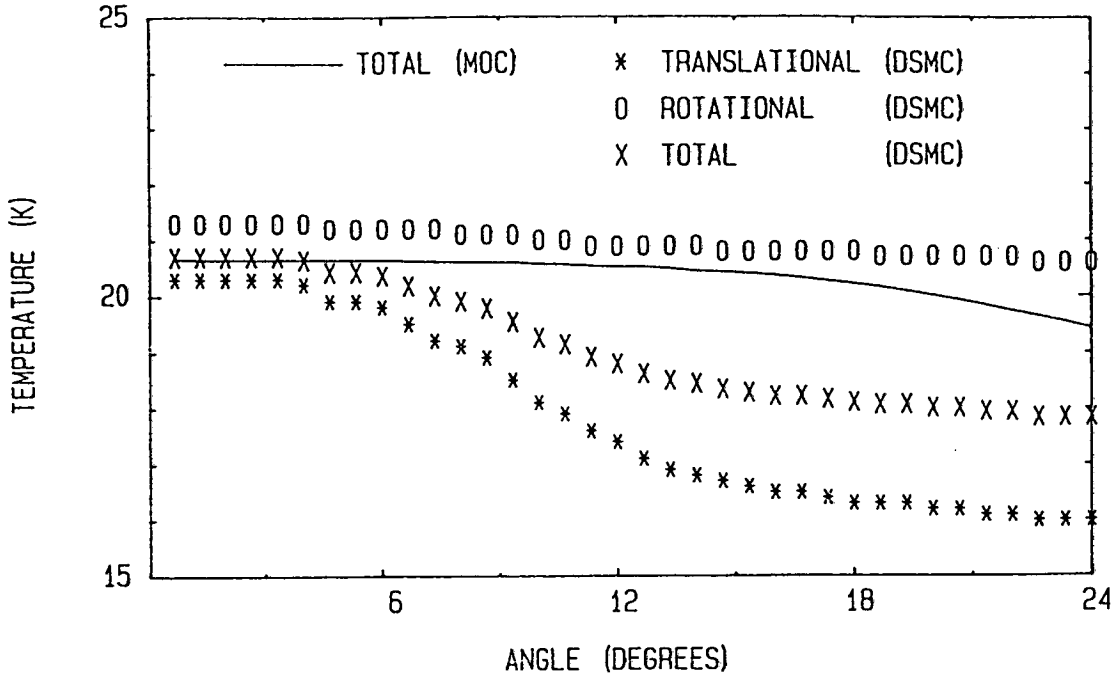

Fig. 5.18 Comparison of MOC and DSMC solutions for temperature along the radius r = 48 exit radii.

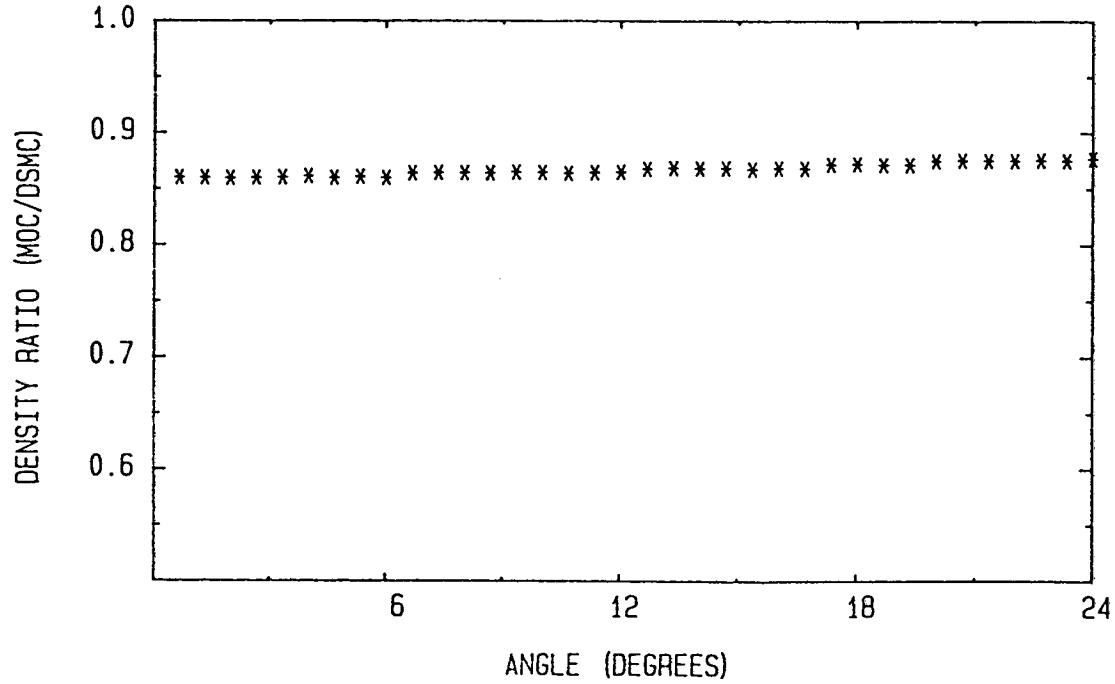

Fig. 5.19 Ratio of MOC and DSMC densities along the radius r = 150 exit radii.

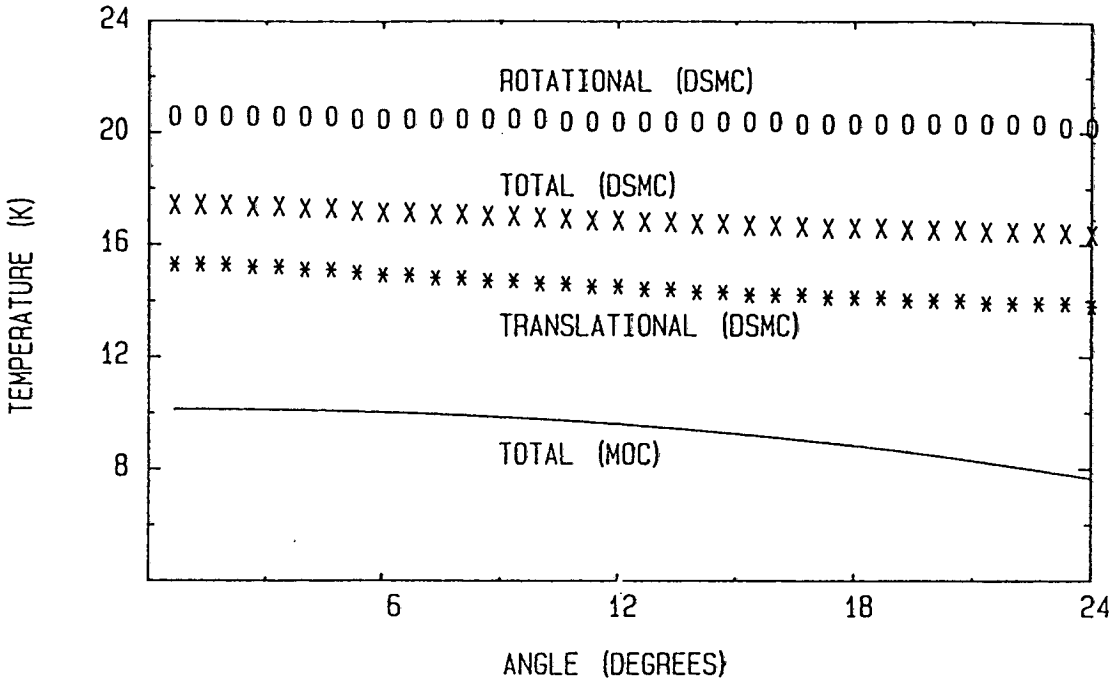

Fig. 5.20 Comparison of MOC and DSMC solutions for temperature along the radius r = 150 exit radii.

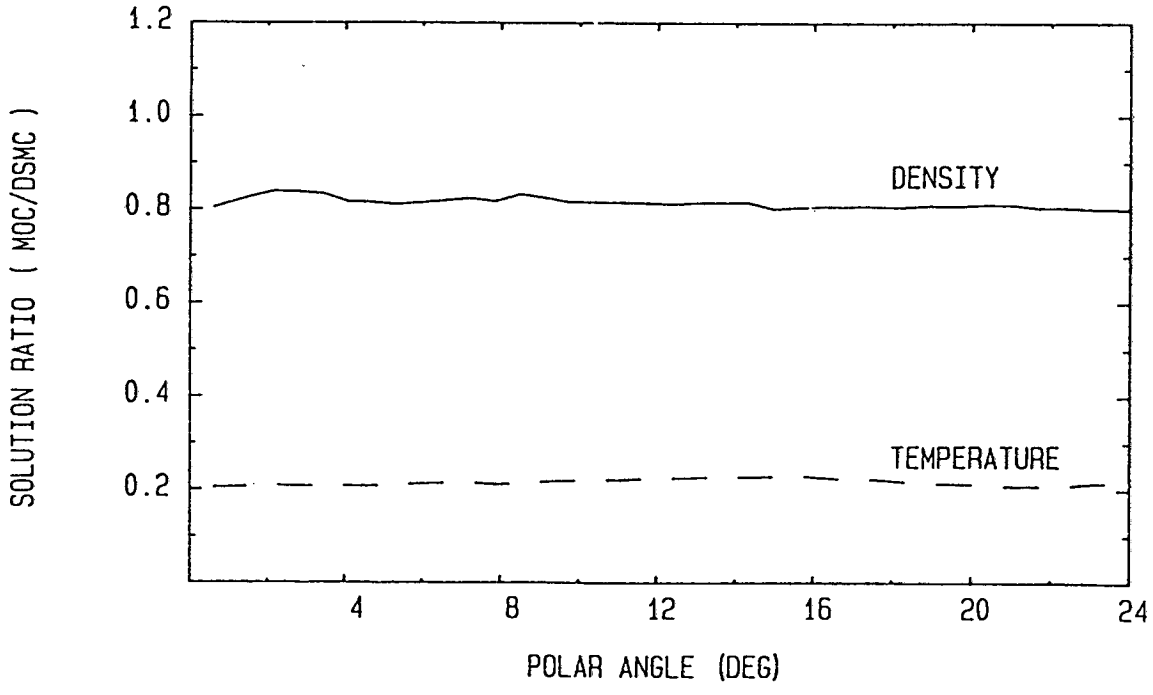

Fig. 5.21 Solution ratios (MOC:DSMC) along the free-molecular locus.

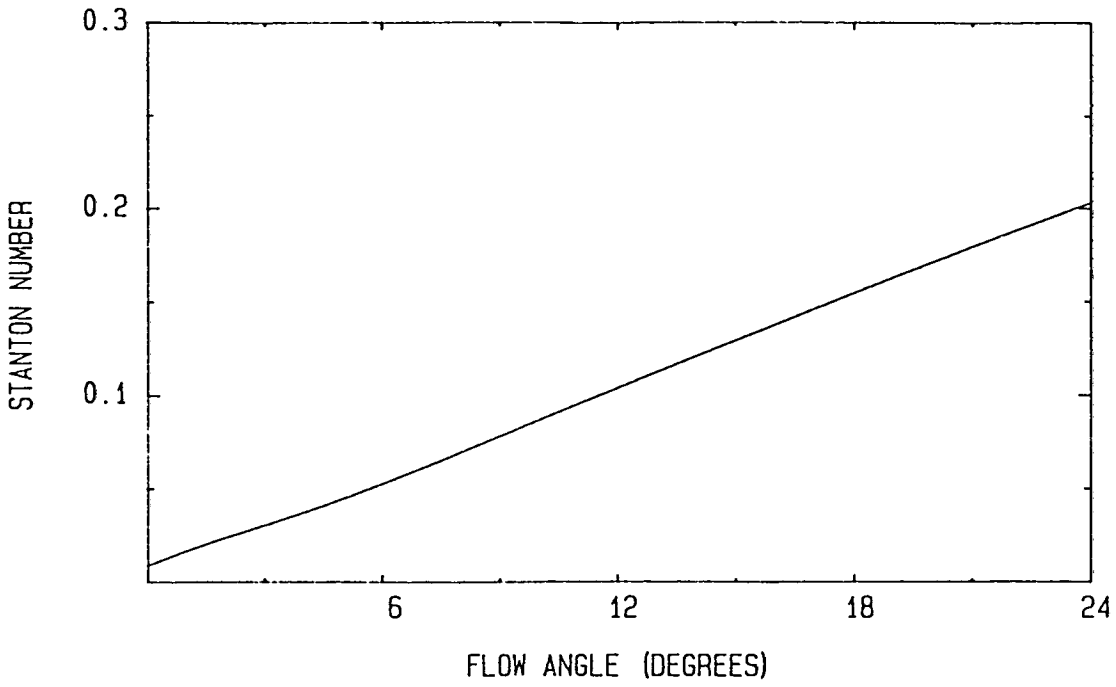

Fig. 5.22 Stanton number derived from MOC results along the free molecular locus.

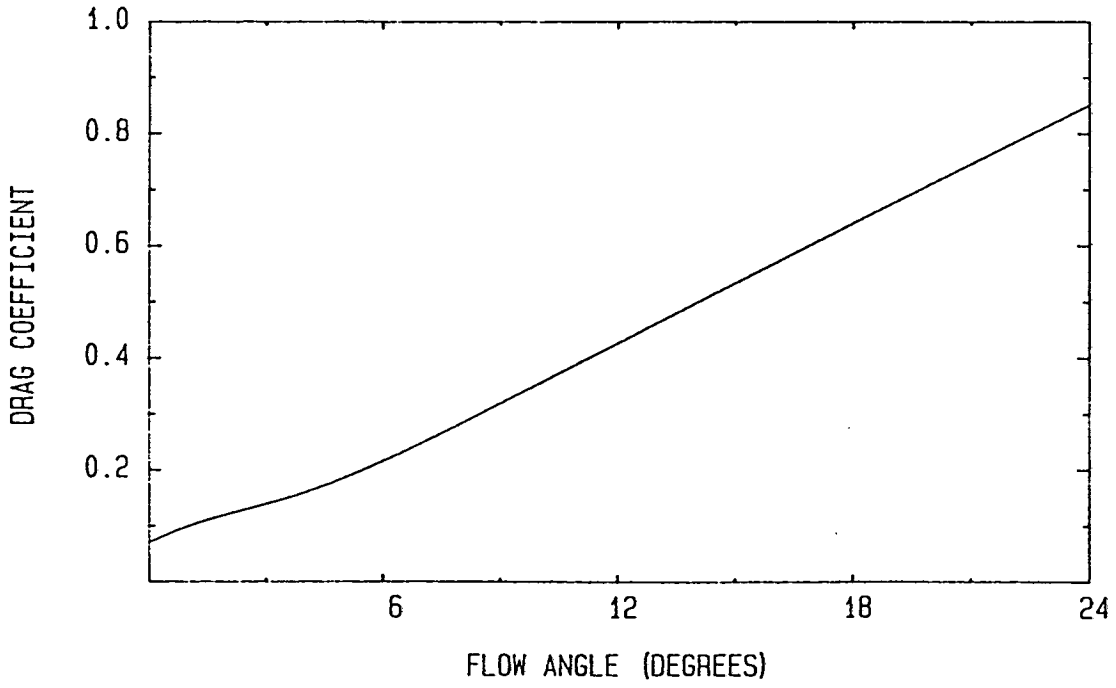

Fig. 5.23 Drag coefficient derived from MOC results along the free molecular locus.

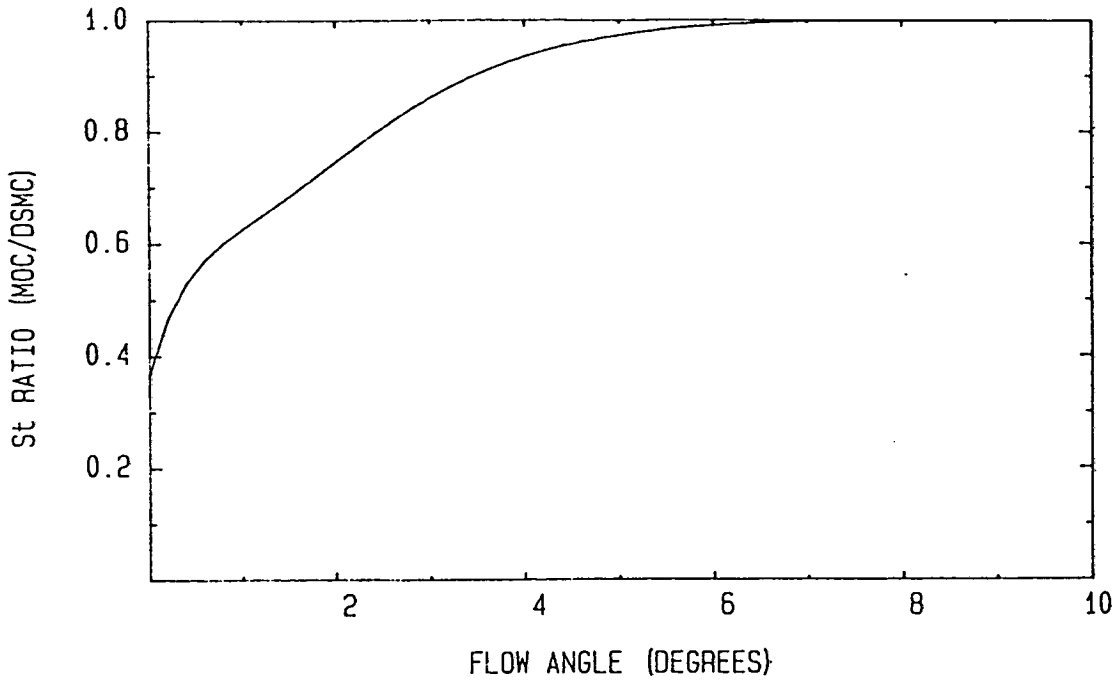

Fig. 5.24 Ratio of MOC and DSMC calculations of Stanton number along the free molecular locus.

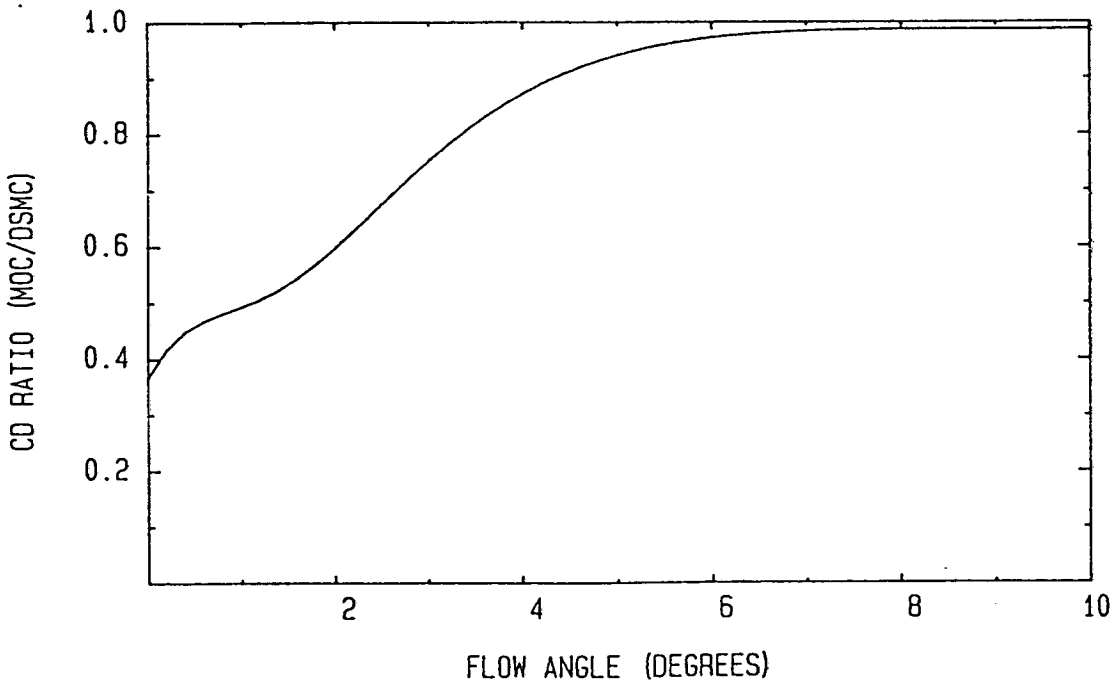

Fig. 5.25 Ratio of MOC and DSMC calculations of drag coefficient along the free molecular locus.

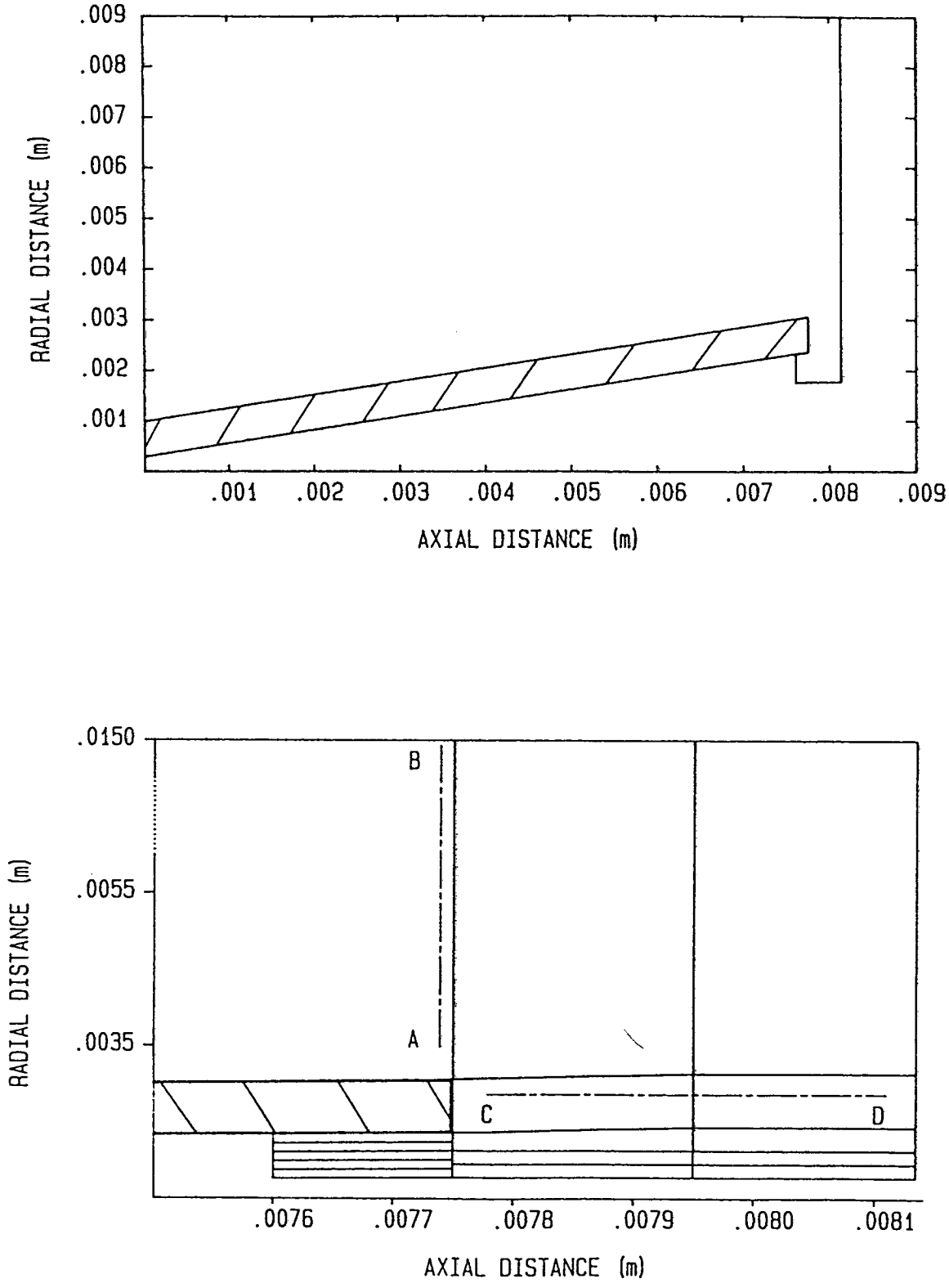

Fig. 5.26 Computational domain for backflow showing regional subdivision.

The hatched section shows the nozzle wall. Calculations are begun just inside the nozzle exit and extend into the backflow region.

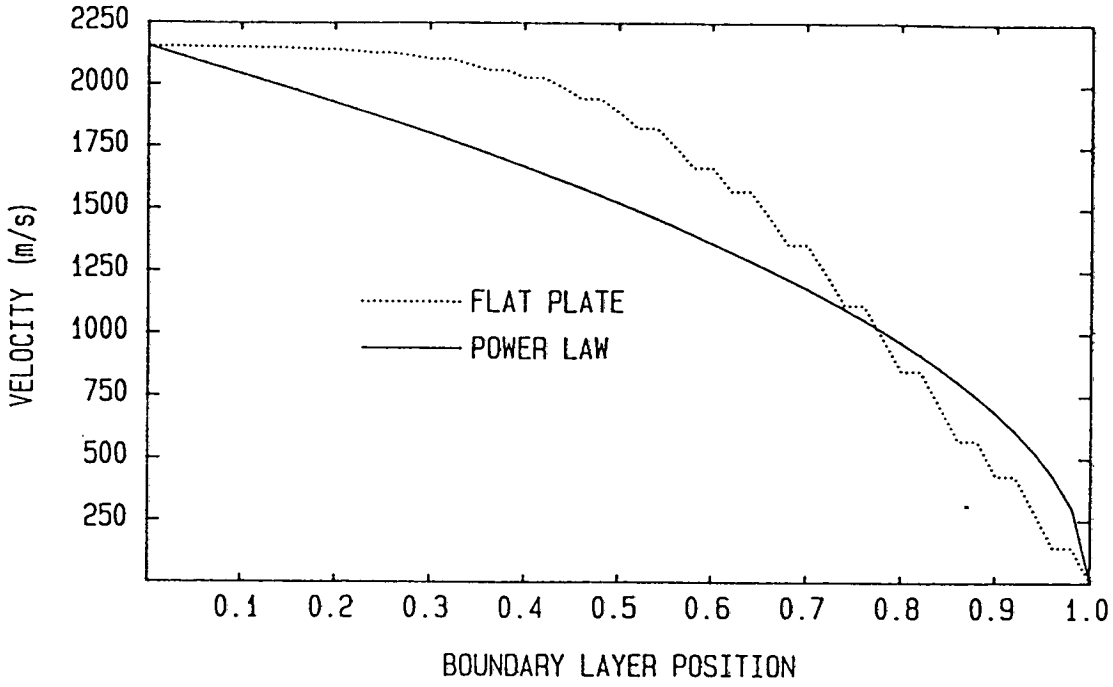

Fig. 5.27 Velocity profiles assumed in the laminar boundary layer.

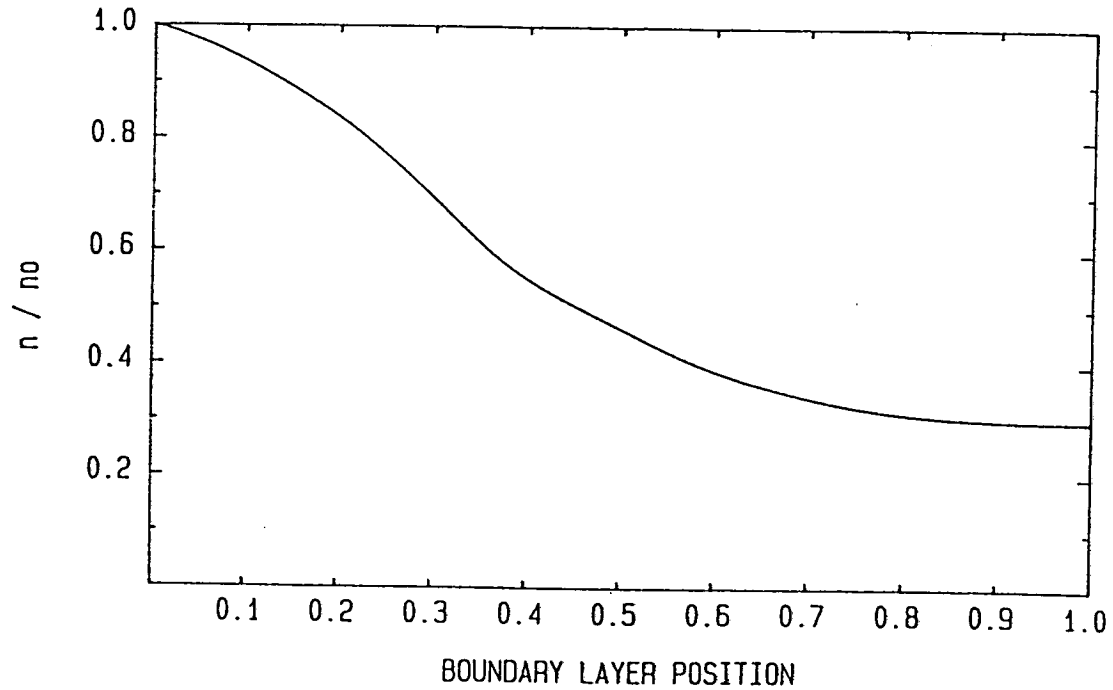

Fig. 5.28 Density profile assumed in the laminar boundary layer.

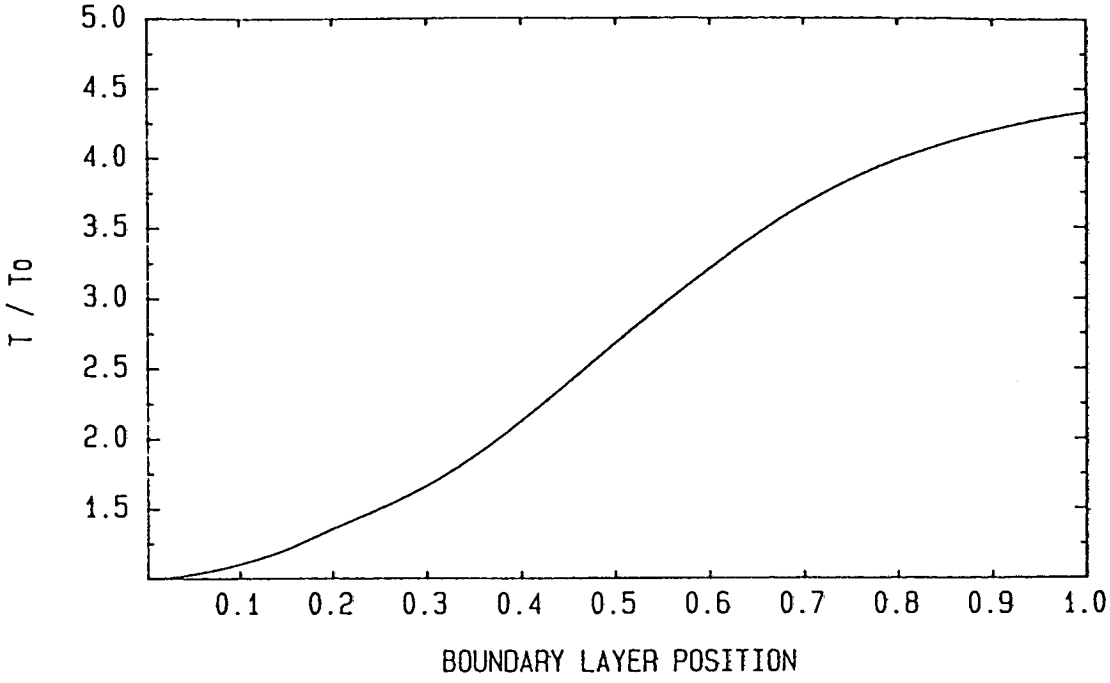

Fig. 5.29 Temperature profile assumed in the laminar boundary layer.

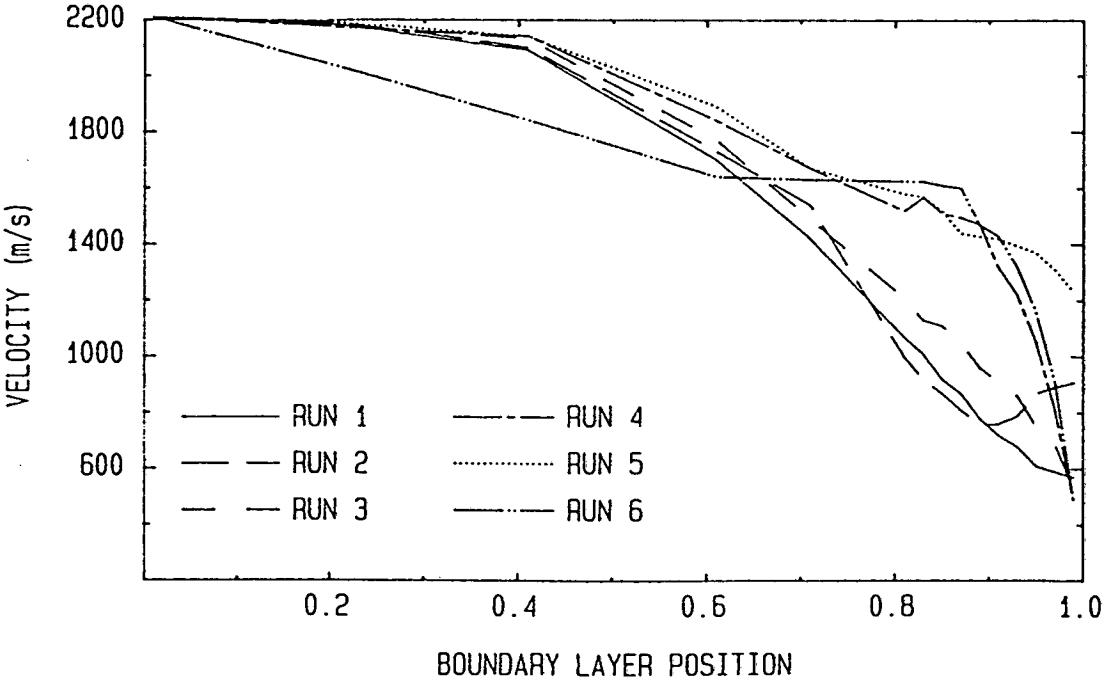

Fig. 5.30 Velocity profiles obtained in the nozzle exit plane.

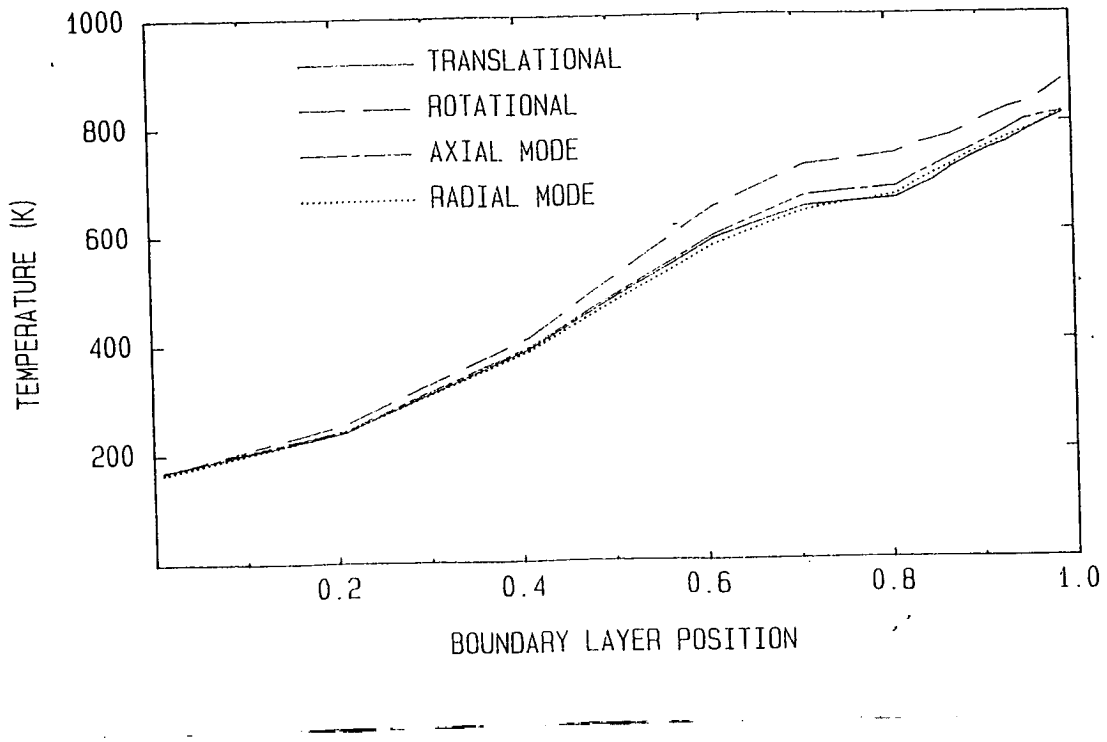

Fig. 5.31 Thermal nonequilibrium in the nozzle exit plane.

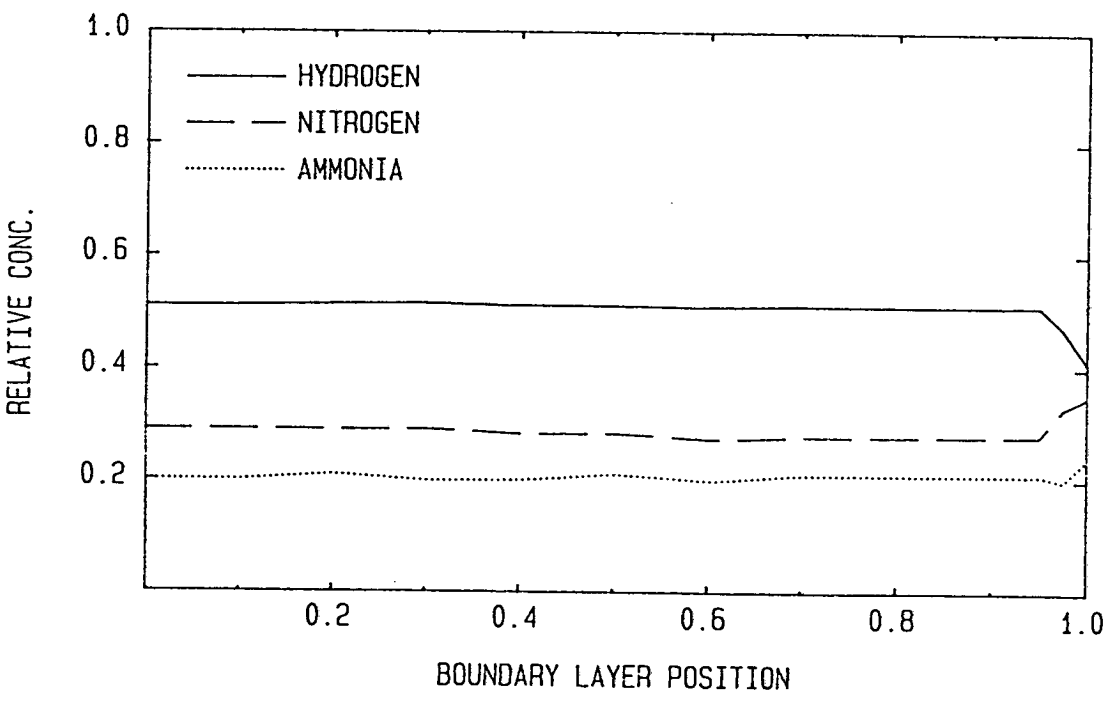

Fig. 5.32 Relative species concentrations in the nozzle exit plane.

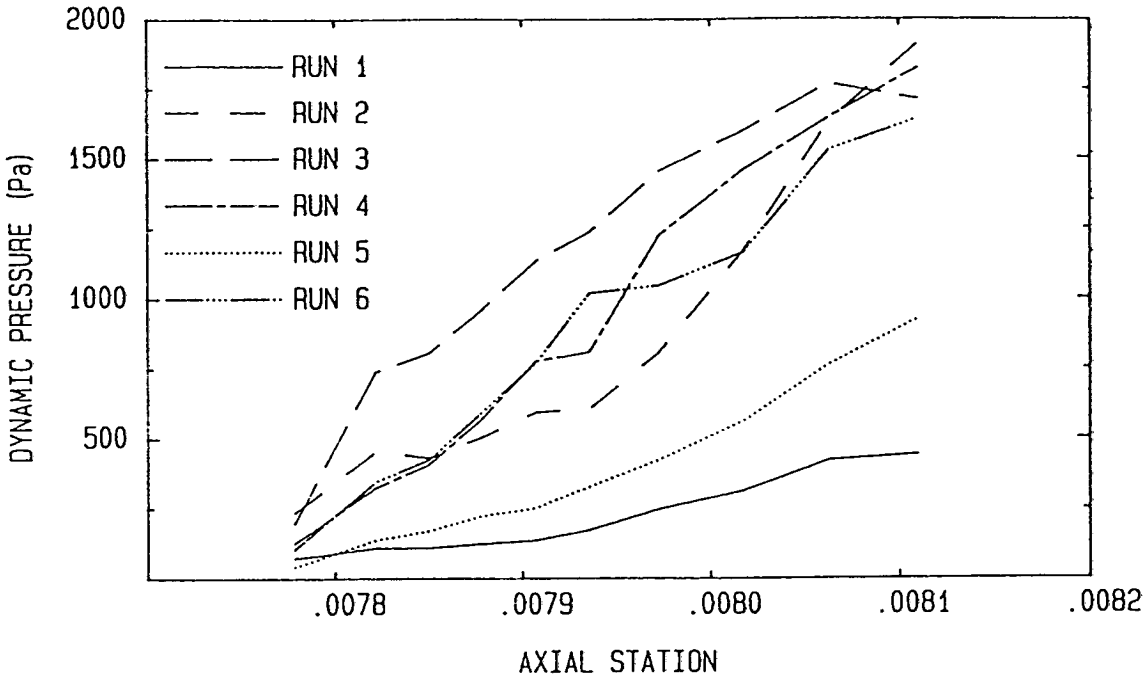

Fig. 5.33 Dynamic pressure in the region forward of the nozzle lip.

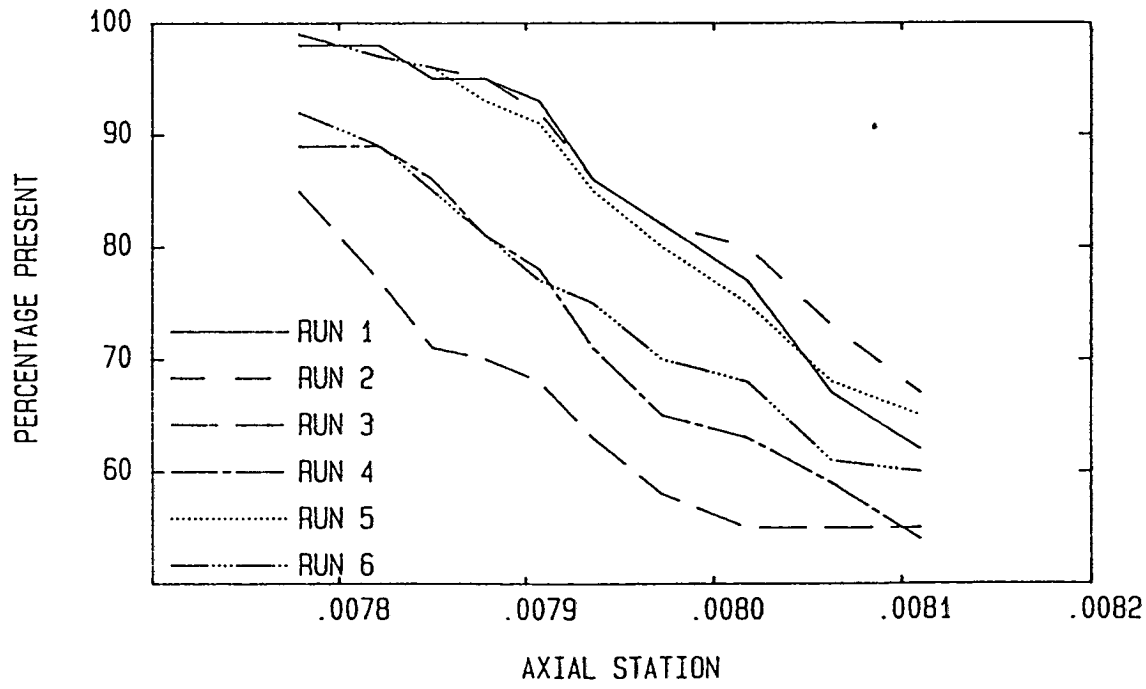

Fig. 5.34(a) Hydrogen concentration in the region forward of the nozzle lip.

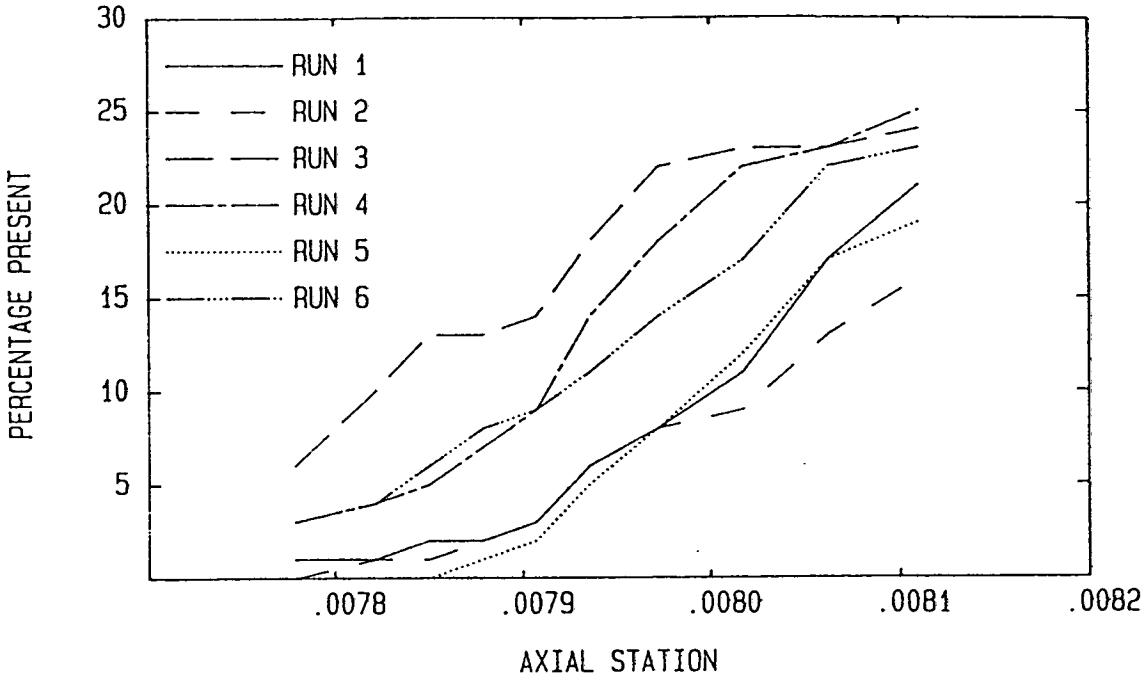

Fig. 5.34(b) Nitrogen concentration in the region forward of the nozzle lip.

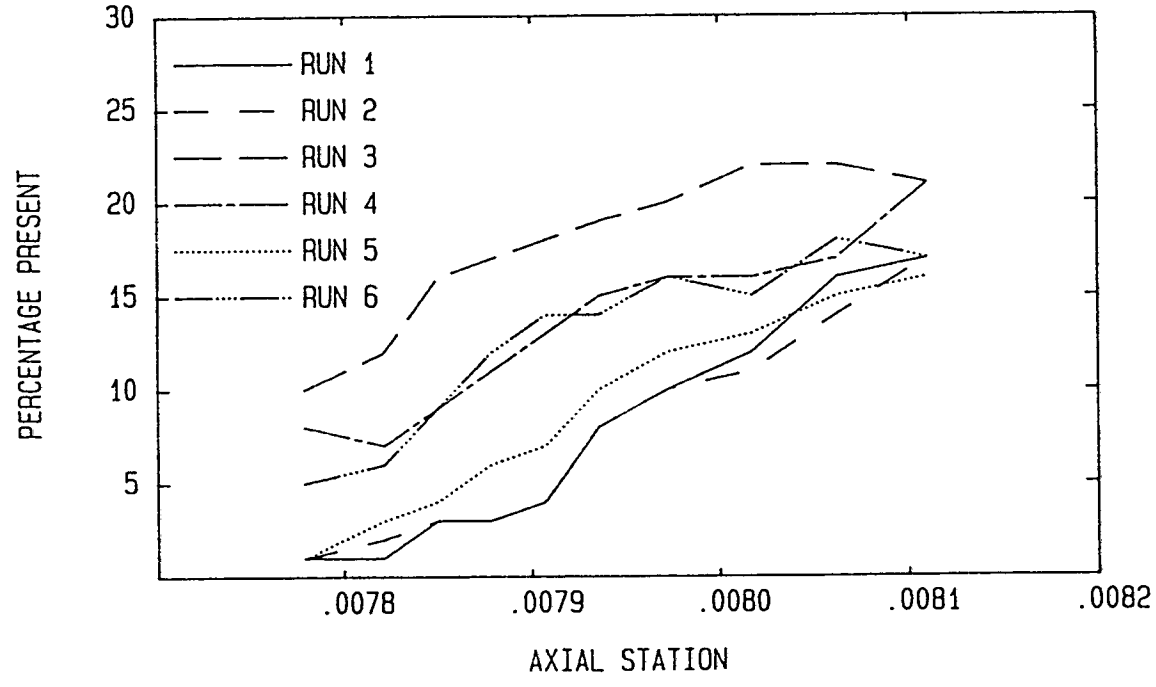

Fig. 5.34(c) Ammonia concentration in the region forward of the nozzle lip.

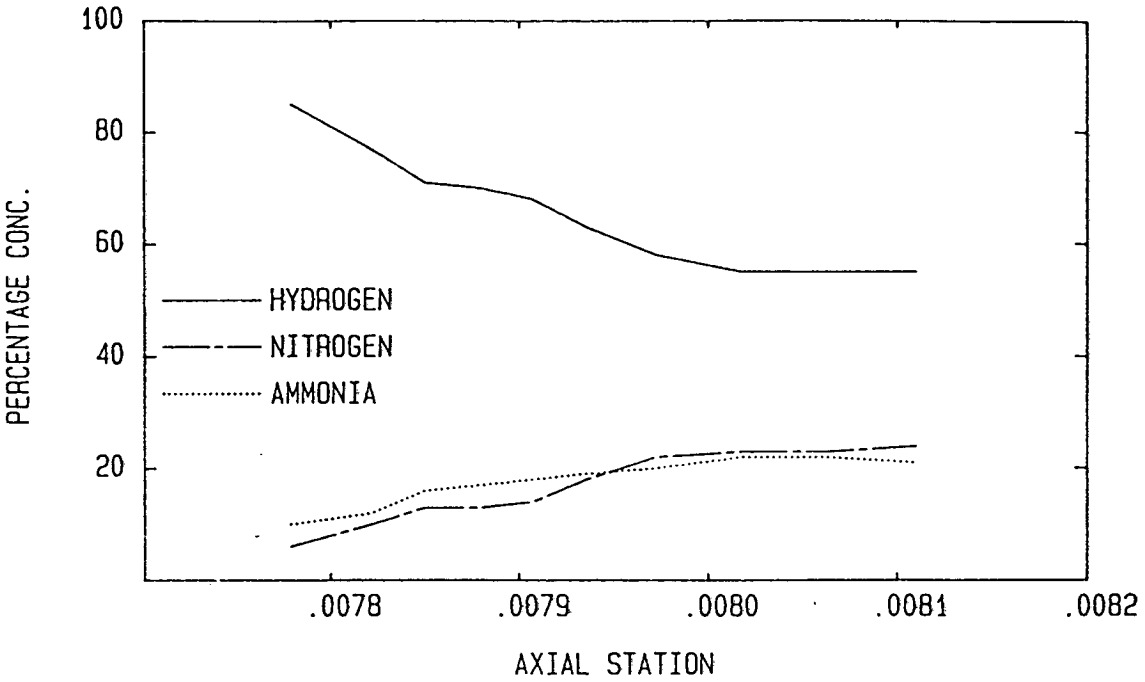

Fig. 5.35 Relative species abundance forward of the nozzle lip for Run 3.

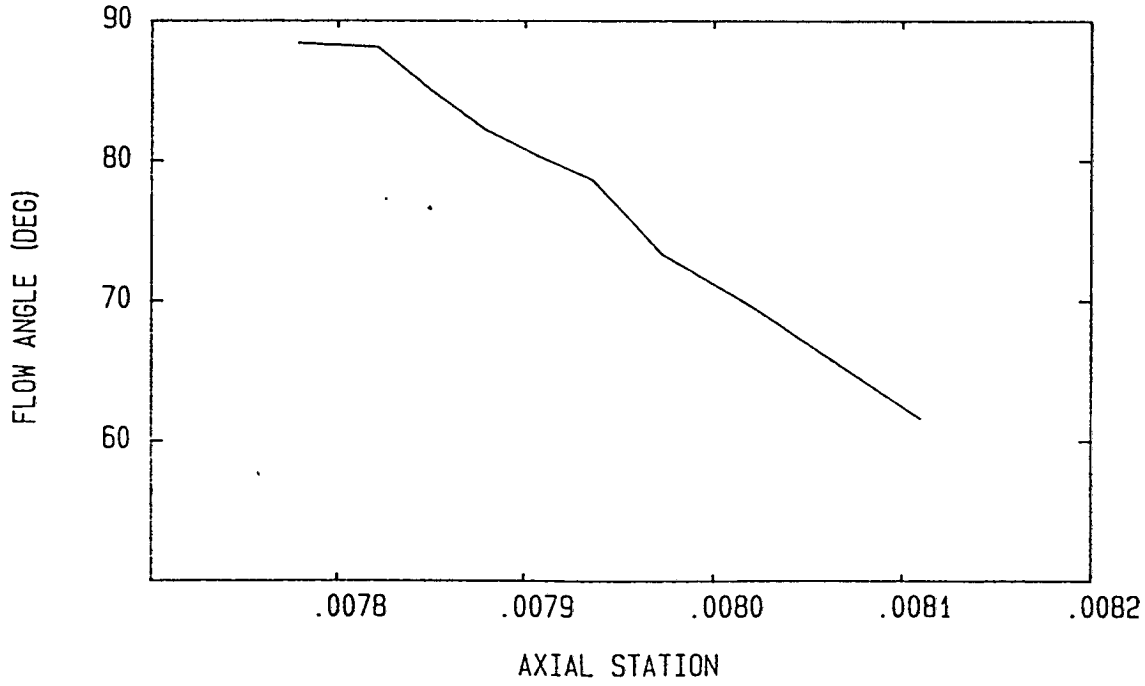

Fig. 5.36 Flow angle in the region forward of the nozzle lip for Run 3.

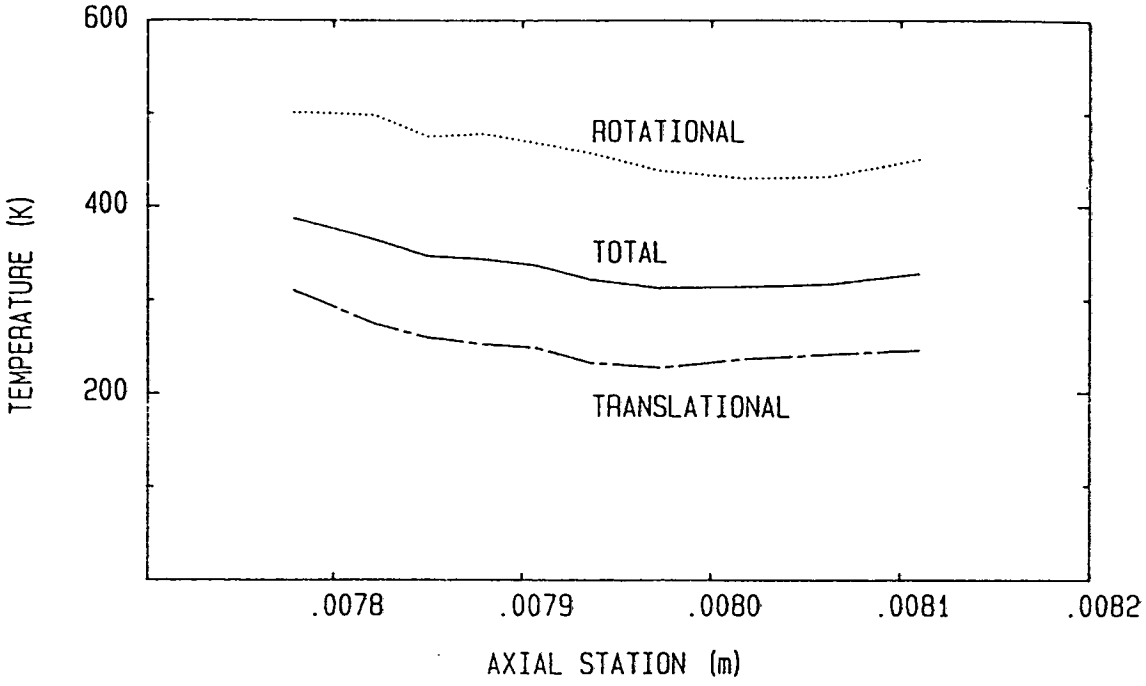

Fig. 5.37 Thermal nonequilibrium in the region forward of the nozzle lip for Run 3.

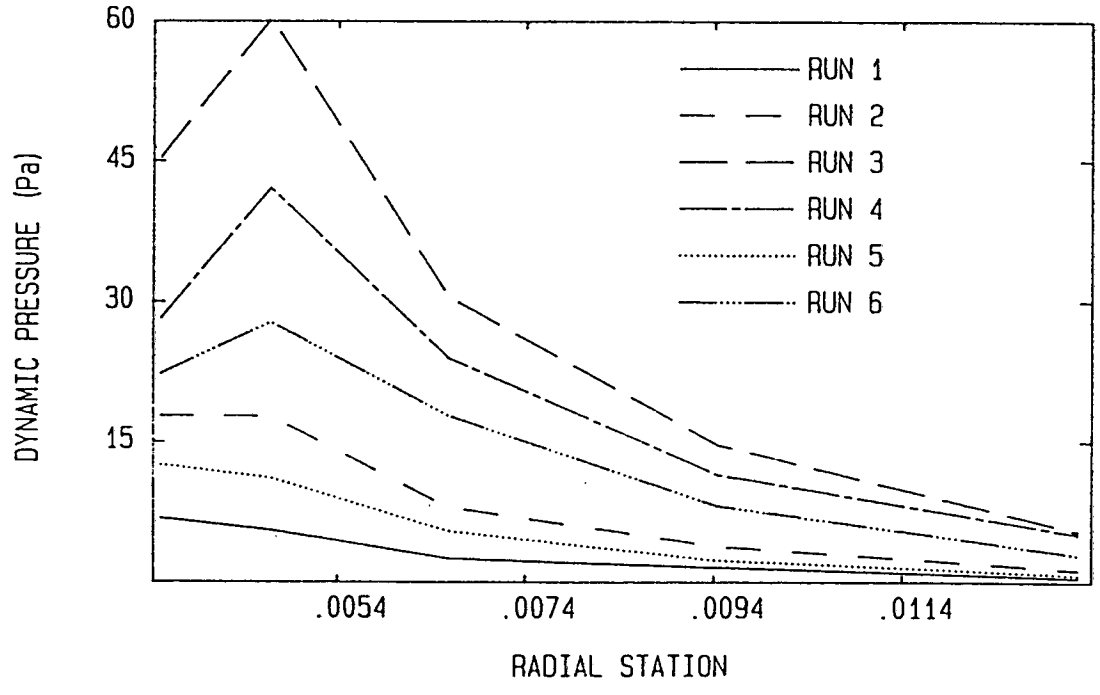

Fig. 5.38 Dynamic pressure in the backflow region.

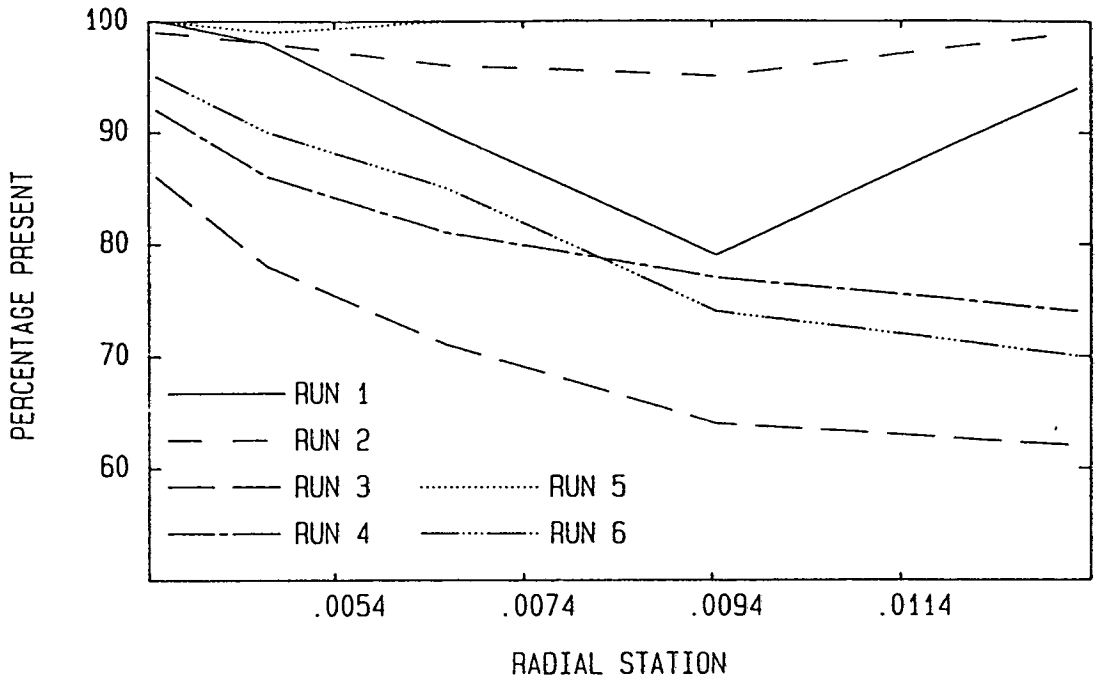

Fig. 5.39(a) Hydrogen concentrations in the backflow region.

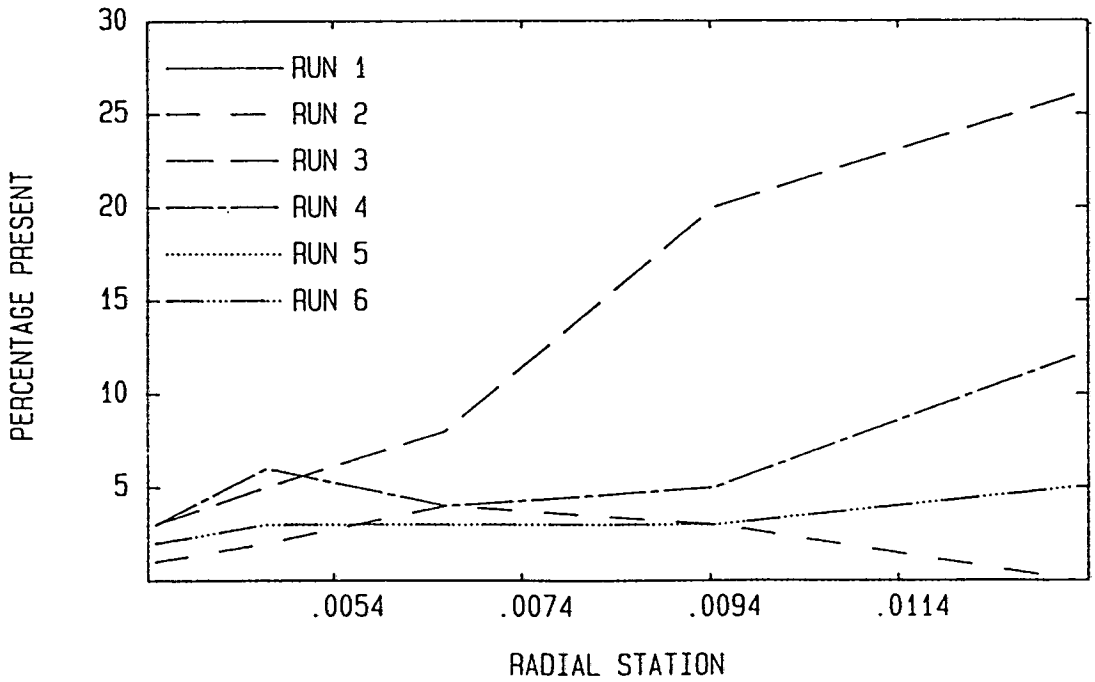

Fig. 5.39(b) Nitrogen concentration in the backflow region.

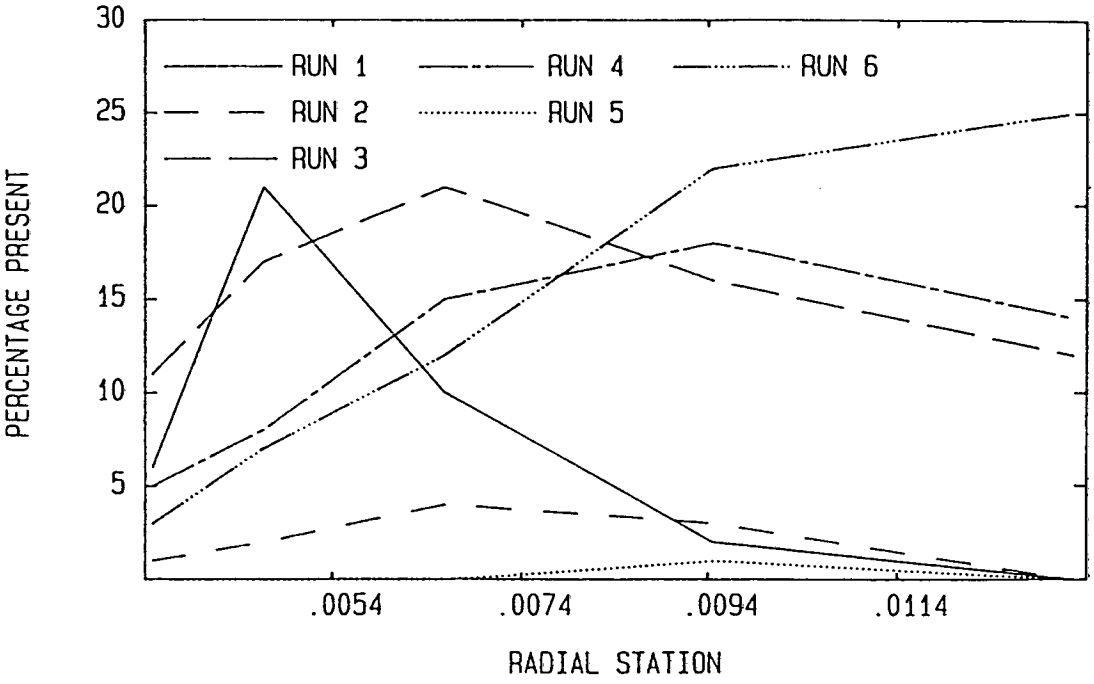

Fig. 5.39(c) Ammonia concentration in the backflow region.

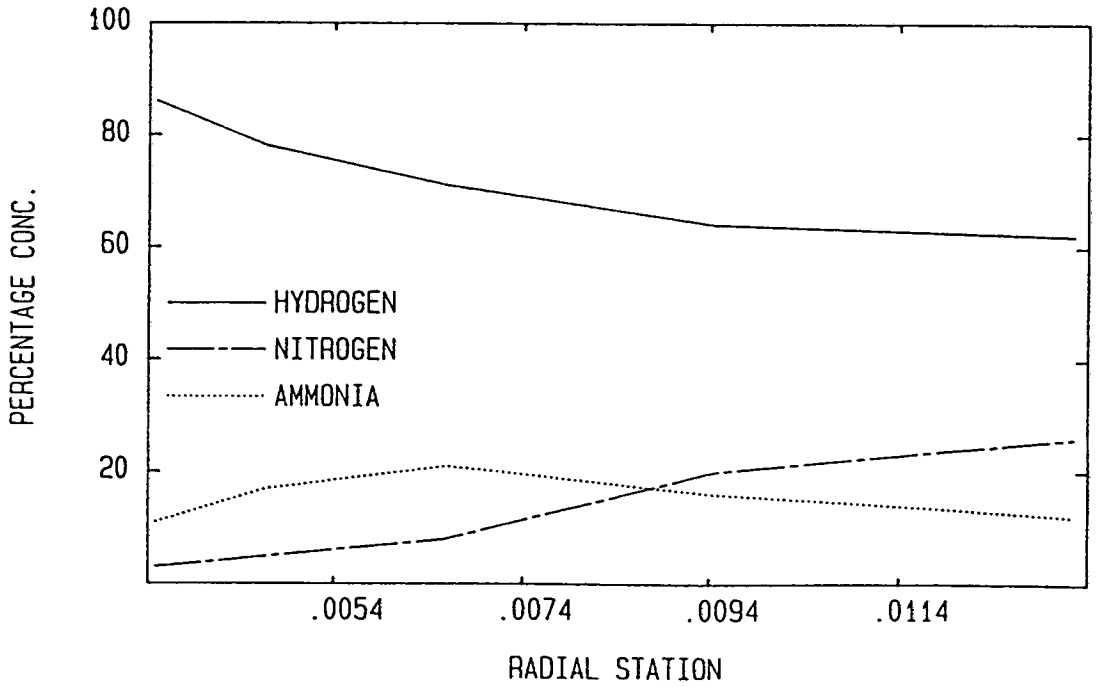

Fig. 5.40 Relative species abundance in the backflow region for Run 3.

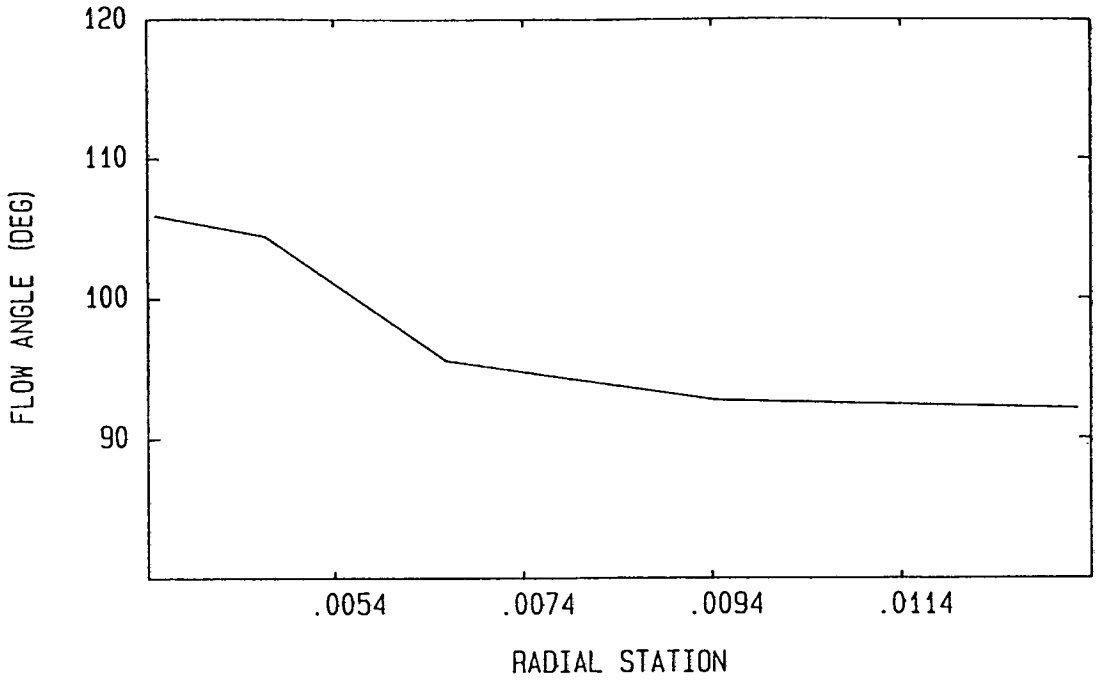

Fig. 5.41 Flow angle in the backflow region for Run 3.

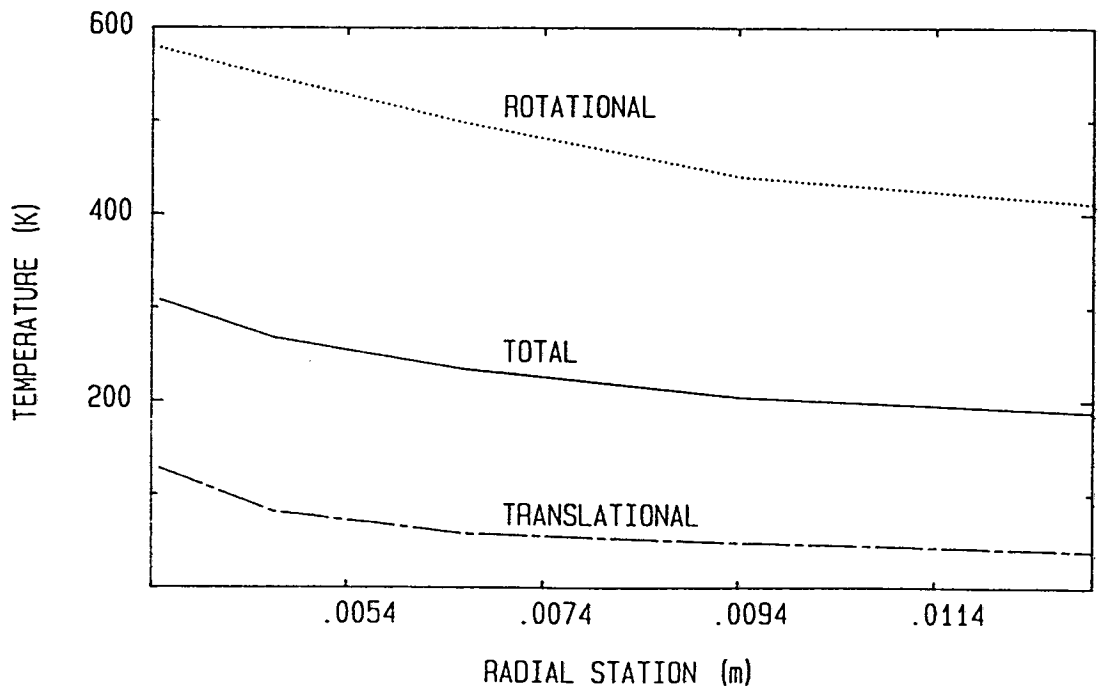

Fig. 5.42 Thermal nonequilibrium in the backflow region for Run 3.